2010

Doctoral Dissertation

Magnetic Suspension Systems Using Permanent Magnet

1118003 Feng SUN
Advisor Koichi OKA

(Special Course for International Students)
Department of Intelligent Mechanical Engineering
Graduate School of Engineering
Kochi University of Technology
Kochi, Japan

August 2010

Contents

Abstract

Magnetic suspension is the technology for supporting an object without contact by means of a magnetic force. Magnetic suspension systems have many advantages, which are the realization of high speed due to no friction, the applications in clean rooms because of no generation of the dirt, and the applications in the cosmos because of the lubrication free. So far, many kinds of magnetic levitation systems have been proposed and developed. These magnetic levitation systems use various methods to control the suspension force. Two types of systems are electromagnetic suspension systems, which control the coil current so as to change the magnetic force in order to levitate an object stably; and mechanical magnetic suspension systems, which use permanent magnets and control the magnetic reluctance so as to vary the suspension force in order to achieve stable suspension. This thesis concentrates on the mechanism magnetic suspension systems, and proposes a zero power control method for a mechanism magnetic suspension system, a noncontact spinning system using permanent magnets and rotary actuators, a novel magnetic suspension system using the variable flux path control method, and the simultaneous suspension of two iron balls using the variable flux path control mechanism.

This thesis consists of three parts, which are Part I Zero Power Control Method, Part II Noncontact Spinning Mechanism, and Part III Variable Flux Path Control Mechanism.

Part I proposes a zero power control method using a spring and an integral feedback loop, and examines the zero power control method on two kinds of magnetic suspension systems with permanent magnets and linear actuators.

First, this zero power control method is examined on a hanging type magnetic suspension system using a permanent magnet and a linear actuator. In this suspension system, a ferromagnetic ceiling is seemed as a track, and a magnetic suspension device is hanging from the ferromagnetic ceiling without contact. The suspension direction of this system is vertical (both the suspension device and the permanent magnet are only moving in the vertical direction). The suspension principle of this hanging type suspension system is that the suspension device is suspended by an attractive force of a permanent magnet that is driven by a linear actuator (that is voice coil motor (VCM) in this prototype.) and positioned from the ferromagnetic ceiling. This suspension system has two parts: the magnet part including a permanent magnet, a slider of VCM and a sensor target; and the frame part including the VCM stator, the three sensors and the frame, which are the remainders of the device except the magnet part. Due to the construction of the suspension device, the VCM has to maintain the gravitational force of the frame part in the stable suspension state, and the frame part holds the most weight of the device and the load has to add on the frame part. Consequently,

the VCM must cost a lot of energy for the gravitational force of the frame part and the load in the stable suspension state. In order to reduce the energy cost in the stable suspension state, a spring is installed between the magnet part and the frame part, and the spring and the VCM sustain the gravitational force of the frame part and the load together. In the control system, two PD feedback loops realize the stable suspension of the device, and a local integral feedback loop makes the VCM current converge to zero in the stable suspension state. As a result, the zero power control is realized in the device by means of the spring and in the control system by means of the integral feedback loop. The model of the suspension system is created and the feasibility of suspension is analyzed theoretically. And then, the optimal feedback gain of the control system is calculated basing on the model and the LQR (linear quadratic regulator) control law. And the nonlinear attractive force of the permanent magnet is used, and the numerical simulations are examined respectively for some typical conditions, such as the magnetic suspension system without springs and without zero power control, with springs and without zero power control, with springs and with zero power control, and using different springs and different gains of the integral feedback loop. Moreover, the suspension experiments are examined in the same cases with the numerical simulations. All simulation and experimental results indicate that the hanging type magnetic suspension system with the permanent magnet and the linear actuator can be levitated stably without contact, the zero power control method using a spring in suspension device and a current integral feedback loop in the controller can reduce energy consumption considerably for this permanent hanging type magnetic suspension system.

Second, this zero power control method is also examined on a mechanical magnetic suspension system for an iron ball, and the good results are obtained.

Part II proposes a novel noncontact spinning mechanism using disk-type permanent magnets and rotary actuators. In this proposed noncontact spinning mechanism, the noncontact suspended-spun object is an iron ball, and the noncontact suspension of the iron ball is achieved using a permanent magnet and a VCM with the air gap control method. The noncontact rotation in horizontal of the suspended object is not realized by exciting coils, but by the rotational, disk-type permanent magnets. The disk-type magnets are arranged around the levitated ball and in the same horizontal plane as the ball. Each magnet has two magnetic poles in the radial direction. The magnetic poles of the disk-type magnets are arranged in a parallel configuration and invert between two adjacent magnets. All of the disk magnets rotate at the same speed and in the same direction. And then, we consider that there are various remanent magnetization points on the surface of the iron ball, and the strongest magnetization determines which will be the upper side of the ball during suspension. Moreover, the next strongest remanent magnetization in the horizontal plane causes the ball to rotate about the vertical axis due to its attraction to the disk-type magnets. Consequently, depending on the remanent magnetization points and the arrangement and number of magnets and the phases of

their magnetic poles, this proposed noncontact spinning mechanism can realize a steady rotation state and fast rotation. Based on the experimental prototype, a numerical model is created and the simulations are carried out in the cases of using only one magnet, using two opposite arranged magnets, and four symmetrically arranged magnets, and the step response, velocity in steady state, and the relationship between the input velocity of the magnets and the output velocity of the iron ball are examined. Moreover, the spinning experiments are completed in the situations same with the simulations using the experimental prototype. All the results indicate that using this proposed noncontact spinning mechanism, the levitated iron ball can be spun using the remanent magnetizations and the rotational disk magnets. The iron ball can be spun regardless of the number of driving magnets used, however, as more magnets were used, the iron ball was spun more smoothly, but the velocity limit decreased. In order to analyze the variation of the flux field of the noncontact spinning mechanism, the IEM (integral element method) analysis for the flux field is carried out using the ELF/MAGIC software in the three same cases with the simulations. And the torque performance is examined by the calculation with the numerical model, the simulation with IEM analysis, and experimental examinations with strain gauges in the three situations. Moreover, the horizontal attractive force of the suspended-spun iron ball is examined by IEM analysis. The examination results indicate that as the number of the driving magnet increases, the rotational torque becomes large and the variation of torque becomes smooth, the horizontal attractive force destroyed the suspension stability of the iron ball, however, becomes large. These results explained the reason caused the spinning velocity results from experiments.

In Part III, first, a novel mechanical magnetic suspension system is proposed with a variable flux path control method using a disk-type permanent magnet and a rotary actuator. This suspension system consists mainly of a disk-type permanent magnet, a rotary actuator containing a gear reducer and an encoder, a pair of opposite F-type permalloy cores, a cuboid permalloy suspension object and two eddy current sensors. The disk-type permanent magnet is magnetized so that its two magnetic poles lay in the radial direction. In this suspension system, the suspension force is provided by the disk-type permanent magnet and is controlled by a magnetic flux path control mechanism, which rotates the disk magnet to change the flux passing through the suspended object. According to the process that is called variable flux path, the attractive force is changed from zero, maximum, and zero, maximum to zero as the disk magnet rotates in one revolution. Consequently, this suspension system can make the attractive force semi-zero, change the polarity of the stator poles, and realize semi-zero power suspension. In order to examine the proposed suspension principle, the flowing of magnetic flux in the magnetic suspension mechanism is examined by the IEM analysis. Moreover, for examining the characteristics of the suspension system, the magnetic flux density and attractive force are simulated by IEM analysis and measured using the experimental prototype with the gauss meter and the force sensor. The results indicate that the proposed suspension

principle is feasible, and this suspension system can change the polarity of the stator poles and realize the semi-zero attractive force. However, the flux leakage causes the attractive forces of two cores different. Based on the examination results, a model is created, and the suspension feasibility is analyzed theoretically. And then, the numerical simulation and suspension experiment are carried out. Owing to the flux leakage, the direct suspension using the cuboid levitated object cannot be succeeded. However, after using a linear rail to balance the unequal attractive forces of the two cores, the suspension has been succeeded. The results indicate that the suspended object can be levitated stably and the actuator current is almost zero at the stable state. That means this magnetic suspension mechanism can levitate a heavy object by means of a small input force, since the gravitational force of suspended object is sustaining by the cores fixed on the base. Moreover, in order to analyze the suspension performance of the suspension mechanism, the variation of the actuator current was examined when the weight of suspended object was changed. And the experiment was carried out in two cases. One case was that, the suspeison force was changing by length of air gap when the angle of magnet was set to 40 degree; the other case was that, the suspension force was changing by the angle of magnet when the air gap was set to 0.9mm. The results indicate that a heavy suspended object can be levitated steadily with a small consumption current, and the actuator current increases as the mass is increased, but the value is very small. Therefore, the system can realize the semi-zero power suspension with the changing air gap and the constant air gap. And the rotational torque of magnet is caused by the potential force of magnetic filed in the mechanism.

Second, the semi-zero suspension force characteristics of the magnetic suspension system have been improved using four methods, which are inserting the ferromagnetic board, using a special type magnet, extending the iron cores, and combination of the special type magnet and the extended cores. The characteristics of the magnetic suspension mechanism using each improvement method are examined by the IEM analysis and the measurement experiments. The results indicate that every method can improve the semi-zero suspension force characteristics. However, using the method of the special type magnet or the extended iron cores can obtain the obvious improvement, and using the combination method can obtain an almost zero suspension force characteristics. Moreover, the suspensions of the simulation and experiment are also carried out using the special type permanent magnet, and the results indicate that the improvement just improved the semi-zero suspension force characteristics of the mechanism, but not influenced the suspension characteristics.

Third, a simultaneous suspension of two iron balls is proposed using the variable flux path control mechanism. The magnetic suspension system using the variable flux path control mechanism has two cores that are seemed as two sources of the suspension forces, and these two cores' attractive forces can be controlled by changing the rotational angle of the disk-type magnet. In order to examine the characteristics of the magnetic suspension system for the

simultaneous suspension of two iron balls, the magnetic flux density and the attractive forces relevant to different size iron balls are examined by the IEM analysis and measurement experiments. The results indicate that the same core generates different attractive force with the different size iron ball, and as the size increases, the attractive force becomes large. Moreover, there is almost no influence to two iron balls suspended by two cores in the suspension direction. According to the examination results, the model is created, and the suspension feasibility is analyzed theoretically. The analyzed results suggest that if the masses of two iron balls are different, this system is controllable and observable. In the control system, the state feedback control is used, and the feedback gains are calculated by LQR. The numerical simulation and suspension experiment are carried out. Since the distance between two levitated iron balls is not long enough, there is an influence of the attractive force between each other. The direct suspension is not succeeded yet. However, after using two linear rails to limit the movement of iron balls in the suspension direction, the simultaneous suspension has been succeeded. The suspension results indicate that the same step is applied to the two suspended iron balls, the response distances of two iron balls are different. The big iron ball moves a larger distance than the small iron ball.

This thesis introduced a zero power control method for the mechanical magnetic suspension systems a noncontact spinning mechanism, and a novel mechanical magnetic suspension system using the variable flux path control method. Based on the examination results, the conclusions can be collected as followings:

A zero power control method using a spring and a current integral feedback loop was proposed. Two kinds of mechanical magnetic suspension systems with permanent magnets and linear actuators were constructed, and the proposed zero power control method was examined on these two systems. The results indicate that this zero power control method is feasible and applicable on the mechanical magnetic suspension systems using the air gap control method.

A noncontact spinning mechanism was proposed with rotational disk-type permanent magnets and rotary actuators. This proposed mechanism could spin the suspended iron ball using the remanent magnetization points regardless of the number of driving magnets used, however, as more magnets were used, the iron ball was spun more smoothly, but the velocity limit decreased.

A novel magnetic suspension system was proposed using a disk-type permanent magnet and a rotary actuator. This suspension system could suspend the cuboid suspended object stably after limiting the movement direction. Moreover, this system could make the attractive force semi-zero, change the polarity of the stator poles, and realize semi-zero power suspension. Through using four kinds of improvement methods, the zero-suspension-force performance was improved. Finally, a simultaneous suspension of two different-weight iron balls was realized using this variable flux path control mechanism.

Keyword: Magnetic suspension, Permanent magnet, Zero power control, Spring, Integral feedback loop, PD control, Noncontact spinning, Flux path control, Actuator, Simultaneous suspension.

Chapter 1 Generation Introduction

1.1 Background of Noncontact Suspension Systems

The noncontact suspension system is a kind of supporting system without mechanical contacts. There are many advantages in noncontact suspension system, such as no contact, no friction and lubrication free. According to these advantages, the noncontact suspension system has many applications, for example, using no contact, the noncontact conveyance vehicles can be developed for semiconductor processing and biotechnology experiments; using no friction, the high speed movement can be realized, such as high speed bearingless motors and high speed trains; using lubrication free, some devices can be developed using in special environment such as high vacuum conditions.

There are many kinds of noncontact suspension systems. Generally, according to the suspension method, there are four major classifications. The four kinds of non-contact suspension systems are electrostatic force suspension systems, air pressure suspension systems, Acoustic levitation systems and magnetic suspension systems as shown in Table. 1.1. Each suspension method has different advantages, problems and limits.

In electrostatic suspension system, the suspension force is an electrostatic force. A photograph of an electrostatic force suspension mechanism is shown in Fig.1.1, and Fig.1.2 shows a basic model of the electrostatic suspension. The floater is electrified by applying a high voltage across the electrodes, and the electrostatic force is generated between the floater and the electrodes. In electrostatic suspension system, since the high voltage control cannot surpass the discharge limit of air, the generation force is weak, and the suspended object must

Table. 1.1 Classification of the non-contact suspension systems

Suspension method	**Generation force**	**Suspended object**	**Problems**
Electrostatic force suspension	weak	Light and large area objects (silicon wafer)	High voltage control Discharge limit of air
Air pressure suspension	Relatively strong	Large area objects	Dust generation
Acoustic levitation floating	Relatively strong	Any objects theoretically	Noise pollution ,Can not use in vacuum condition
Magnetic suspension	**strong**	**Ferromagnetic material**	**Limited material**

be light and large area objects, such as silicon wafer [1]-[3].

In air pressure suspension system, the non-contact suspension force is a pressure force of the flowing air. The general application of the air pressure suspension is an air bearing that is a non-contacting system where air acts as the lubricant that separates the two surfaces in relative motion. Fig.1.3 shows a basic model of an air bearing drilling spindle. In air pressure suspension system, the generation force is relatively strong, and the suspended object must be

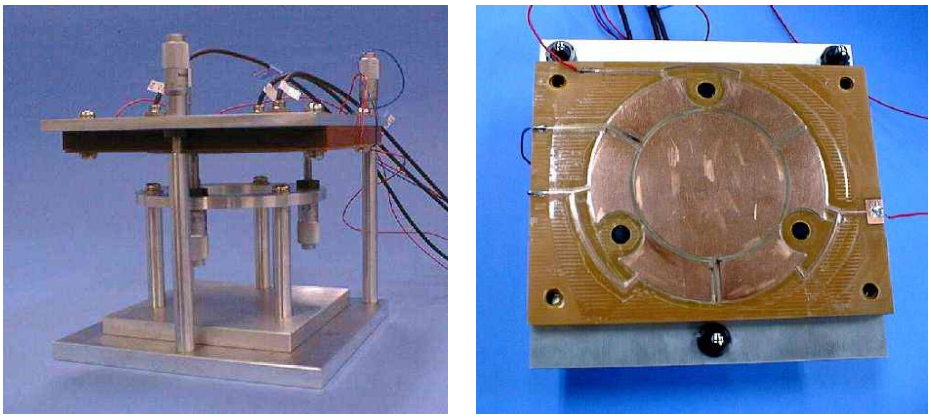

http://www.aml.t.u-tokyo.ac.jp/research/vac_lev/es_lev_vac_j.html

Fig.1.1 An electrostatic suspension mechanism

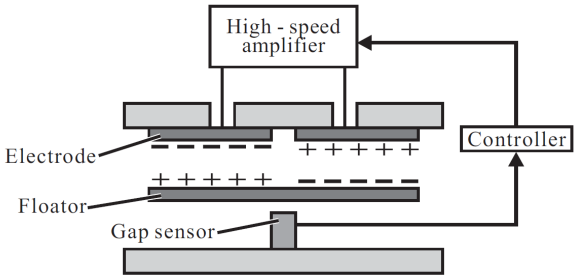

Fig.1.2 Basic model of the electrostatic suspension

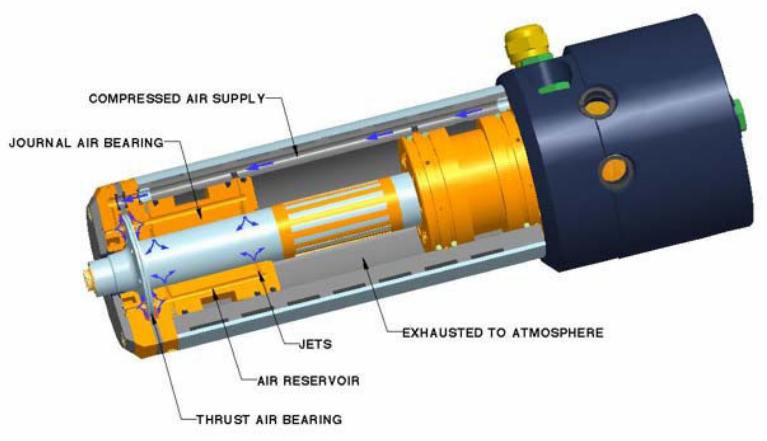

http://www.westwind-airbearings.com/airBearing/index.html

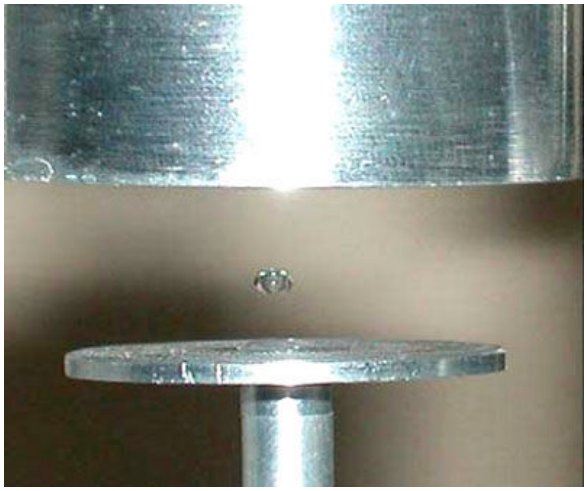

http://science.howstuffworks.com/acoustic-levitation2.htm

Fig.1.4 An acoustic levitation of a water droplet

http://image2.sina.com.cn/dy/c/2007-05-30/U1831P1T1D13114168F21DT20070530184821.jpg

Fig.1.5 A MAGLEV train moving in high speed in Shanghai, China

a large area object. Due to airflow, dust will be generated [4][5].

Acoustic levitation is a method for suspending matter in a medium by using acoustic radiation pressure from intense sound waves in the medium. Fig.1.4 shows a photograph of an acoustic levitation of a water droplet. Acoustic levitation takes advantage of the properties of sound to cause solids, liquids and heavy gases to float. The process can take place in normal or reduced gravity. In other words, the acoustic levitation system can levitate objects on Earth or in gas-filled enclosures in space [6]. There is no known limit to what acoustic levitation can lift given enough vibratory sound, but currently the maximum amount that can be lifted by this force is a few kilograms of matter. Acoustic levitators are used mostly in industry and for researchers of anti-gravity effects such as NASA [7][8]. However, the problems of the acoustic levitation systems are the noise pollution and cannot use in vacuum condition.

Finally, magnetic suspension is a kind of supporting method without any mechanical contact, where the gravitational force is balanced by the magnetic forces only. The position of the suspended object has to remain stable when subject to “reasonable ” disturbance forces. In magnetic suspension system, the generation force is strong, and there are some advantages such as no friction, dirty free, lubrication free. However, the suspended object must be ferromagnetic material or magnetic objects. Using these advantages, various magnetic suspension systems have been proposed and applied in many fields [9]~[11], i.g. the magnetic levitation transport systems and the rotor bearings shown in Fig. 1.5 and Fig. 1.6.

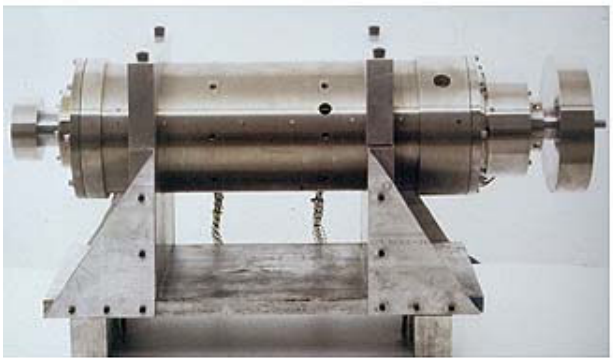

http://www.adixen.co.uk/media/produkte/ATH-M-Series_ID40_412_40.jpg

Fig.1.6 A photo of a NASA turbine unit with Magnetic Bearings

1.2 Classification of Magnetic Suspension Systems

1.2.1 Classification by Magnetic Force

In magnetic suspension systems, there are two basic types of magnetic forces, “Lorentz force” and “Reluctance force” [9]~[11].

The Lorentz force is not across the air gap, but transverse, i.e. in the direction of the air gap. The Lorentz force f in the magnetic suspension system can be expressed as the following equation:

$$f = i \times B \tag{1.1}$$

Where,

i : following current.

B : magnetic flux density.

The reluctance force is across the air gap. The reluctance force is obtained from the principle of virtual work in arrangements of different magnetic permeability μ, and always arises at the surface of media of different relative permeability μ_r, e.g. iron and air. The greater the difference of μ_r, the greater the reluctance force f. The force direction is

perpendicular to the surface of the different materials. And the force is computed from

$$f = \partial w / \partial s \tag{1.2}$$

Where,

w : the field energy.

s : a virtual displacement of the supported body.

Moreover, Table 1.2 sums up the differences of the two force types in magnetic suspension system.

Table 1.2 The two types of magnetic force computation used in practice

	Group 1: Lorentz Force	Group 2: Reluctance Force
Basic computation principle	Cross-product of current and flux density	Energy in magnetic field, principle of virtual work
Computation formula	$f = i \times B$	$f = \partial w / \partial s$
Direction of force	Perpendicular to flux density	Perpendicular to the surface of materials of different μ_r
Basic dependence on current and air gap	Linear when current and flux are not depending on each other, independent of air gap	Quadratic to current Inverse quadratic to air gap

Classification in Lorentz force magnetic suspension systems

According to the source of the current i in the equation (1.1), the magnetic suspension systems can be classified into four types shown in Fig.1.7. The four types are passive electrodynamic levitation of systems in relative motion, passive system with interaction of AC and induced current, active system with interaction of AC and induced current, interaction of controlled current and static flux.

The current i in the equation (1.1) can be either induced or active controlled. When the current is induced, there are two possible mechanisms of induction: either there is an interaction between a permanent magnetic field and a moving conductor, or the interaction takes place without relative motion, between a conductor and an AC powered electromagnet. These two basic types are the passive electrodynamic levitation of systems in relative motion and the passive system with interaction of AC and induced current.

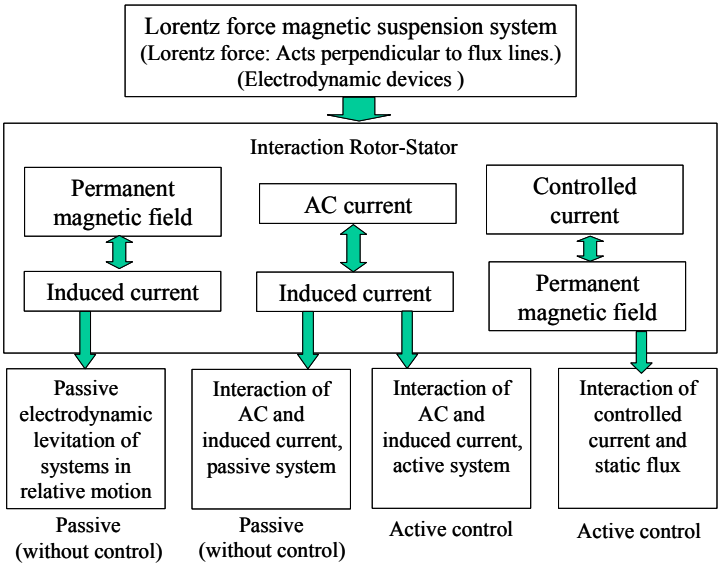

Fig.1.7 Classification in Lorentz force magnetic suspension systems

When the current is active controlled to interact with a magnetic field, there are two possibilities: either, the magnetic field is produced by a permanent magnet or there is an interaction between the controlled current and an induced current. These two levitation types are the active system with interaction of AC and induced current and the system with interaction of controlled current and static flux.

1.2.2 Classification in Reluctance Force Magnetic Suspension Systems

In the magnetic suspension systems using the reluctance forces, the magnetic suspension systems can first be classified according to the value of the relative permeability μ_r of the suspended object' material, which involves paramagnetic material, diamagnetic material, and ferromagnetic material. Of these, the paramagnetic material as well as the diamagnetic material can produce small magnetic forces without superconductors. On the other hand, the ferromagnetic material and the Meissner-Ochsenfeld effect can produce large magnetic forces. Therefore, according to the relative permeability μ_r, the magnetic suspension systems can be classified as shown in Fig.1.8.

CASE 1: Diamagnetic material (μ_r <1)

Many common materials such as water, wood, plants, animals, diamonds, fingers, etc. are usually considered to be non-magnetic but in fact, they are very weakly diamagnetic. Diamagnets repel, and are repelled by a strong magnetic field. The electrons in a diamagnetic material rearrange their orbits slightly creating small persistent currents, which oppose the external magnetic field. The forces created by diamagnetism are extremely weak, millions of times smaller than the forces between magnets and such common ferromagnetic materials as iron. However, in certain carefully arranged situations, the influence of diamagnetic materials can produce startling effects in diamagnetic levitation systems. Up to now, many diamagnetic

levitation systems have been proposed [12]~[14]. Of these suspensions, the most interesting one is that the levitation of a permanent magnet was stabilized by the small diamagnetism of water in human fingers as shown in Fig.1.9 [15].

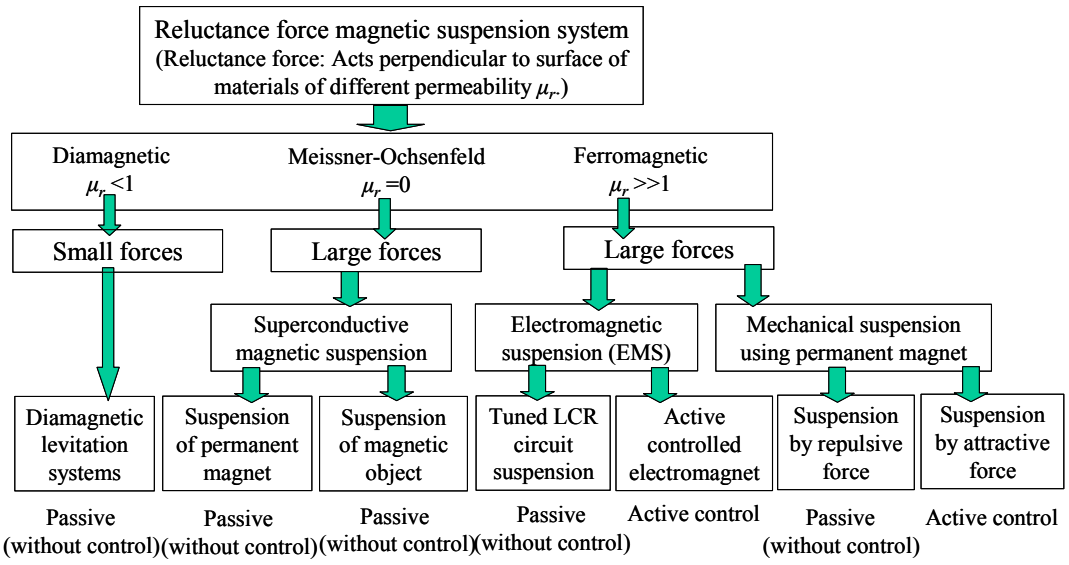

Fig.1.8 Classification in reluctance force magnetic suspension systems

CASE 2: Meissner-Ochsenfeld effect (μ_r =0)

Superconductors may be considered as perfect diamagnets (μ_r = 0), as well as the property they have of completely expelling magnetic fields due to the Meissner-Ochsenfeld effect when the superconductivity initially forms. The levitation of the magnet is further stabilized due to flux pinning within the superconductor; this tends to stop the superconductor leaving the magnetic field, even if the levitated system is inverted. A photograph when a magnet is levitating above a superconductor cooled by liquid nitrogen is shown in Fig.1.10. Using this property, many superconductive magnetic suspension systems have been developed with high temperature superconductors [16]~[18]. Moreover, a suspension of soft magnetic materials using high Tc superconductors has also been proposed using the phenomenon that the usual inverse relationship between the attractive magnetic force and gap distance reverts to a direct relationship for small gap length for a field-cooled superconductor and an adjacent magnetic material [19].

CASE3: Ferromagnetic material (μ_r >>1)

Since the large magnetic force can be produced between the ferromagnetic materials and electromagnets or permanent magnets, the magnetic suspension systems can be realized. According to the magnetic forces generated from electromagnets and permanent magnets, the magnetic suspension systems can be classified into two types, i.e. electromagnetic suspension system and mechanical magnetic suspension system using permanent magnets. Moreover, according to the stability of the magnetic suspension systems, the systems can be classified into passive (without control) systems and actively controlled systems, i.e. passive

electromagnetic suspension system, active electromagnetic suspension system, passive permanent magnetic suspension system, and active permanent magnetic suspension system. The passive system is stable without control loop. And the active system needs the control

Fig.1.9 A permanent magnet is levitating between fingers

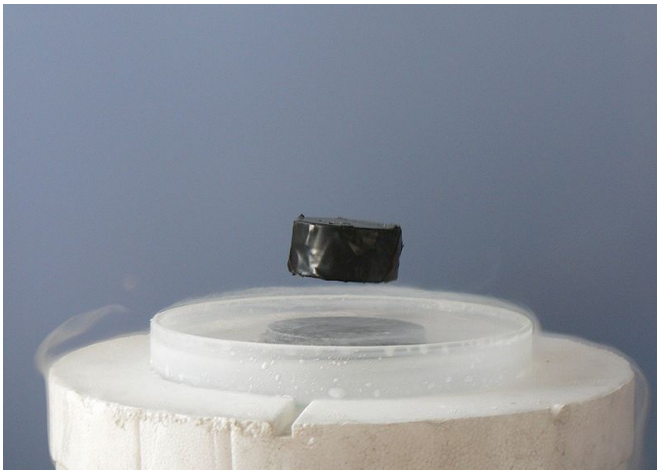

http://en.wikipedia.org/wiki/File:Meissner_effect_p1390048.jpg

Fig.1.10 A magnet is levitating above a superconductor cooled by liquid nitrogen.

loop and the actuator for stabilization.

The suspension system using tuned LCR circuit shown in Fig.1.8 is a kind of passive electromagnetic suspension system. This system achieves a stable stiffness characteristic in an LC-circuit excited slightly off resonance. The LC-circuit is formed with the inductance of the electromagnetic coil and a capacitor. The mechanical displacement of the flotor changes the inductance of the electromagnetic. The LC-circuit is operated near resonance and tuned in this way, that it approaches resonance as the flotor moves away from the electromagnet. This result in an increased current from the AC voltage source and thus pulls the flotor back to its nominal position. The forces and stiffnesses obtained are not very large, but sufficient for certain instrumentation applications. The power supply consists of an AC source operating at a constant frequency [20][21]. The main drawback of this kind of system is that there is no damping, i.e. without additional measures such as mechanical damping or active bearings such systems tend to go unstable.

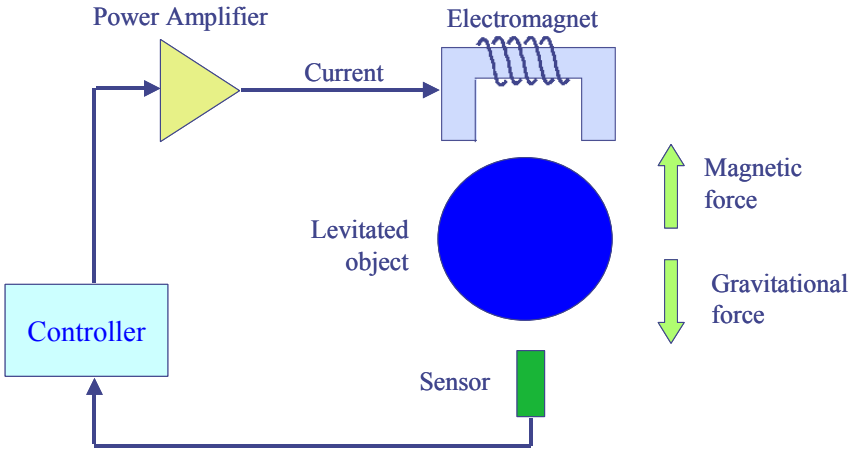

Fig.1.11 A basic model of EMS system.

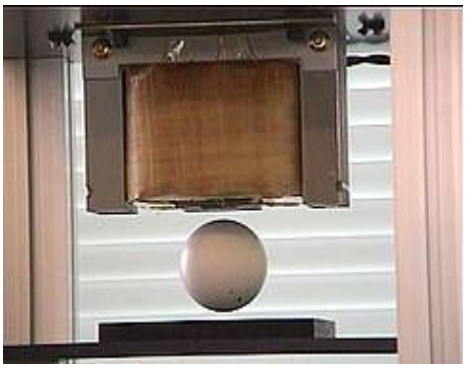

http://www.eee.kagoshima-u.ac.jp/~dc-lab/lab/maglev.html

Fig.1.12 An iron ball suspension by an EMS system.

The active electromagnetic suspension (EMS) system is well known as a basic type of magnetic suspension system. In this kind of system, position signals from gap sensors are used by a controller-power amplifier unit to set the appropriate currents and voltages of the electromagnets in such a way, that stable levitation takes place. Fig.1.11 shows a basic model of the EMS system, which consists of an electromagnet, a levitated object, a sensor, a controller and a power amplifier. In this system, according to the signals of sensor, the controller controls the current of the electromagnet to adjust the magnetic force. When the magnetic force equals the gravitational force, the object can be levitated stable.

In this kind of EMS system, it can be said that magnetic force is controlled by varying magnetomotive force in the magnetic circuit of levitation system. Moreover, the magnetomotive force is varied by actively controlling the coil currents or voltages. As a result, the suspension force f can be expressed as the following equation in the active magnetic suspension systems.

Table.1.3 Summation of suspension force control method in active suspension systems

Active magnetic suspension system by reluctance force Suspension force: $f = k\frac{i^2}{d^2}$			
Suspension method	Electromagnetic suspension (EMS)	Mechanical suspension using permanent magnets	
		The length of air gap control method	Variable flux path control method
Suspension force control method	Actively control the current of the coil	Actively control the length of air gap	Actively control the flux flowing path in device
Changing parameter in the equation of suspension force	i	d	k
Advantages	Realize easily; But energy cost and heat are generated.	No heat, easy to realize long distance operations	No heat, easy to realize save energy mechanisms
Applications	Many fields, e.g. MAGLEV, magnetic bearings	Transportation and operation mechanisms without contact	Transportation and save energy mechanisms without contact

$$f = k\frac{i^2}{d^2} \tag{1.3}$$

Where,

i : the coil current;

d : the length of air gap;

k : the constant of suspension force.

Using EMS systems, various noncontact suspension/levitation systems have been proposed and applied in many fields [9][10][22][23]. And a simple EMS system is shown in Fig.1.12.

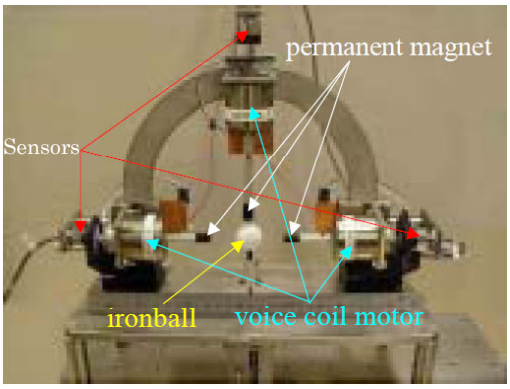

Fig.1.13 A photograph of a 2 DOF suspension mechanism.

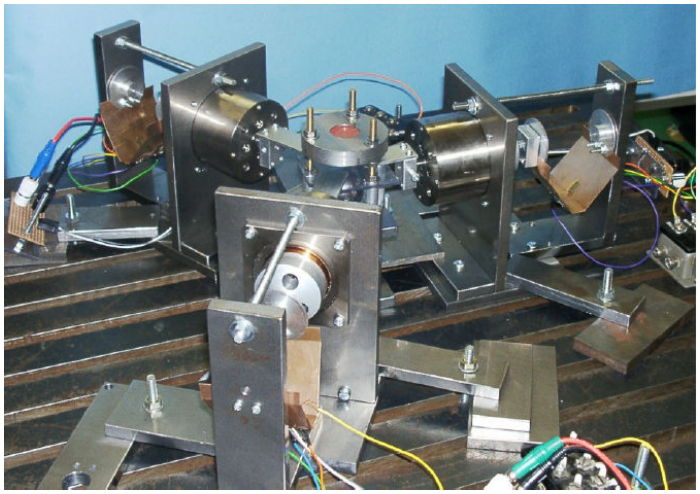

Fig.1.14 A photograph of a flux path control suspension mechanism.

http://www.physics.ucla.edu/marty/levitron/

Fig.1.15 A spin stabilized magnetic levitation of a magnetic top.

The active permanent magnetic suspension system is a kind of system using the attractive force between the permanent magnets and the ferromagnetic materials or the different poles of permanent magnets. The magnetic force is controlled by varying the reluctance of the magnetic circuit in the suspension mechanism. As no electromagnets are used, it is effective for saving energy and avoiding heat generation.

Moreover, in active permanent magnetic suspension systems, since the magnetic force is produced by the permanent magnets, the method of controlling the suspension force is different from the EMS systems. According to the equation (1.3), the control method of suspension force in the active permanent magnetic suspension systems using the reluctance forces can be classified into two types, i.e. the length of air gap control method and the variable flux path control method [24]. And the summation of the suspension force control method in active magnetic suspension systems using reluctance forces is shown in Table.1.3.

The length of air gap control method controls the suspension force through varying the air gap d in the equation (1.3) using a varying gap mechanism, e.g. linear actuators. Using this

control method, many noncontact magnetic suspension systems have been developed for transportation vehicles and noncontact operation mechanisms [25]~[30]. A photograph of a 2 DOF suspension mechanism for noncontact manipulation is shown in Fig.1.13.

The variable flux path control method controls the suspension force through varying the constant k in the equation (1.3) using a varying flux path mechanism, e.g. using composite of magnetostrictive/piezoelectric material in flux circuit of the proposed device. A lot of researchers have presented some suspension mechanisms as saving energy devices [31]~[35]. A photograph of a flux path control suspension mechanism is shown in Fig.1.14.

In addition, the passive permanent magnetic suspension system is a kind of system using the repulsive force between the like poles of permanent magnets. In this kind of system, the stability is only in one degree that the magnets are facing, and other degrees are unstable. Using the repulsive force of permanent magnets, a lot of systems have been developed

http://en.wikipedia.org/wiki/File:Transrapid.jpg

Fig.1.16 The Transrapid at the Emsland test facility in Germany

http://en.wikipedia.org/wiki/File:JR-Maglev-MLX01-2.jpg

Fig.1.17 The MLX01 maglev train at Yamanashi test track in Japan

[36]~[38]. And Fig.1.15 shows a spin stabilized magnetic levitation of a magnetic top using the repulsive force between the permanent magnets [39].

1.3 Application of Magnetic Suspension Systems

Using the advantages, magnetic suspension has two main fields of application: Transport Systems and Magnetic Bearings.

In Transport Systems, MAGLEV vehicles may be better known to the public due to the high speed. Up to now, several MAGLEV vehicles have been developed already as commercial transportation systems [40]~[42].

First, in San Diego of USA. General Atomics has a 120 meter test facility, which is being used as the basis of Union Pacific's 8 km freight shuttle in Los Angeles. The technology is "passive" (or “permanent”), requiring no electromagnets for either levitation or propulsion.

Second, in Emsland of Germany. Transrapid, a German maglev company, has a test track with a total length of 31.5 km. The single-track line runs between Dörpen and Lathen with turning loops at each end. The trains, shown in Fig.1.16, regularly run at up to 420 km/h (260 mph). The construction of the test facility began in 1980 and finished in 1984.

Third, in Yamanashi of Japan. JR-Maglev, shown in Fig.1.17, is a magnetic levitation train system developed by the Central Japan Railway Company and Railway Technical Research Institute (association of Japan Railways Group). JR-Maglev MLX01 (X means experimental) is one of the latest designs of a series of Maglev trains in development in Japan since the 1970s. It is composed of a maximum five cars to run on the Yamanashi Maglev Test Line. On December 2, 2003, a three-car train reached a maximum speed of 581 km/h (world speed record for railed vehicles) in a manned vehicle run.

Forth, in Chengdu of China. The first crewed high-temperature superconducting maglev,

http://www.swjdcy.cn/qqlw_view.asp?newsid=767

Fig.1.17 The high-temperature superconducting maglev CFC-01 in China

shown in Fig.1.18, was tested successfully on December 31, 2000, at Southwest Jiaotong University, Chengdu, China. This system is based on the principle that bulk high-temperature superconductors can be levitated or suspended stably above or below a permanent magnet. The load was over 530 kg and the levitation gap over 20 mm. The system uses liquid nitrogen to cool the superconductor.

Magnetic bearings' advantages include very low and predictable friction, ability to run without lubrication and in a vacuum. Magnetic bearings are increasingly used in industrial

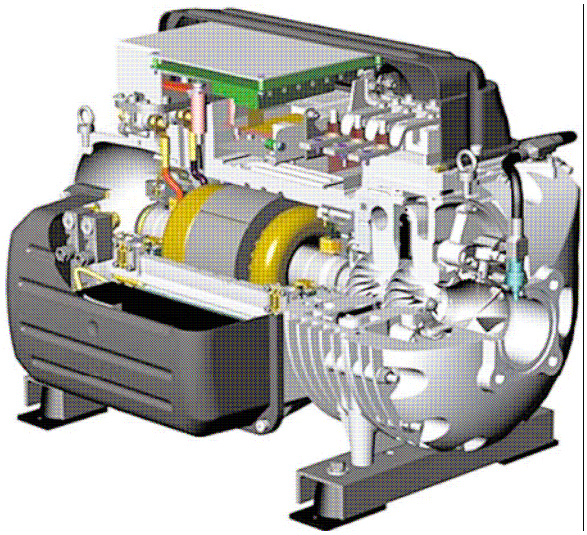

http://www.mcquay.com/mcquaybiz/literature/lit_ch_wc/Brochures/ASP_WMC_Comp.pdf

Fig.1.18 Cutaway View of a Magnetic Bearing Compressor, Nominal 75 Tons

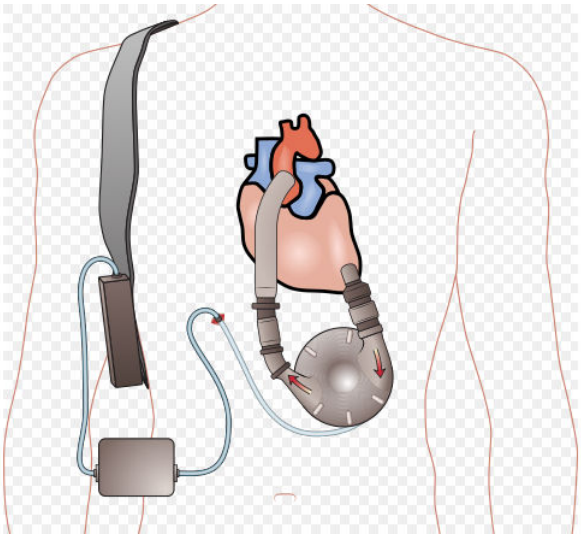

http://commons.wikimedia.org/wiki/File:Ventricular_assist_device.svg

Fig.1.19 Graphic of a ventricular assist device

machines such as compressors, turbines, pumps, motors and generators [10][43]~[45]. Magnetic bearings are commonly used in watt-hour meters by electric utilities to measure home power consumption. Magnetic bearings are also used in high-precision instruments and to support equipment in a vacuum, for example in flywheel energy storage systems. A flywheel in a vacuum has very low windage losses, but conventional bearings usually fail quickly in a vacuum due to poor lubrication. Magnetic bearings are also used to support maglev trains in order to get low noise and smooth ride by eliminating physical contact surfaces. Moreover, a magnetic bearing compressor is shown in Fig.1.18.

A new application of magnetic bearings is their use in artificial hearts. The use of magnetic suspension in ventricular assist devices was pioneered by Prof. Paul Allaire and Prof. Houston Wood at the University of Virginia culminating in the first magnetically suspended ventricular assist centrifugal pump (VAD) in 1999 [46]~[49]. And the graphic of a ventricular assist device is shown in Fig.1.19.

1.4 Reaserch Motivation

1.4.1 Disadvantage of EMS System

Since there are some coils in EMS system, the EMS system has some disadvantages of heat generation, high power, low efficiency, and the big size of coil. Because of these problems, the EMS system cannot suitable for develop some miniature devices, and some devices using in constant temperature plant.

1.4.2 Advantage and Disadvantage of Mechanical Magnetic Suspension System

With the development of permanent magnet, the power of permanent magnet is getting stronger day by day. And the permanent magnet can overcome all the problems of the coils. Therefore, the mechanical magnetic suspension system using permanent magnet can be used to develop some miniature devices, and some devices using in constant temperature plant.

However, the mechanical magnetic suspension system using permanent magnet also has some disadvantages of slow responsibility and difficult control.

This thesis will focus on developing the actively control mechanical magnetic suspension systems using permanent magnet.

1.5 Structure of This Thesis

According to the different control method and experimental device, this thesis is divided into three parts.

1.5.1 Part I Zero Power Control Method for Permanent Magnetic Suspension

In Part I, a zero power control method using a spring and a current integral feedback loop is proposed. Two kinds of mechanical magnetic suspension systems with permanent magnets and linear actuators are constructed, and the proposed zero power control method is examined on these two systems. The results indicate that this zero power control method is feasible and applicable on the mechanical magnetic suspension systems using the air gap control method.

1.5.2 Part II A Novel Noncontact Spinning Mechanism

In Part II, a noncontact spinning mechanism is proposed with rotational disk-type permanent magnets and rotary actuators. This proposed mechanism can spin the suspended iron ball using the remanent magnetization points regardless of the number of driving magnets used.

1.5.3 Part III Variable Flux Path Control Mechanism

In Part III, a novel magnetic suspension system is proposed using a disk-type permanent magnet and a rotary actuator. This suspension system can suspend the cuboid suspended object stably after limiting the movement direction. Moreover, this system can make the attractive force semi-zero, change the polarity of the stator poles, and realize semi-zero power suspension. Through using some improvement methods, the zero-suspension-force performance is improved. Finally, a simultaneous suspension of two different-weight iron balls is realized using this variable flux path control mechanism.

Part I　Zero Power Control Method

Chapter 2 Zero Power Control Method for a Hanging Type Magnetic Suspension System

2.1 Introduction

Conveyance vehicles have been in increasing demand because of the need for an ultra-clean environment in many fields, such as semiconductor processing, biotechnology experiments and material processing. The mechanisms and tools used in these fields must be ultra-clean so as not to contaminate samples. Moving frictional parts in direct contact, such as reduction gears, bearings, wheels and rails, are the main sources of dust and particles, which cannot be avoided. In order to resolve these problems, some noncontact conveyance vehicles have been proposed with magnetic suspension systems [50]-[52]. Fig.2.1 shows a hanging type noncontact conveyance vehicle using electromagnetic suspension system. Most of these systems are using electromagnetic suspension systems. The electromagnetic suspension has some disadvantages, such as heat generation, high cost, low efficiency, big size of the suspension device. Because there are some coils in the device, the heat is generated by coils when the attractive force is generating, and a large attractive force needs a big size coil to generate. For hanging type conveyance vehicles, when the suspension device is levitated in a stable state, the electromagnet must generate the attractive force to balance the gravitational

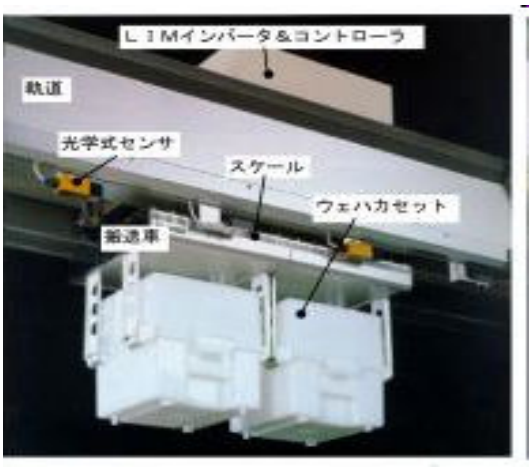

http://www.dbjet.jp/pub/cgi-bin/detail_jr.php?id=323

Fig.2.1 A hanging type transmission vehicle of Toshiba using electromagnets

force of the suspended device, i.e. a lot of power is consumed to generate a constant force for counterbalancing the gravitational force. Moreover, this kind of system requires a minimum driving power consumption because it has battery for supplying driving electric power by itself. With regards to this, many researchers have done a lot of work focus on saving the consumption energy in the stable state. Morishita et al. proposed a zero power control method using a hybrid magnet of permanent magnet and electromagnet. Using this method, the DC power loss of the hybrid magnet under load variation can be drastically reduced, because the hybrid magnet uses the electric power only in the transient condition [50]. This kind of hybrid magnet has become a long standing proved method as an energy saving maglev system. Basing on the hybrid magnet, many zero power control methods have been developed using different control methods [53]-[56].

However, the disadvantages of coils cause the noncontact conveyance vehicles using electromagnets cannot be used in the constant temperature plants, and it is difficult to manufacture some miniature transmission devices. With the development of high power permanent magnet, the magnetic suspension systems using permanent magnets have been proposed [26]~[29], [35], [56]~[59]. The advantages of permanent magnetic suspension systems are no heat generation and no requirement for a coil.

This chapter proposes a hanging type magnetic suspension system using a permanent magnet. This suspension system can be used to realize noncontact conveyance mechanisms. In this suspension system, the attractive force is controlled through varying the air gap distance between the permanent magnet and the ferromagnetic ceiling. The system's characteristics are the nonuse of an electromagnet and the utilizations of a permanent magnet and a linear actuator. However when this type of magnetic levitation system suspends with noncontact, the actuator has to support the mostly weight of the whole device including itself. Therefore, the energy consumption becomes a significant problem. In order to solve this problem, a zero power control method is adopted to reduce the energy consumption. A spring is assembled in the device and an integral feedback loop is used in the control system, and then almost no energy is consumed in the suspending state.

In this chapter, first the principle of the permanent magnetic suspension is explained. Second, a magnetic suspension system prototype is introduced and a mathematical model is created. Third, the realization of zero power control is analyzed in device, mathematical model, and control system. Last, some results of numerical simulations and experiments are shown and discussed, and these results indicate that the zero power control makes the levitation system almost consume no energy in the stable suspension state.

2.2 Suspension Principle

The principle of this hanging type magnetic suspension system can be understand from Fig.2.2, a schematic of the proposed magnetic suspension system. The suspension system mainly consists of a permanent magnet, an actuator and a mass. In this system, the permanent

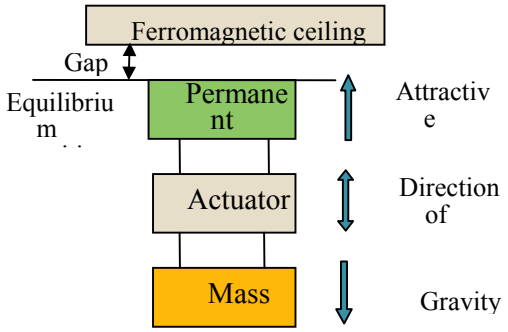

Fig.2.2 The schematic of hanging type magnetic suspension system

magnet generates the suspension force; the actuator performs the suspension control; and the ferromagnetic ceiling acts as a track. The suspension device is hung from the ferromagnetic ceiling by the attractive force of the permanent magnet. When the suspension device is levitating, the levitation direction is vertical, and the magnet's attractive force is equal to the gravitational force on the suspension device in the equilibrium position. Then, based on the principle that the magnetic force is inversely proportional to the square of the gap between the magnet and the ferromagnetic ceiling [65], the actuator controls the distance between the magnet and the mass so as to adjust the gap. When the gap is larger than the balance gap, the actuator increases its distance in response to the magnet's motion from the equilibrium position towards the ceiling. When the gap is smaller than the balance gap, the actuator decreases its distance in response to the magnet's motion away from the ceiling. In this way, the suspension mechanism is able to levitate stably without contact.

2.3 Experimental Prototype

2.3.1 Experimental Prototype

A prototype photograph of a permanent magnetic suspension device is shown in Fig.2.3. The prototype mainly consists of a permanent magnet, a voice coil motor (VCM), a spring, three eddy current displacement sensors and a frame. The weight of the experimental prototype is 746.8 g. This prototype consists of two parts: the magnet part and the frame part. The magnet part includes a permanent magnet, a slider of VCM and a sensor target. The frame part includes all the remainders of the prototype besides the magnet part, which are the VCM stator, three eddy current sensors and the frame. The weight of the magnet part is 79.5 g,

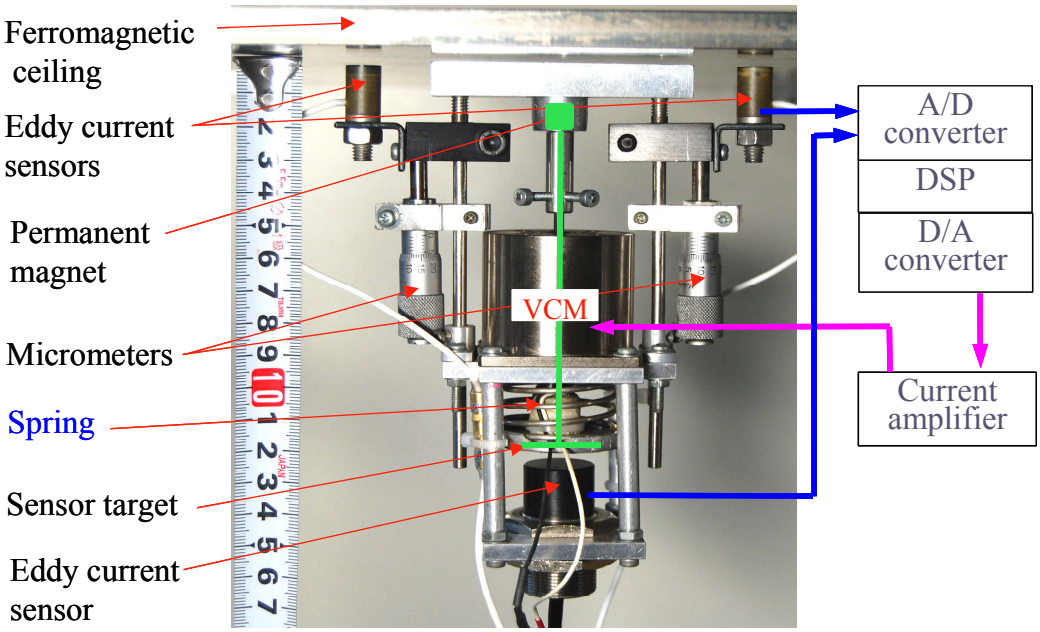

Fig.2.3 The experimental prototype of the hanging type suspension device

and the weight of the frame part is 667.3 g.

The VCM (voice coil motor) used in this experimental prototype is a linear actuator powered by Lorentz force. The VCM's important characteristics are fast response, high-frequency vibration capability, zero nonlinear friction and a direct drive mechanism. These advantages are indispensable for levitating an object steadily without contact. The VCM used here has a driving length of 15 mm. This VCM can generate a driving force of 10 N by a coil current of 2 A. This VCM consists of a stator and a slider. The stator mainly consists of a permanent magnet and an iron core, which is belonging to the frame part. And the slider with a coil is belonging to the magnet part. The VCM is the only active driving element, which is utilized to suspend the device stably.

A spring is installed between the frame part and the magnet part of the device. When the VCM current is zero, the spring generates a force to counterbalance the gravitational force acting on the frame part at the balance position. This is the primary requirement for zero power control.

Three displacement sensors installed in the prototype are eddy current sensor. The upper two sensors measure the distance between the frame part and the ferromagnetic ceiling. The resolution these two sensors is 0.5 μm, and the measurement rang is 4 mm. These two sensors are installed on the stays of the frame, and can be adjusted precisely in the vertical direction by two micrometers along the stays. Moreover, these two sensors were arranged at two sides of the permanent magnet symmetrically for co-locating. Therefore, the position of the frame part is determined by the average of these two sensors' signals. Additionally, the lower sensor

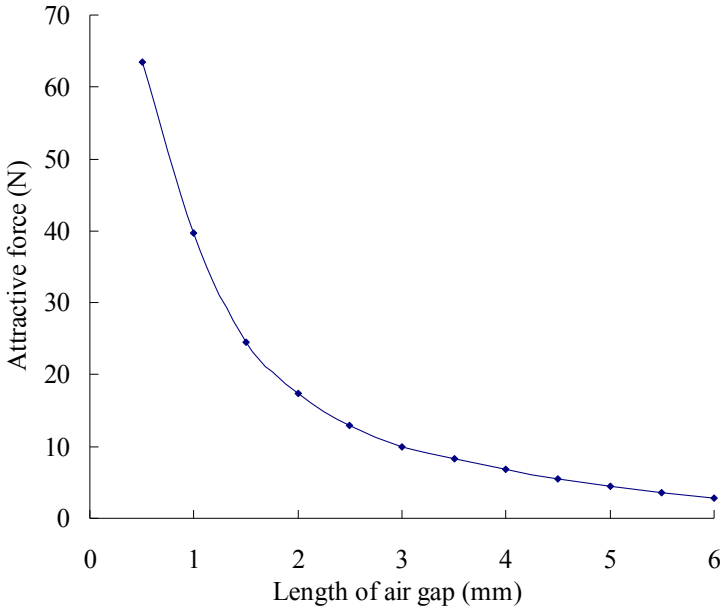

Fig.2.4 The attractive force characteristic of permanent magnet

measures the relative position between the magnet part and the frame part. The lower sensor has a resolution of 5 μm and a measurement range of 10 mm.

2.3.2 Examination of Attractive Force

First, the relationship between the attractive force and the air gap of the permanent magnet was measured by a load sell. The measurement results are shown in Fig.2.4. The results indicate that the attractive force becomes larger when the air gap becomes smaller.

2.4 Mathematical Model and Analysis of Suspension Feasibility

2.4.1 Mathematical Model

According to the experimental prototype, a model is created and shown in Fig.2.5. Basing on the model, the motion equations of the system can be expressed as following:

$$m_0\ddot{z}_0 = k_s\left(z_1 - z_0\right) + c\left(\dot{z}_1 - \dot{z}_0\right) - f_a - m_0 g \tag{2.1}$$

$$m_1\ddot{z}_1 = k_s\left(z_0 - z_1\right) + c\left(\dot{z}_0 - \dot{z}_1\right) + f_a + f_m - m_1 g \tag{2.2}$$

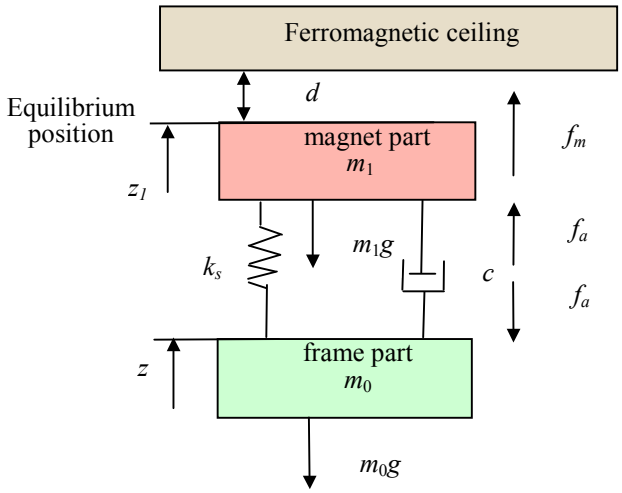

Fig.2.5 Model of suspension system

$$f_a = k_t i \tag{2.3}$$

$$f_m = \frac{k_m}{d^2} \tag{2.4}$$

Where,

m_0: the mass of the frame part

m_1: the mass of the magnet part

z_0: the displacement of the frame part

z_1: the displacement of the magnet part

f_a: the generation force of VCM

f_m: the attractive force of the permanent magnet

k_s: the spring constant

c: the damping coefficient

d: the length of the air gap between the permanent magnet and the ceiling

k_t: the propulsive coefficient of VCM

i: the current of the VCM

2.4.2 Analysis of Suspension Feasibility

The attractive force of permanent magnet fm is represented as a nonlinear function of the length of the air gap becomes larger as the air gap decreases. By linearization of this function around the equilibrium position, we obtain

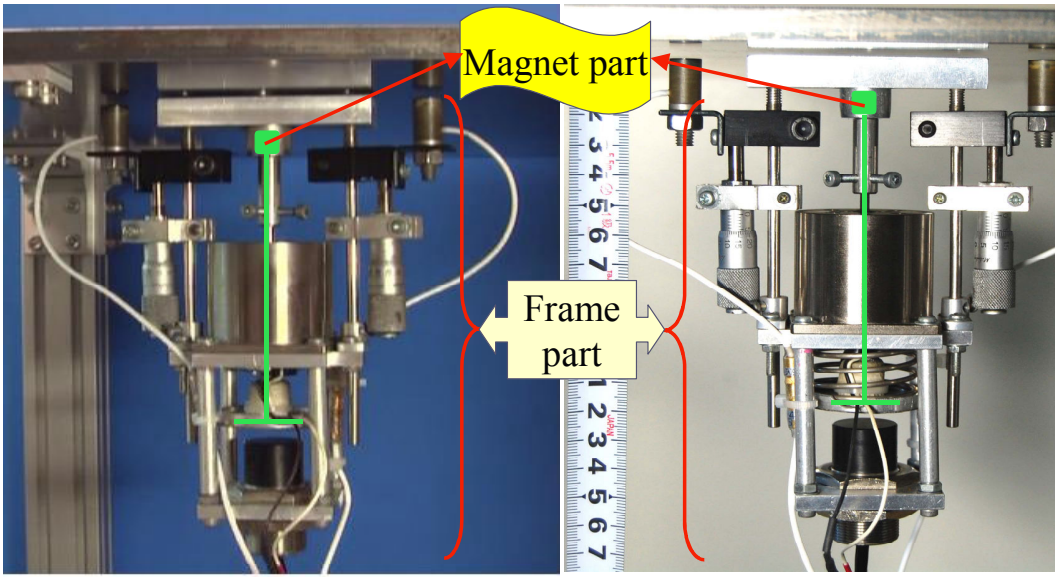

(a) The device without the spring (b) The device with the spring

Fig.2.6 Realization of zero power control in device

$$f_m = \frac{k_m}{(d_0 + \Delta d)^2} = \frac{k_m}{d_0^2 + 2\Delta d d_0 + \Delta d^2} \tag{2.5}$$

$$= \frac{k_m\left(d_0^2 - 2\Delta d d_0 - \Delta d^2\right)}{\left(d_0^2 + 2\Delta d d_0 + \Delta d^2\right)\left(d_0^2 - 2\Delta d d_0 - \Delta d^2\right)}$$

$$= \frac{k_m\left(d_0^2 - 2\Delta d d_0 - \Delta d^2\right)}{d_0^4 - \left(2\Delta d d_0 - \Delta d^2\right)^2}$$

Around the balance point, Δd is much smaller than d. Thereforce the second-order items in Equation (2.5) can be neglected.

$$f_m = \frac{k_m\left(d_0^2 - 2\Delta d d_0\right)}{d_0^4} = \frac{k_m}{d_0^2} - \frac{2k_m}{d_0^3}\Delta d = f_{m0} + \Delta f_m$$

$$\Delta f_m = -\frac{2k_m}{d_0^3}\Delta d \tag{2.6}$$

In this model, we can conclude following equations around the equilibrium position:

$$\Delta d = \Delta z_1 \tag{2.7}$$

Then

$$\Delta f_m = -\frac{2k_m}{d_0^3}\Delta z_1 \tag{2.8}$$

Then the equations can be translated to followings at the equilibrium position:

$$\Delta \ddot{z}_0 = \frac{c}{m_0}\left(\Delta \dot{z}_1 - \Delta \dot{z}_0\right) + \frac{k_s}{m_0}\left(\Delta z_1 - \Delta z_0\right) - \frac{k_t}{m_0}\Delta i \tag{2.9}$$

$$\Delta \ddot{z}_1 = \frac{c}{m_1}\left(\Delta \dot{z}_0 - \Delta \dot{z}_1\right) + \frac{k_s}{m_1}\Delta z_0 - \left(\frac{k_s}{m_1} + \frac{2k_m}{m_1 d_0^3}\right)\Delta z_1 + \frac{k_t}{m_1}\Delta i \tag{2.10}$$

We can set the state variables as:

$$x = \begin{bmatrix} \Delta z_0 \\ \Delta \dot{z}_0 \\ \Delta z_1 \\ \Delta \dot{z}_1 \end{bmatrix} \tag{2.11}$$

Then the state space equation and the output equation are:

$$\dot{x} = Ax + Bu \tag{2.12}$$

$$y = Cx \tag{2.13}$$

Where,

$$A = \begin{bmatrix} 0 & 1 & 0 & 0 \\ -\frac{k_s}{m_0} & -\frac{c}{m_0} & \frac{k_s}{m_0} & \frac{c}{m_0} \\ 0 & 0 & 0 & 1 \\ \frac{k_s}{m_1} & \frac{c}{m_1} & -\frac{\left(k_s + \frac{2k_m}{d_0^3}\right)}{m_1} & -\frac{c}{m_1} \end{bmatrix}$$

$$B = \begin{bmatrix} 0 \\ -\frac{k_t}{m_0} \\ 0 \\ \frac{k_t}{m_1} \end{bmatrix}$$

$$C = \begin{bmatrix} 1 & 0 & 0 & 0 \end{bmatrix}$$

The controllability matrix of the system is:

$$P_c = \begin{bmatrix} B & AB & A^2B & A^3B \end{bmatrix} \tag{2.14}$$

$$\det(P_c) = \frac{4k_m^2 k_t^4}{d_0^6 m_0^2 m_1^4} \tag{2.15}$$

Therefore,

$$Rank(P_c) = 4 \tag{2.16}$$

The controllability matrix of the system is full rank, so the system is controllable.
The observability matrix of the system is:

$$Q = \begin{bmatrix} C \\ CA \\ CA^2 \\ CA^3 \end{bmatrix} \tag{2.17}$$

$$\det(Q) = \frac{k_s^2}{m_0^2} + \frac{2c^2 k_m}{d_0^3 m_0^2 m_1} \tag{2.18}$$

$$Rank(Q) = 4 \tag{2.19}$$

The observability matrix of the system is full rank, so the system is observable.

2.5 Realization of Zero Power Control

2.5.1 Realization in Device

Zero power control in this system means that the current of VCM is 0 when the device is suspending stable. In the stable suspension state, the magnetic force of the permanent magnet supports the gravitational force of the whole device. However, the gravitational force of the frame part must be transmitted to the magnet. If there is no spring installed in the device shown as Fig.2.6 (a), the gravitational force of the frame part must be transmitted through the VCM. That means the VCM force equals the gravitational force of the frame part constantly. Therefore, it is impossible to make the force of VCM zero, i.e. the current of VCM cannot be zero. However, if there is a spring installed in the device shown as Fig.2.6 (b). Generally, the gravitational force of the frame part can be transmitted to the permanent magnet through the spring instead of the VCM, and the VCM only generates force in the transient condition. As a result, in the stable suspension state, there is no current flowing through the VCM, and no power is consumed, theoretically.

2.5.2 Realization in Mathematical Model

Moreover, the zero power control in this system also can be understood from the mathematical model. If there is no spring installed in the device, the motion equations of the system can be expressed as following.

$$m_0\ddot{z}_0 = c\left(\dot{z}_1 - \dot{z}_0\right) - f_a - m_0 g \tag{2.20}$$

$$m_1\ddot{z}_1 = c\left(\dot{z}_0 - \dot{z}_1\right) + f_a + f_m - m_1 g \tag{2.21}$$

In this case, if the system is in the stable suspension state, the dynamic items in Equation (2.5) and (2.6) equal zero. In order to maintain the balance of the system, the force of VCM f_a must equal the gravitational force of the frame part. Therefore, the current of VCM cannot be zero.

On the other hand, if there is a spring installed in the device, the motion equations of the system are shown as Equation (2.1) and (2.2). In the stable suspension state, the dynamic items in Equation (2.1) and (2.2) equal zero. In this time, the force of VCM and the spring support the gravitational force of the frame part together. When the force of VCM verges to zero, the force of spring supports the gravitational force. As a result, the current of VCM can verge to zero, i.e. the zero power control can be realized.

2.5.3 Realization in Control System

The controller of this suspension system is a DSP controller shown in Fig.2.3. Signals from three sensors are input to the DSP controller through 12-bit A/D converters. Based on these signals, appropriate current values are computed by the controller. The current values are converted to analog current by D/A converters, and then amplified by a current amplifier. The

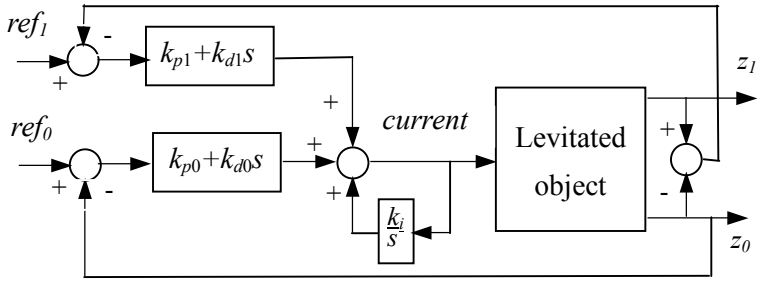

Fig.2.7 Block diagram of control system

final actual current controls the VCM to maintain the system suspension stably.

The block diagram of control system for zero power magnetic suspension system is shown in Fig.2.7. As shown in Fig.2.7, there are two large PD feedback loops in the block diagram. The lower PD feedback loop controls the distance between the frame part and the ceiling. The upper PD feedback loop controls the relative displacement between the magnet part and the frame part. Both PD feedback loops calculate the current values based on the sensors' signals in order to make the VCM maintain the system levitation robustly. When the magnetic suspension system is suspended, no external input is imported, and the system simply maintains itself suspension stable in an equilibrium position. To some degree, this suspension system is an autonomous system, and the control system is an adaptive control system. The requirements of the control system are quick response and reliable stability. Moreover the equilibrium positions are not fixed. When the load varies, the equilibrium position changes. When the controller was designed, all above-mentioned factors were considered. Therefore the proportional controller and differential controller were adopted and the integral controller was not used in both feedback loops.

Moreover, when using these two PD feedback loops to suspend the device stably, only an optimal distance between the permanent magnet part and the frame part can make the current of VCM approximately zero. If the distance between the permanent magnet part and the frame part is not equals to the optimal distance, there are two cases in regard to the force of VCM. When the distance is larger than the optimal distance, the force of spring is deficient to support the frame part, and the force of VCM compensates the deficiency. In this case, the direction of the VCM's force is upward, and is same with the force of the spring. If the distance is shorter than the optimal distance, the force of spring is larger than the gravitational

force of the frame part, and the force of VCM counteracts the redundant force of the spring. In this case, the direction of the VCM's force is downward, and is reverse to the force of the spring.

In order to always approximate the VCM's force to zero in the stable suspension state, besides the two large PD feedback loops, a local current integral feedback loop is used before the levitated object block to implement zero power control in the control system. When current flows through the VCM circuit, this integral feedback loop reduces the current. The current reduction affects the distance between the frame part and the magnet part, and the resulting distance variation causes the spring length and the generating force to change. Finally, when the spring force becomes equal to the frame part weight, i.e. the distance between the permanent magnet part and the frame part equals the optimal distance, the VCM current verges to zero. Nevertheless the load is not varying, so the air gap between the permanent magnet and the ceiling never changes. Furthermore, the k_i shown in Fig.2.7, the gain of the integral current feedback loop influences the speed of current variation. If the value is large, the current reaches zero quickly. However, that works against to the system's stability. Rapid current variation will cause the system unstable. Therefore, a proper value of k_i is very important for the system's stability.

After analyzing the realization of the zero power control in device, mathematical model, and the control system, the feasibility of zero power control in this system can be understood obviously.

Table 2.1 Parameters using in numerical simulation

Parameter	Value	Parameter	Value
m_0 (kg)	0.6673	c (N/(m/s))	0
m_1 (kg)	0. 0795	k_m (Nm^2)	9. 518×10^{-5}
d_0 (m)	2.5×10^{-3}	k_t (N/A)	5
g (m/s^2)	9.8	k_s (N/m)	600

2.6 Numerical Simulation

According to the mathematical model of Equation (2.12) and (2.13), first, the feedback gains were calculated using the LQR (linear quadratic regulator) full state feedback control law. Second, the numerical simulation was carried out with a nonlinear attractive force.

2.6.1 Calculation of Feedback Gains

All the parameters using in the numerical simulation are shown in Table.2.1, which are

measured from the experimental prototype. Moreover, the value of k_m is measured from Fig.2.4

Many methods can design the controller for a linear system. In terms of linear control theory, due to this proposed system is controllable and observable, the LQR can be used to get the feedback gains. Based on the characteristics of the system, we chose the state weighting matrix Q and input weighting matrix R as following:

$$Q = \begin{bmatrix} 1 & 0 & 0 & 0 \\ 0 & 1 & 0 & 0 \\ 0 & 0 & 1 & 0 \\ 0 & 0 & 0 & 1 \end{bmatrix} \tag{2.22}$$

$$R = 1 \tag{2.23}$$

Using MATLAB software, the feedback gain K is calculated as following:

$$K = \begin{bmatrix} 2600 & 10 & 3300 & 30 \end{bmatrix} \tag{2.24}$$

2.6.2 Numerical Simulation

For feasibility study, numerical simulations carried out with the nonlinearization of the attractive force. The simulations are examined in the following cases.

- Case 1: the magnetic suspension system without spring and without zero power control.
- Case 2: the magnetic suspension system with spring (600 N/m) and without zero power control.
- Case 3: the magnetic suspension system with spring (600 N/m) and with zero power control.
- Case 4: the magnetic suspension system with spring (700 N/m) and without zero power control.
- Case 5: the magnetic suspension system with spring (700 N/m) and with zero power control.

The simulations were carried out using the calculated feedback gains in the five cases. In the simulations, when a 10 grams weight was cut off from the frame part as a step during the stable suspension state, the VCM current, the frame part displacements, the relative displacements between the magnet part and the frame part, and the displacement of the magnet part were recorded. The step was implied at 0.2 second, and the responses were recorded until 1 second. The varieties of the current and the displacements were plotted in figures, as the upward direction is positive.

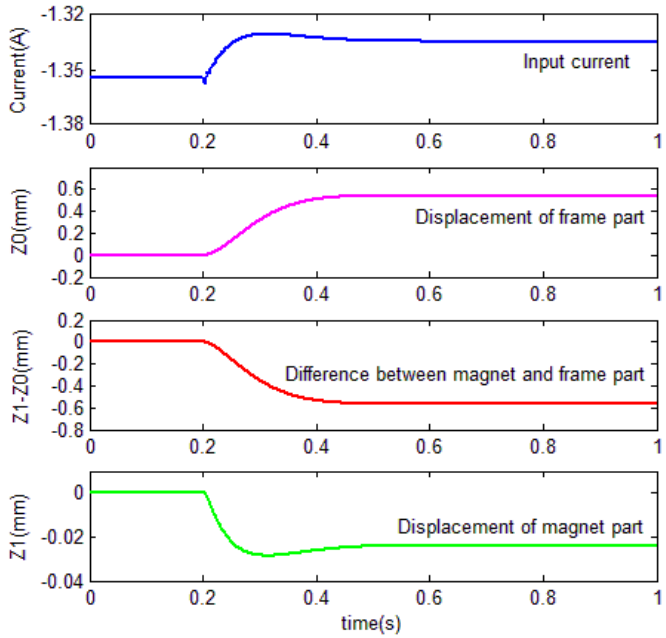

Fig.2.8 Simulation results in Case 1

The results of the simulation in Case 1 are in shown in Fig.2.8. The first graph shows the VCM current response. The second one indicates the frame part displacement. The third one shows the relative displacement between the magnet part and the frame part. The final graph shows the displacement of the magnet part. When the weight is cut off from the frame part, the original balance state is broken since the gravitational force is smaller than the attractive force of the magnet. Therefore, the displacement of the frame part shown in the second graph increases. In order to make the system return to balance, the actuator must enlarge the air gap between the magnet and the ceiling, and then the attractive force will increase until it is equal to gravitational force of the device. Therefore, the displacement of the magnet from the ceiling decreases. In this process, the magnet part descends, and the VCM decreases the distance between the magnet part and the frame part. Since the gravitational force of the frame part that is supporting by the VCM is decreased, the VCM needs a smaller current than before cutting the weight of disturbance. The process is same as shown in Fig.2.8. After the transient process, the suspension system reaches the balance state again. Moreover, in the final stable suspension state, the VCM current is approximately –1.33 (A). This current is used to generate the propulsion force that is supporting the gravitational force of the frame part. The changing value of the current is 0.02A for responding to the decreased weight.

The results of the simulation in Case 2 are shown in Fig.2.9. In this simulation, the used spring constant is 600 N/m. All results are similar to the results of the simulation in Case 1 at the beginning of the control process. However, in the steady state in Fig.2.9, the changing value of the current is approximate 0.01 (A), which is smaller than in Fig.2.8. The reason is

that the gravitational force of the frame part is supporting by the propulsion force of the spring and the force of the VCM.

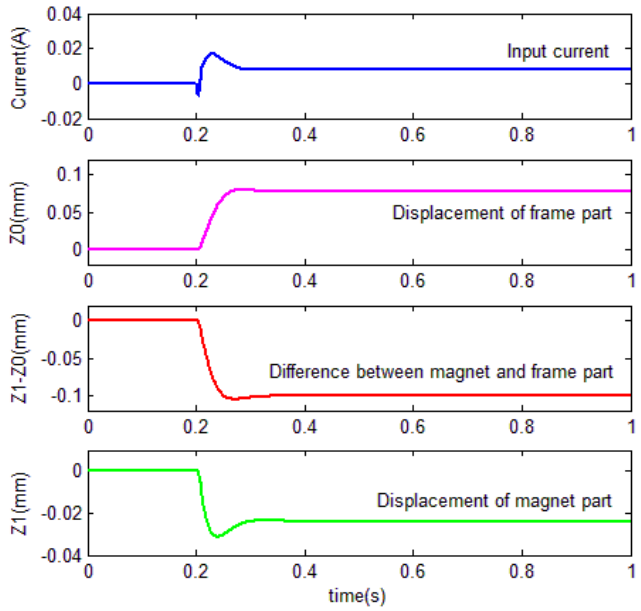

Fig.2.9 Simulation results in Case 2

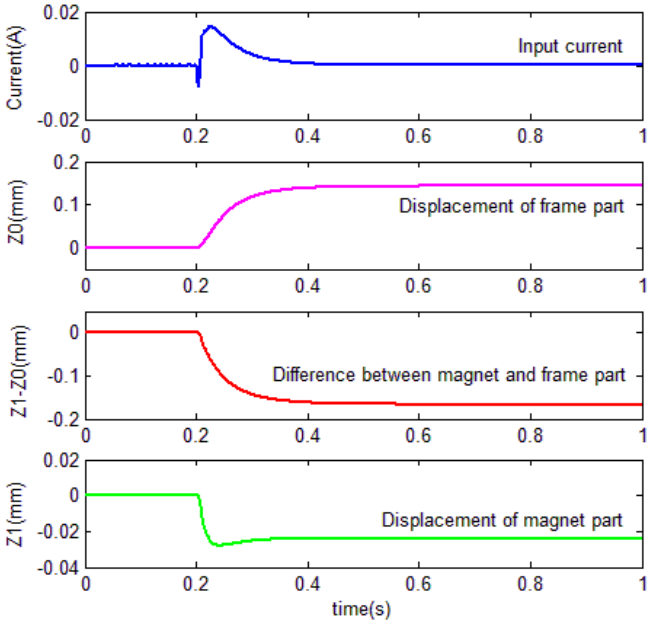

Fig.2.10 Simulation results in Case 3

The results of the simulation in Case 3 are shown in Fig.2.10. In this figure, the spring constant and all the feedback gains are same to Fig.2.9, except for the gain of the current integral feedback loop. The gain k_i is 35 in the simulation of Case 3. The comparison between Fig.2.9 and Fig.2.10 suggests that, even though the same gains was used in these two

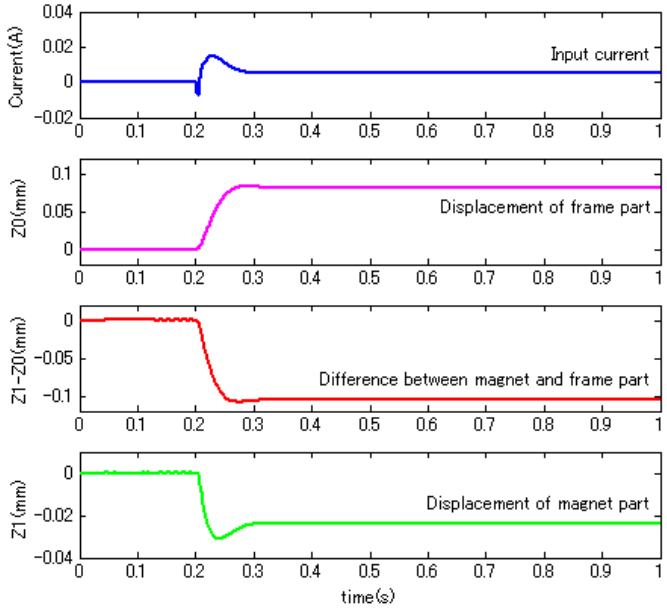

Fig.2.11 Simulation results in Case 4

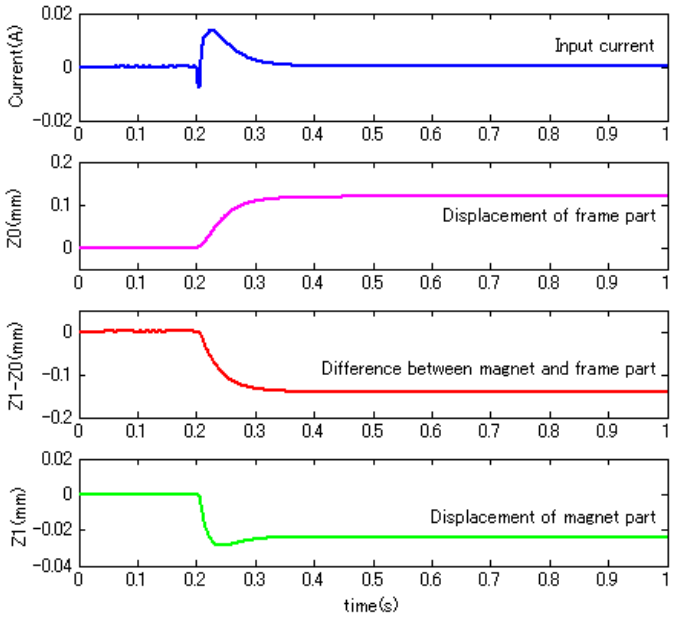

Fig.2.12 Simulation results in Case 5

simulations, the time of reaching balance state is different, and the time in Fig.2.10 is longer than in Fig.2.9. However, the VCM input current converges to zero in the stable state in Fig.2.10. That means, in this simulation with spring and with zero power control, the VCM consumes no energy, and the spring force counterbalances all the gravitational force of the frame part in the equilibrium state. Moreover, since only the spring force supports the gravitational force of the frame part, the changing distance between the permanent magnet part and the frame part is larger than Case 2.

The results of the simulation in Case 4 are shown in Fig.2.11. In this simulation, the spring constant is 700 N/m, which is stronger than the spring constant in Case 2 and 3. In Fig.2.11, the changing value of current is smaller than the result in Fig.2.10. Since the strong spring can generate a larger force than the weak spring with the same changing distance, the VCM may generate a smaller force in this case than in Case 2.

The results of the simulation in Case 5 are shown in Fig.2.12. In this simulation, the gain k_i is 25, which is smaller than Case 3. However, because of the big spring constant, the transient time is shorter, and the changing distance of the frame part and the difference between the

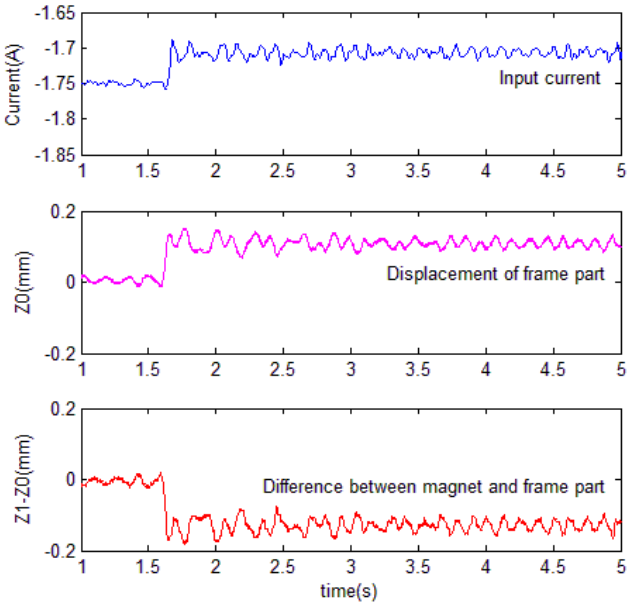

Fig.2.13 Experimental results in Case 1

magnet part and the frame part are smaller than Case 3.

Moreover, in the simulation results of all cases, because the decreased weights are equal, the changing distances between the magnet and the ceiling are same. All numerical simulation results imply that zero power control used a spring and an integral current feedback loop is feasible in this permanent magnet suspending system.

2.7 Experimental Results

Furthermore, the noncontact suspension experiments have been implemented with the prototype shown in Fig.2.3 that is a suspension photograph. The experiments were carried out in the same conditions and feedback gains with the numerical simulations. The experimental results are shown in Fig.2.13 ~ Fig.2.17. In these results, the responses of the suspension system were investigated with a step disturbance of cutting off 10 grams weight from the frame part. The weight was cut off at the time between 1.5 seconds and 2 seconds, and the

responses were recorded from 1 second to 5 seconds. All the current results in figures were passed through the low pass filters.

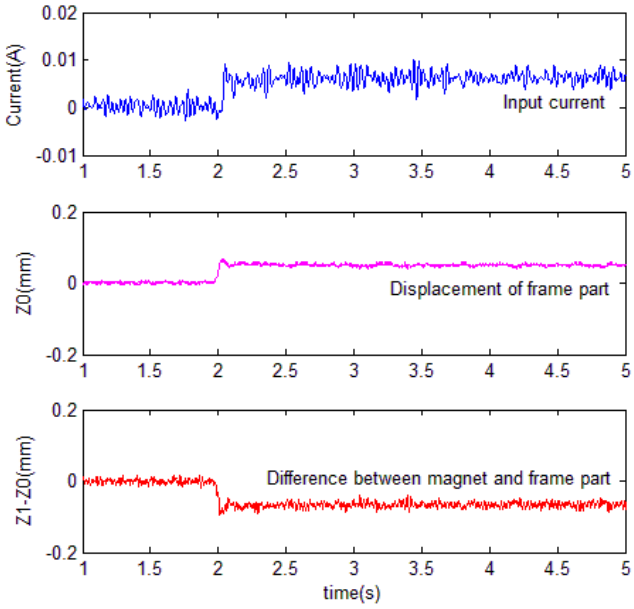

Fig.2.14 Experimental results in Case 2

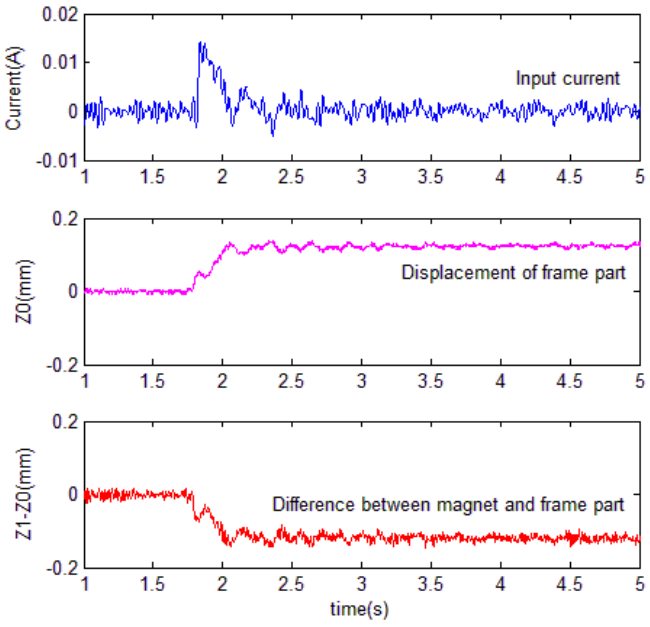

Fig.2.15 Experimental results in Case 3

The results of the experiment in Case 1 are shown in Fig.2.13. This experiment was carried out in the same conditions and using the same feedback gains with the simulation in Case 1. The results indicate that, when the suspension device suspends stably, the device is not resting at the equilibrium position, but it is vibrating around the equilibrium position. After cutting off the weight and reaching the stable suspension state, the input current decreases 0.05 (A)

because of the cutting weight. However, this current value is bigger than the simulation result. It may be caused by the deformation of the VCM core.

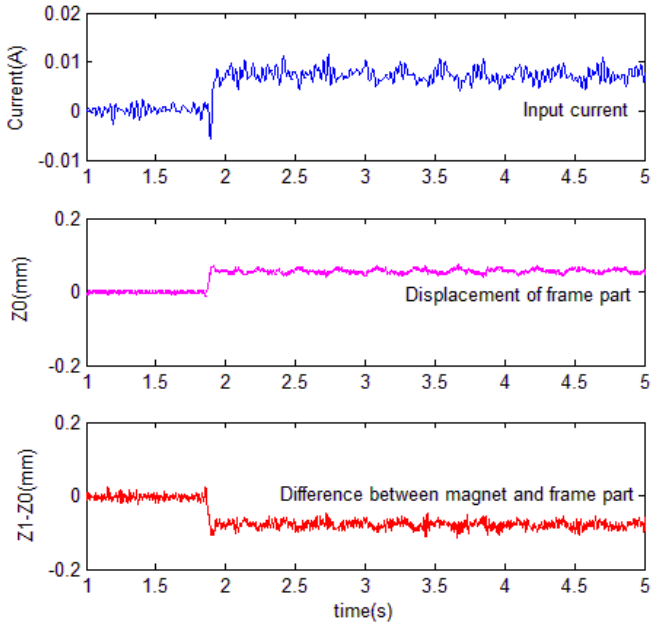

Fig.2.16 Experimental results in Case 4

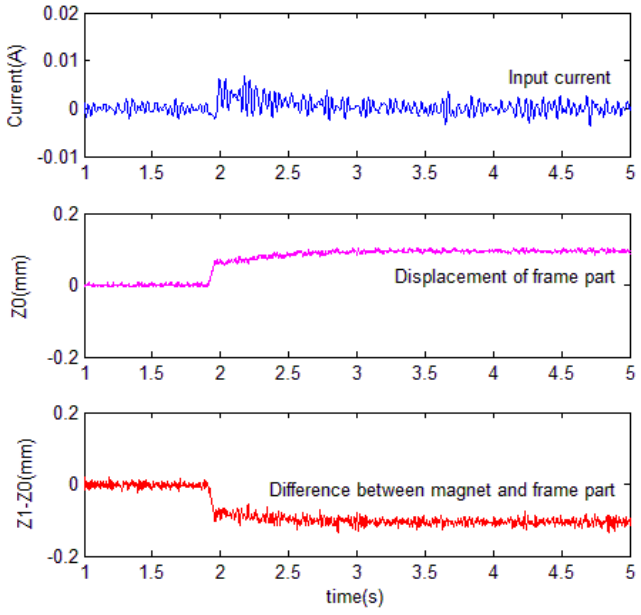

Fig.2.17 Experimental results in Case 5

Fig.2.14 and Fig.2.15 show the results of the experiments in Case 2 and Case 3. From the current graph in Fig.2.14, after cutting off the weight, the current value is just approximate 0.006 (A) in the stable state. Which is much smaller than the current in Case 1. The reason is that the resultant force of the VCM and the spring si supporting the gravitational force of the

frame part. In Fig.2.15, however, the current is converging to zero, and the variation values of the displacement of frame part and the difference between magnet and frame part are greater than them in Fig.2.14. The current integral feedback loop arouses all variations between Fig.2.14 and Fig.2.15. The integral loop decreases the VCM input current converging to zero, and then the VCM generates no force, so all gravitational force of the frame part maintains by the spring. Therefore, the spring length becomes short, and the changing length equals the value of the difference between the magnet and frame part. However, the integral loop is not able to affect the air gap between the magnet and the ceiling, so the increasing displacement of the frame part is larger than in Fig.2.14.

Moreover, the experiments were also investigated in Case 4 and Case 5 using different springs and different gain of k_i. The results are shown in Fig.2.16 and Fig.2.17. The experiment in Case 4 was carried out using the same feedback gains and same conditions with Case 2, except the spring. The spring constant is 700 N/m in Case 4. The differences of the experiments between Case 3 and Case 5 are the spring constant and the gain of the current integral feedback loop. The gain of k_i in Case 3 was 35, but it was 25 in Case 5. Because different springs require different gains, and stronger springs require smaller gains. Comparing Fig.2.16 and Fig.2.17 with Fig.2.14 and Fig.2.15, there is a little difference. The changing displacement of the frame part and the variation between the magnet part and the frame part become small, because a stronger spring can generate the same propulsion force by a small variation length.

2.8 Conclusions

This chapter proposed a hanging type magnetic suspension system using a permanent magnet and the VCM. In order to reduce the power consumption of the system in the stable suspension state, a kind of zero power control method was proposed for this hanging type magnetic suspension system using a spring and an integral feedback loop of current.

According to the suspension principle, an experimental prototype was set up. A mathematical model was created. The suspension feasibility of the system was examined theoretically. The realization of zero power control was analyzed in device, mathematical model, and control system. The numerical simulations and experiments were carried out in five cases. All the simulation and experimental results indicate that this hanging type magnetic suspension system can be suspended stably. Moreover, comparing the results in the five cases, the validity of the zero power control was examined.

Moreover, the miniature transmission device and the conveyance vehicle applied in constant temperature plant can be developed using this kind of hanging type magnetic suspension system, and the zero power suspension can also be realized in the development device using the zero power control method.

Chapter 3 Zero Power Non-Contact Suspension System with Permanent Magnet Motion Feedback

3.1 Introduction

Magnetic suspension systems have been extensively studied and have found numerous applications. Most magnetic suspension systems are electromagnetic suspension systems (EMS systems) that utilize electromagnets. Morishita and Azukizawa have proposed a zero power control method for EMS systems with the aim of reducing steady state energy consumption [53], which is introduced in the last chapter. Moreover, Misuno et al. have proposed a transfer-function approach to analyze and design the zero power controllers for magnetic suspension system [61]. This zero power control method for EMS systems has been adopted by many researchers and used in various magnetic suspension systems, which are not applied as the transmission devices. Misuno et al. have developed a vibration isolation system using this zero power magnetic suspension system that behaves as a spring capable of infinite negative stiffness [62][63]. Ishino et al. have presented a method of increasing the load capacity of the magnetic suspension system with this zero power control method [64]. Kim et al. have presented a zero power control scheme using an extended Luenberger observer, taking into consideration nonlinear gap and current characteristics to improve the magnetic levitation performance [65]. Myounggyu et al. have proposed a virtual zero power (VZP) controller consisting of a standard linear-quadratic (LQ) regulator and a Kalman filter [66]. The controller is used in an axial bearing in a pediaflow ventricular assist device. The Kalman filter estimates both the equilibrium position to which the feedback controller drives the system, and the covariance of sensor noise and axial disturbance forces on the rotor, which is used to select LQ regulator optimal gains. In this way, the controller can bring the actuator force to zero.

Recently, some researchers have proposed some zero-power magnetic suspension systems with permanent magnets for manipulation devices. Misuno et al. have proposed a magnetic suspension system with a permanent magnet and three flux-path control modules consisting of a ferromagnetic plate, a voice coil motor (VCM), and a displacement sensor [57]. This system controls the attractive force of the magnet by changing the flux path with the flux-path

control modules. Ueno and Higuchi presented a zero-power magnetic levitation technique using a composite of magnetostrictive and piezoelectric materials [33][34]. That technique utilized the capacitive property of the piezoelectric materials so that no current flowed in static operation, to realize the zero power control at any reference gap or load. Finally, Oka et al. proposed a magnetic suspension system with a permanent magnet and a rotary actuator that drove the permanent magnet varying magnetic flux path [35]. The suspension force was controlled through the variable magnetic flux path. That system resulted in a zero attractive force, changed the polarity of stator poles, and realized zero power control in an equilibrium state.

So far, we have proposed several kinds of permanent magnetic suspension systems with permanent magnets and linear actuators [26]~[29], [35], [56]~[59]. In this chapter, a zero power control method is proposed in a magnetic suspension system for manipulation devices. This system consists of a permanent magnet, a VCM, and a suspended iron ball, and no electromagnet. As a result, there is no heat generation and it is easy to realize remote non-contact manipulation by using a long rod, and realize the miniature manipulation devices using in a narrow space. However, when this system suspends an object with non-contact, the actuator has to support all the weight of the moving part and the suspended object. Therefore, the energy consumption becomes a significant problem. In order to solve this problem, a zero power control method that is same with the method using in last chapter, is adopted to reduce the energy consumption. A spring is assembled in the device, and an integral feedback loop is used in the control system. Quasi-zero power is then consumed in the steady state.

In this chapter, first, the principle of the permanent magnetic suspension is explained. The realization of zero power control method is then analyzed in a prototype, through a model, and in the controller. Finally, some numerical simulation and experimental results are shown and discussed.

3.2 Principle of Magnetic Suspension

The principle of this levitation system is explained in terms of the suspension system scheme shown in Fig.3.1. The suspension system consists of an actuator, a permanent magnet, and a suspended object. The permanent magnet generates the suspension force, the actuator drives the magnet keeping the suspension stable, and the suspended object is a ferromagnetic body. When the object is suspended with non-contact in a steady state, the relationship between attractive force and gravitational force is as shown in Fig.3.2. The levitation direction is vertical, and in the equilibrium position, the magnet's attractive force is equal to the gravitational force of the suspended object. Then, based on the principle that the magnetic force is inversely proportional to the square of the gap between the magnet and the ferromagnetic body, the actuator controls the air gap between the magnet and the object so as

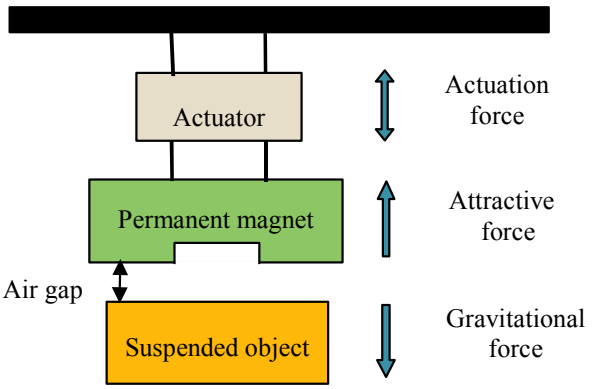

Fog.3.1 A suspension system scheme

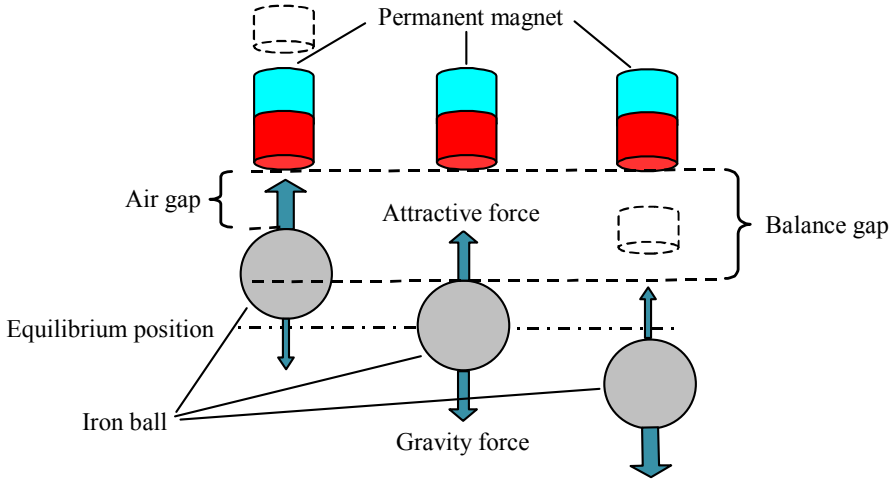

Fig.3.2 Relationship between attractive force and gravitational force

to adjust the attractive force. When the air gap is smaller than the balance gap, the actuator raises the magnet to increase the air gap; when the air gap is larger than the balance gap, the actuator lowers the magnet to decrease the air gap. In this way, the suspended object is levitated steadily without contact.

3.3 Realization of Zero Power Control

3.3.1 Zero Power Control in Experimental Prototype

A photograph of the prototype of the permanent magnetic suspension device is shown in Fig.3.3. Fig.3.4 shows the configuration of this magnetic suspension system. The prototype

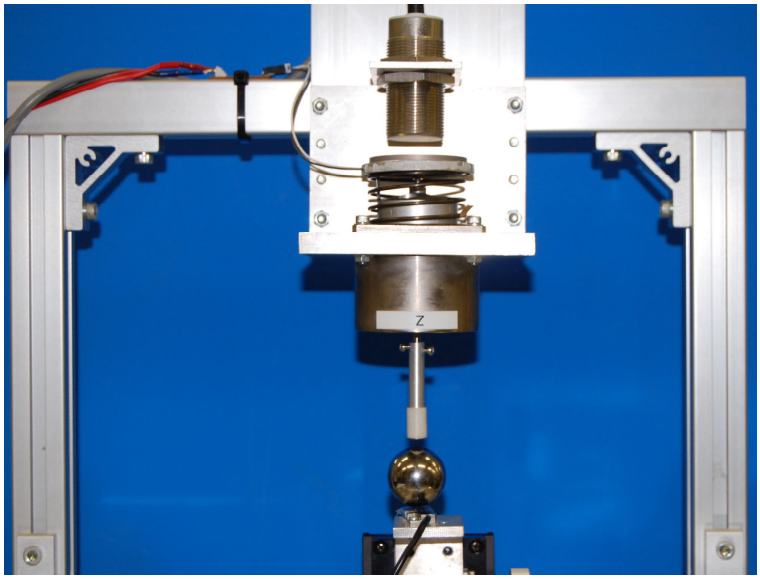

Fig.3.3 Photograph of experimental prototype

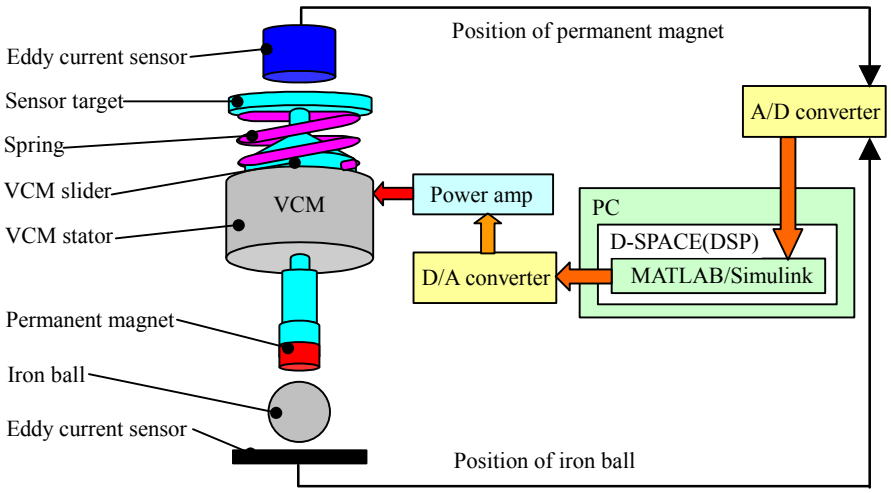

Fig.3.4 Configuration of magnetic suspension system

principally consists of a permanent magnet, a VCM, a spring, and two eddy current displacement sensors. The whole device has three parts: the suspended object is an iron ball whose diameter is 30 mm; the moving part consists of a permanent magnet, a slider of VCM, and a sensor target; and the base part consists of the VCM stator, two sensors, and the frame. The weight of the iron ball is 0.1098 kg, and that of the moving part is 0.1478 kg. The VCM used in this magnetic suspension prototype has a driving length of 15 mm and a maximum generating force of 20 N at a coil current of 2 A. The VCM is the only active driving element that is used to control the device suspension stably in the equilibrium. The two sensors are eddy current displacement sensors. The upper sensor measures the permanent magnet's

position and has a resolution of 0.02 mm and a measurement range of 10 mm. The lower

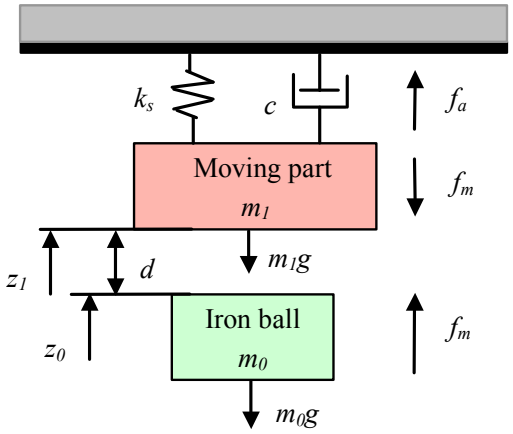

Fig.3.5 Model of suspension system

sensor measures the iron ball's position and has a resolution of 0.001mm and a measurement range of 4 mm.

As shown in Fig.3.4, in order to obtain the zero power control, a spring is installed between the VCM stator and the sensor target in the device. When the iron ball is steadily suspended, the gravitational force of the moving part and the iron ball must be transmitted to the base part. If there is no spring in the device, the force must be transmitted through the VCM, which means that the VCM normal force equals the gravitational force of the moving part and the iron ball. However, if there is a spring in the device, the spring's force can counterbalance the gravitational force acting on the moving part and the iron ball in the balanced state, and the VCM force can reach zero.

The controller of this suspension system is a DSP controller, as shown in Fig.3.4. Signals from two sensors are input to the DSP controller through 12-bit A/D converters. Based on these signals, appropriate current values are computed by the controller. The current values are converted to analog current by D/A converters, and then amplified by a current amplifier. The final actual current controls the VCM to steadily maintain suspension of the ball.

3.3.2 Zero Power Control in Model

A model of this permanent magnetic suspension system as shown in Fig.3.5 has been set up for feasibility studies, stability confirmations, numerical simulations, and feedback gains calculations. According to the model, the equations of motion for the moving part and the suspended object are, respectively,

$$m_0\ddot{z}_0 = f_m - m_0 g \tag{3.1}$$

$$m_1\ddot{z}_1 = -c\dot{z}_1 - k_s z_1 + f_a - f_m - m_1 g \tag{3.2}$$

In these equations, m_0, m_1 are the mass of the iron ball and the moving part; z_0, z_1, whose positive directions are upward, are the displacements of the iron ball and the moving part; f_a is the generating force of VCM; fm is the attractive force of the permanent magnet; k_s is the spring constant; and c is the damping coefficient including spring fading characteristics, VCM bearings frictions, and air viscosities.

Additionally, the relationship between the input current and the VCM generating force is represented by the equation

$$f_a = k_t i \tag{3.3}$$

where k_t is the VCM propulsive coefficient and i is the VCM input current.

The relationship between the permanent magnet attractive force and the air gap distance is described by

$$f_m = \frac{k_m}{d^2} \tag{3.4}$$

Where k_m is the coefficient of magnetic attractive forces and d is the air gap distance between the permanent magnet and the iron ball.

According to Equation (3.1) and (3.2), when the iron ball is suspended in a static state, the differential terms become zero, i.e., the acceleration terms and the damping force become zero. If there is no spring in the device, the spring force is zero. Consequently, in order to maintain the balance, the VCM force has to equal the gravitational force of the moving part and the iron ball. During this time, the VCM current can never be zero. However, if there is a spring in the device, the spring force and the VCM force together afford the gravitational force acting on the moving part and the iron ball. Therefore, the VCM current can become zero in the static state. This means that the zero power control is mathematically feasible.

3.3.3 Zero Power Control in Controller

There are many ways to realize zero power control in the magnetic suspension system controller, such as using an observer, a current integral feedback, or object weight estimation. In this chapter, the current integral feedback method is investigated.

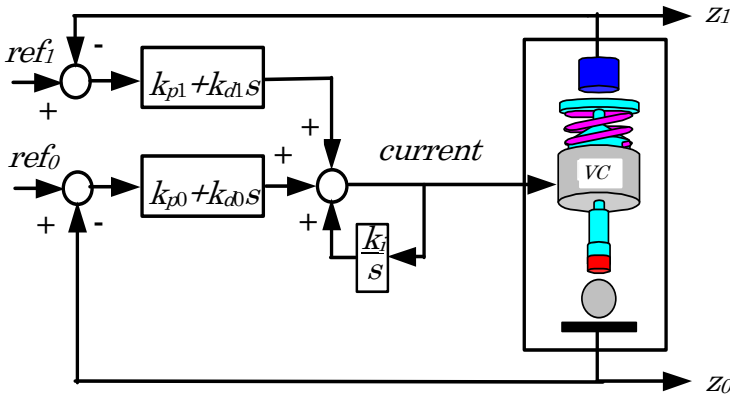

Fig.3.6 Block diagram of control system

As shown in Fig.3.6, the block diagram is the controller of the permanent magnetic suspension system, having an integral current feedback loop for zero power control. There are two large PD feedback loops. The lower PD feedback loop measures the position of the iron ball. The upper PD feedback loop observes the position of the permanent magnet. Both PD feedback loops calculate the current values based on the sensors' signals in order to make the VCM robustly maintain the system levitation. In addition to the two large PD feedback loops, a local current integral feedback loop is used before the levitated object block to implement zero power control. When current flows through the VCM circuit, this integral feedback loop reduces the current. The current reduction diminishes the generating force of the VCM, and the resulting variation causes the spring length and the generating force to change. Finally, when the spring force equals the gravitational force of the moving part and the iron ball, the VCM current reaches zero. Furthermore, the k_i value for the gain of the integral current feedback loop influences the speed of current variation. If the value is large, the current reaches zero quickly. However, that works against system stability. Rapid current variation will result in system instability. Therefore, a proper k_i value is very important for system stability.

3.4 Feasibility Analysis of Suspension

The attractive force of permanent magnet f_m is represented as a nonlinear function of the length of the air gap becomes larger as the air gap decreases. By linearization of this function around the equilibrium position, we obtain

$$f_m = f_{m0} + \Delta f_m = \frac{k_m}{d_0^2} - \frac{2k_m}{d_0^3}\Delta d \tag{3.5}$$

$$\Delta f_m = -\frac{2k_m}{d_0^3}\Delta d \tag{3.6}$$

In this model, we can conclude following equations around the equilibrium position:

$$\Delta d = z_0 - z_1 \tag{3.7}$$

Then

$$\Delta f_m = \frac{2k_m}{d_0^3}(z_1 - z_0) \tag{3.8}$$

Then the equations can be translated to followings at the equilibrium position:

$$\ddot{z}_0 = \frac{2k_m}{m_0 d_0^3}(z_1 - z_0) \tag{3.9}$$

$$\ddot{z}_1 = -\frac{c}{m_1}\dot{z}_1 - \frac{k_s}{m_1}z_1 - \frac{2k_m}{m_1 d_0^3}(z_1 - z_0) + \frac{k_t}{m_1}i \tag{3.10}$$

We can set the state variables as:

$$x = \begin{bmatrix} \Delta z_0 \\ \Delta \dot{z}_0 \\ \Delta z_1 \\ \Delta \dot{z}_1 \end{bmatrix} \tag{3.11}$$

Then the state space equation and the output equation are:

$$\dot{x} = Ax + Bu \tag{3.12}$$

$$y = Cx \tag{3.13}$$

Where,

$$A = \begin{bmatrix} 0 & 1 & 0 & 0 \\ -\frac{2k_m}{m_0 d_0^3} & 0 & \frac{2k_m}{m_0 d_0^3} & 0 \\ 0 & 0 & 0 & 1 \\ \frac{2k_m}{m_1 d_0^3} & 0 & -\frac{\left(k_s + \frac{2k_m}{d_0^3}\right)}{m_1} & -\frac{c}{m_1} \end{bmatrix}$$

$$B = \begin{bmatrix} 0 \\ 0 \\ 0 \\ \frac{k_t}{m_1} \end{bmatrix}$$

$$C = \begin{bmatrix} 1 & 0 & 0 & 0 \end{bmatrix}$$

The controllability matrix of the system is:

$$P_c = \begin{bmatrix} B & AB & A^2B & A^3B \end{bmatrix} \tag{3.14}$$

$$\det(P_c) = \frac{4k_m^2 k_t^4}{d_0^6 m_0^2 m_1^4} \tag{3.15}$$

Therefore,

$$Rank(P_c) = 4 \tag{3.16}$$

The controllability matrix of the system is full rank, so the system is controllable.
The observability matrix of the system is:

$$Q = \begin{bmatrix} C \\ CA \\ CA^2 \\ CA^3 \end{bmatrix} \tag{3.17}$$

$$\det(Q) = \frac{4k_m^2}{d_0^6 m_0^2} \tag{3.18}$$

$$Rank(Q) = 4 \tag{3.19}$$

The observability matrix of the system is full rank, so the system is observable.

3.5 Numerical Simulation

According to the mathematical model of Equation (3.12) and (3.13), first, the feedback gains were calculated using the LQR (linear quadratic regulator) full state feedback control law. Second, the numerical simulation was carried out with a nonlinear attractive force.

Table 3.1 Parameters using in numerical simulation

Parameter	Value	Parameter	Value
m_0 (kg)	0.1098	c (N/(m/s))	0
m_1 (kg)	0. 1478	k_m (Nm^2)	3. 758×10^{-6}
d_0 (mm)	1.85	k_t (N/A)	10
g (m/s^2)	9.8	k_s (N/m)	400

3.5.1 Simulation Conditions

In this feasibility study, numerical simulations were carried out with a nonlinear attractive force. The simulations were examined in same 5 cases, which are:

- Case 1: the magnetic suspension system without spring and without zero power control.
- Case 2: the magnetic suspension system with spring (400 N/m) and without zero power control.
- Case 3: the magnetic suspension system with spring (400 N/m) and with zero power control.
- Case 4: the magnetic suspension system with spring (300 N/m) and without zero power control.

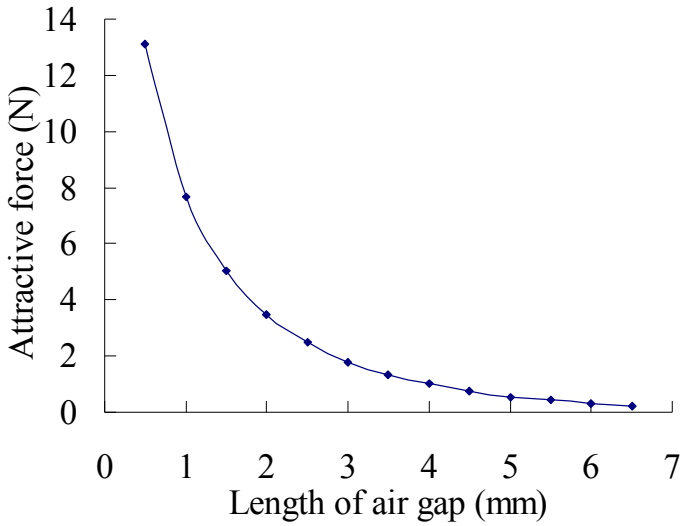

Fig.3.7 The attractive force characteristic of the permanent magnet

- Case 5: the magnetic suspension system with spring (300 N/m) and with zero power control.

3.5.2 Calculation of Feedback Gains

All the parameters using in the numerical simulation are shown in Table.3.1, which are measured from the experimental prototype. Moreover, the value of k_m is measured from Fig.3.7, which is the measured attractive force of the using permanent magnet when the length of air gap is changing.

Many methods can design the controller for a linear system. In terms of linear control theory, due to this proposed system is controllable and observable, the LQR can be used to get the feedback gains. Based on the characteristics of the system, we chose the state weighting matrix Q and input weighting matrix R as following:

$$Q = \begin{bmatrix} 1 & 0 & 0 & 0 \\ 0 & 1 & 0 & 0 \\ 0 & 0 & 1 & 0 \\ 0 & 0 & 0 & 1 \end{bmatrix} \tag{3.22}$$

$$R = 1 \tag{3.23}$$

Using MATLAB software and considering the conditions of the device with spring and without spring, the feedback gains K_1 (without spring) and K_2 (with spring) are calculated as following:

$$K_1 = \begin{bmatrix} -748 & -6.4 & 742 & 4.9 \end{bmatrix} \tag{3.24}$$

$$K_2 = \begin{bmatrix} -830 & -6.8 & 750 & 4.8 \end{bmatrix} \tag{3.25}$$

3.5.3 Simulation Results

Using the mathematical model and the calculated feedback gains, the simulations were carried out. When the iron ball was levitated, a –0.05 mm step value was added to the iron ball. After the step was added, the VCM current, the iron ball displacements, and the moving part displacements were recorded. The step was added at 1.5 seconds, and the responses were recorded until 5 seconds. The varieties of current and displacement were plotted, with the upward direction as positive.

The results of simulation in Case 1 are shown in Fig.3.8. The upper plot shows the VCM current response, the middle one indicates the iron ball displacement, and the lower one shows the moving part displacement. When the iron ball was levitated in a stable condition, before adding the step, the current was approximately –0.258 A, which was used to generate the force counterbalancing the gravitational force on the moving part and the iron ball. The negative current caused the VCM to generate an upward force. When the step was added, the iron ball moved downward as shown in the middle graph, the air gap length between the magnet and the iron ball increased, and the attractive force of the magnet decreased. In order to make the levitation return to equilibrium, the actuator drove the magnet lower to reduce the

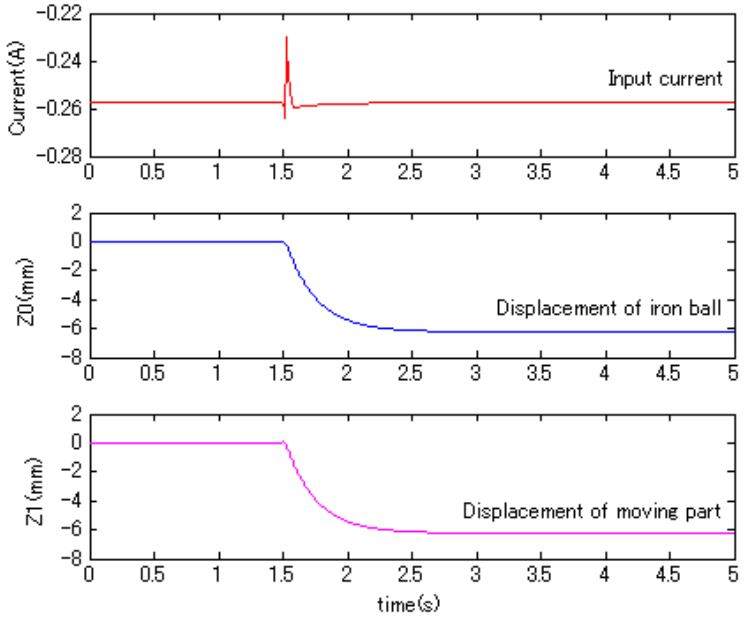

Fig.3.8 Simulation results in Case 1

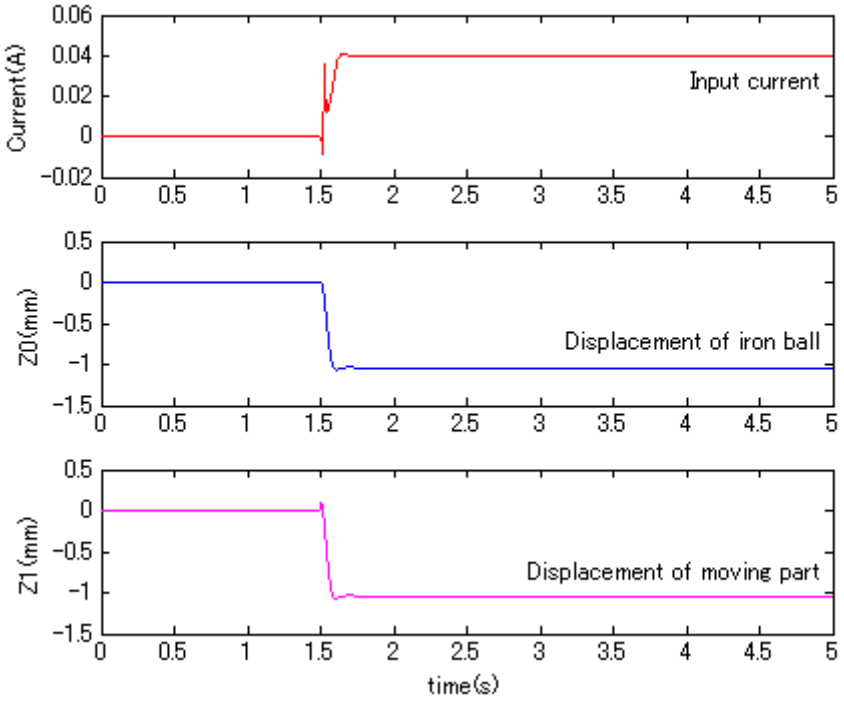

Fig.3.9 Simulation results in Case 2

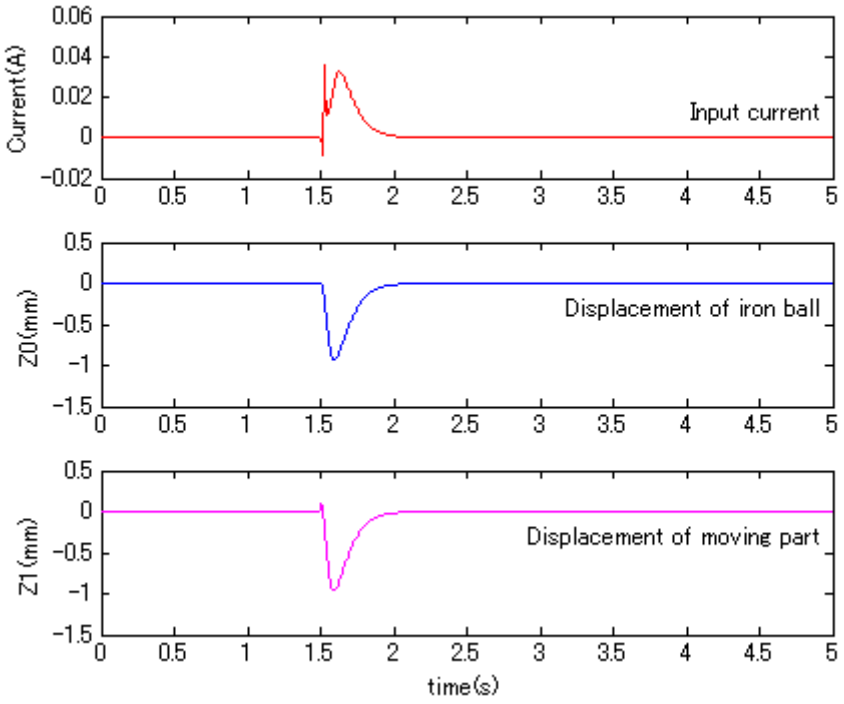

Fig.3.10 Simulation results in Case 3

air gap between the magnet and the iron ball, and then the attractive force increased until it was equal to the gravitational force. Thereafter, the levitation reached the balanced state again. Moreover, the VCM current after equilibrating was the same as that in the original

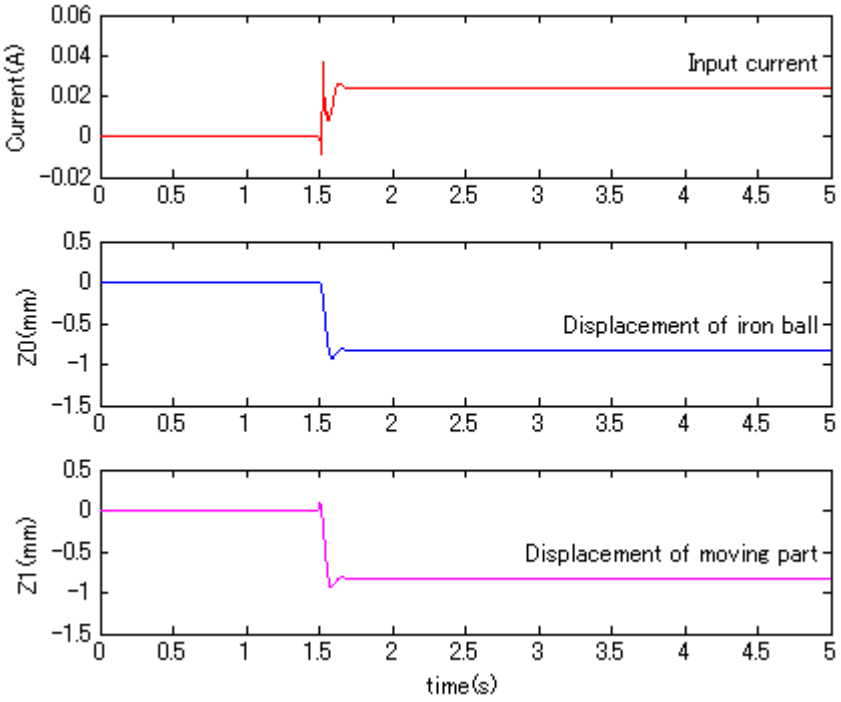

Fig.3.11 Simulation results in Case 4

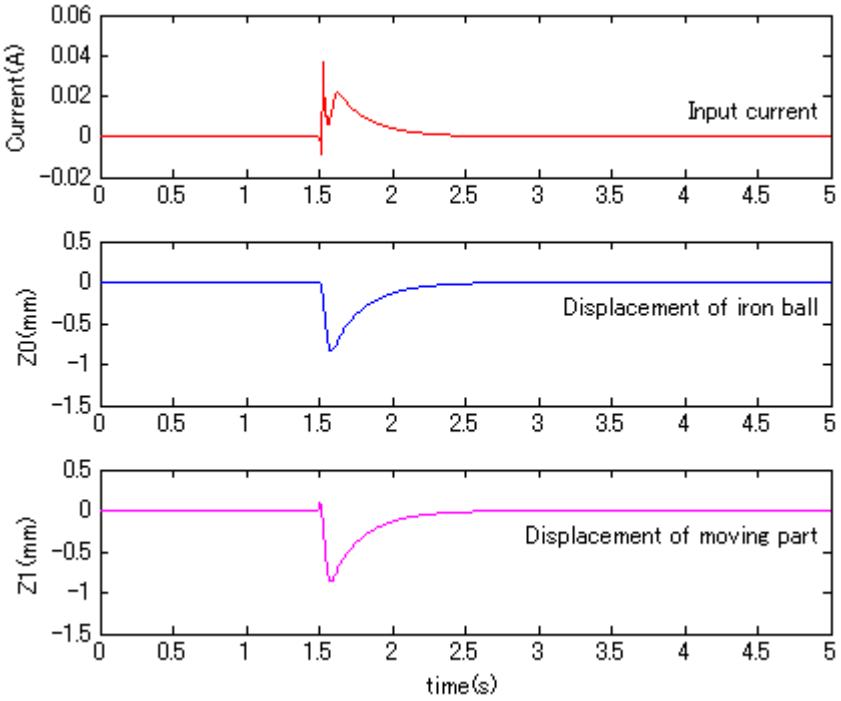

Fig.3.12 Simulation results in Case 5

equilibrium state since the generating force did not change.

The results of the simulation in Case 2 are shown in Fig.3.9. In this simulation, the spring constant used was 400 N/m. After adding the step, the current value was approximately 0.04

A, which generated a downward force to counterbalance the spring force. The value was smaller than that shown in Fig. 5. In that moment, the spring force was equal to the summations of the VCM force and the gravitational forces of the iron ball and the moving part. In the changing progress, there was a sharp variation in the current because the VCM responded to the step, and subsequently changed the variation resulting from the spring's actions.

The results of the simulation in Case 3 are shown in Fig.3.10. In this simulation, except for the current integral feedback loop, all of the conditions and feedback gains were the same as in the simulation shown in Fig.3.9. As shown in Fig.3.10, after adding the step and reaching the equilibrium state, the current and the displacements of the iron ball and the moving part returned to zero. This result indicates that in the simulation with spring and with zero power control, the VCM consumed no energy and the spring force counterbalanced all the gravitational forces in the equilibrium state.

The results of the simulation in Case 4 are shown in Fig.3.11. In this simulation, the spring constant used was 300 N/m. These results are similar with the results in Case 2. However, after adding the step, the current value is approximately 0.025 A, which is smaller than the current in Case 2. The reason is that weak spring needs a weak force to change the distance between the permanent magnet part and the frame part.

The results of the simulation in Case 5 are shown in Fig.3.12. In these results, the current also can be converged to zero and the displacements also can be returned back to the original position. However, the response time is longer in Case 5 than in Case 3, even the same current integral feedback gain is same.

All numerical simulation results imply that the zero power control using a spring and an integral current feedback loop is feasible in this suspension system with a permanent magnet motion feedback loop.

3.6 Experimental Results

Non-contact suspension experiments were also implemented using the experimental prototype shown in Fig.3.3. Fig.3.13 shows an iron ball levitating in a stable state. Experiments in same cases with the numerical simulations were completed. However, on account of the upper sensor in the experimental prototype having poor linearity, the feedback gains used in the experiments differed from those used in the simulations. Some experimental results are shown here, and all the current results in the figures were passed through low pass filters.

The results of the experiment in Case 1 are shown in Fig.3.14. From these results, it can be seen that when the iron ball was suspended in a stable state, the VCM current was approximately –0.26 A, which generated a force counterbalancing the gravitational force of

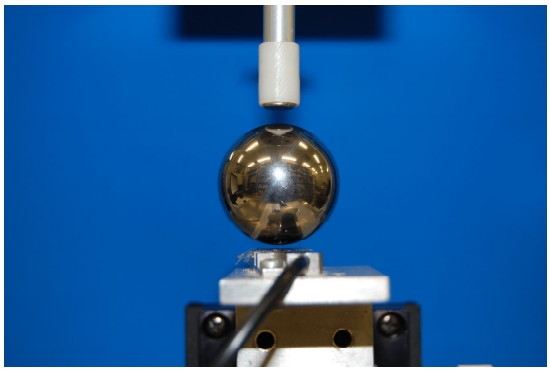

Fig. 3.13 Photograph of suspended iron ball

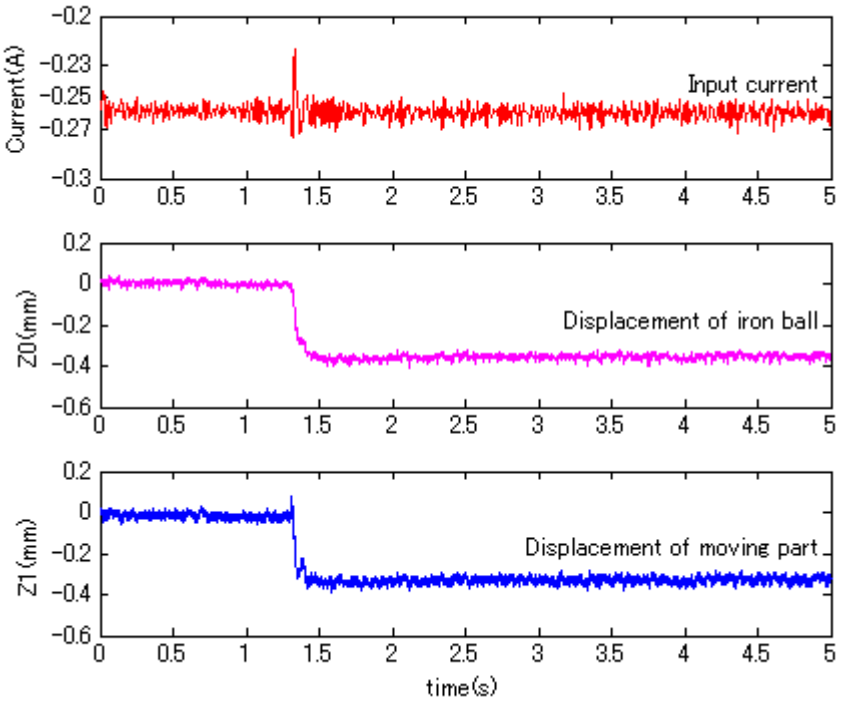

Fig.3.14 Experimental results in Case 1

the iron ball and the moving part. After adding the step value, the iron ball and the moving part moved downward together, and the current returned to the original value, in agreement with the simulation results. The step only changed the position of the iron ball but did not change the loads; therefore, the current did not change. Fig.3.14 indicates that the VCM current in the normal suspension state was approximately –0.26 A.

Fig.3.15 shows the experimental results in Case 2. The spring constant was 400 N/m. In the current graph in Fig.3.15, it can be seen that after adding the step, the current value was approximately 0.02 A in the stable state. This was much smaller than the current in Fig.3.14.

Fig.3.16 shows the experimental results in Case 3. As shown in Fig.3.16, the current and the displacements all converged to zero in the stable state. The current integral feedback loop caused all the variation. The integral loop reduced the VCM input current to zero, and then

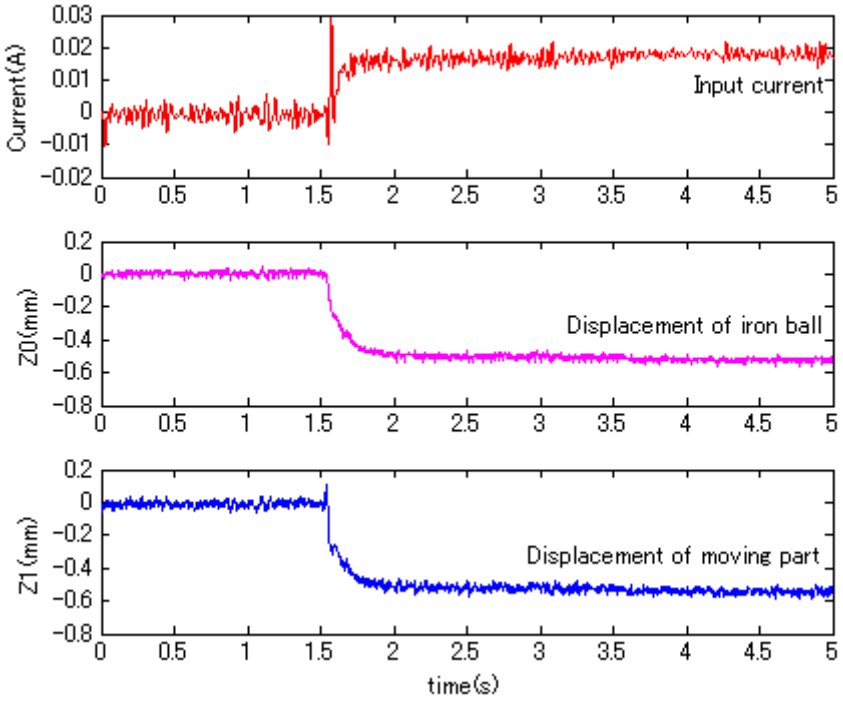

Fig. 3.15 Experimental results in Case 2

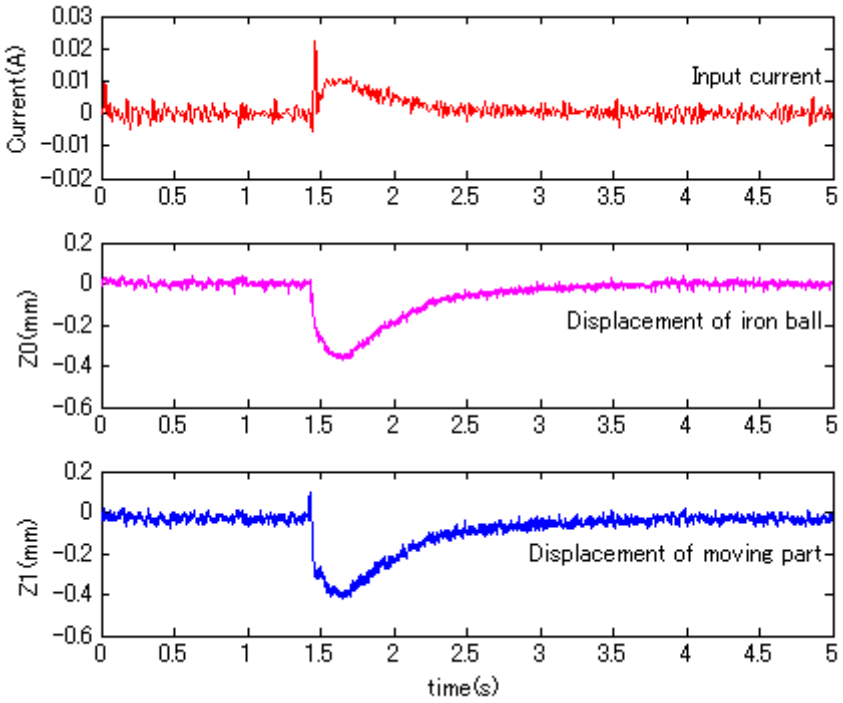

Fig.3.16 Experimental results in Case 3

the VCM generated no force. Therefore, the spring maintained all of the gravitational forces, and the iron ball and the moving part returned to their original positions.

Fig.3.17 and Fig.3.18 show the experimental results in Case 4 and 5, which used a different spring whose spring constant was 300 N/m. The experiments were carried out with the same

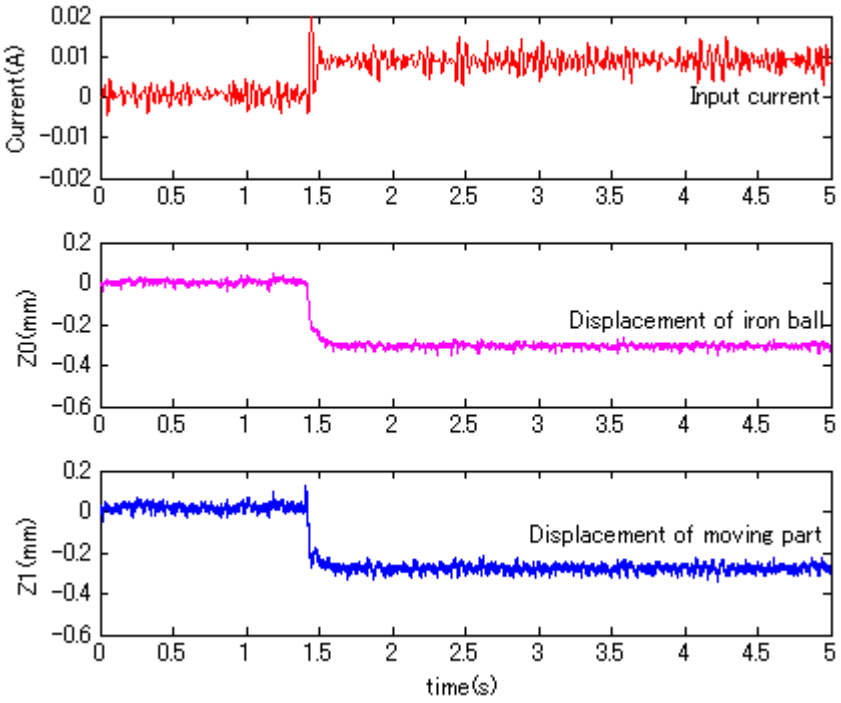

Fig. 3.17 Experimental results in Case 4

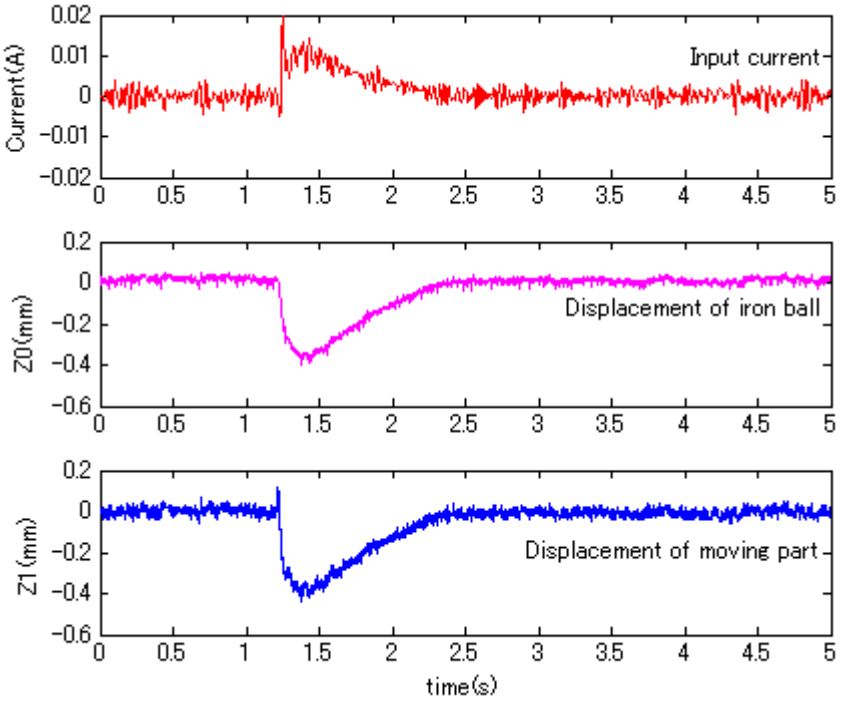

Fig.3.18 Experimental results in Case 5

feedback gains and conditions with Case 2 and 3. As shown in Fig.3.17, after adding the step, the current was approximately 0.01 A in the stable state, which was smaller than that in Fig.3.15. This was because weak springs require small forces to counterbalance. Moreover,

the current and displacements in Fig.3.18 converged to zero as well.

In conclusion, the experimental and simulation results are very similar, and they suggest that the zero power control can be successfully applied in this suspension system with a permanent magnet motion feedback loop.

3.7 Conclusions

A zero power control method was proposed in a permanent magnetic suspension system used as a noncontact manipulation device. Based on the analysis of the feasibilities of zero power control in an experimental prototype, in a model, and in a controller and on the results of the numerical simulations and experiments, the following conclusions can be drawn.

First, through the use of a digital controller with two PD feedback loops, the suspension system with the permanent magnet and linear actuator can be levitated steadily without contact.

Second, the zero power control method using a spring in suspension device and a current integral feedback loop in the controller can reduce energy consumption considerably in this suspension system with a permanent magnet motion feedback loop.

Third, this kind of zero-power magnetic suspension system can be used to develop a miniature noncontact manipulation device or a long distance noncontact manipulation mechanism.

Part II Noncontact Spinning Mechanism

Chapter 4 Development of a Noncontact Spinning Mechanism Using Rotary Permanent Magnets

4.1 Introduction

Currently, the developments in machinery are aimed at two goals: miniaturization and high precision. However, reducing the size of the machinery requires the parts to be small and easy to distort, and the high precision targets require clean assembly. Consequently, noncontact manipulation of machinery parts is desirable. Since magnetic force is strong, clean and fit for ferromagnetic materials, magnetic suspension is adequate for manipulating and spinning machinery parts without contact.

So far, many kinds of noncontact suspension systems and manipulation systems have been proposed using electromagnets and permanent magnets [9]. For noncontact manipulation systems, Oka et al. have proposed an active magnetic levitation system using a permanent magnet and a motion control mechanism [24]. In this system, noncontact levitation was realized by adjusting the magnetic force via the control of the air gap between the permanent magnet and the ferromagnetic suspended object. Cui et al. have proposed a 2D, noncontact manipulation system using permanent magnets and linear actuators with an air gap control method [27]. Nakamura et al. proposed a three-dimensional manipulation mechanism for manipulating a small permanent magnet [67]. Verma et al. have presented a novel electromagnetic actuation scheme for nanoscale positioning with a six-axis, magnetic-levitation stage [68]. For noncontact spinning system, many magnetic bearings and bearingless motors have been proposed [10]. Magnetic bearings support a rotor without physical contact, and a bearingless motor combines a rotary motor and an active magnetic bearing. Moreover, others have proposed noncontact spinning systems. Ikuta et al. have proposed a noncontact magnetic gear acting as a transmission mechanism to develop safe mechanisms for use in homes and hospitals [69]. Fujiwara et al. have developed a noncontact spinning mechanism using permanent magnets and linear actuators to magnetically suspend an object [58]. In this system, four magnets were sequentially driven in the horizontal plane toward the object, causing it to spin. This spin mechanism, however, pulsated the object vertically, and high rotation speeds could not be realized. It is hypothesized that this result is due to abrupt alterations in the flux distribution.

This chapter proposes a new type of noncontact spinning mechanism using disk magnets

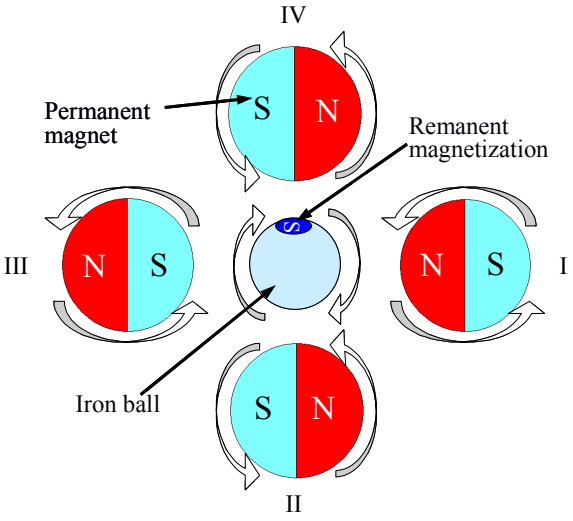

Fig.4.1 Principle of spinning system using rotational magmets

and rotary actuators in place of magnets and linear actuators. In this proposed noncontact spinning mechanism, the noncontact suspension of the suspended object is achieved using a permanent magnet and a VCM (Voice Coil Motor) with the air gap control method. The noncontact rotation in horizontal of the suspended object is not realized by exciting coils, but by the rotational, disk-type permanent magnets. Depending on the arrangement and number of magnets and the phases of their magnetic poles, this proposed noncontact spinning mechanism can realize a steady rotation state and fast rotation. In this paper, the spinning principle is explained, and the prototype of the proposed spinning system is introduced. Next, spinning experiments were performed, and the rotational torque of the spinning object was calculated using mathematical models and IEM analysis. Finally, some results are shown and discussed.

4.2 Noncontact Spinning Principle

The principle of the spinning system is shown in Fig.4.1. The figure is a plane view from the top of the device. An iron ball, the spun object, is located in the center of the four disk magnets. The iron ball is suspended in the vertical direction by a permanent magnetic suspension system. The four disk magnets are arranged around the levitated ball and in the same horizontal plane as the ball. Each magnet has two magnetic poles in the radial direction. The magnetic poles of the four disk magnets are arranged in a parallel configuration and invert between two adjacent magnets. All of the disk magnets rotate at the same speed and in the same direction.

The remanent magnetization on the surface of the iron ball is used for spin control. The iron ball has various remanent magnetizations. The strongest magnetization determines which

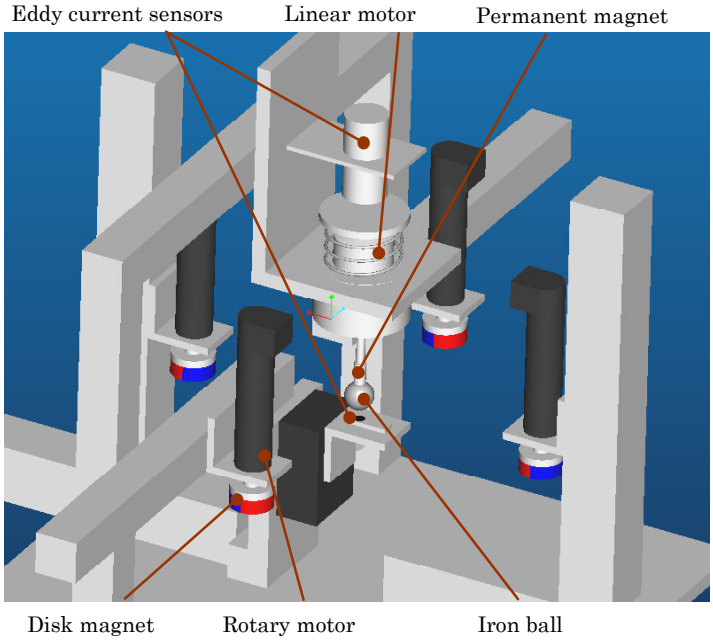

Fig.4.2 Configuration of the spinning system

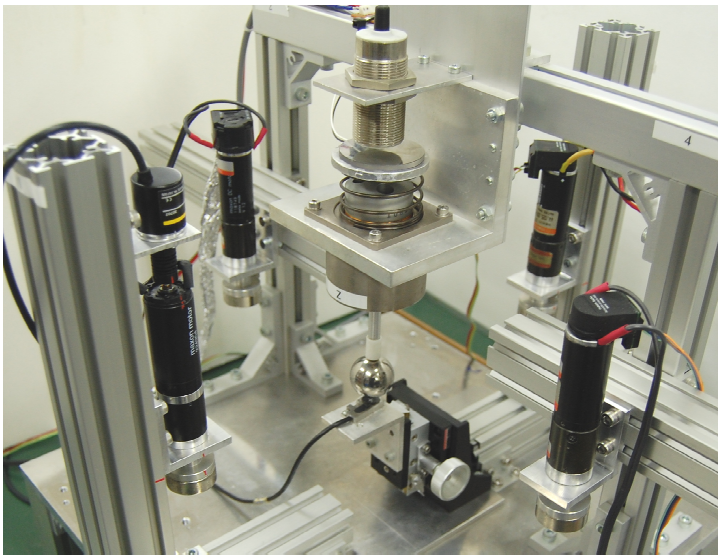

Fig.4.3 Photograph of spinning system

will be the upper side of the ball during suspension. The next strongest remanent magnetization in the horizontal plane, indicated in Fig.4.1, causes the ball to rotate about the vertical axis due to its attraction to the four disk magnets. We assumed the remanent magnetization is S. In the situation shown in Figure 1, the remanent magnetization is attracted by disk magnet I, and the ball will rotate to face disk magnet I. At the same time, the four magnets also rotate. Consequently, when the remanent magnetization faces magnet I, the iron ball has rotated 90 degrees, and the four magnets have rotated 90 degrees as well. At this point, the remanent magnetization will then be attracted to magnet II. Theoretically,

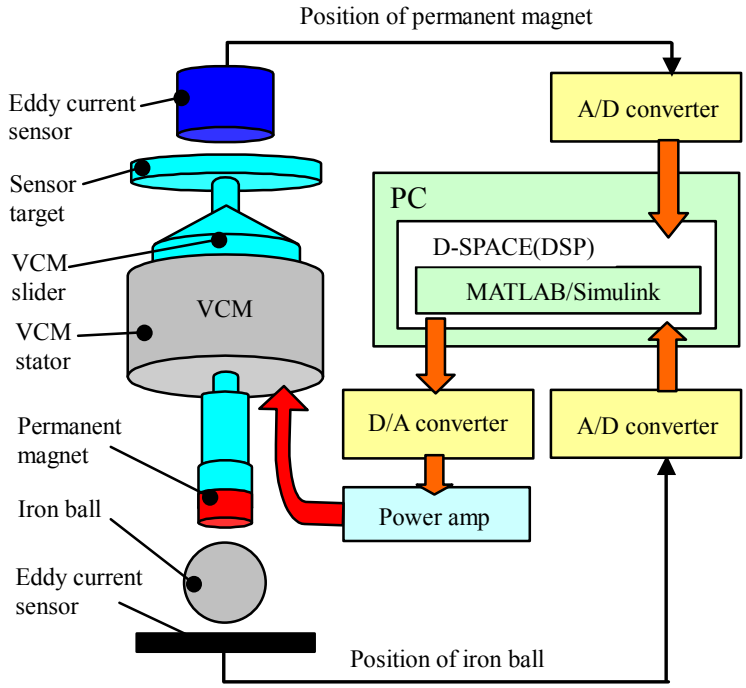

Fig.4.4 Schematic draw of magnetic suspension system

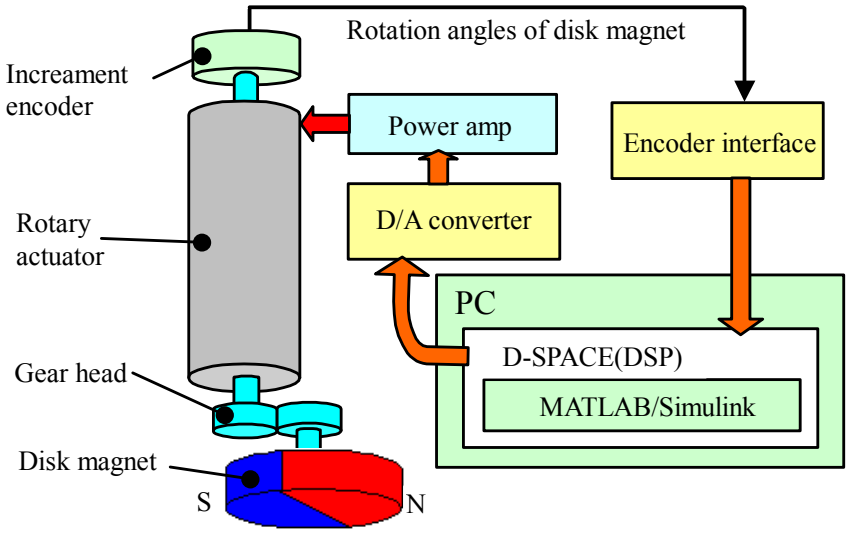

Fig.4.5 Schematic draw of spinning system

repetitions of this rotation cycle can cause the iron ball to spin in the reverse rotational direction at the same rotational speed as the rotational disk magnets.

4.3 Noncontact Spinning System

Fig.4.2 shows the configuration of the noncontact spinning system, and Fig.4.3 shows a photograph of the prototype. The mechanism has two parts: a suspension part and a spinning

part. The suspension part consists of a permanent magnet, a voice coil motor and two eddy current sensors, and the spinning part consists of four disk-type permanent magnets and four rotary motors that include reduction mechanisms and encoders.

4.3.1 Suspension Part

In the suspension part shown in Fig.4.4, the suspended object was an iron ball with a diameter of 30 mm and a mass of 0.1098 kg. A cylindrical permanent magnet with a diameter of 8 mm and length of 8 mm was attached to the lower top of the slider of the VCM, and a sensor target was installed on the upper top of the slider. The permanent magnet and the sensor target moved with the slider together. The upper sensor measured the magnet position through the sensor target with a resolution of 0.02 mm and a measurement range of 10 mm. The lower sensor measured the position of the iron ball with a resolution of 0.001 mm and a measurement range of 4 mm. The VCM used in this magnetic suspension prototype has a driving length of 15 mm and a maximum generating force of 20 N at a coil current of 2 A.

As shown in Fig.4.4, a DSP controller (DSPACE1104) and the PID control method were used in the control system of the suspension system. Based on the feedback position signals of the iron ball and the permanent magnet, the control system controlled the suspended object to maintain stable levitation.

4.3.2 Spinning Part

In the spinning part, four disk-type permanent magnets were installed on the rotary motor's shafts. As shown in Fig.4.3, the motors were installed on the rail-frames, which allowed the magnets' positions to be adjusted in the vertical and horizontal directions. The four magnets were placed in the same horizontal plane as the levitated ball and at the same distance from the suspended ball. The four disk-magnets were arranged as shown in Fig.4.1 and had been magnetized into two magnetic poles in their radial directions. Each disk magnet had a diameter of 30 mm and a thickness of 10 mm.

A schematic drawing of the control system of the one forth spinning part is shown in Fig.4.5. Based on the signals from the encoder, the DSP controller controlled the disk magnet rotation. Fig.4.6 shows the control diagram of the spinning system. In this system, the rotational angle of one of the magnets was used as a reference to control the other three magnets, and both the angle and speed were controlled. Consequently, the four magnets could maintain a phase relationship with each other, rotate at same speed and start and stop at the same time.

4.3.3 Characteristic Experiment

To examine the magnetic characteristics of the disk magnets and the influence of the distance between the magnet and the levitated ball, the magnetic flux density of the disk magnet was measured using a gauss-meter. While the magnet rotated, the flux density was recorded at distance of 20 mm, 30 mm, 50 mm, 70 mm and 100 mm. The measurement data

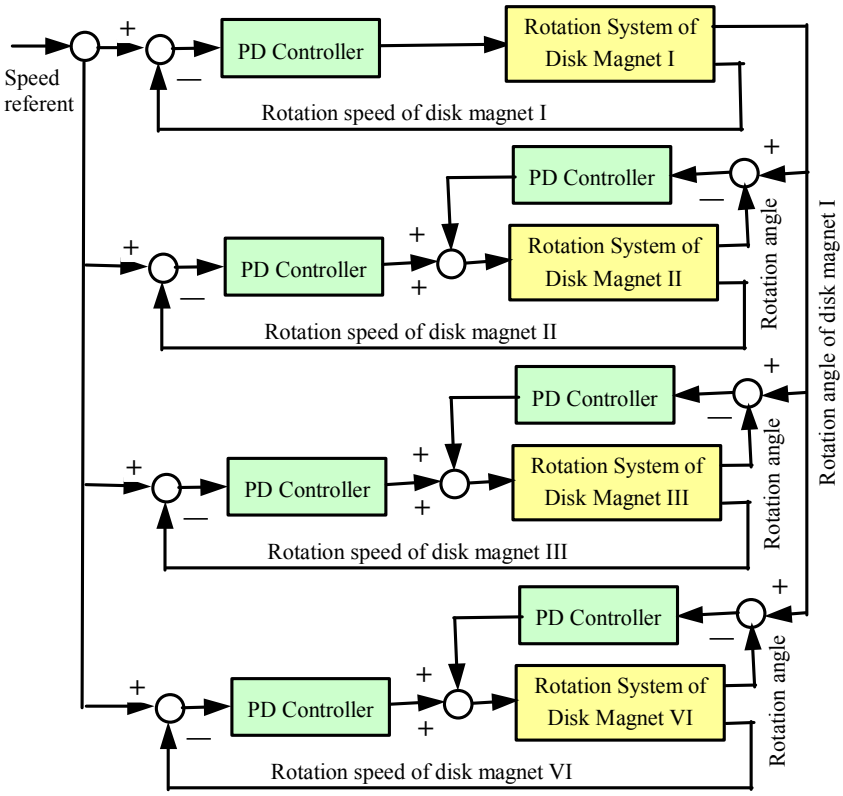

Fig.4.6 Control diagram of spinning system

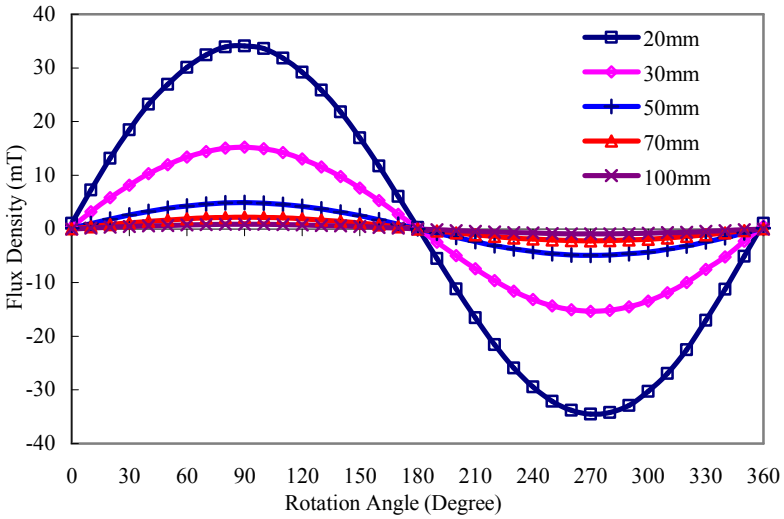

Fig.4.7 Magnetic flux density characteristic of disk magnet.

are shown in Fig.4.7. From the results, it can be seen that the flux density curves resemble sine curves at all points, and smaller distances yield greater flux density. This means that the influence on the remanent magnetization of the ball surface is periodic while the magnet is rotating; therefore, the magnet generates a greater force at the point nearest the levitated ball.

To examine the remanent magnetization points on the surface of the iron ball, the magnetic flux density of the surface of an iron ball was carried out using the gauss meter. Fig.4.8 shows

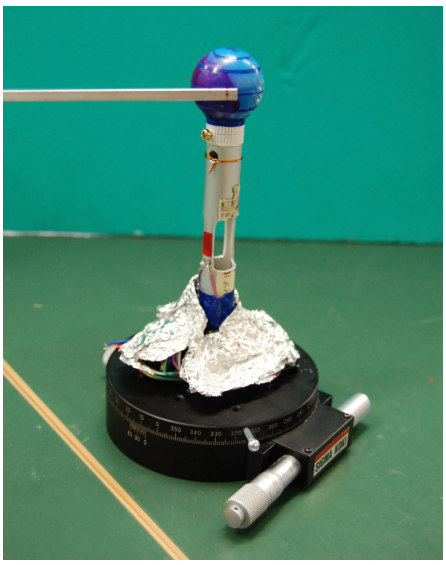

Fig.4.8 The photograph of measurement device

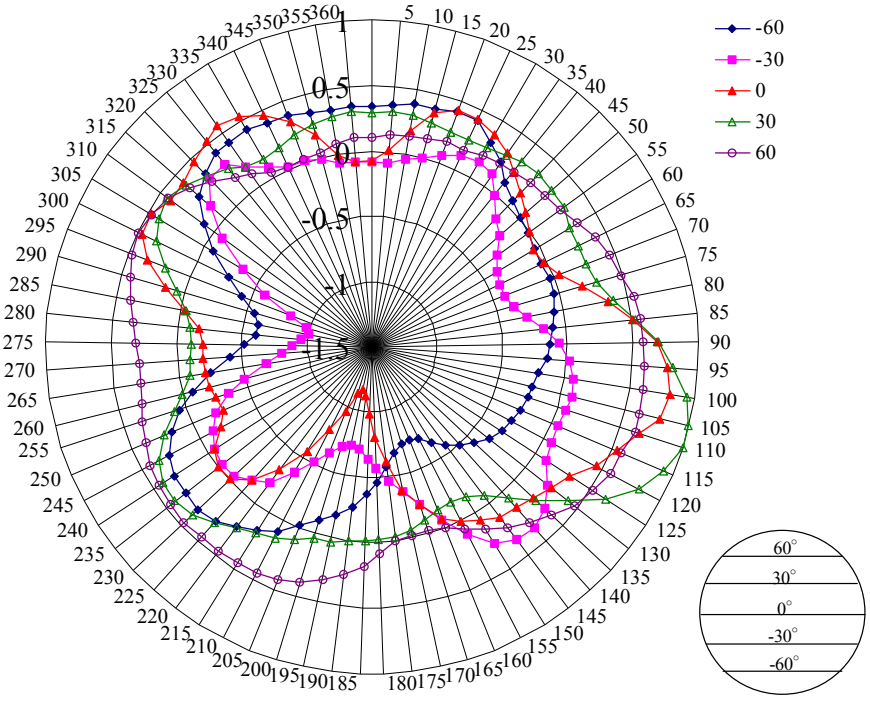

Fig.4.9 Magnetic flux density ditribution on the surface of iron ball

the photograph of measurement experiment. In the experiment, first, an iron ball was suspended to decide the position of maximum magnetization point on its surface. Second, the position of the maximum magnetization point was maintained on the top of the iron ball, and fixed on the top of the aluminum pipe, which was installing on the a rotational stage. Third, the longitude of the iron ball was marked, and the magnetic flux density along the longitude was measured in one revolution at a step of 5 degrees.

Fig.4.9 shows the results of magnetic flux density on the surface of the iron ball. In the

figure, the outside circle expresses the magnetic flux density as 1 mT, and the center point expresses as –1.5 mT. The results indicate that the magnetic flux density on the different place of the iron ball is different. Some place looks like the S pole, and some place looks like the N pole. The maximum magnetic flux density appears at the longitude of 0 degree, and the value is –1.16 mT. Therefore, we know that there are many remanent magnetization points on the surface of the iron ball.

4.4 Mathematical Model

4.4.1 Rotational Torque Modeling

In order to analyze the proposed spinning principle and examine the rotational characteristics of the spinning mechanism, a mathematical model of the spinning system was created as shown in Fig.4.10, where is only using magnet I (using the numbering configuration shown in Fig.4.1.) as a driving magnet. In this model, we assumed the following:

(1) There is one remnant magnetization point A as an S pole on the surface of the iron ball and a N pole located at the center of the sphere.

(2) The magnetic poles of the disk magnet are at points B (N pole) and C (S pole), and all magnetic flux comes out of point B and returns into point C.

According to the model, the remanent magnetization point A is attracted by point B and repulsed by point C, and the attractive force f_{m1} between point A and B and repulsive force f_{m2} between point A and C are expressed as

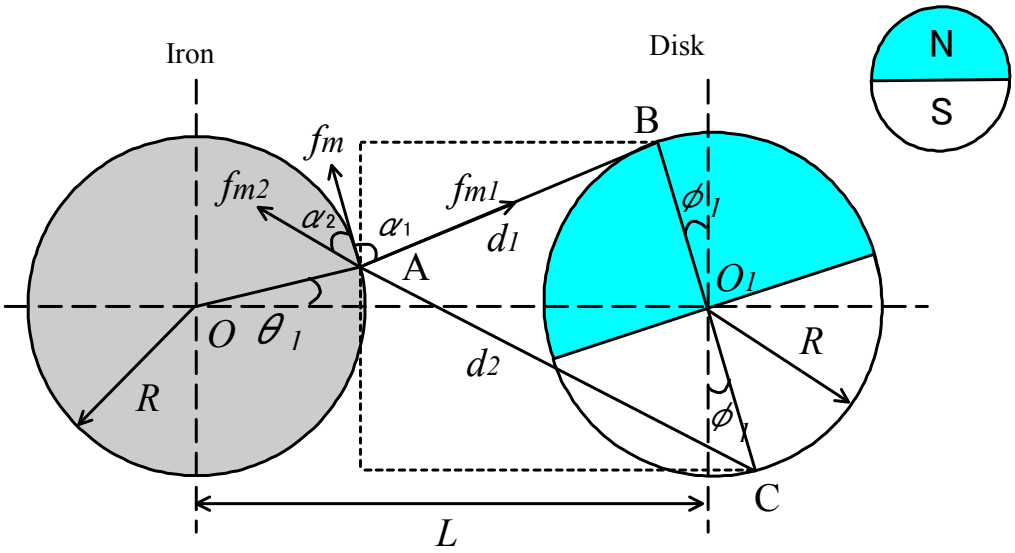

Fig.4.10 Model of the spinning system using magnet I

$$f_{m1} = \frac{k_1}{d_1^2} \tag{4.1}$$

$$f_{m2} = -\frac{k_2}{d_2^2} \tag{4.2}$$

$$\begin{aligned} f_{mI} &= f_{m1}\cos\alpha_1 + f_{m2}\cos\alpha_2 \\ &= k_1 \frac{R\cos(\theta_1 - \varphi_1) - L\sin\theta_1}{((R\cos\varphi_1 - R\sin\theta_1)^2 + (L - R\cos\theta_1 - R\sin\varphi_1)^2)^{\frac{3}{2}}} \\ &\quad - k_2 \frac{R\cos(\theta_1 - \varphi_1) + L\sin\theta_1}{((R\cos\varphi_1 + R\sin\theta_1)^2 + (L - R\cos\theta_1 + R\sin\varphi_1)^2)^{\frac{3}{2}}} \end{aligned} \tag{4.3}$$

$$\tau_{z1} = f_{mI} R \tag{4.4}$$

Where d_1 and d_2 are the distances from point A to points B and C, and k_1 and k_2 are factors of the attractive force and repulsive force. α_1 is the angle between f_{mI} and f_{m1}, α_2 is the angle between f_{mI} and f_{m2}. θ_1 is the rotational angle of the iron ball with respect to magnet I, and φ_1 is the rotational angle of magnet I. R is the radius of the iron ball and the magnets, and L is the distance between the centers of the iron ball and the magnets. τ_{z1} is the rotational torque on the iron ball around the z-axis using magnet I.

According to the arrangement of the iron ball and the disk magnets shown in Fig.4.1, the angular relationship between the magnets can be expressed by the following relationships:

$$\theta_2 = \theta_1 + \frac{\pi}{2} \tag{4.5}$$

$$\theta_3 = \theta_1 + \pi \tag{4.6}$$

$$\theta_4 = \theta_1 + \frac{3\pi}{2} \tag{4.7}$$

$$\varphi_2 = \varphi_1 + \frac{3\pi}{2} \tag{4.8}$$

$$\varphi_3 = \varphi_1 + \pi \tag{4.9}$$

$$\varphi_4 = \varphi_1 + \frac{\pi}{2} \tag{4.10}$$

Where θ_2 , θ_3 and θ_4 are the rotational angles of the iron ball with respect to magnets II, III and IV, respectively, and φ_2 , φ_3 and φ_4 are the rotation angles of magnets II, III and IV, respectively. Based on these relationships, the rotational torques of the other magnets can be calculated as well. Since all magnets are uniform in the mechanism, the factors of the attractive force and repulsive force are same. Since the rotational velocity of magnets is equivalent in experiments, the rotational angles of magnets can be expressed by φ_1.

Consequently, the rotational torque on the iron ball, τ_z, can be expressed for three different configurations of the disk magnets:

(1) Using disk magnet I as the driving magnet.

$$\tau_z = \tau_{z1} \tag{4.11}$$

(2) Using disk magnets I and III as the driving magnets.

$$\tau_z = \tau_{z1} + \tau_{z3} \tag{4.12}$$

(3) Using all four disk magnets as the driving magnets.

$$\tau_z = \tau_{z1} + \tau_{z2} + \tau_{z3} + \tau_{z4} \tag{4.13}$$

Where τ_{z2}, τ_{z3} and τ_{z4} are the rotational torques on the iron ball with respect to magnets II, III and IV, respectively.

4.4.2 Rotation Equation of Iron Ball

According to the mathematical model of the rotational torque of iron ball, the rotational equations of the iron ball can be obtained.

$$J\ddot{\theta} = \tau_z \tag{4.14}$$

$$J = m_0 R^2 \tag{4.15}$$

Where J is the moment of iron ball, m_0 is the mass the iron ball.

4.5 Spinning Examination by Numerical Simulation

According to the rotational equation of the iron ball, the spinning examination was carried out. In the simulation, the rotational velocity of the iron ball was not feedback to the control system, i.e. the spinning system was an open loop system. The parameters using in the simulations are shown in Table 4.1. Step responses of the velocity of the levitated object, its velocity in steady states conditions and the relationship of velocity between the iron ball and the rotational magnets with a ramp input of the rotational magnets were examined.

Table 4.1 Parameters using in numerical simulation

Parameter	Value	Parameter	Value
m_0 (kg)	0.1098	k_1 (Nm^2)	9×10^{-6}
L (mm)	90	k_2 (Nm^2)	9×10^{-6}
R (mm)	15		

4.5.1 Step Response

A step response was performed for the three different driving magnet configurations used in the above-mentioned model. In each simulation, a step velocity input of -0.5 rps was applied to the magnet after 2 seconds, and the responses of the iron ball and magnet were recorded for 20 seconds.

The step response results of iron ball using magnet I are shown in Fig.4.11. These results indicate that when the velocity step of the rotational magnets is input, the velocity of the iron ball responds to vibrate in the reverse direction to the magnet.

The step response results of iron ball using magnet I and III are shown in Fig.4.12. The results show that the velocity of iron ball responds to the input step immediately, and also vibrates. However, the mean velocity is almost equal to the velocity of the magnets.

The step response results of iron ball using all four magnets are shown in Fig.4.13. The velocity of iron ball also responds to the input step immediately and vibrates. However, the amplitude and period of the vibration are less than those in Fig.4.12. That means the numbers

of magnets become large, the velocity responsibility of the iron ball becomes quick and the velocity vibration becomes small.

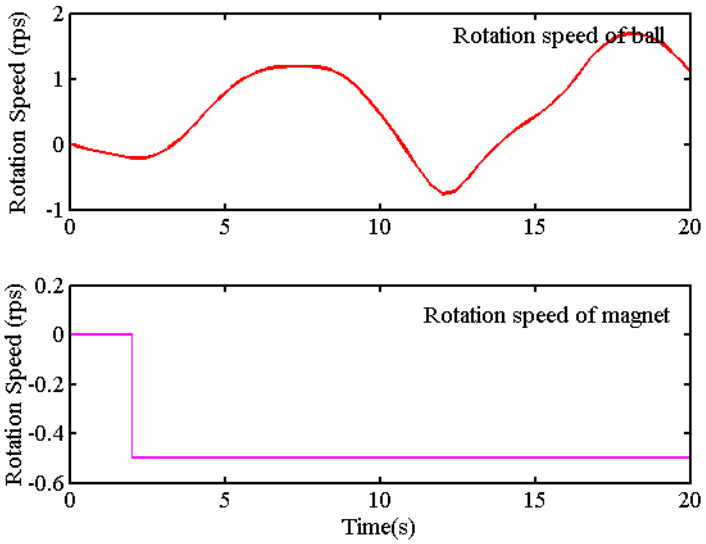

Fig.4.11 Step response of iron ball using magnet I in simulation

4.5.2 Velocity in Steady State

The rotational velocity of the iron ball was simulated in the steady state at about 0.5 rps. The simulation results of the steady velocity are shown in Fig.4.l4 to Fig.4.16. In the figures, the rotational velocity of the iron ball and the magnet was recorded from 80 s to 100s. In Fig.4.14 and Fig.4.15, the velocity of the iron ball is vibrating around 0.5 rps. In Fig.4.16, the velocity of the iron ball is almost 0.5 rps. Therefore, in the steady state, the velocity of the iron ball in the case with four magnets is more stable than other two cases.

4.5.3 Relationship between Input Velocity and Output Velocity

In order to examine the relationship between the input velocity of magnets and the output velocity of the iron ball, the velocities of the magnet and the iron ball were recorded until 5 rps, when a ramp signal was applied to the rotational magnet. The results are shown in Fig.4.17 to Fig.4.19. In the figures, the horizontal axis is the velocity of the magnet, and the vertical axis is the velocity of the iron ball.

Fig.4.17 shows the relationship results using magnet I only. The results indicate that the gradient is almost 1, i.e. the velocity of the iron ball is almost equal to the velocity of the magnet.

Fig.4.18 shows the relationship results using magnet I and III. The trend of the figure is similar to the Fig.4.17, but the differences between the velocity of iron ball and the magnets are large.

Fig.4.19 shows the relationship results using four magnets. The gradient of the graph is

almost 1, and there are some small differences between the velocity of iron ball and the magnets.

All the simulation results indicate that as the number of the magnet increases, the step response becomes quick, the steady rotational velocity becomes stable, and the linearity of the relationship between the velocity of the iron ball and the magnets becomes good.

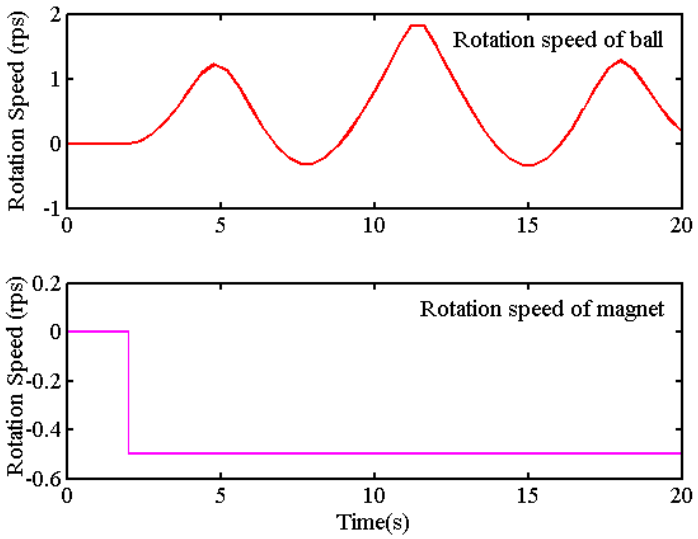

Fig.4.12 Step response of iron ball using magnet I and III in simulation

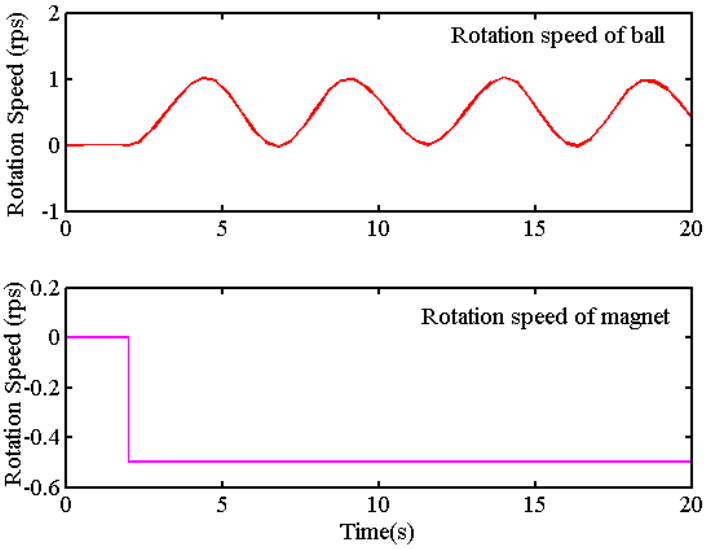

Fig.4.13 Step response of iron ball using four magnets in simulation

4.6 Spinning Examination by Experiments

Experiments were carried out to investigate the performance of the proposed spinning system. In the experiments, the velocity of the same spinning object was recorded. Step

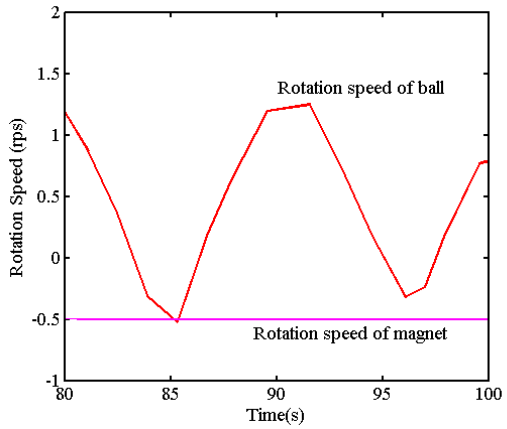

Fig.4.14 Steady velocity of iron ball using magnet I only in simulation

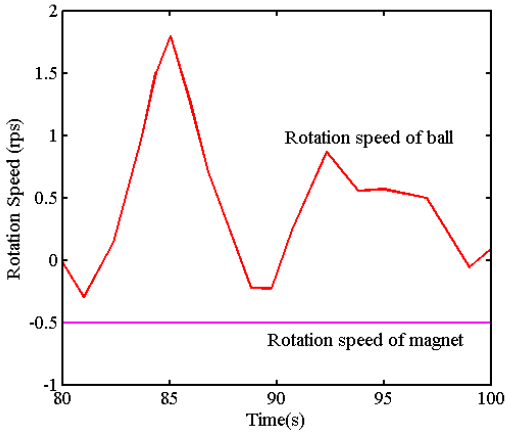

Fig.4.15 Steady velocity of iron ball using magnet I and III in simulation

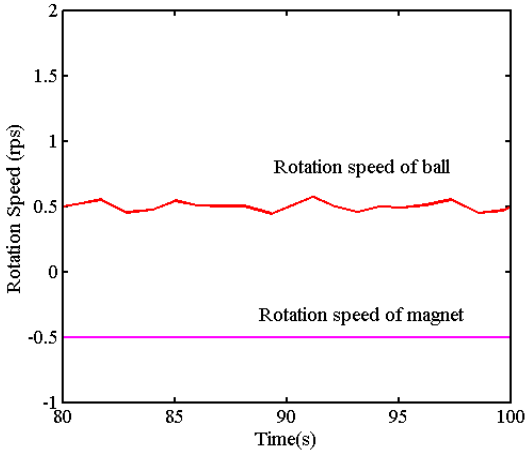

Fig.4.16 Steady velocity of iron ball using four magnets in simulation

responses of the velocity of the levitated object, its velocity in steady states conditions and the relationship between the input and output velocities were also examined.

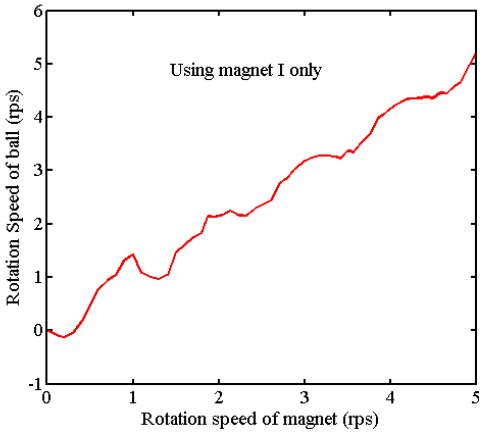

Fig.4.17 Velocity relationship using magnet I only in simulation

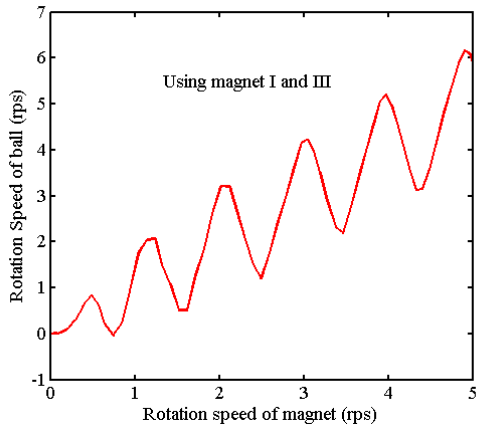

Fig.4.18 Velocity relationship using magnet I and III in simulation

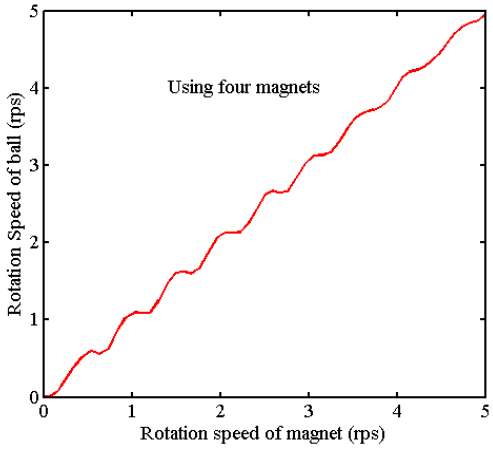

Fig.4.19 Velocity relationship using four magnets in simulation

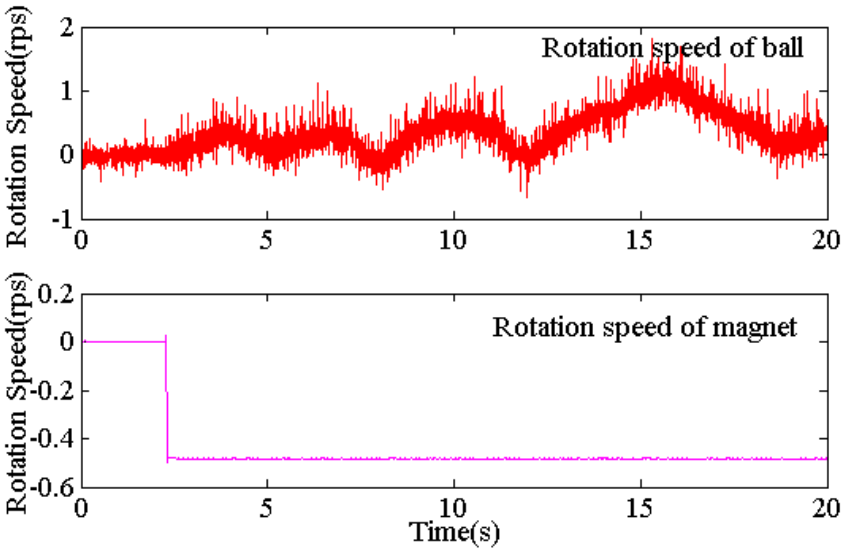

Fig.4.20 Step response of iron ball using magnet I in experiment

4.6.1 Step Response

A step response was performed for the three different driving magnet configurations used in the above-mentioned simulations. In each experiment, a step velocity input of -0.5 rps was applied to the magnet after 2 seconds, and the responses of the iron ball and magnet were recorded for 20 seconds. The velocity response of the iron ball was measured using a FC-2000/FC-2010 of KEYENCY laser sensor for the length and speed measurements. The measurement range of the velocity was less than 42 rps, and the measurement error was less than ±0.09 rps. The results are shown in Fig.4.20 to Fig.4.22. In these results, the upper graph is the velocity of the iron ball, and the lower graph is the velocity of disk magnets.

The result of the experiment using magnet I as the only driving magnet is shown in Fig.4.20. As shown in the figure, the velocity response does not follow the input velocity, which means that the object does not rotate; it vibrates. We can see, however, that the vibration becomes large. A possible explanation for this result is that the strongest remanent magnetization point in horizontal plane on the surface of iron ball was stopping at the reverse side to the magnet, where the driving stiffness was low and the rotational torque was small.

Fig.4.21 shows the step response results when magnet I and III are used for spinning. As shown in the figure, the spinning movement starts as the input is applied, and the mean output velocity is about 0.5 rps. This is the same as the input velocity, since the rotational torque using two magnets is bigger than using one magnet as shown in the results of the calculations and simulations; however, the velocity vibrates with a period of about 4 seconds.

The velocity step response for the experiment using all four magnets to drive the suspended object is shown in Fig.4.22. As shown in the figure, the velocity responds as the input changes. The mean output velocity is about 0.5 rps, which is the same as the input. Velocity vibration also occurs, but the period is shorter than the result shown in Fig.4.21. Compared with the

result using two magnets, a quicker response can be seen in this case.

These step response results indicate that rotation can be realized regardless of the number of driving magnets; however, increasing the number of disk magnets causes a quicker response.

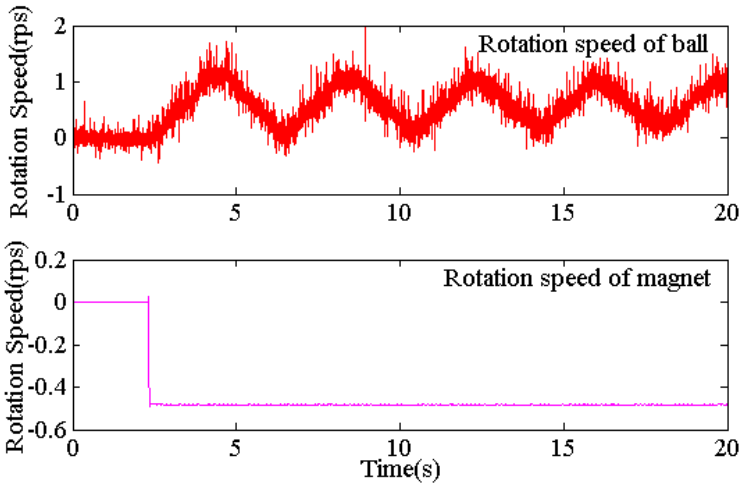

Fig.4.21 Step response of iron ball using magnet I and III in experiment

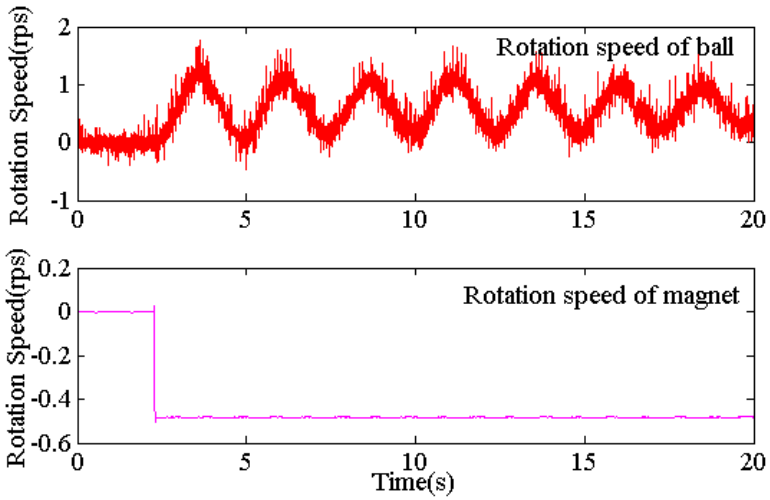

Fig.4.22 Step response of iron ball using four magnets in experiment

4.6.2 Velocity in Steady State

Using the same configurations mentioned above, the velocities of the iron ball were recorded 20 seconds after the step input occurred 5 minutes, and the results are shown in Fig.4.23 to Fig.4.25.

As shown in these figures, the means of output velocities are almost 0.5 rps, which is the same as the input velocity. A small velocity error can be seen in all figures, which may be caused by the sensor gain error. These experimental velocity results from a stable rotation state agree with the results of simulation, which indicate that a higher number of installed magnets generate steadier rotational velocity of the iron ball.

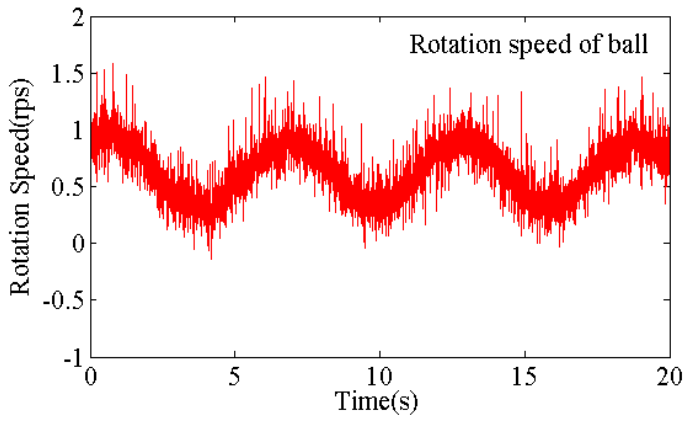

Fig.4.23 Steady velocity of iron ball using magnet I in experiment

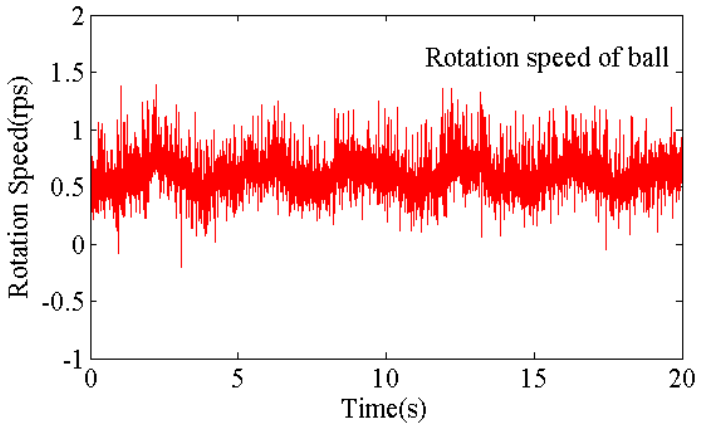

Fig.4.24 Steady velocity of iron ball using magnet I and III in experiment

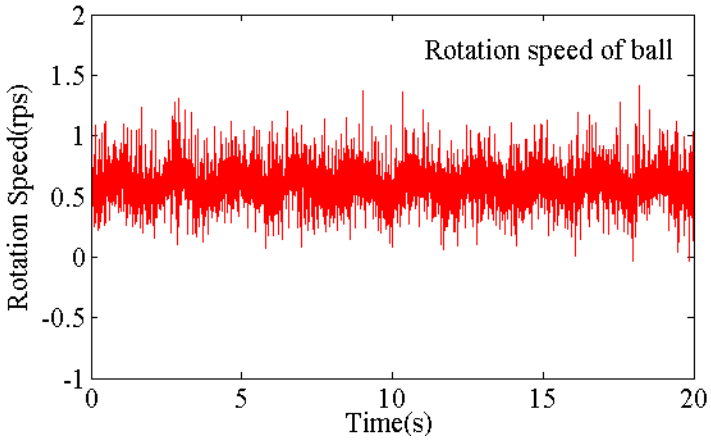

Fig.4.25Steady velocity of iron ball using four magnets in experiment

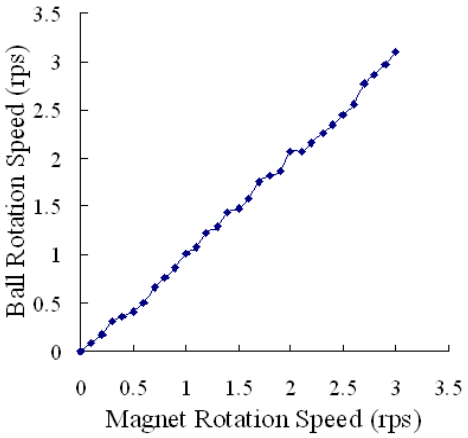

Fig.4.26 Velocity relationship of iron ball using magnet I in experiment

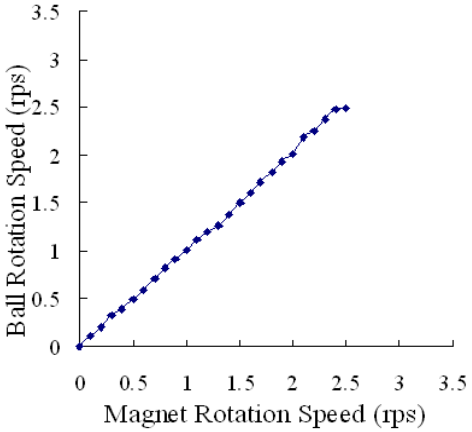

Fig.4.27 Velocity relationship of iron ball using magnet I and III in experiment

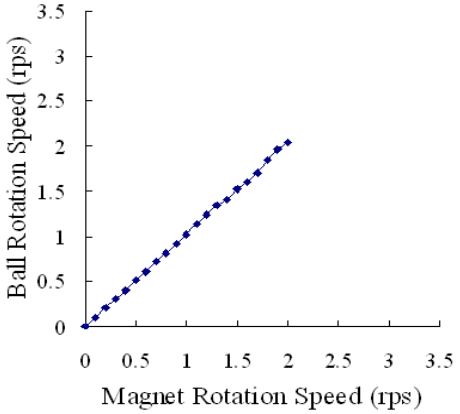

Fig.4.28 Velocity relationship of iron ball using four magnets in experiment

4.6.3 Relationship Between Input Velocity and Output Velocity

The relationship between the input and output velocities was examined to verify the linearity of the system. In the experiments, the input velocity to the system was increased in increments of 0.1 rps until the iron ball could not be stably suspended. For each experiment, the average velocity for 10 seconds was measured after steady state was achieved. The results are shown in Fig.4.26 to Fig.4.28.

The result using only magnet I is shown in Fig.4.26. During this experiment, the other 3 magnets were removed from the system. The spinning velocity of the iron ball increased with the increasing input velocity of the disk magnet as shown in the figure. The input and output velocities were differed slightly, and the gradient was not 1; however, the number of rotations of the magnet was same as that of the iron ball, and the relationship between the input and output velocity was almost linear. Therefore, the difference is assumed to be caused by the sensor gain error. The correct velocity is represented by the magnet rotation velocity. The iron ball could be spun up to 3 rps.

The result using magnets I and III is shown in Fig.4.27. During this experiment, the magnet II and IV were removed from the system. In this case, the iron ball could be spun up to about 2.5 rps.

When all four magnets were used for spinning, the result is shown in Fig.4.28. As shown in the figure, the iron ball velocity was able to reach about 2 rps.

As shown in these three figures, as the number of the magnet increases, the linearity of the relationship improves, but the velocity limit decreases. The reason for the lower velocity limit can be considered that increasing the number of magnets generates an increased attractive force in the horizontal plane.

Compared with the velocity limit of 1 rps in the previous prototype spinning system, this proposed spinning system has better performance than the previous system.

4.7 Conclusions

A noncontact spinning method using disk magnets and rotary motors has been proposed. A prototype of the spinning system was constructed to verify the performance of the proposed method. A mathematical model was created, and simulations were performed. Noncontact spinning experiments using the prototype were performed, and the results indicate that a levitated iron ball can be spun using the remanent magnetizations and the rotational disk magnets. The iron ball could be spun regardless of the number of driving magnets used, however, as more magnets were used, the iron ball was spun more smoothly, but the velocity limit decreased.

Chapter 5 Performance analysis of noncontact spinning mechanism

5.1 Introduction

The last chapter introduced a noncontact spinning system using permanent magnets and rotary motors. An experimental prototype of the spinning mechanism was set up, and the noncontact spinning simulations and the spinning experiments were examined. All examinations indicate that this spinning system can realize the noncontact spin of the noncontact suspended object (here is an iron ball) by means of the remanent magnetization on the surface of the suspended object and the rotation disk-type permanent magnets. The rotation of the suspended object had been realized using one magnet, two magnets, and four magnets, respectively. Moreover, the spinning experimental results indicated that the suspended object could be spun regardless of the number of driving magnets used; however, as more magnets were used, the suspended object was spun more smoothly, but the velocity limit decreased.

In order to examine the reasons of the spinning results, this chapter will examine the characteristics of the noncontact spinning mechanism by IEM (Integral Element Method) analysis [70] and experimental examinations. In this chapter, first, the magnetic filed of the spinning mechanism is examined by a 2-D analysis model. Second, the rotational torque of the suspended iron ball is calculated using the mathematical model created in last chapter. Third, after modeling the remanent magnetization point, the 3-D IEM analysis model is created, and the rotational torque is examined. Forth, a measurement device is set up according to the model of the remanent magnetization point, and the rotational torque is also examined by experiments. Finally, the attractive force in the horizontal direction is examined. Moreover, all the examinations are carried out three figurations of the permanent magnets, which are same as the simulations and experiments in last chapter.

5.2 Magnetic Field Examination by IEM Analysis

In order to examine the magnetic field of the spinning mechanism in the horizontal plane, the 2-D analysis models were created in the ELF/Magic software in three cases. In the models,

the diameters of the iron ball and the magnets are 30 mm, which is same as the experimental

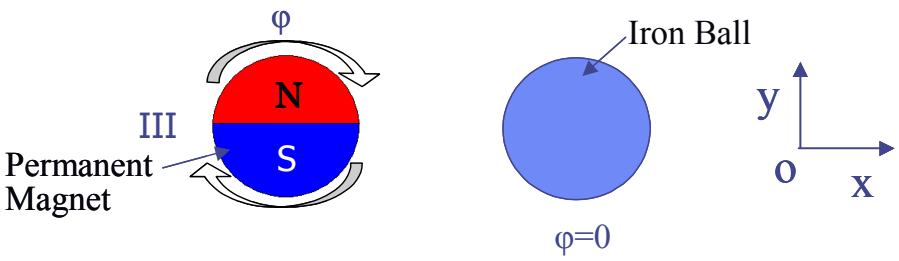

Fig.5.1 2-D analysis model using one magnet only

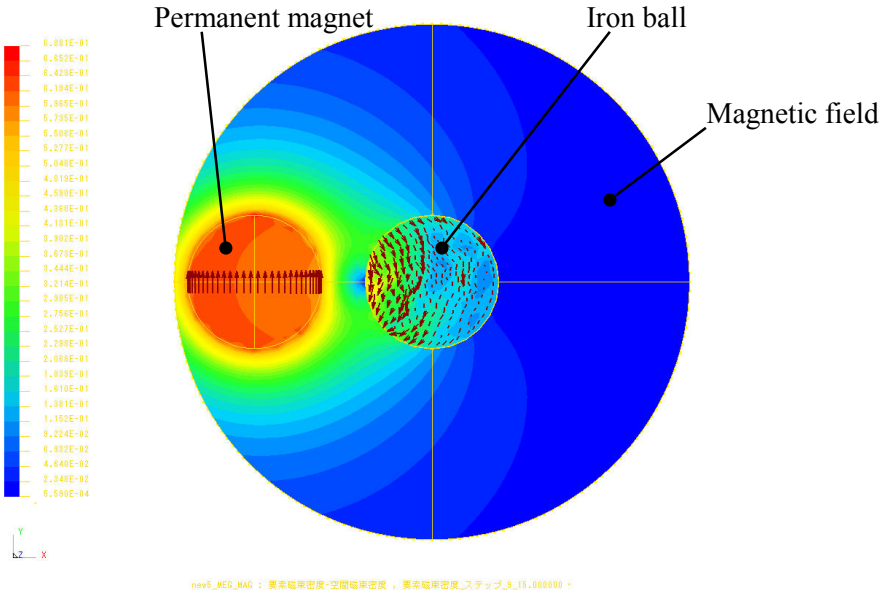

Fig.5.2 Analysis result when φ=0˚

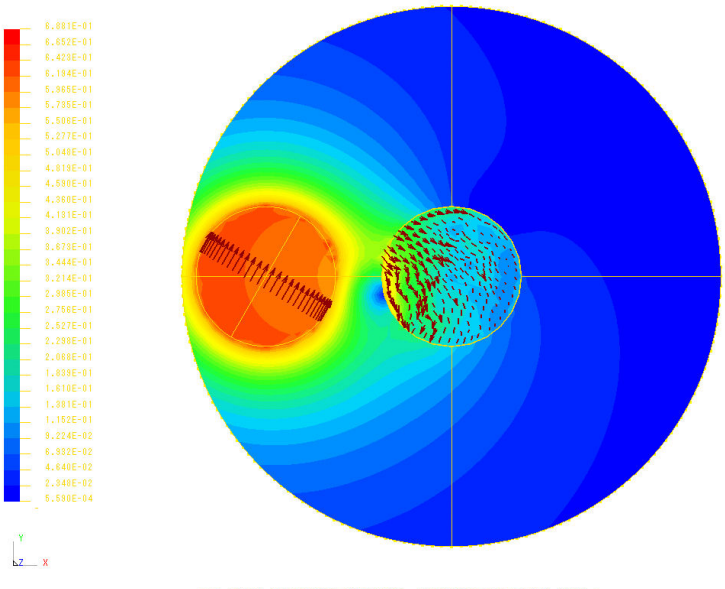

Fig.5.3 Analysis result when φ=30˚

mechanism. The distance from the center of iron ball to the center of magnets is 40mm. The range of the magnetic field expressed is round and including the iron ball and the all magnets. The diameter of the magnetic field is 120mm. The material of iron ball is Fe, and the material of the magnets is N48 of neodymium.

5.2.1 Analysis Using one Magnet only

In this case, an analysis model is created and shown in Fig.5.1. In this model, the rotational angle of magnet III (this number is same with the number shown in Fig.4.1) is assumed as φ, and φ is equal to 0 degree when the situation is shown as Fig.5.1. The analysis results when the magnet rotates from 0 degrees to 90 degrees, are shown in Fig.5.2 to Fig.5.5, where the left roundness is permanent magnet, the right roundness is the iron ball. The big and blue roundness is the expressed magnetic field. The arrows express the direction of the magnet flux, and the color expresses the magnetic density. The results indicate that the strong magnetic density point around the surface of the iron ball varies when the magnet rotates. Therefore, if there is a remanent magnetization as S pole on the surface of the iron ball, the remanent magnetization will be attracted by the rotational magnet, and will follow the variation of the strong magnetic density point. These results can prove that the iron ball can be spun using one magnet only.

5.2.2 Analysis Using Two Magnets (I and III)

An analysis model with two magnets is created and shown in Fig.5.6. The analysis results are shown in Fig.5.7 to Fig.5.10. These results indicate that the strong magnetic density points around the surface of the iron ball vary when the magnets rotate as well, the number of the strong magnetic density points, however, is two. The two strong magnetic density points are symmetry, and move to the same rotational direction, as the two magnets rotate in same direction. Therefore, these two rotational magnets also can spin the iron ball without contact. Moreover, since there are two strong magnetic density points around the surface of the iron ball, it may be easier to spin the iron ball using two magnets than using one magnet.

5.2.3 Analysis Using Four Magnets

An analysis model with four magnets is created and shown in Fig.5.11. The analysis results are shown in Fig.5.12 to Fig.5.15. These results indicate that the strong magnetic density points around the surface of the iron ball vary when the magnets rotate as well. The number of the strong magnetic density points is also two. Moreover, the intensity of the magnetic density is seemed as equal at all the rotational angle of magnets, and the variation angle of the strong magnetic density points on the surface of the iron ball is almost equal to the rotational angle of the magnets. Therefore, the iron ball will be spin smoothly when using four magnets as the driving magnets.

All the analysis results of the magnetic field by IEM are agreed with the simulation results and experimental results shown in last chapter. Using four magnets as driving magnets, the

mechanism is easy to spin the iron ball, and the spinning state will be steadier than other two cases.

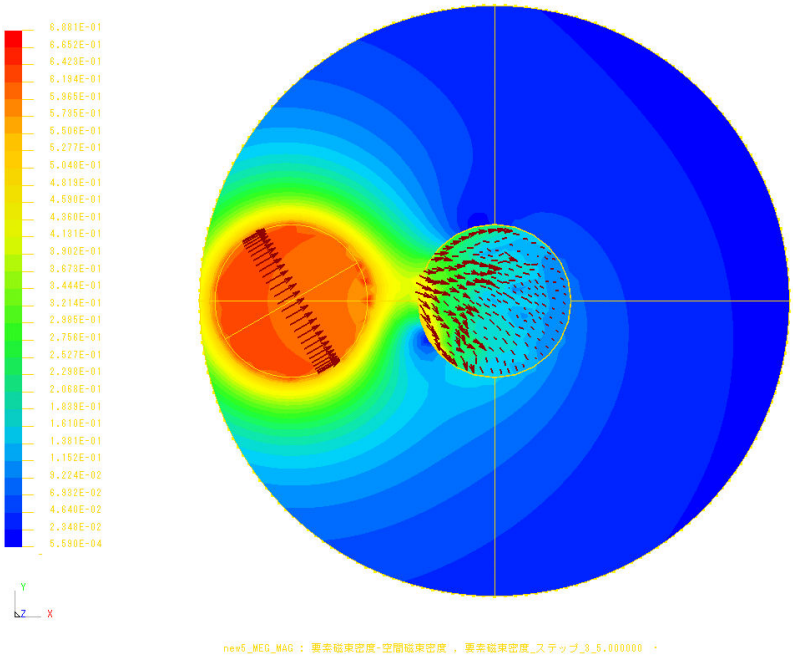

Fig.5.4 Analysis result when φ=60˚

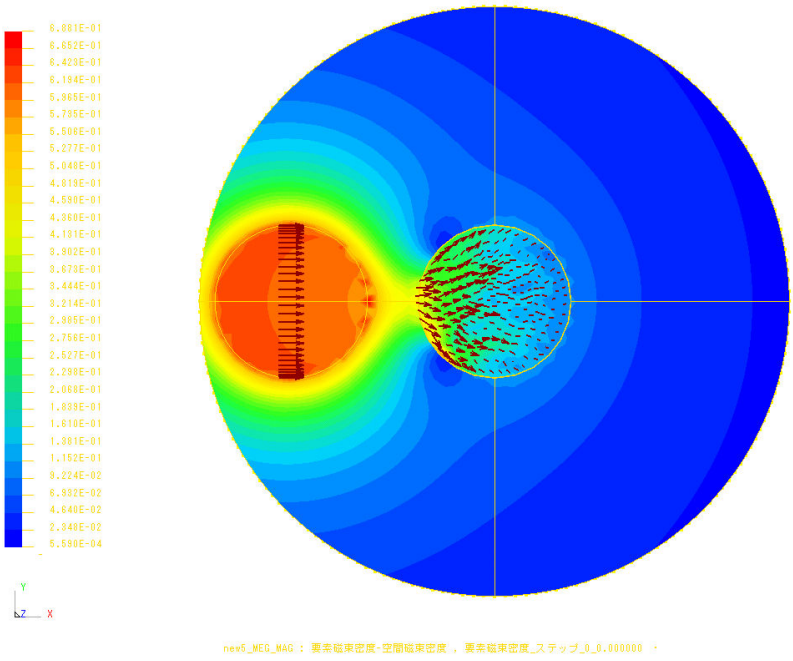

Fig.5.5 Analysis result when φ=90˚

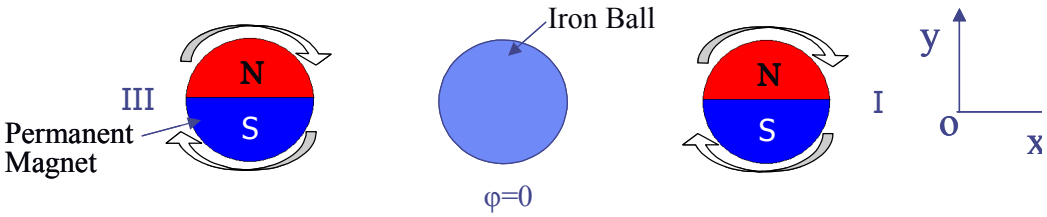

Fig.5.6 2-D analysis model using two magnets

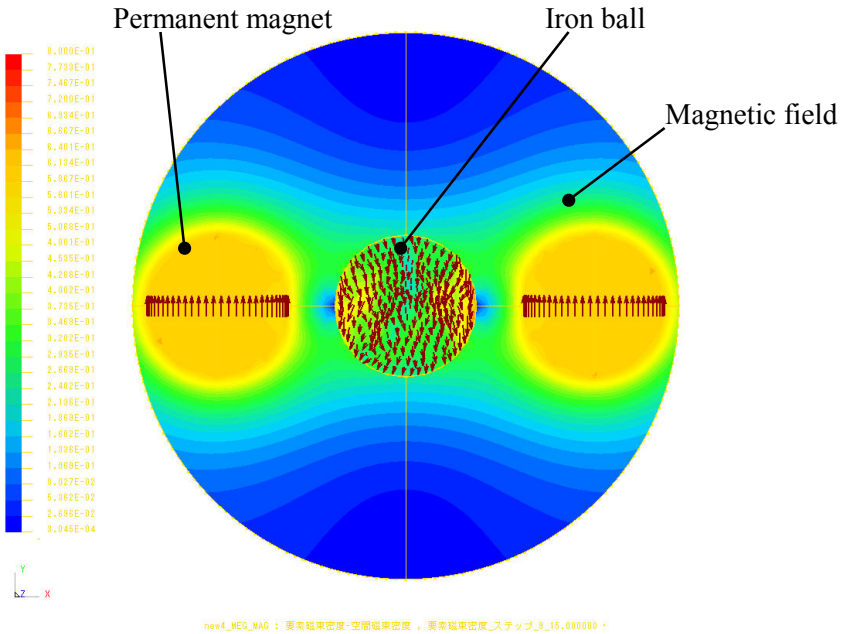

Fig.5.7 Analysis result when φ=0˚

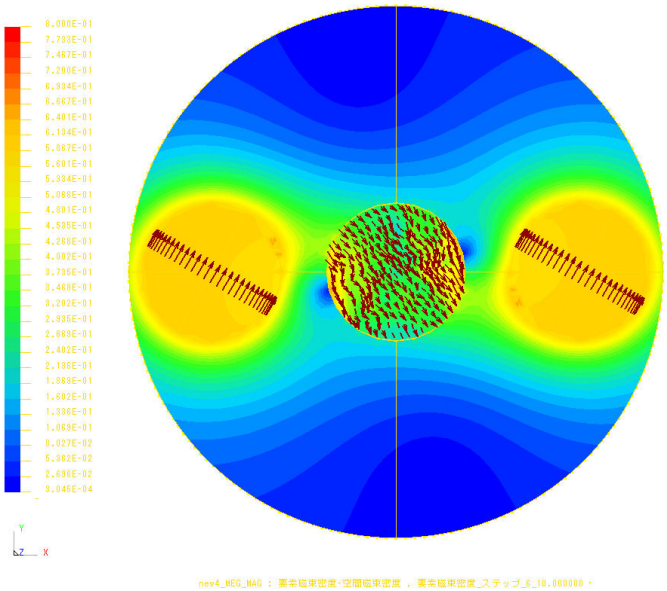

Fig.5.8 Analysis result when φ=30˚

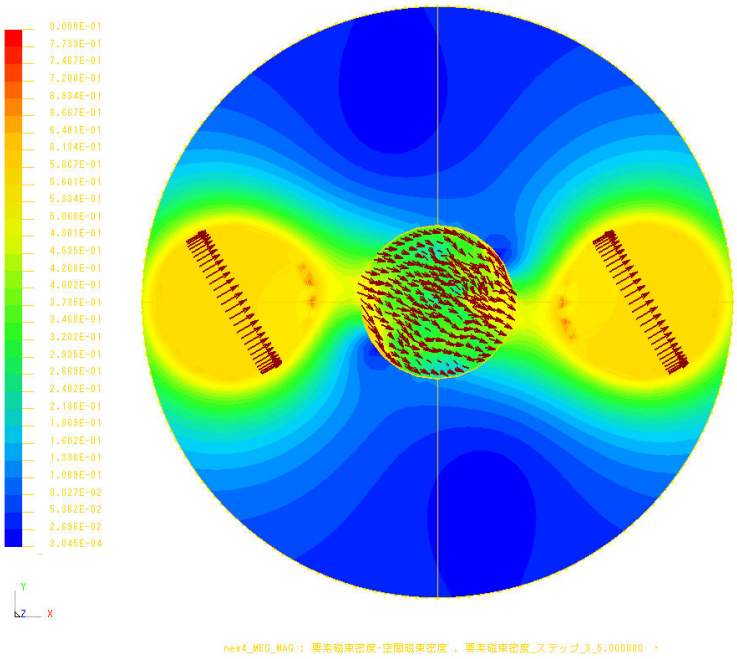

Fig.5.9 Analysis result when φ=60˚

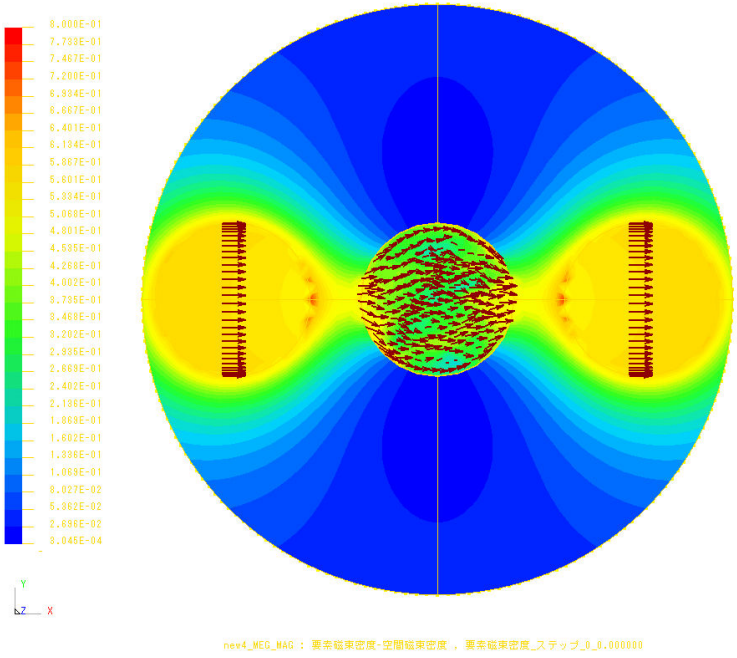

Fig.5.10 Analysis result when φ=90˚

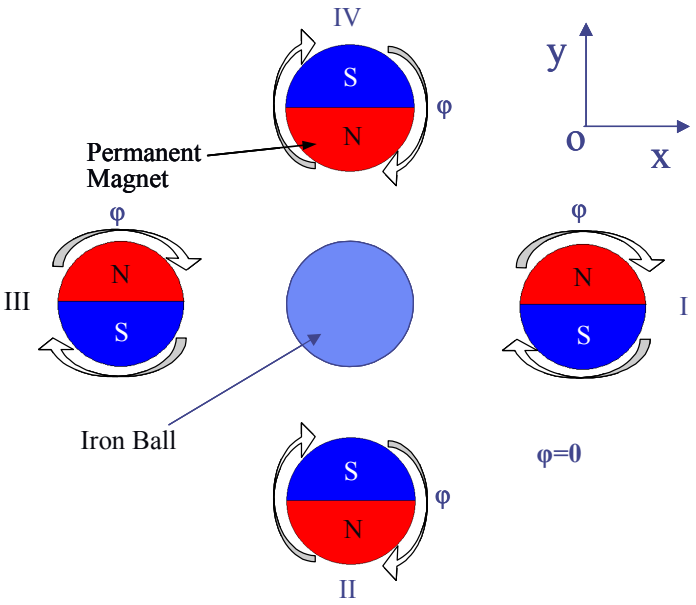

Fig.5.11 2-D analysis model using four magnets

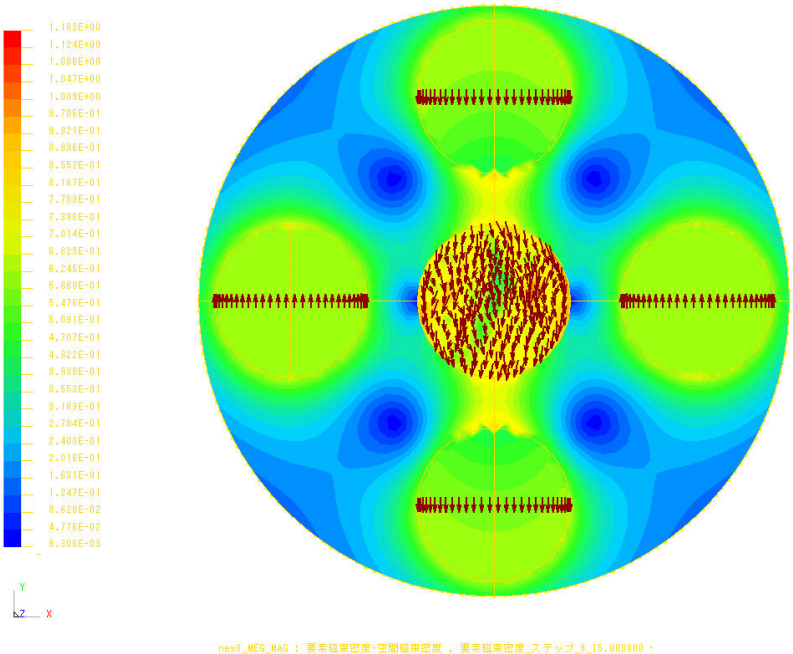

Fig.5.12 Analysis result when φ=0˚

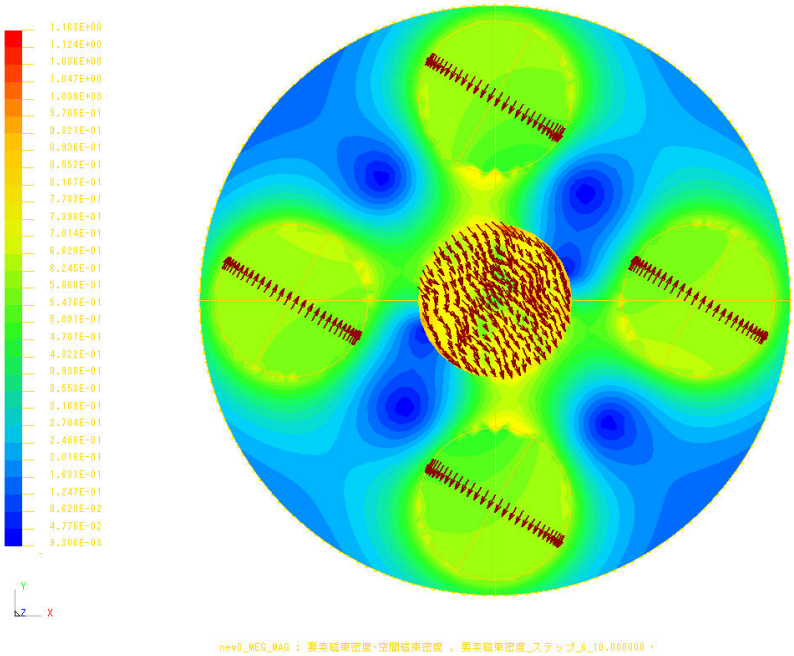

Fig.5.13 Analysis result when φ=30˚

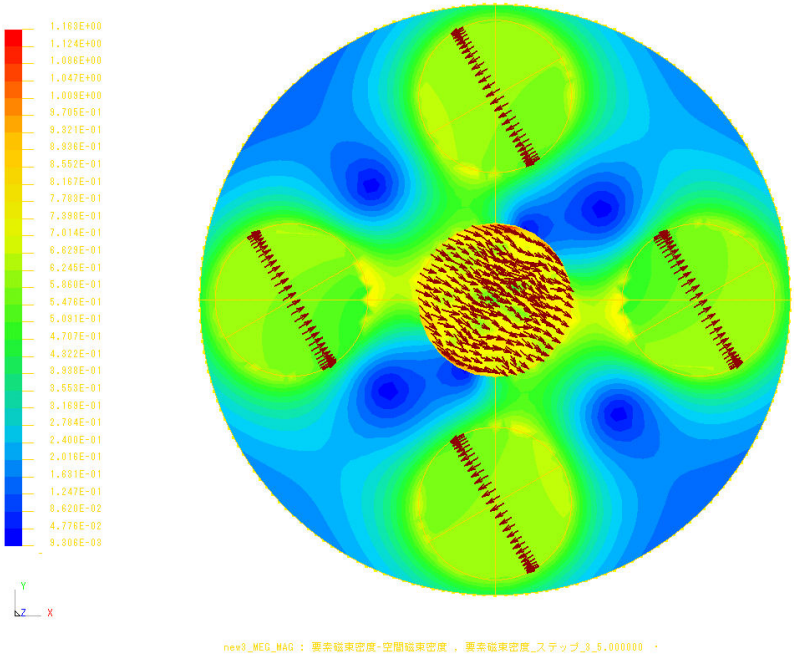

Fig.5.14 Analysis result when φ=60˚

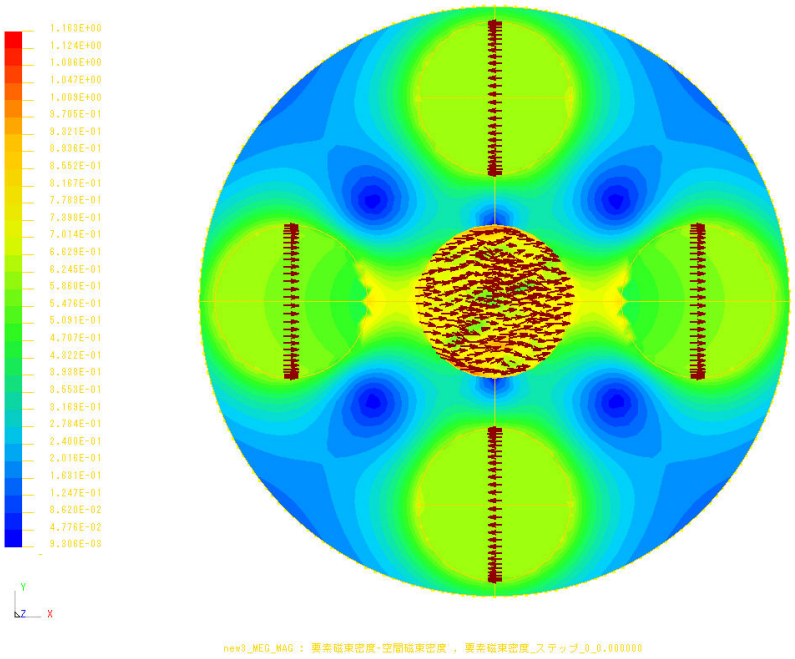

Fig.5.15 Analysis result when φ=90˚

Table 5.1 Parameters using in simulation of rotational torque

Parameter	Value	Parameter	Value
L (mm)	60	k_1 (Nm^2)	9×10^{-3}
R (mm)	15	k_2 (Nm^2)	9×10^{-3}

5.3 Simulation Examination of Rotational Torque of Iron Ball

In order to examine the rotational characteristics of the spinning mechanism, the rotational torque of the iron ball was simulated using the mathematical model (from Equation (4.3) to Equation (4.13)) expressed in the last chapter. The parameters used in the simulation are shown in Table 5.1.

The simulation used magnet I only was carried out as shown in Fig.5.16. The remnant magnetizations are assumed to be two elliptical points on the surface of the iron ball. One remanent magnetization point as N pole is on the top of the iron ball, facing the upper magnet for suspension, and the other as S pole is on the side of the iron ball in the same horizontal plane with the disk magnet. We also assumed that θ is the rotational angle of the iron ball and φ is the rotational angle of the disk magnet. θ and φ are equal to 0° when the iron ball and the

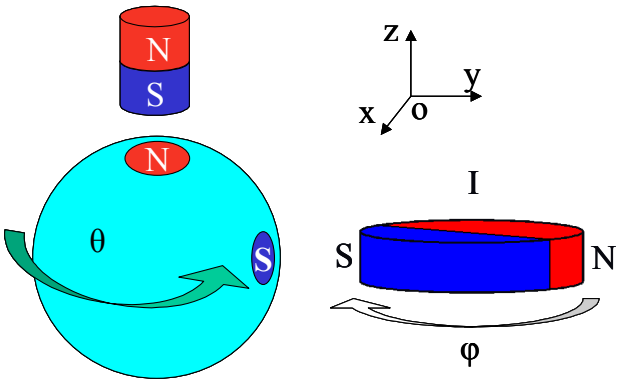

Fig.5.16 The schematic model of simulation using magnet I only

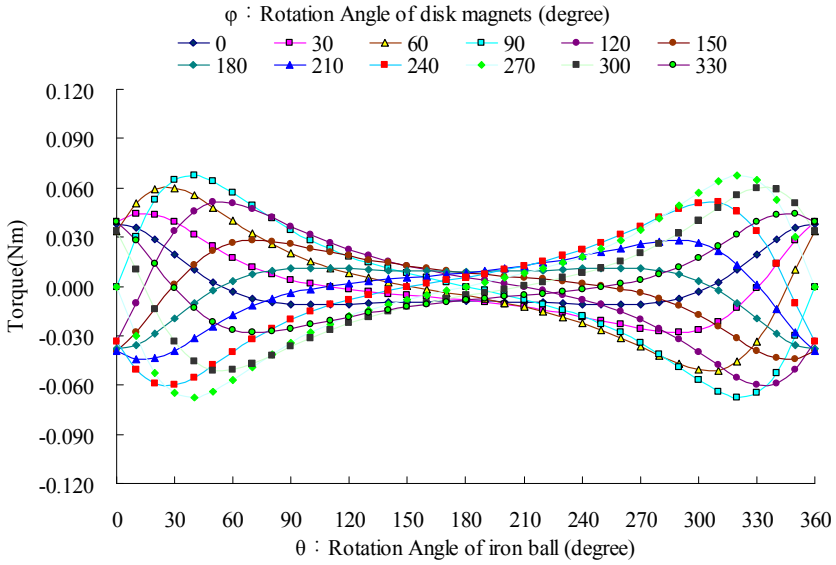

Fig.5.17 Rotational torque of the iron ball using magnet I only

disk magnets are stopped at the position shown in Fig.5.16. The simulation process is as follows:

(1) When φ = 0°, θ rotated in steps of 10° from 0° to 360°, and the torque around the vertical axis was calculated at each step.

(2) Then φ rotated in steps of 30° until it completed one revolution.

The simulation results used magnet I only are shown in Fig.5.17. In the figure, the horizontal axis expresses θ, the rotational angle of the iron ball, and the vertical axis expresses the torque around the vertical axis of the iron ball, and the parameters on the top of figures express φ, the rotational angle of the disk magnets. In these results, the torque is expressed with respect to the rotational angle of the iron ball. The intersection where the downward-sloping section of torque graph intersects the horizontal axis is called a stable point. When the remanent magnetization point is at the stable point, the torque equals zero, and if the iron ball rotates around the stable point, the direction of the torque will make the remanent magnetization point return to the stable point. If the stable point moves, the

remanent magnetization point will follow it. As a result, the iron ball spins. Moreover, the interval of two adjacent stable points indicates the rotational angles of the iron ball while the disk magnets rotate 30°, and the slope of intersections indicates the driving stiffness, which is the rate of the change in torque with respect to the rotational angle of the iron ball. The rotational stability of the iron ball depends on the interval of two adjacent stable points and the driving stiffness. If the intervals and the driving stiffness are identical for an entire revolution, the iron ball will spin smoothly.

From Fig.5.17, it can be seen that the torque varies with respect to the rotational angle of the iron ball and the disk magnet. The maximum torque appears at about 55° and 305° of rotation of the iron ball when the magnet stops at 90° or 270°. The maximum torque is approximately 0.07 Nm. The stable points are concentrated around θ = 0° and θ = 180°, and scarce around θ = 90° and θ = 270°. The interval between marked stable points becomes longer from the first to the fourth stable points, which means the iron ball will spin faster and faster until point four while the magnet rotates at constant velocity. After point four, the iron ball will decelerate. Moreover, the driving stiffness is high around θ = 0°, when the remanent

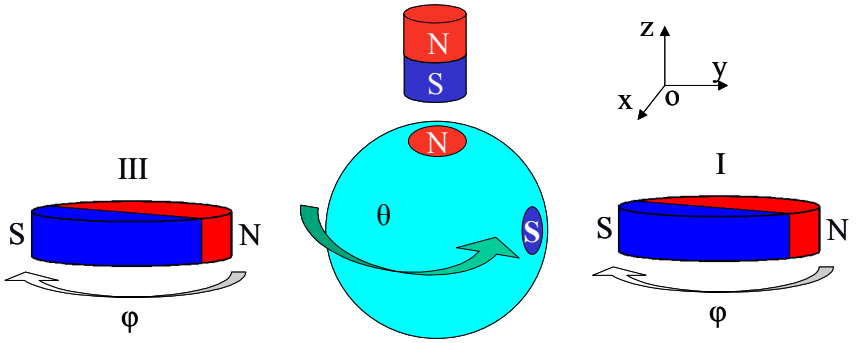

Fig.5.18 The schematic model of simulation using magnet I and III

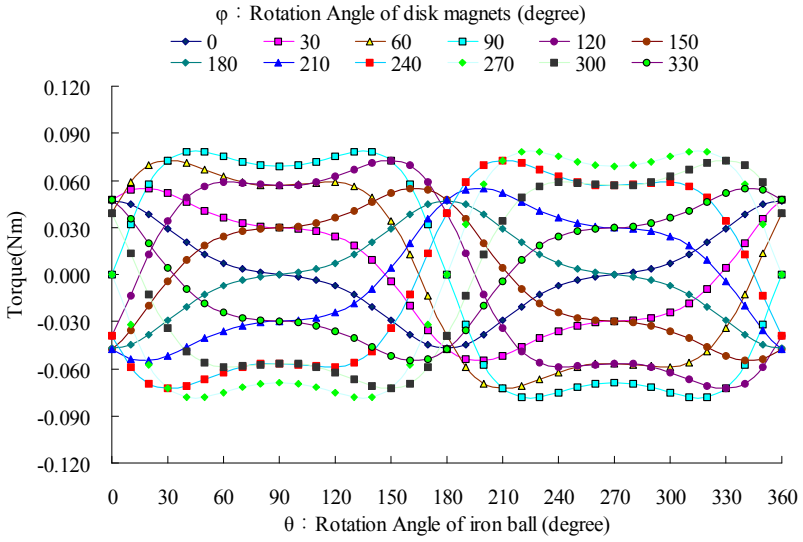

Fig.5.19 Rotational torque of the iron ball using magnet I and III

magnetization is facing magnet I, and is low around θ = 180°, when the remanent magnetization is farthest away from magnet I. These results indicate that the relationship between the rotational velocity of the disk magnet and the rotational velocity of the iron ball is nonlinear, and the rotational velocity of the iron ball is sometimes fast and sometimes slow even though the magnet rotates at a constant velocity. Consequently, when only using magnet I as the driving magnet, the iron ball can be spun, but the spinning speed will not be constant.

Fig.5.18 shows the schematic model of simulation using magnet I and III. And Fig.5.19 shows the simulation results. In these results, the maximum torque appears at about 45°, 135°, 225° and 315° of the iron ball when the magnets stop at 90° or 270°. The maximum torque is approximately 0.08 Nm, which is equal to the sum of the maximum torque using just magnet I and the torque after the iron ball and the magnet I were rotated 180° from the maximum-torque angle. Because magnets I and III were on opposite sides of the iron ball, the phase difference between the two magnets was 180° with respect to iron ball. As a result, the

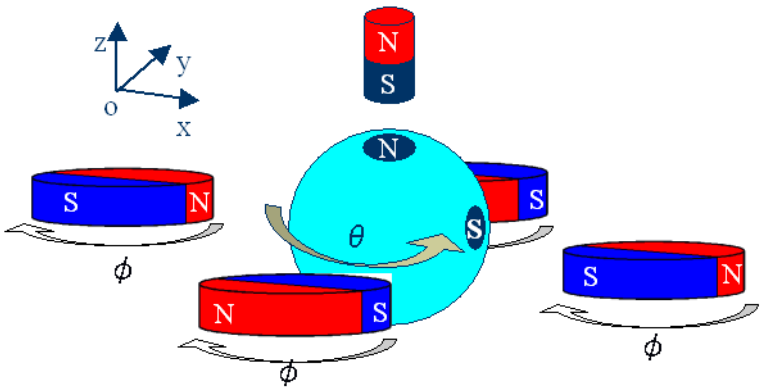

Fig.5.20 The schematic model of simulation using four magnets

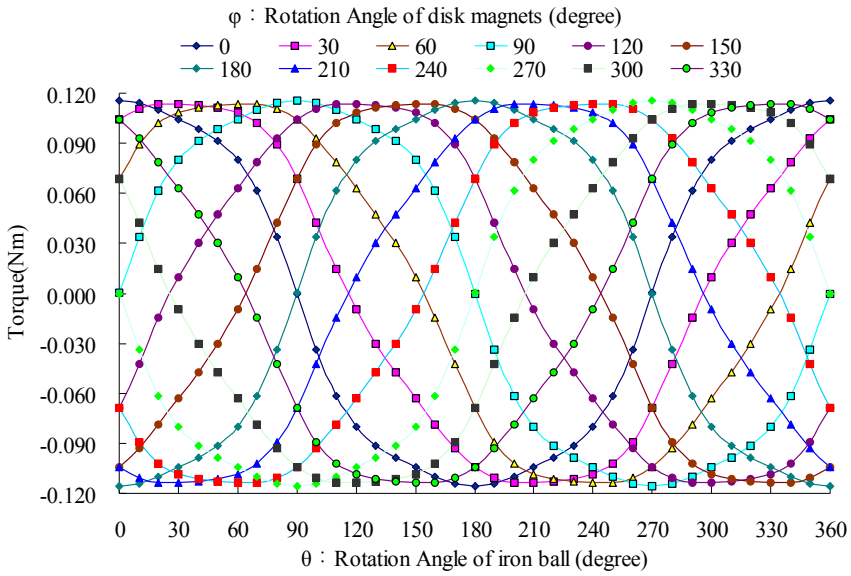

Fig.5.21 Rotational torque of the iron ball using four magnets

maximum torque in Fig.5.20 is not twice the maximum torque shown in Fig 5.18. Moreover, the system exhibits high driving stiffness around θ = 0° and θ = 180°, where the intervals between stable points are short, and the ball will be spun slowly around these angles. High torque appears around θ = 90° and θ = 270°, and the intervals between stable points are long. The ball will be spun fast around these angles. From these results using magnets I and III as the driving magnets, the angular velocity of the iron ball will also be unstable.

Fig.5.20 shows the schematic model of simulation using four magnets. Fig.5.21 shows the simulation results using all four disk-magnets as the driving magnets, which are different from the results from Fig.5.17 and Fig.5.19. The graph of each rotational angle of the disk magnets is regular and resembles a sine curve. The maximum torques is approximately 0.12 Nm and is nearly the same at each rotational angle of the disk magnets. The maximum torque in this figure is equal to the sum of the maximum torque produced using magnets I and III and the torque after the iron ball and the magnets rotated 90°. Moreover, the interval between adjacent stable points is 30°, which is the same as the variation in the rotational angle of the disk magnets. The driving stiffness is almost the same at all of the intersections. The results in Fig.5.21 indicate that, when using four disk magnets as driving magnets, the iron ball can be smoothly spun at the same speed as the disk magnets.

5.4 IEM Analysis of Rotational Torque of Iron Ball

In order to examine the validity of the simulation results, the remanent magnetization point on the iron ball was simplified and modeled. The IEM analysis of the rotational torque of the iron ball was completed using the ELF/Magic software.

5.4.1 Modeling the Remnant Magnetization Points

According to the measurement results of the magnetic flux density on the surface of the iron ball and the model of simulation, the remanent magnetization point on the surface of the iron ball can be seemed as a permanent magnet, whose one pole is on the surface of the iron

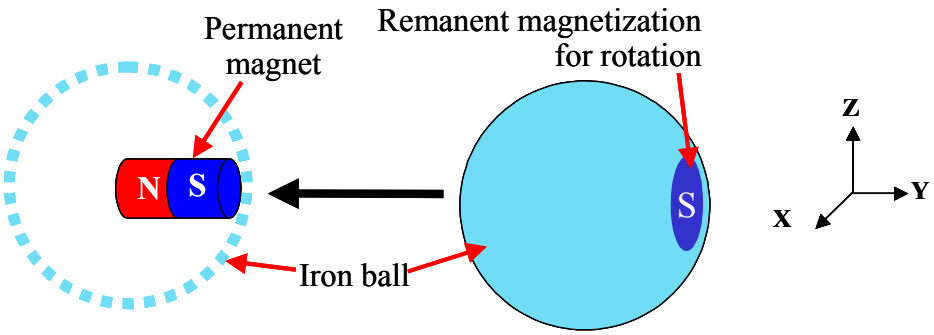

Fig.5.22 The model of the remanent magnetization point

ball, and the other pole is in the center of the iron ball. Therefore, the pole of the permanent magnet in the center of the iron ball will not influence the rotational torque of the iron ball around the vertical axis of the ball. Based on the model of the simulation, if we assume the S pole is the pole of the remanent magnetization point on the side of iron ball, the model who causes the iron ball rotate in the horizontal direction, can be created as Fig.5.22. Using this simplification of the remanent magnetization point, the IEM model was created and analyzed.

5.4.2 IEM Analysis Model and Results

The IEM analysis model used magnet I only is shown in Fig.5.23. In the model, the upper permanent magnet is using for suspending the iron ball, and the diameter and the length are 8mm. The round disk magnet is using for spinning, and the diameter is 30mm and the thickness is 10mm. The two thin and long permanent magnets are regarded as the remanent magnetization points, and the diameter is 5mm and the length is 15mm. The material of all the permanent magnets is N48 of Neodymium. The distance between the center of the iron ball and the disk magnet is 60mm.

The IEM analysis was carried out with the same process with the simulation of the

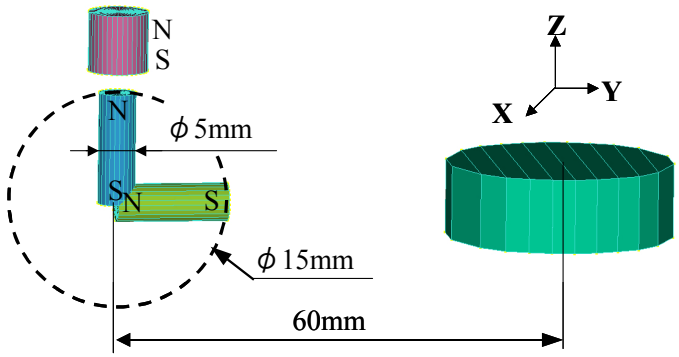

Fig.5.23 IEM analysis model using magnet I only

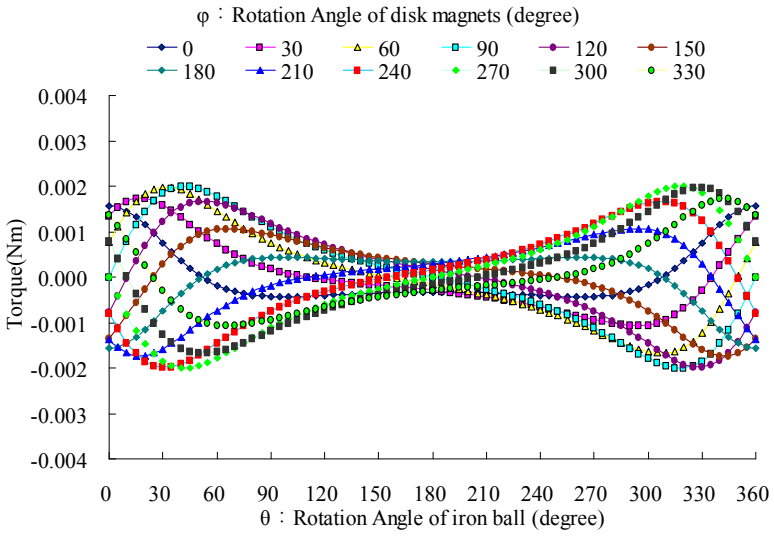

Fig.5.24 Rotational torque of IEM analysis using magnet I only

rotational torque. The analysis result used magnetic I only is shown in Fig.5.24. This result is similar to the simulation result, but the value of the torque is different. The different magnetic field density of the remanent magnetization point causes the difference of the value.

The IEM analysis model used magnet I and III is shown in Fig.5.25, and the analysis result is shown in Fig.5.26.

The IEM analysis model used four magnets is shown in Fig.5.27, and the analysis result is shown in Fig.5.28. The result is also similar to the simulation result, and the value is also different.

However, the relationship of the maximum value between the results in three cases is almost same.

5.4.3 Rotational Torque in Stable Rotational State

In order to examine the rotational stability of the iron ball, its rotational torque was examined using IEM analysis for $\theta = -\varphi+90°$, and the results are shown in Fig.5.29. From the results, we can see that the torques in all three cases oscillate about 0 Nm; however, the

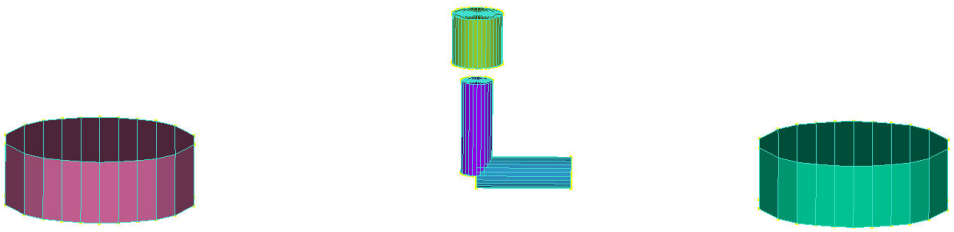

Fig.5.25 IEM analysis model using magnet I and III

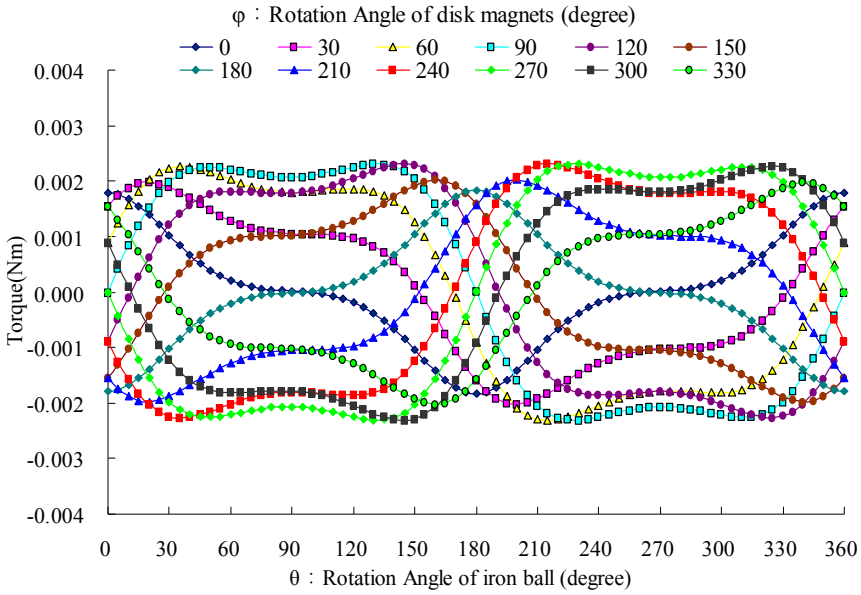

Fig.5.26 Rotational torque of IEM analysis using magnet I and III

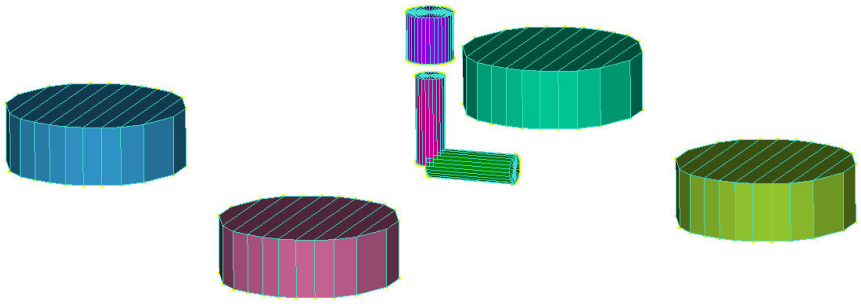

Fig.5.27 IEM analysis model using magnet I and III

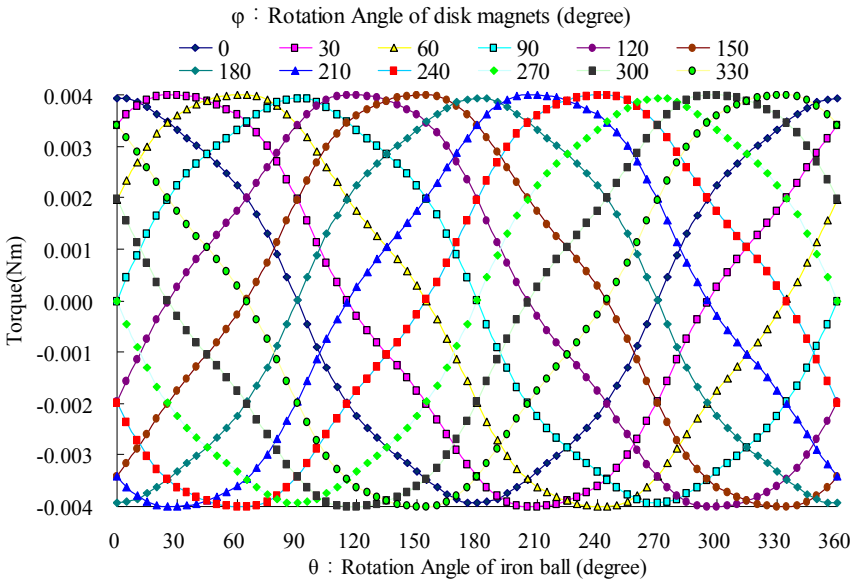

Fig.5.28 Rotational torque of IEM analysis using four magnets

amplitude of the torque when using all four magnets as the driving magnets is much smaller than the other two cases. There are two vibration periods in one revolution with one and two driving magnets, and four vibration periods with all four magnets. Consequently, the rotational stability with four magnets is better than the other two cases.

5.4.4 Horizontal Force

To examine the effect of the number of magnets on suspension stability, the attractive force of the iron ball was examined by IEM analysis, and the results are shown in Fig.5.30. These results indicate that the higher the number of installed magnets, the larger the generated attractive force in the x-y plane. As a result, the suspension stability will be destroyed by the centrifugal force when the iron ball spins at high angular velocities.

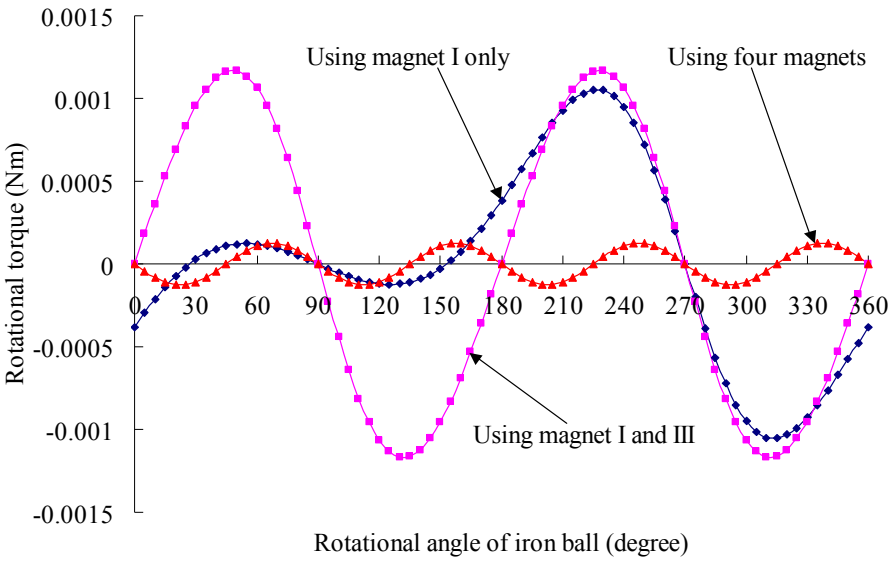

Fig.5.29 Rotational torque when θ = -φ+90° in the stable state

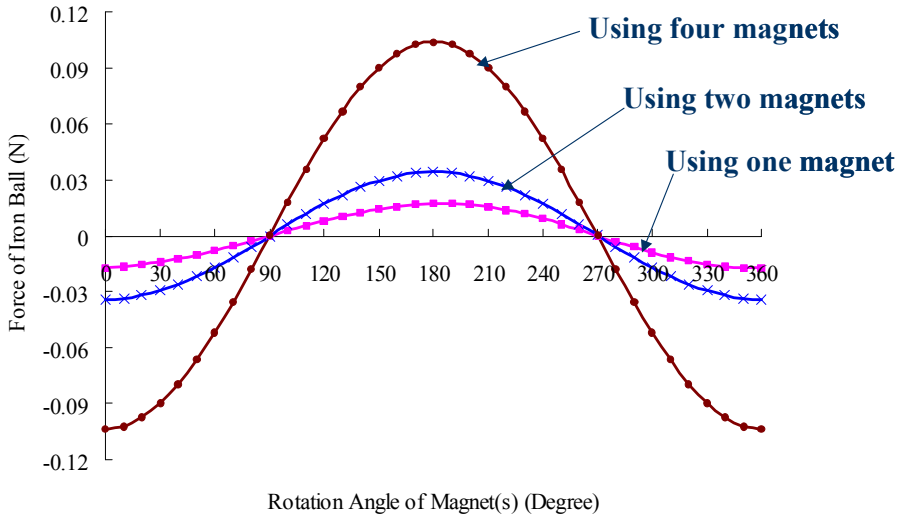

Fig.5.30 Attractive force of the iron ball in the x-y plane

5.5 Experimental Measurement of Rotational Torque

5.5.1 Measurement device set up

According to the model in IEM analysis, and considering about that the remanent magnetization point on the top of the iron ball cannot influence the rotational torque in horizontal direction, a measurement device was set up with one remanent magnetization point

on the side of the iron ball. The modeling process and the configuration of the measurement device are shown in Fig.5.31. In the measurement device, an aluminum pipe was installed on a rotational stage. A permanent magnet that was regard as a remanent magnetization point was installed on the pipe. The diameter of the magnet is 5mm, and the length is 15mm. The S pole of the magnet is at the position where is the surface of the iron ball, and the N pole of the magnet is at the position where is the center of the iron ball. Two pieces of strain gauges for rotational torque were pasted on the opposite side of the aluminum pipe. The strain gauge has two axes (0˚/90˚), whose resistance is 350Ω, and the ratio of gauge is about 2.1. Using this measurement device, the rotational torque of the mechanism was measured in the same process with the simulation and the IEM analysis. Fig.5.32 shows the photograph when the measurement experiment is carried out.

5.5.2 Experimental Results of Rotational Torque

The experimental results of the rotational torque are shown in Fig.5.33 to Fig.5.35. The results are almost same with the simulation results and the IEM analysis results, although there are some errors, which are caused by the accuracy of the measurement experiments. The rotational characteristics of the mechanism also can be illuminated according to the results.

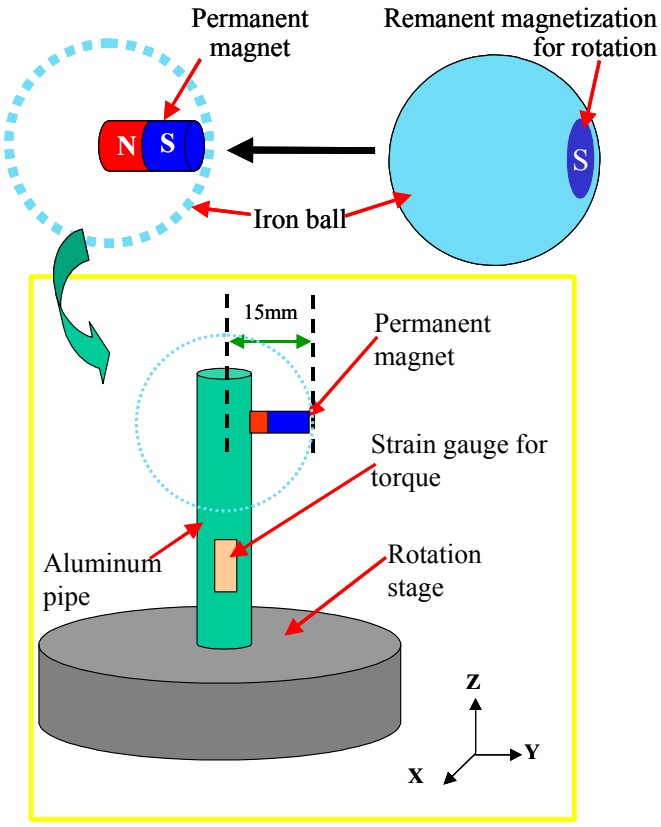

Fig.5.31 The configuration of the measurement device

Fig.5.32 Experimental measurement photograph

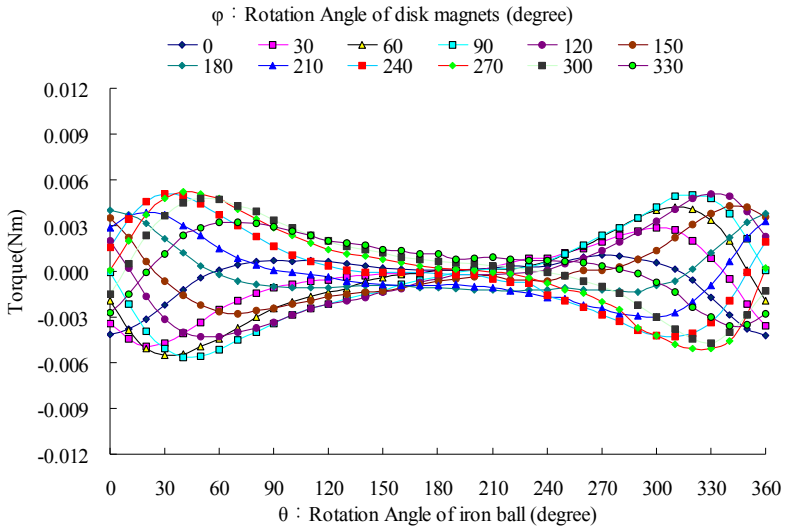

Fig.5.33 Rotational torque of experimental measurement using magnet I only

The measurement results of the rotational torque in the stable rotational state are shown in Fig.5.36. The trend of the graph is similar to the IEM analysis results. The vibration of the torque using four magnets is smallest.

Since all the experimental results are similar to the simulation and IEM analysis results, the validity of the simulation results and the IEM analysis results are verified.

5.6 Conclusions

In order to understand the variation of magnetic flux field of the mechanism, when the disk magnets was rotating, the 2-D analysis model was created, and the magnetic flux field was

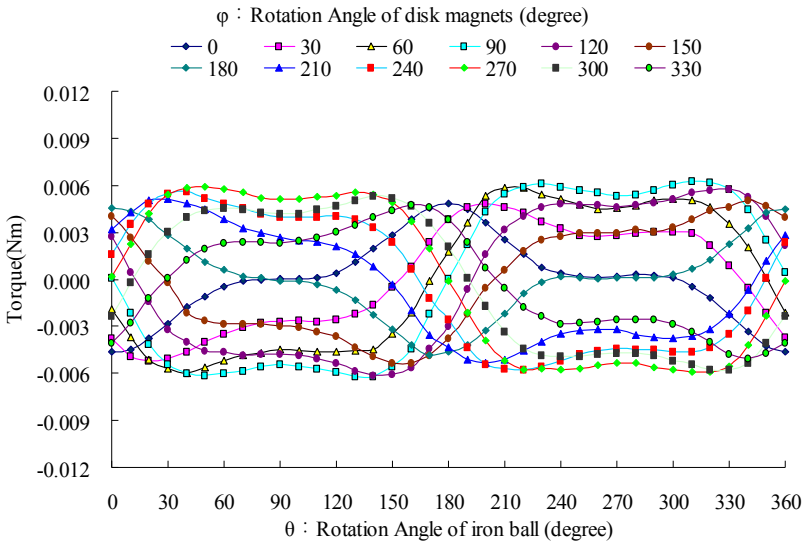

Fig.5.34 Rotational torque of experimental measurement using magnet I and III

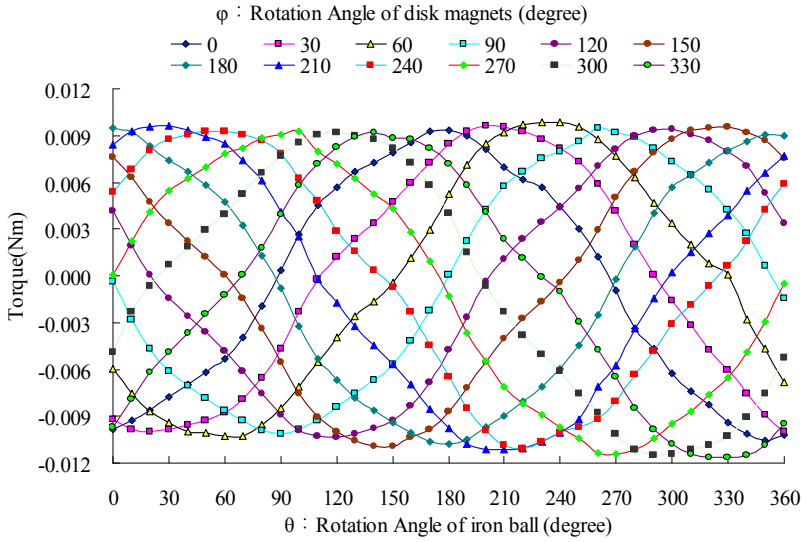

Fig.5.35 Rotational torque of experimental measurement using four magnets

analyzed. The analysis results indicate that the magnetic flux field around the iron ball can be changed while the magnet rotates. As the number of the magnet increases, the variation of the magnetic flux field becomes well proportioned.

In order to examine the rotational characteristics of the mechanism, the 3-D analysis model and the measurement device were created, and the rotational torque was examined by simulation, IEM analysis, and experimental measurement. All the results indicate that the iron ball could be spun regardless of the number of driving magnets used, however, as more magnets were used, the iron ball was spun more smoothly. But the attractive force of the iron ball in the horizontal direction also increased, the centrifugal force increased. As a result, the

velocity limit decreased.

Therefore, all the examination results in this chapter illuminate the reasons of the rotational characteristics of this noncontact spinning mechanism.

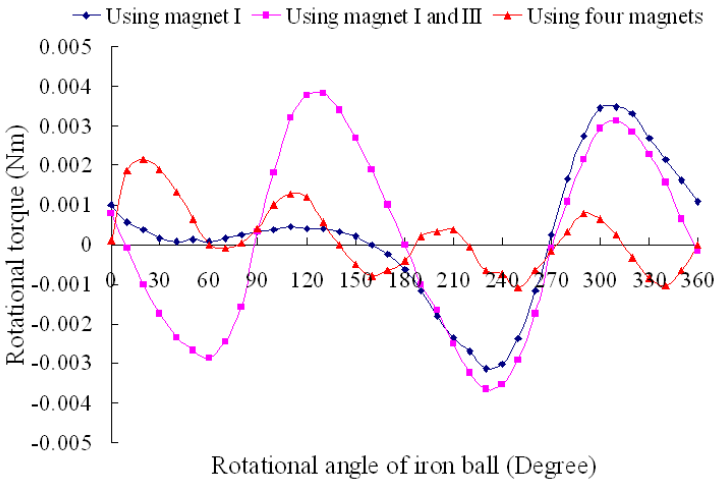

Fig.5.36 Rotational torque when θ = -φ+90° in the stable state

Part III Variable Flux Path Control Mechanism

Chapter 6 Development of a Magnetic Suspension System Using Variable Flux Path Control Method

6.1 Introduction

So far, many magnetic suspension systems have been developed, and various control methods of suspension force have been proposed [9]. In the magnetic suspension systems using permanent magnets, there are mainly two control methods of suspension forces, which are the air gap length control and the variable flux path control [24]. Using the air gap length control, some magnetic suspension systems have been proposed for noncontact transmission and manipulation applied in the super-clean room [25,26]. Using the variable flux path control, the zero-power magnetic suspension system has been developed with the composite of magnetostrictive and piezoelectric materials [53]. Moreover, a flux path control magnetic suspension system has been reported with the motion control of a part of ferromagnetic yokes in a magnetic circuit [31]. However, most magnetic suspension systems have a disadvantage, which is once the suspended object adheres to the permanent magnets or the magnetic yokes, the suspended object cannot be controlled any more, unless another force is used to detach the suspended object from the magnets or magnetic yokes.

This chapter proposes a magnetic suspension system using a disk-type permanent magnet and a rotary actuator. In this suspension system, the suspension force is controlled by a variable magnetic flux path mechanism where the flux path is changed by varying the angle of the magnet. This system can generate a semi-zero suspension force, which can overcome the fore-mentioned disadvantage of the magnetic suspension system using permanent magnets. Moreover, this system also can realize the variable magnetic poles and an energy-saving suspension. In this chapter, the variable flux path control method of the suspension forces is introduced, and an experimental prototype is manufactured. An IEM analysis is carried out to verify the variable flux path control method. Some basic experiments and IEM analysis for the magnetic flux density and the attractive force are implemented to examine the basic characteristics of the mechanism and model the suspension force. According to the experimental results, the mathematical model is created, and the suspension feasibility is examined. Finally, the numerical simulation, and suspension experiments are carried out. The characteristics of the proposed mechanism are analyzed.

6.2 Principle of Variable Flux Path Control Mechanism

The principle of variable flux path control mechanism can be understood from Fig.6.1. This figure shows a schematic diagram of a disk permanent magnet, two opposite F-type iron cores and a suspended object. In order to understand easily, we assume that: (I) The magnet has an N pole of 90 degrees and an S pole of opposite side 90 degrees as shown in Fig. 1; (II) There is no flux leakage to the air in this magnetic suspension system. Fig.6.1 (a) shows that the magnetic poles of the magnet are aligned in the vertical direction, and the N pole is at the upper side and the S pole is in the lower side. In this case, the facing angle of the N pole and S pole to each core are same, so all magnetic flux comes from the N pole and is absorbed into the S pole through each core respectively. There is no flux flowing through the suspension object, so zero attractive force generates between the cores and the levitated object. However, Fig.6.1 (b) shows the magnet rotated a certain angle, the facing angle of the N pole becomes bigger than the S pole in the right core, and that is reverse in the left core. Since that, the flux from the N pole in the right core is more than that in the left core. Some of the flux in the right core flow through the suspension object to the left core and is absorbed by the S pole. Consequently, there are some flux flowing through the levitated object, and the attractive force is generated. The flux flowing through the levitated object becomes more as the rotated angle is larger, until the rotated angle reaches 90 degrees. After 180 degrees, the direction of the flux flowing through the levitated object is reversed. The magnetic suspension system changed the magnetic poles of the stator cores. According to this process that is called variable flux path, the attractive force is changed from zero, maximum, and zero, maximum to zero as the magnet rotates in one revolution.

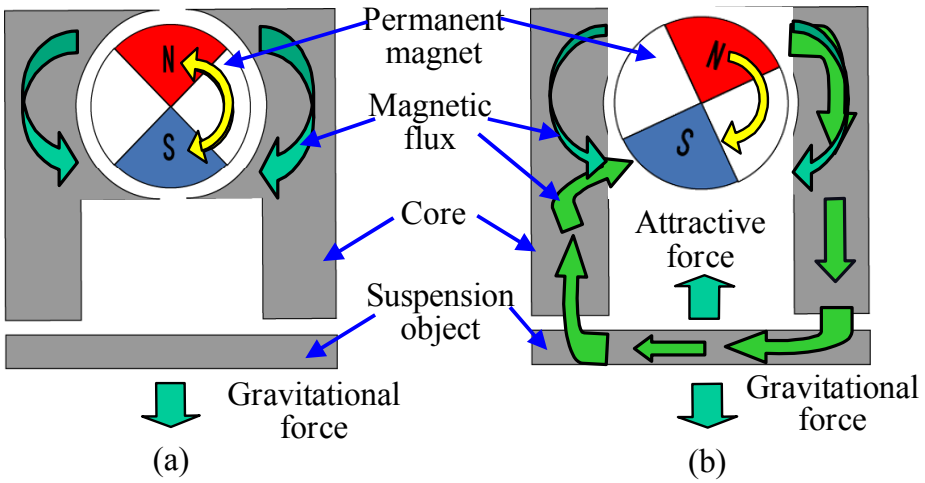

Fig.6.1 Principle of variable flux path control mechanism

6.3 Experimental Prototype

Fig.6.2 shows an illustration of the proposed magnetic suspension device. And an experimental prototype of the proposed magnetic suspension system was constructed, and the photograph of the prototype is shown in Fig.6.3. This prototype consists mainly of a disk-type permanent magnet, a rotary actuator containing a gear reducer and an encoder, a pair of opposite F-type permalloy cores, a suspended object and two eddy current sensors. The magnet that is located in the opposite F-type cores is a neodymium magnet and magnetized in radial direction. The diameter of the magnet is 30 mm and the thickness is 10 mm. A rotary actuator behind of the magnet drives the magnet rotate. The actuator that has an encoder

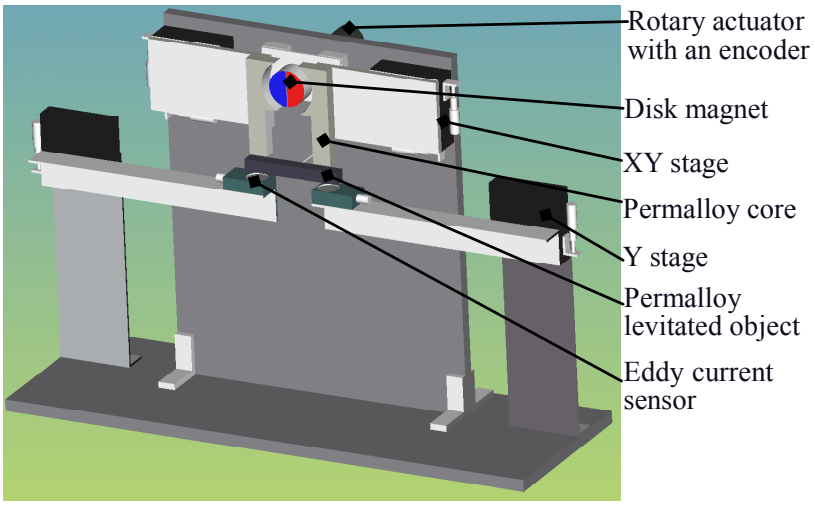

Fig.6.2 Illustration of the developed prototype

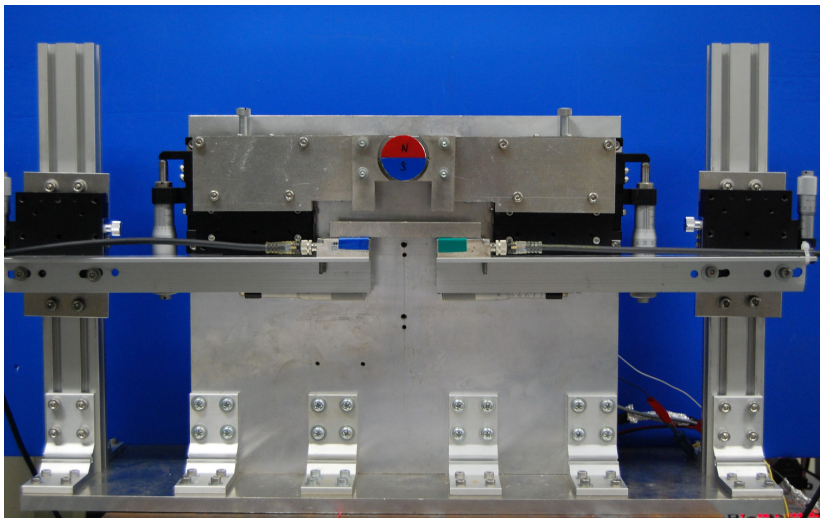

Fig.6.3 Photograph of the developed prototype

measuring the angle of the magnet cannot be seen in Fig.6.3. the encoder of the actuator The thickness of the two cores is 10 mm that is same as the magnet. The suspended object is a Permalloy tetragonal prism. The position of the levitated object is measured by an eddy current sensor, of which the measurement range is from 2 mm to 3 mm and the repeat accuracy is 10 μm.

Fig.6.4 shows the whole configuration of the magnetic suspension system. In the control system, the PD feedback loops are used to realize the suspension of the suspended object. Based on the signals of the eddy current sensors and the encoder, the DSP controller calculated the optimal current of the actuator to control the angle of the permanent magnet.

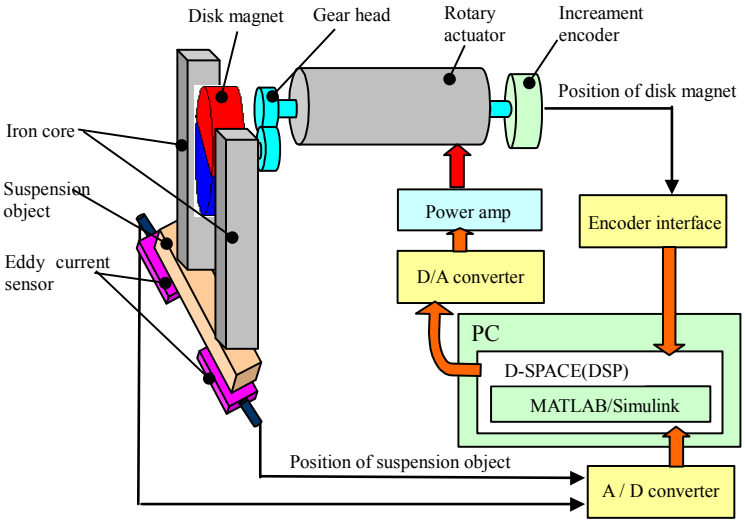

Fig.6.4 Configuration of the magnetic suspension system

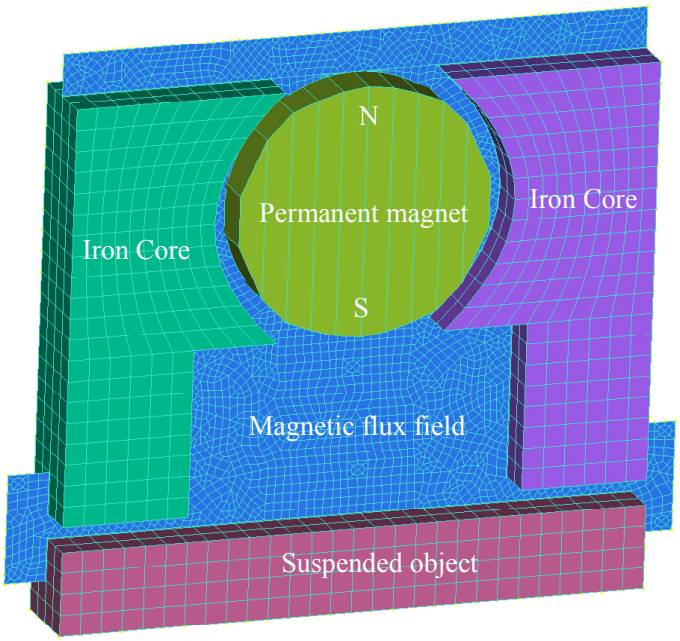

Fig.6.5 IEM analysis model in ELF/Magic software

6.4 IEM Analysis of the Suspension Mechanism

In order to verify the variable flux path control method, an analysis model was created, and the magnetic flux field of the mechanism was examined. Moreover, the magnetic flux density and the attractive force between the iron cores and the suspended object were calculated.

6.4.1 Analysis of Magnetic Flux Field

First, a 3-D analysis model was created in the same dimension with the experimental prototype using the ELF/Magic software, and shown in Fig.6.5. In the model, the magnetic flux field in air space is expressed as the blue field in 2-D, and in the middle position of the thickness direction of the mechanism. The magnet is the roundness in the center of the cores, and when the N pole and S pole are arranged as shown in Fig.6.5, the rotational angle of the

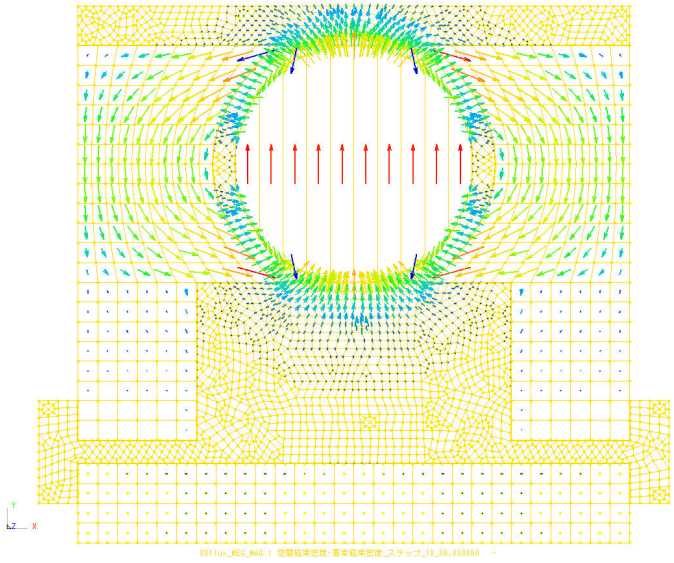

Fig.6.6 Analysis result of magnetic flux field (0 degree)

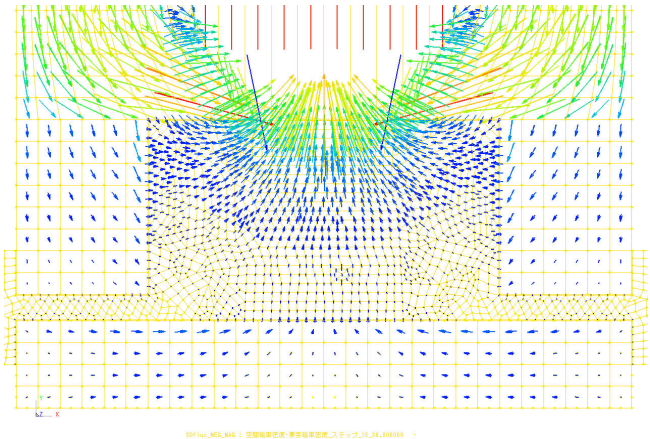

Fig.6.7 Enlarged analysis result with 4 times (0 degree)

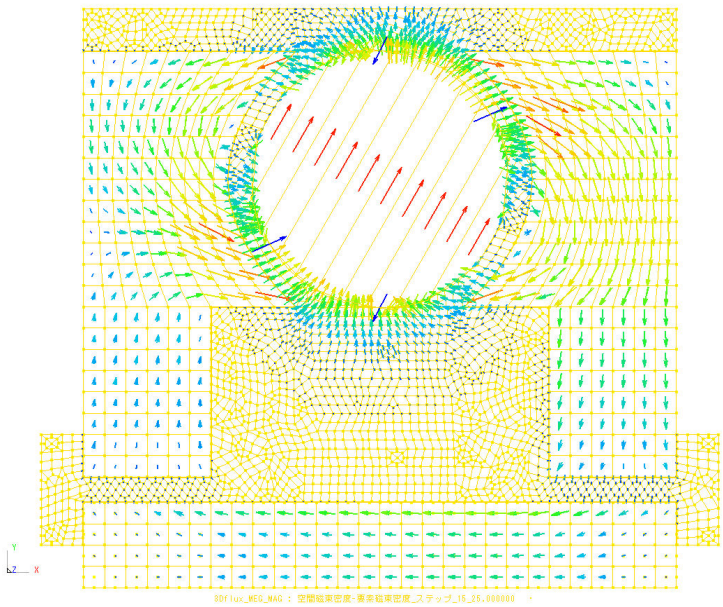

Fig.6.8 Analysis result of magnetic flux field (30 degrees)

magnet is assumed as 0 degree. The air gap between the magnet and the iron cores is 2mm, and the distance between the iron cores and the suspended object is 3mm.

Using the analysis model shown in Fig.6.5, the magnetic flux field was analyzed. The analysis results are shown in Fig.6.6 to Fig.6.9. In the figures, the direction of arrows express the direction of the magnetic flux, and the size and color of the arrows express the intensity of the magnetic flux density.

Fig.6.6 shows the analysis result when the magnet stops at 0 degree. Fig.6.7 shows the 4-time enlarged figure of the lower side of Fig.6.6. In these results, the magnetic flux that comes from N pole of the magnet almost returns to the S pole only through the upper side of the iron cores, and there is a little part of magnetic flux flows through the lower side of the iron cores, the suspended object, and the air space, finally returns to the S pole. Therefore, the attractive force between the iron cores and the suspended object is not zero exactly, but is very small. This problem is caused by the magnetic flux leakage in the mechanism. However, if the magnetic reluctance of the cores is small enough, the results will be same with the proposed principle.

Fig.6.8 shows the analysis result when the magnet stops at 30 degrees. From this result, we can see that one part of magnetic flux flows though the upper side cores, and returns to S pole directly. However, the other part of magnetic flux flows through the right core, the right air gap, the suspended object, the left air gap, and the left core, returns to the S pole that is facing the left core. Therefore, the attractive force generated at the air gap between the iron cores and the suspended object. Moreover, as the rotational angle of the magnet becomes large until 90 degrees, the part of the magnetic flux flowing through the suspended object will be large.

Fig.6.9 shows the analysis result when the magnet stops at 90 degrees, and Fig.6.10 shows the analysis result when the magnet stops at 270 degrees. From these results, we can see that almost magnetic flux flows through the suspended object, so the attractive force between the iron cores and the suspended object becomes maximal. And the direction of the magnetic flux is reverse to each other. Therefore, the magnetic poles of the two stators were changed each other.

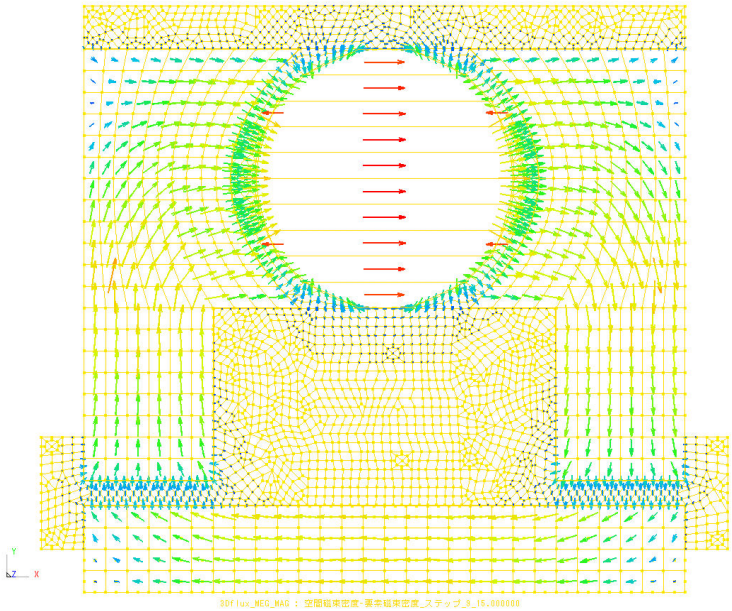

Fig.6.9 Analysis result of magnetic flux field (90 degree)

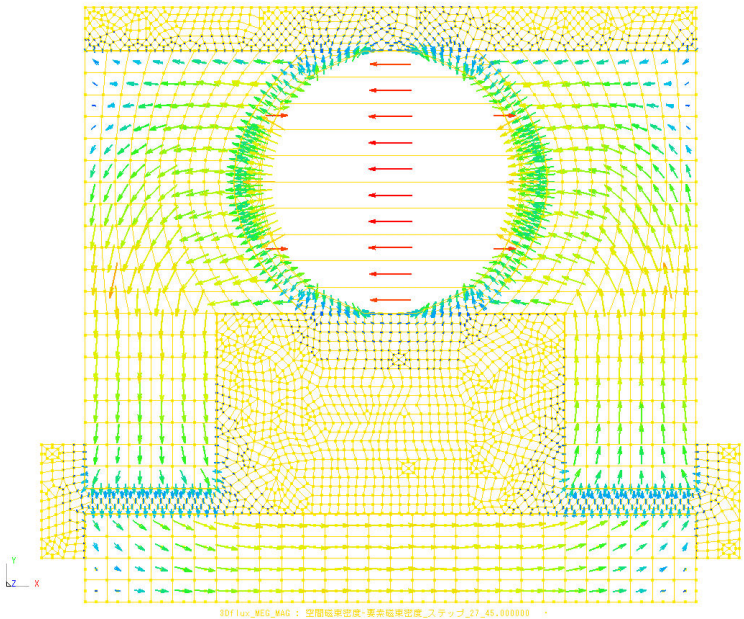

Fig.6.10 Analysis result of magnetic flux field (270 degrees)

6.4.2 Analysis of Magnetic Flux Density and Attractive force

The magnetic flux densities and attractive forces from the cores were calculated, when the permanent magnet was rotated at 10 degrees as one step in one revolution, and the air gap length between the cores and the levitated object was from 2 mm to 10 mm, and increased at 1 mm as one step.

Fig.6.11 shows the calculated magnetic flux density. The flux densities resemble sine curves according to the magnet's angles at all air gap lengths, and smaller distance yields greater flux density. Moreover, the flux direction is changing at about 180 degrees.

Fig.6.12 shows the calculated attractive forces. The force in each position varies according

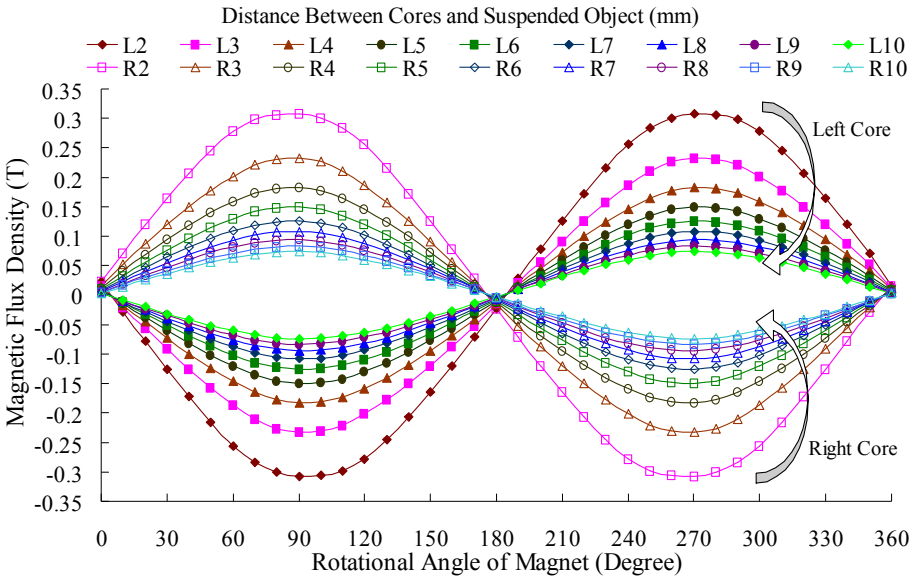

Fig.6.11 Magnetic flux density between cores and levitated object in IEM

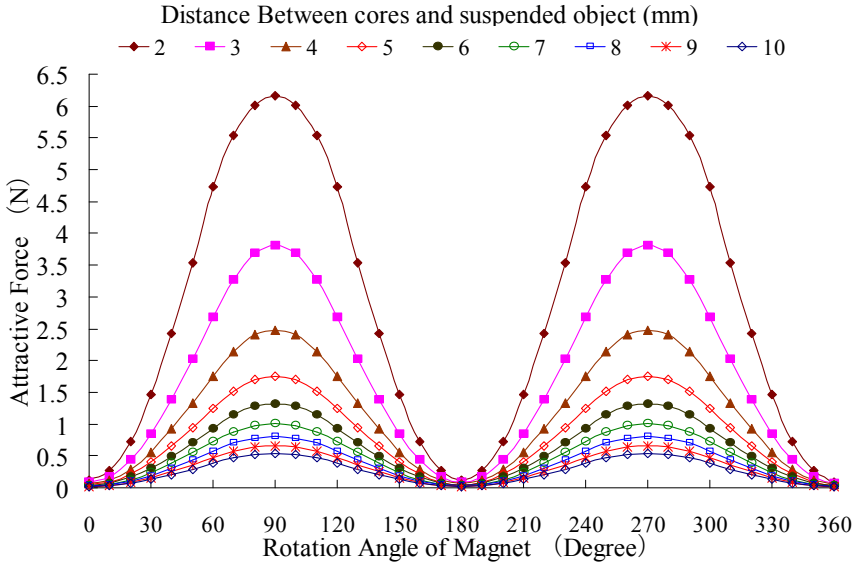

Fig.6.12 Attractive force between cores and levitated object in IEM

to the rotated angle of the permanent magnet, and has 2 maximum points at about 90 degrees and 270 degrees and 2 approximately zero points at about 0 degree and 180 degrees. Moreover, the forces become smaller when the gap becomes larger.

Moreover, Fig.6.13 shows the calculated rotational torque of the magnet. The results indicate that the toque of the magnet varies as a sine curve with a period of 180 degrees, and becomes large as the air gap between the cores and the suspended object becomes small.

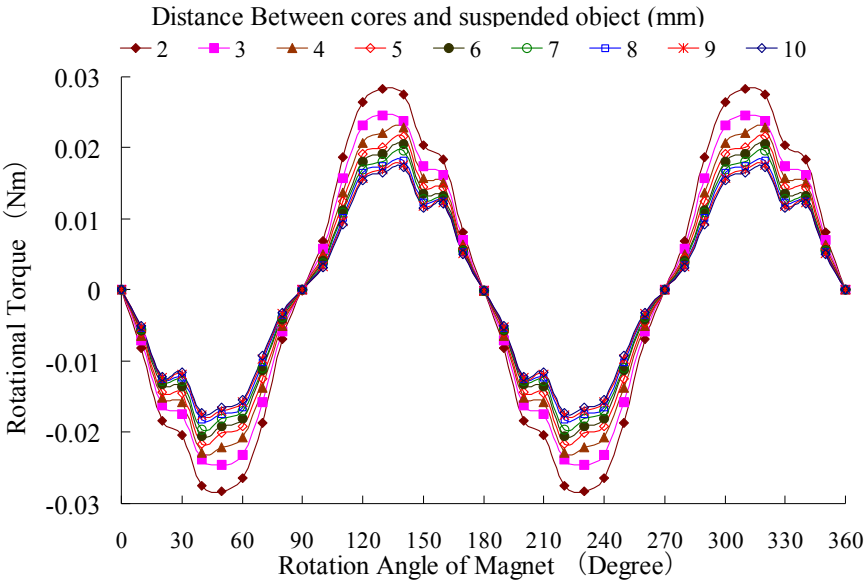

Fig.6.13 Rotational torque of the magnet in IEM

6.5 Basic Characteristics Examination by Experimental Measurement

In order to examine the basic characteristics of the magnetic suspension mechanism, some measurement experiments were carried out.

6.5.1 Magnetic Flux Density of the Permanent Magnet

To examine the magnetic characteristic of the permanent magnet and the influence of the distance from the magnet, the magnetic flux density of the permanent magnet was measured using a gauss-meter. The flux density was recorded, while the magnet rotated in one revolution and increased at 10 degrees as a step, and the distance from the magnet was changed from 1 mm to 8 mm and increased at 1 mm as a step. The measurement results are shown in Fig.6.14. From the results, it can be seen that the flux density curves resemble sine curves at all points, and smaller distance yields greater flux density. It means that the distance between magnet and iron cores is smaller; the attractive force generated by cores will be

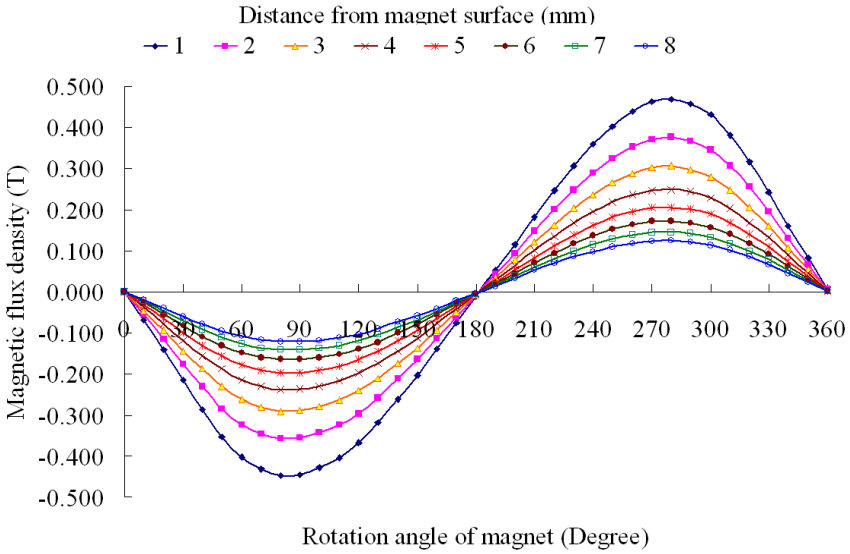

Fig.6.14 Magnetic flux density of permanent magnet

larger. In this prototype, the distance between the magnet and cores was set in 2 mm for considering the radial precision of magnet rotation.

6.5.2 Magnetic Flux Density Examination by Experiment

In order to examine the basic characteristics of the suspension mechanism, the magnetic flux density between the suspended object and two iron cores, the attractive force of two iron cores, and the rotational torque of magnet were measured. In the measurement experiment, the permanent magnet was rotated at 10 degrees as one step in one revolution, and the air gap length between the cores and the suspended object was increased at 1 mm as one step. The magnetic flux density was measured when the air gap length varied from 3 mm to 10 mm.

The magnetic flux density between the suspended object and two iron cores was measured with gauss meters. Measured results of magnetic flux density are shown in Fig.6.15 and Fig.6.16. Fig.6.15 shows the relationship between the magnetic flux density and the rotational angle of magnet. The graphs of magnetic flux density resemble sine curves according to the rotational angle of magnet at all air gap lengths, and the smaller distance yields greater magnetic flux density. Moreover, the magnetic flux direction is changing at about 180 degrees. Fig.6.16 shows the relationship between the magnetic flux density and the air gap. The graph indicates that the flux density is approximately in inverse proportion to the length of air gap.

6.5.3 Attractive Force Examination by Experiment

The attractive force between the suspended object and two iron cores was measured with a load sell, when the air gap length varied from 2 mm to 8 mm. The measured results of attractive force are shown in Fig.6.17 and Fig.6.18. Fig.6.17 shows the relationship between

the attractive force and the rotational angle of magnet. In the figure, the force is expressed when the rotational angle of magnet is changing and the length of air gap is seemed as a parameter. The results indicate that, the attractive force varies as the rotational angle of magnet changes, and smaller distances yield greater attractive force. Moreover, the attractive forces are almost zero when the rotational angle is around 0 and 180 degrees, i.e. the N pole and S pole stop at directly above or below. The forces are maximums when the rotational angle is around 90 and 270 degrees. Fig.6 shows the relationship between the attractive force and the length of air gap. The figure indicates that the attractive force becomes large as the length of air gap becomes short.

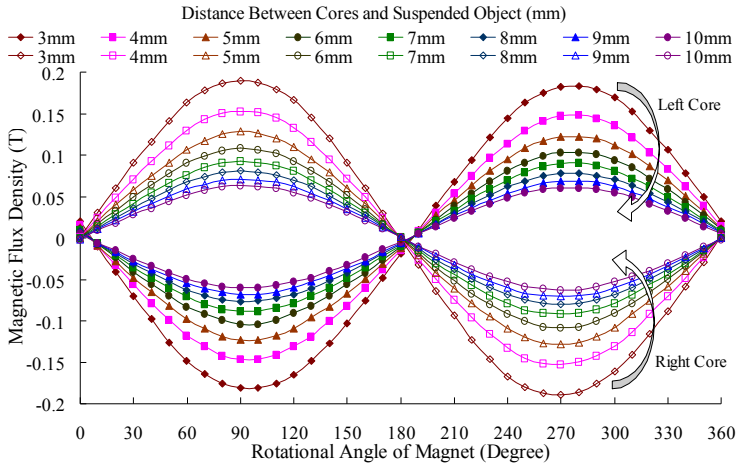

Fig.6.15 Relationship between flux density and rotation angle

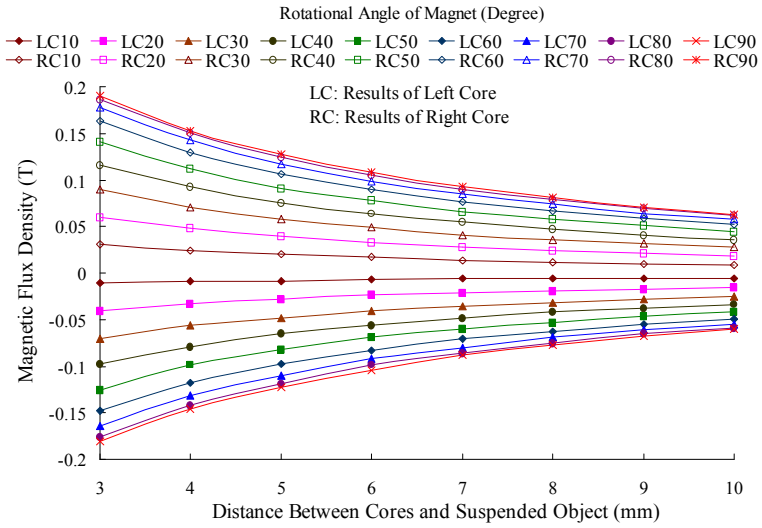

Fig.6.16 Relationship between flux density and air gap

6.5.4 Semi-zero Suspension Force Examination by Experiment

In order to examine the semi-zero attractive force characteristic, the force was measured when varying the distance between magnet and cores and the distance between cores and the suspended object. Fig.6.19 and Fig.6.20 show the results of attractive forces when the distance between the permanent magnet and the iron cores is expanded to 6 mm and 10 mm. These results indicate that the distance between the magnet and the iron cores cannot influence the variation tendency of the attractive force. However, comparing these results with Fig.6.15, when the distance is enlarged, the maximal magnitude of the attractive force becomes small, and the minimal magnitude of the attractive force at about 0 and 180 degrees becomes large between the permanent magnet and the iron cores.

Moreover, Fig.6.21 shows the results of attractive force as varying the distance between magnet and cores and the distance between cores and the suspended object, when the

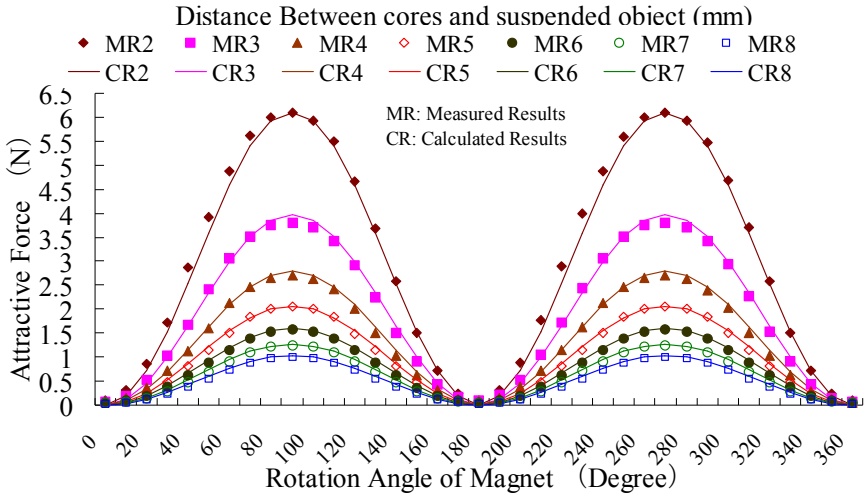

Fig.6.17 Relationship between attractive force and rotation angle

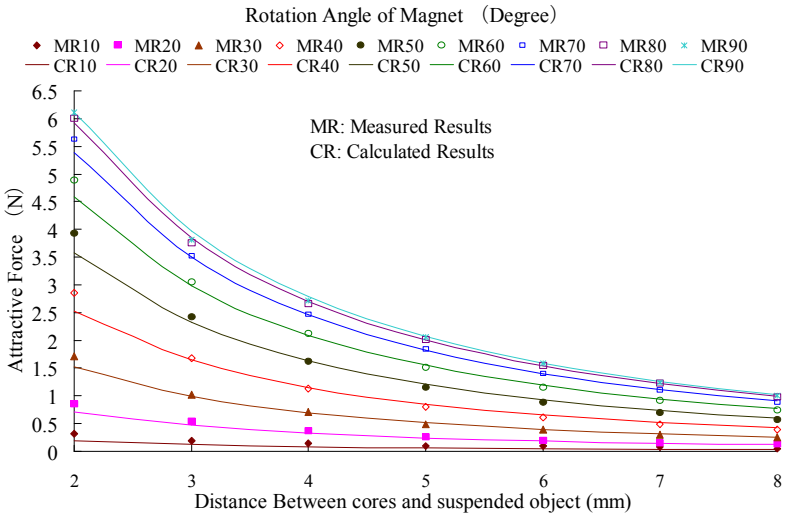

Fig.6.18 Relationship between attractive force and air gap

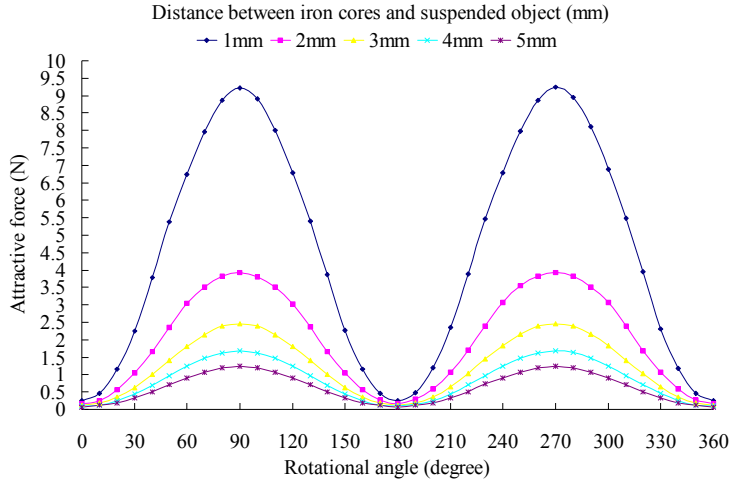

Fig.6.19 Suspension force when the distance between the permanent magnet and the cores is expanded to 6mm.

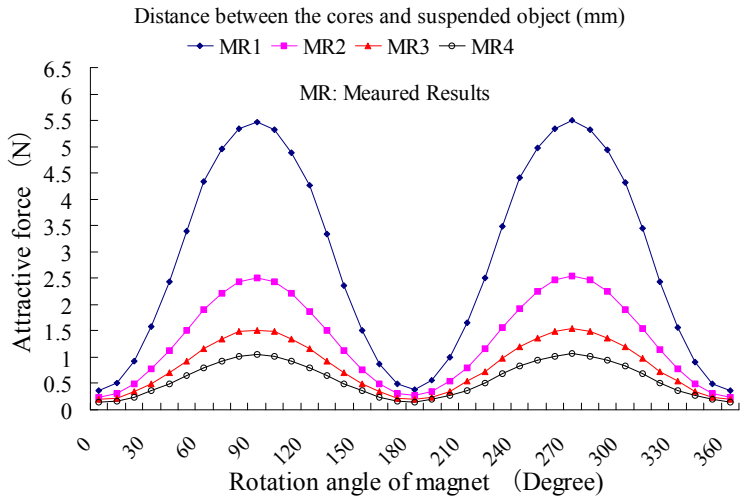

Fig.6.20 Suspension force when the distance between the permanent magnet and the cores is expanded to 10 mm.

rotational angle of magnet is at 0 degree. The results indicate the characteristic of the semi-zero suspension force as that smaller distance between cores and suspended object generates greater attractive force, and larger distance between cores and magnet generates greater attractive force. These are caused by the magnetic flux leakage of the device. As a result, the larger distance can cause the semi-zero suspension force characteristics of the magnetic suspension mechanism worse.

6.5.5 Experimental Examination of Rotational Torque of Magnet

For examining the effect of the magnetic potential to the permanent magnet, the rotational torque of magnet was measured with strain gauges, when varied the rotational angle of the permanent magnet and the air gap between iron cores and the suspended object. Two pieces of

strain gauges for measuring torques were pasted on the side of the connector between the rotary motor and the permanent magnet, and the rotational torque was measured in the same condition with measurement experiment of attractive force. The air gap length varied from 2 mm to 8 mm. The measurement device is shown in Fig.6.22. The measured results of the

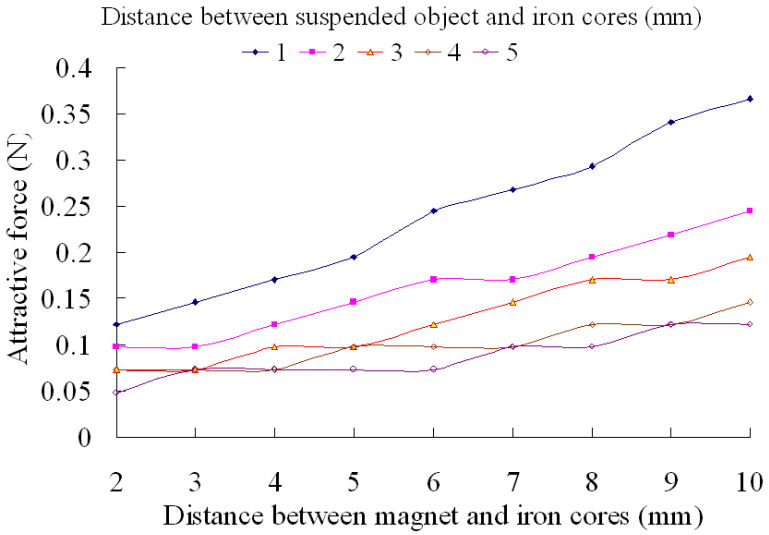

Fig.6.21 Attractive force when magnet stops at 0º

rotational torque are shown in Fig.6.23. The results are similar to the IEM analysis results, and indicate that the rotational torque is similar to a sine curve of two times of rotational angle, and decreases with increasing the air gap.

6.6 Mathematical Model and Feasibility Analysis

6.6.1 Modeling Suspension Force

According to the relationship of the flux density with the rotational angle θ and the length of air gap d shown in Fig.3 and Fig.4, and considering about the square relationship between the attractive force and the magnetic flux density, the attractive force f can be expressed as the following equation.

$$f = k_m \frac{\sin^2 \theta}{\left(d + \Delta d_f\right)^2} \tag{6.1}$$

Where k_m is a proportionality coefficient of attractive force and Δd_f is a compensation coefficient of air gap. Comparing the attractive force calculated by Equation (6.1) with the

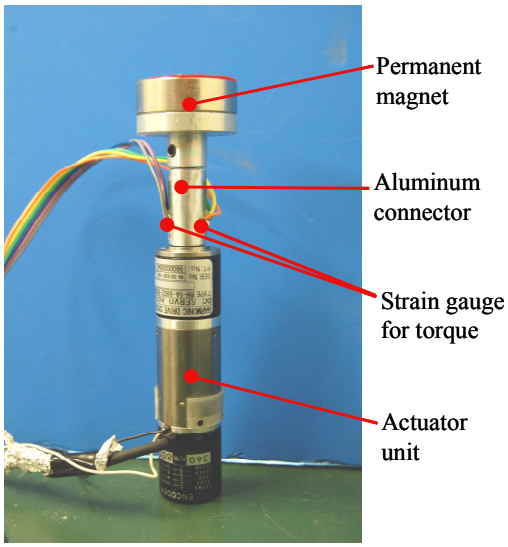

Fig.6.22 Measurement device for rotational torque of magnet

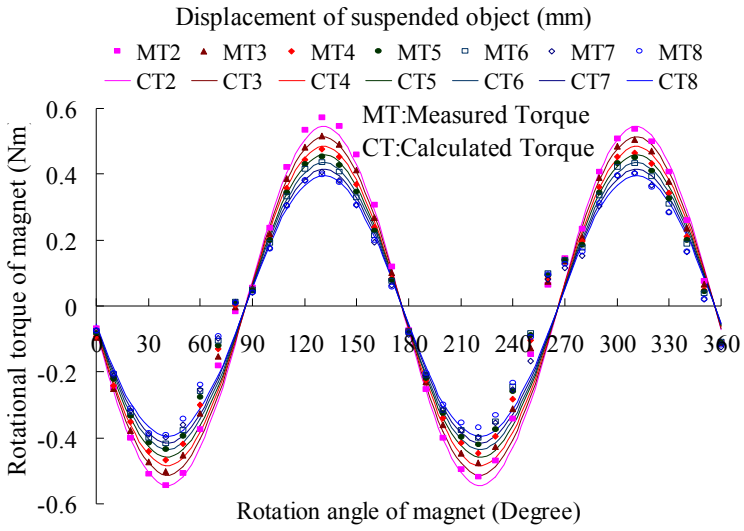

Fig.6.23 Rotational torque of permanent magnet

measurement results, the coefficients k_m and Δd_f can be decided as 1.06×10^{-4} Nm^2 and 2.17 mm. The comparison results shown in Fig.6.17 and Fig.6.18, where the solid line expresses the calculation force and the point mark expresses the measurement force. The comparison indicates that Equation (6.1) expresses the measurement results of the attractive force very well, and the validity of attractive force model is proved.

6.6.2 Modeling Rotational Torque of Permanent Magnet

According to the results shown in Fig.6.23, the rotational torque of magnet τ can be expressed by the rotational angle θ and the air gap d as the following equation.

$$\tau = k_\tau \frac{\sin 2\theta}{d + \Delta d_\tau} \tag{6.2}$$

Where k_τ is a proportionality coefficient of rotational torque and Δd_τ is a compensation coefficient of air gap. The coefficients k_τ and Δd_τ can be obtained from Fig.6.23 as -8.726×10^{-3} Nm^2 and 14 mm.

6.6.3 Motion Equations of Motor and Suspended Object

Using the mathematical model of the attractive force and the rotational torque of magnet and assuming the displacement of the suspended object as z in the upward direction, the motion equations of the motor and the suspended object can be expressed as:

$$J\ddot{\theta} = c_1\dot{\theta} + k_\tau \frac{\sin 2\theta}{d + \Delta d_\tau - z} + k_t i \tag{6.3}$$

$$m\ddot{z} = c_2\dot{z} + k_m \frac{\sin^2 \theta}{\left(d + \Delta d_f - z\right)^2} - mg \tag{6.4}$$

Where, J is the moment of inertia of motor and magnet; k_t is the torque constant of motor; m is the mass of the suspended object; c_1 and c_2 are the damping coefficients of the motor and the suspended object, respectively.

6.6.4 Suspension Feasibility Analysis

In the motion equations of this system, the attractive force fm is represented as a nonlinear function of the rotation angle of permanent magnet and the distance between core and iron ball. Moreover, the attractive force becomes larger as the rotation angle increases and becomes smaller as the distance decreases. Through linearization of the attractive force around the equilibrium position, the linear relationship of attractive force, rotation angle and the distance can be obtained.

$$\Delta f_m = \frac{2k_m(\sin\theta_0)^2}{(d_0 + \Delta d_f)^3} z + \frac{k_m \sin 2\theta_0}{(d_0 + \Delta d_f)^2} \Delta\theta \tag{6.5}$$

where,

Δf_m, z, $\Delta\theta$: the small value around the equilibrium position

θ_0, d_0 : the value at the equilibrium position

At same time, linearization of the rotational torque around the equilibrium position, the linear relationship of rotational torque, rotation angle and the distance can be obtained.

$$\Delta\tau = \frac{k_\tau \sin 2\theta}{(d_0 + \Delta d_\tau)^2} z + \frac{2k_\tau \cos 2\theta}{d_0 + \Delta d_\tau} \Delta\theta \tag{6.6}$$

Assuming that:

$$d_f = d_0 + \Delta d_f \tag{6.7}$$

$$d_\tau = d_0 + \Delta d_\tau \tag{6.8}$$

According to the equations from Equation (6.1) to Equation (6.8), the state space equation and the output equation are represented as:

$$\begin{aligned} \dot{x} &= Ax + Bu \\ y &= Cx \end{aligned} \tag{6.9}$$

where

$$x = \begin{pmatrix} z & \dot{z} & \theta & \dot{\theta} \end{pmatrix}'$$

$$A = \begin{bmatrix} 0 & 1 & 0 & 0 \\ \frac{2k_m(\sin\theta_0)^2}{md_m^3} & \frac{c_2}{m} & \frac{k_m \sin 2\theta_0}{md_m^2} & 0 \\ 0 & 0 & 0 & 1 \\ \frac{k_\tau \sin 2\theta}{Jd_\tau^2} & 0 & \frac{2k_\tau \cos 2\theta}{Jd_\tau} & \frac{c_1}{J} \end{bmatrix}$$

$$B = \begin{pmatrix} 0 & 0 & 0 & \frac{k_t}{J} \end{pmatrix}'$$

$$C = \begin{pmatrix} 1 & 0 & 0 & 0 \\ 0 & 0 & 1 & 0 \end{pmatrix}$$

$$u = i$$

The controllability matrix of the system of Equation (6.9) is

$$P_c = \begin{pmatrix} B & AB & A^2B & A^3B \end{pmatrix} \tag{6.10}$$

Then determinant of the controllability matrix is

$$\det(P_c) = \frac{k_m^{\,2} k_t^{\,4} \sin^2 2\theta}{d_m^{\,4} J^4 m^2} \neq 0 \tag{6.11}$$

$$Rank(P_c) = 4 \tag{6.12}$$

The determinant of the controllability matrix is nonzero, and the rank of the controllability matrix is full rank. Consequently, the proposed magnetic suspension system is controllable, and suspension feasibility is verified, theoretically.

6.7 Examination of Suspension Performance

In this study of suspension feasibility, first, the control system was introduced. Second, the feedback gains were calculated using the LQR (linear quadratic regulator) full state feedback control law with the linear mathematical model of Equation (6.9). Third, the numerical simulation was carried out using the calculated feedback gain with a nonlinear attractive force.

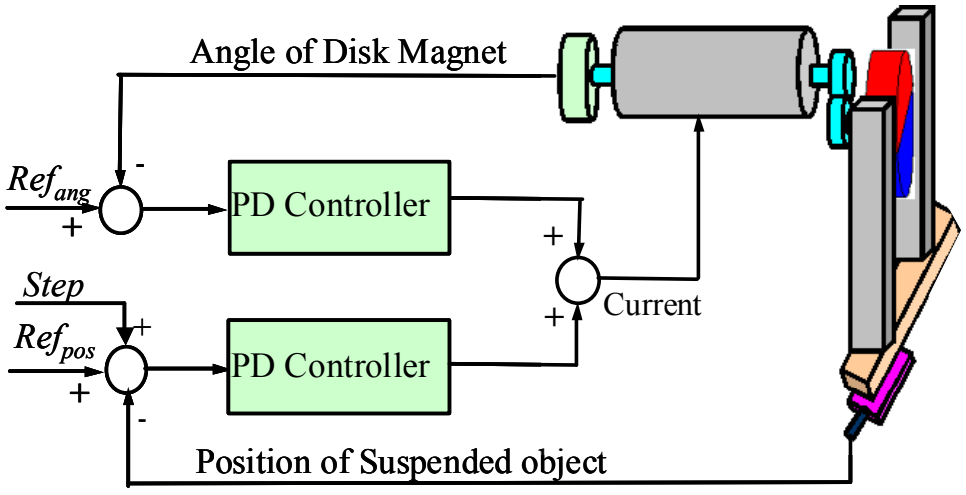

Fig.6.24 Structure of control system

Table.6.1 Parameters using in numerical simulation

Parameter	Value	Parameter	Value
m (kg)	0.232	c_1 (N/(m/s))	0.5
d_0 (mm)	1.8	c_2 (N/(m/s))	100
Δd_f (mm)	2.17	J (kgm^2)	6.37×10^{-4}
Δd_τ (mm)	14	k_t (Nm/A)	0.69
θ_0 (degree)	40	k_m (Nm^2)	1.06×10^{-4}
g (m/s^2)	9.8	k_τ (Nm^2)	-8.726×10^{-3}

Then, the experiment of suspension was carried out, and the performance of the semi-zero power suspension was also examined.

6.7.1 Control System

The structure of the control system is shown in Fig.6.24. In this control system, two PD controllers are used. Basing on the feedback signals of the encorder and the eddy current sensor, the input current of the motor is calculated, and the suspension force is controlled.

6.7.2 Calculation of Feedback Gains

All the parameters using in the numerical simulation are shown in Table.6.1, which are measured from the experimental prototype and the measurement experiment.

Many methods can design the controller for a linear system. In terms of linear control theory, due to this proposed system is controllable and observable, the LQR can be used to get the feedback gains.

Based on the characteristics of the system and Equation (6.9), we chose the state weighting matrix Q and input weighting matrix R as following:

$$Q=\begin{bmatrix} 10000000000 & 0 & 0 & 0 \\ 0 & 1 & 0 & 0 \\ 0 & 0 & 1 & 0 \\ 0 & 0 & 0 & 1 \end{bmatrix} \tag{6.13}$$

$$R=1 \tag{6.14}$$

Using MATLAB software, the feedback gain K is calculated as following:

$$K=\begin{bmatrix} 125930 & 282.87 & 145.48 & 0.615 \end{bmatrix} \tag{6.15}$$

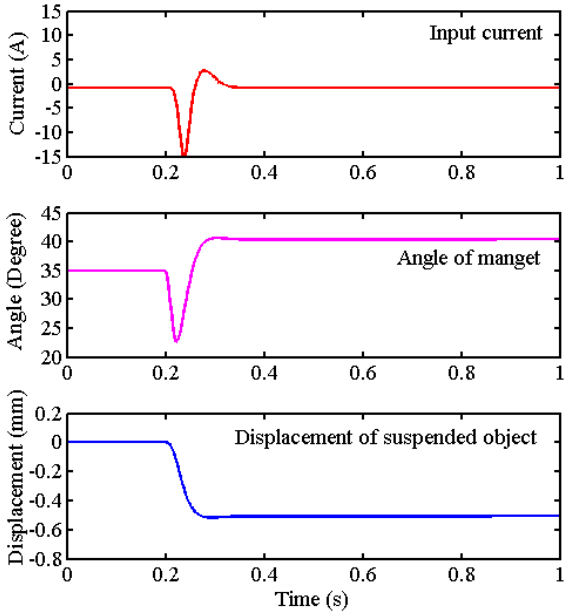

Fig.6.25 Simulation results with a suspended object of 0.232 kg

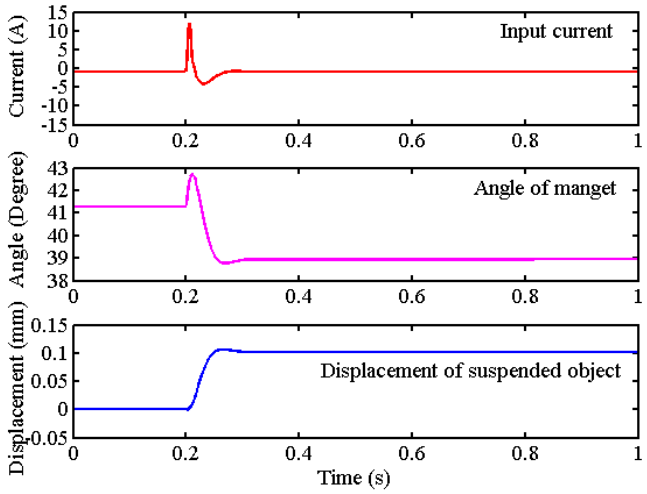

Fig.6.26 Simulation results with a suspended object of 1 kg

6.7.3 Simulation Results

In the simulation, the nonlinear attractive force and the nonlinear rotational torque are used directly, and the mass of suspended object is 0.232 kg. An input disturbance of a step of -0.4 mm was applied to the displacement of the suspended object, and the response was recorded until 1 second. The results of the response are shown in Fig.6.25. Moreover, the simulation with the suspended object of 1 kg also was carried out with an input step of 0.05 mm. And the simulation results are shown in Fig.6.26. The figures show the input current of motor, the angle of magnet, and the displacement of suspended object from up to down. As shown in

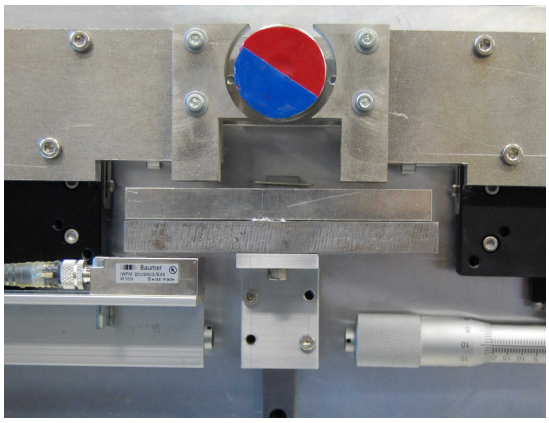

Fig.6.27 Suspending photograph with a linear rail

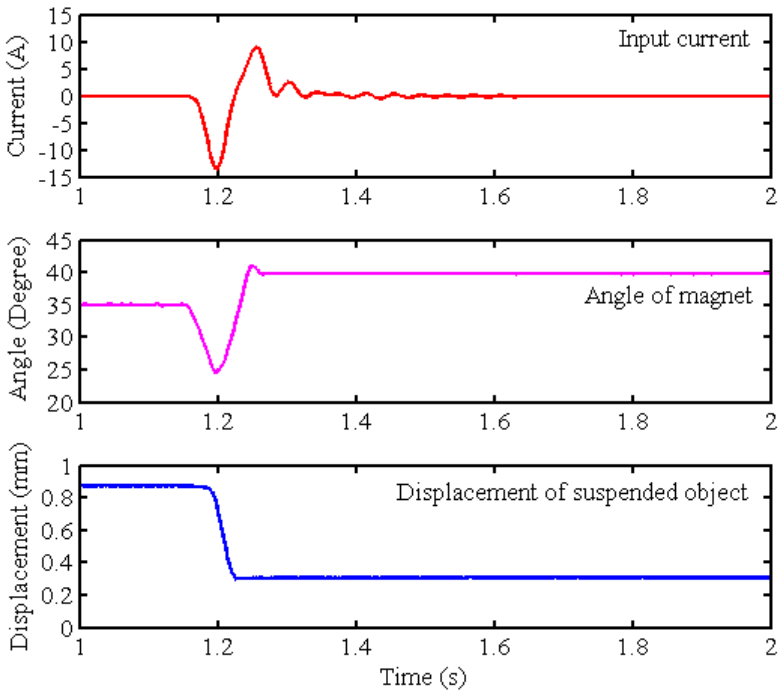

Fig.6.28 Experimental results with a suspended object of 0.232 kg

Fig.6.25 and Fig.6.26, after applying the disturbance, the system returns to stable state quickly, and the current is very small in the stable state.

6.7.4 Experimental Suspension Results

So far, owing to the flux leakage, the direct suspension using the cuboid levitated object cannot be succeeded. However, after using a linear rail to balance the unequal attractive forces of the two cores, the suspension has been succeeded. The photograph of successful suspension experiment is shown in Fig.6.27.

Fig.6.28 shows the step response results when the mass of suspended object is 0.232 kg,

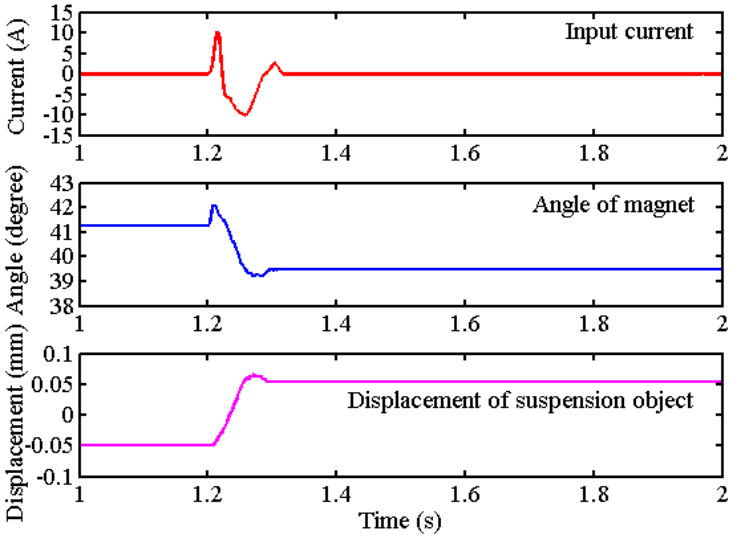

Fig.6.29 Experimental results with a suspended object of 1 kg

and the step input is –0.4 mm. Fig.6.29 shows the step response results when the mass of suspended object is 1 kg, and the step input is 0.05 mm. In the figures, the input current, the rotational angle of magnet, and the displacement of suspended object are recorded from 1 second to 2 seconds. The results indicate that the suspended object can be suspended stably and the input current is almost zero at the stable state. That means this magnetic suspension mechanism can suspend a heavy object by means of a small input force, since the gravitational force of suspended object is sustaining by the cores fixed on the frame. Therefore, this system can realize an energy-saving suspension.

6.7.5 Examination of Semi-zero Power Suspension Characteristic

In order to analyze the semi-zero power suspension performance of the suspension mechanism, the variation of the actuator current was examined when the weight of suspended object was changed. In the experiment, two kinds of examinations were carried out, which are fix angle examination and fix air gap examination.

In the fix angle examination, when the angle of magnet was adjusted to 40 degree each time after the suspended weight was changed, the actuator current was measured. The mass of the suspended object was changed from 0 to 1.44kg. The experiment results are shown in Fig.6.30. The results indicate that the actuator current increases as the mass is increased. If the rotational angle of magnet is maintained at same degree, the attractive force of the iron cores is constant. In this time, if increasing the weight of the suspended object and maintaining the suspended object in the stable suspension state, the length of air gap between the suspended object and the iron cores decreases. As the length of air gap decreasing, the potential force of

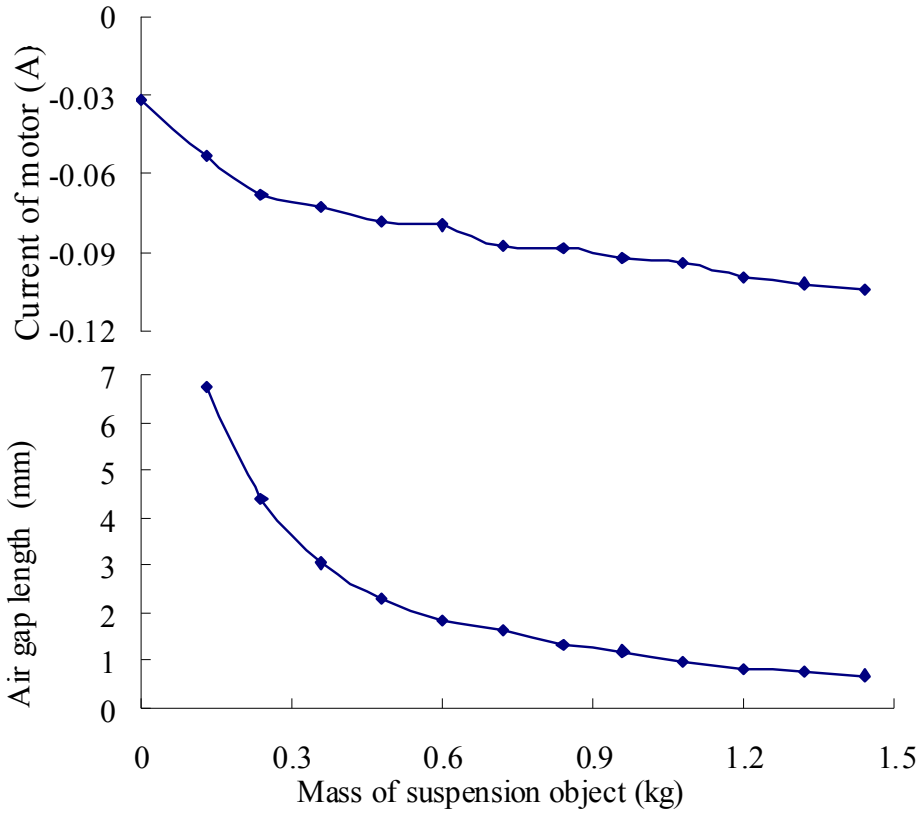

Fig.6.30 Semi-zero power suspension with changing air gap

magnetic filed is increased. Therefore, the current of the rotary actuator increases while the weight of the suspended object is increased. However, the current of the motor is very small. The maximum value is about 0.1 A. At the same time, the air gap becomes small. Comparing the current consumption with the weight of the suspended object, the semi-zero power suspension characteristic with changing air gap, and the minus stiffness characteristic of this suspension mechanism are affirmed, which are same with the general zero power magnetic suspension systems with an electromagnets.

Moreover, in the fix air gap examination, the current of motor was recorded when the mass was changing. The results are shown in Fig.6.31. From these results, we can see the angle of magnet is increasing, and the current increases, but the value of current is also very small. Therefore, these results indicate the semi-zero power suspension characteristics with the contant air gap.

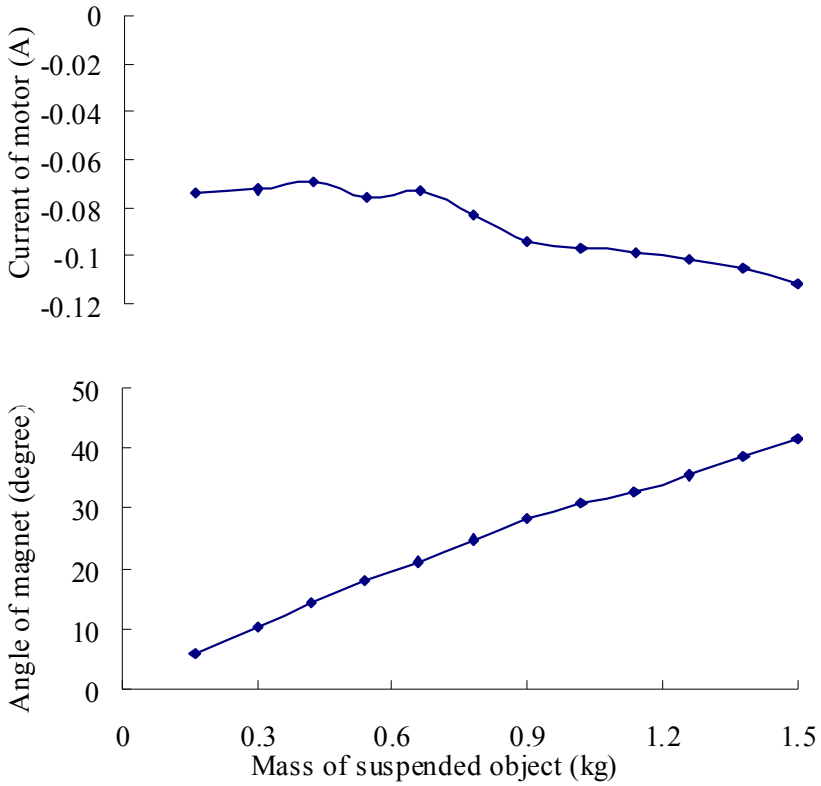

Fig.6.31 Semi-zero power suspension with constant air gap

6.8 Conclusions

A magnetic suspension system using a permanent magnet and a rotary motor was proposed, which controls the suspension force by variable flux path mechanism. First, the principle of the variable flux path control method was introduced, and a experimental prototype was designed and manufactured. According to the IEM analysis, the magnetic flux field of the mechanism was examined, and the magnetic flux density and the attractive force between the cores and the suspended object were calculated with a 3-D analysis model. At the same time, the rotational torque of the magnet was also calculated. Moreover, the magnetic flux density, attractive force, and the rotational torque of the magnet were measured by experiments. The mathematical model was created, and the suspension feasibility and the simulation were carried out. Finally, the suspension experiments were succeeded, and the energy-saving suspension characteristic was examined. Based on the results, the follows can be concluded.

According to control the rotational angle of the disk magnet that is installed on a rotary actuator, the magnetic flux path can be varied by a variable flux path control mechanism. As a

result, the suspension force can be controlled.

Through changing the rotational angle of the magnet, it not only can control the magnitude of the magnetic flux, but also can change the direction of the flux flowing in the mechanism.

The semi-zero suspension force can be generated by this mechanism. However, the suspension force is not zero exactly, since there is a leakage of the magnetic flux.

The suspension can be succeeded using this mechanism with a linear rail to limit the motivation direction to the vertical direction.

Since the iron cores support the gravitational force of the suspended object, and a reducer is used in the actuator, this system can suspend a heavy object by a small input current. This mechanism can realize two kinds of semi-zero power suspension characteristics with changing air gap and the constant air gap.

Chapter 7 Improvement for zero suspension force characteristics of variable flux path control mechanism

7.1 Introduction

The last chapter proposed a magnetic suspension system using a variable flux path control method. This magnetic suspension system has suspended the suspended object successfully, and the semi-zero suspension force, the variable magnetic poles, and the energy-saving suspension have been realized. However, the semi-zero suspension force was not exact zero yet. For this reason, this chapter try to improve the semi-zero suspension force characteristics on the basis of maintaining others characteristics of the mechanism.

According to the Fig.6.7, we have known that the attractive force was generated mainly by the leakage of magnetic flux between the permanent magnet and the suspended object, when the magnetic poles of S pole and N pole stopped at the vertical positions. In order to reduce the leakage of magnetic flux between the permanent magnet and the suspended object, we considered three kinds of methods to resolve the problem.

Insert a piece of ferromagnetic board to shield the leakage of magnetic flux between the permanent magnet and the suspended object.

Use a special type permanent magnet to reduce the magnetic flux leakage of the magnet when the magnetic poles of S pole and N pole stopped at the vertical positions.

Extend the distance between the permanent magnet and the suspended object to reduce the arrival magnetic flux.

Combine the method (2) and (3), use the special type permanent magnet and the extended iron cores.

In this chapter, the examinations of the semi-zero suspension force characteristics are carried out by IEM analysis and the measurement experiment. The comparison of the semi-zero suspension force characteristics is implemented between these four improvement methods and the original mechanism. Moreover, the suspension of simulation and experiment is also done with method (2).

7.2 Performance Comparison by IEM Analysis

In order to evaluate the performance of the mechanism improved by these three methods, three kinds of models were created, and the magnetic flux field, the magnetic flux density, and the attractive force were calculated by IEM analysis.

7.2.1 IEM Analysis for Inserting Ferromagnetic Board Method

7.2.1.1 Analysis Model

Fig.7.1 shows the analysis model of inserting a ferromagnetic board. This model is same with the model shown in Fig.6.5 in last chapter, and a ferromagnetic board is inserted to the air space between the magnet and the suspended object. The inserted board is an iron board, whose size is 3x10x20 mm. In Fig.7.1, since the half model is used, a half part of the inserted board can be seen in the length direction. The distance from the magnet to the inserted board is 5 mm, and the distance from the inserted board to the iron cores is 14 mm. The aim of inserting the iron board is to interdict the direct magnetic flux path from the magnet to the suspended object.

7.2.1.2 Analysis of Magnetic Flux Field

First, the magnetic flux field of the mechanism was analyzed. And the result when the magnet stops at zero degree is shown in Fig.7.2. Fig.7.3 shows the 4-time enlarged figure of the lower side of Fig.7.2. Compare them with Fig.6.6 and Fig.6.7, we can see that the flux flowing in the iron cores and the suspended object is not less than that in the original

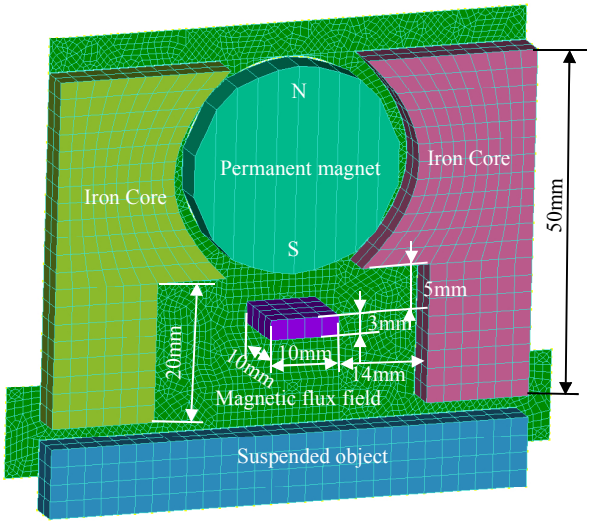

Fig.7.1 IEM analysis model of inserting a ferromagnetic board

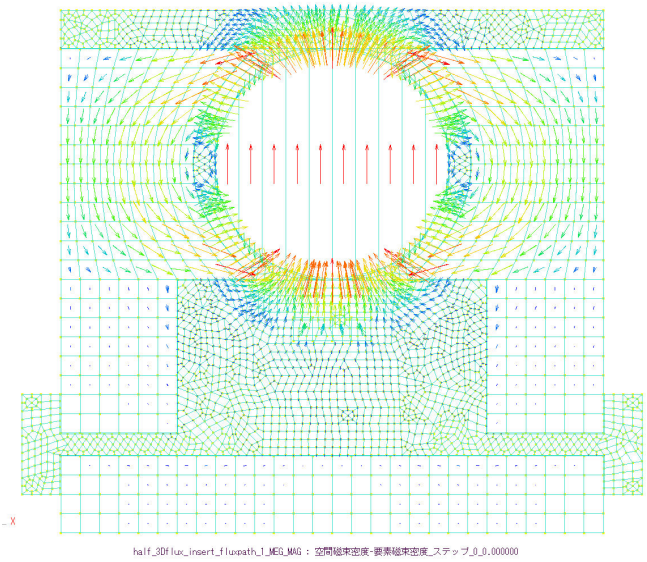

Fig.7.2 Analysis result of magnetic flux field (0 degree)

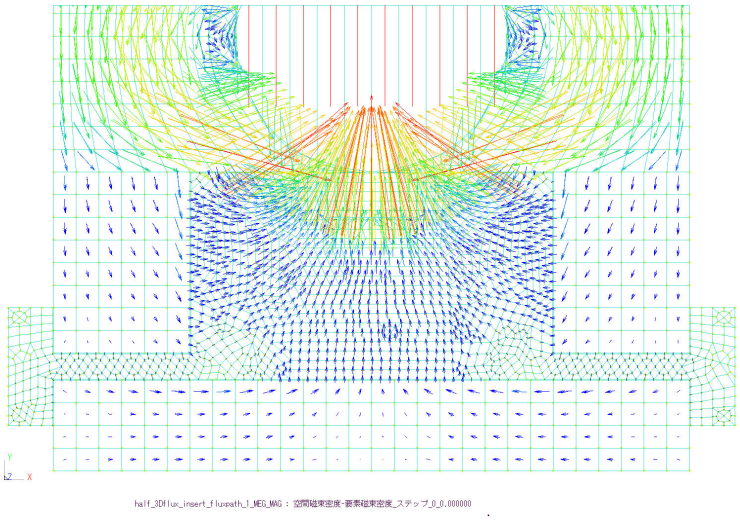

Fig.7.3 Enlarged analysis result with 4 times (0 degree)

mechanism almost, when the magnet stops at 0 degree. These results indicate that using the inserting ferromagnetic board method almost cannot reduce the magnetic flux between the magnet and the suspended object.

7.2.1.3 Analysis of Magnetic Flux Density

Fig.7.4 shows the analysis results of magnetic flux field using the inserting ferromagnetic board method. These results are similar to the results of the original mechanism.

7.2.1.4 Analysis of Attractive Force

Fig.7.5 shows the analysis results of attractive force using the inserting ferromagnetic board method. These results are also similar to the results of the original mechanism, but the

inserting the ferromagnetic board causes the attractive force at 2 mm of air gap and the 90 degrees of the angle a little difference from the origianal mechanism. This difference cannot influence the attractive force characteristics of the mechanism. However, these results are difficult to compare the the semi-zero suspension force charateristics, so the folowing section will compare the semi-zero suspension force charateristics of all the improvement methods.

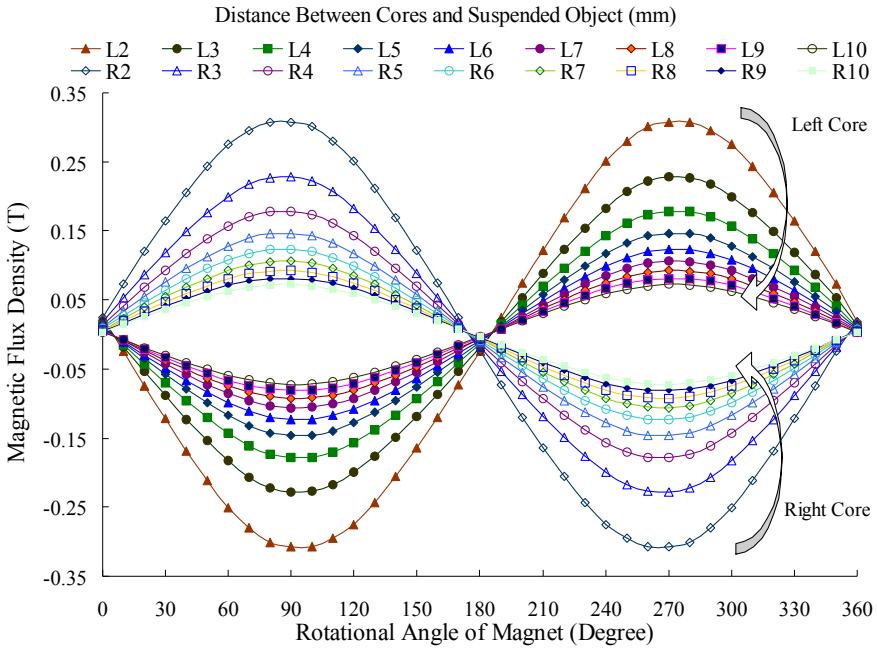

Fig.7.4 Analysis of magnetic flux field of inserting ferromagnetic board

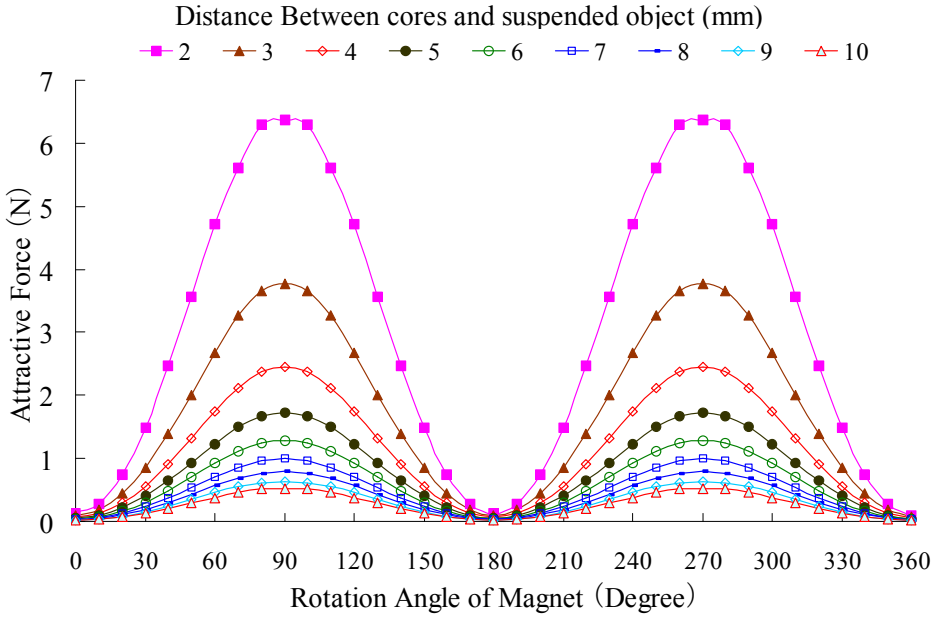

Fig.7.5 Analysis results of magnetic flux field of inserting ferromagnetic board

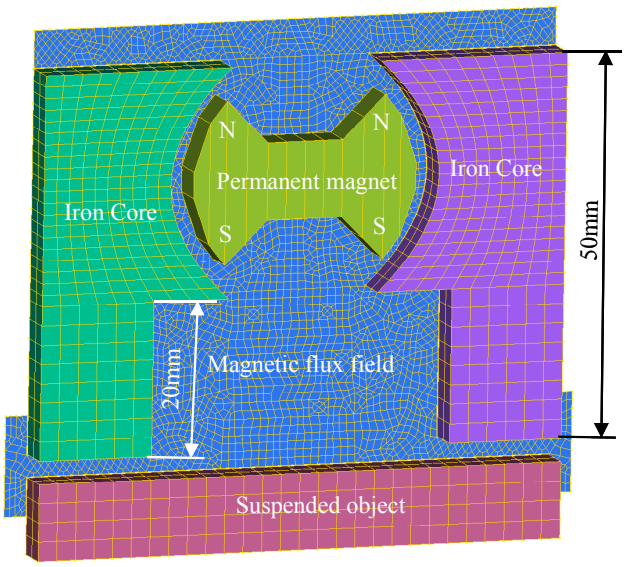

Fig.7.6 IEM analysis model using the special type magnet

7.2.2 IEM Analysis for Special Type Permanent Magnet Method

7.2.2.1 Analysis Model

Fig.7.6 shows the analysis model used in IEM analysis. This model is revised from the model shown in Fig.6.5. The round magnet was changed to this special type permanent magnet. Using this model, the IEM analysis was carried out.

7.2.2.2 Analysis of Magnetic Flux Field

First, the magnetic flux field of the mechanism was analyzed using the special type magnet. And the result when the magnet stops at zero degree is shown in Fig.7.7. Fig.7.8 shows the 4-time enlarged figure of the lower side of Fig.7.7. Compare them with Fig.6.6 and Fig.6.7, we can see that the flux flowing in the iron cores and the suspended object using this special type magnet is much less than that in the original mechanism using the round magnet, when the magnet stops at 0 degree. These results indicate that using this special type magnet can obviously reduce the leakage magnetic flux between the magnet and the suspended object, and the improvement using this method is feasible.

7.2.2.3 Analysis of Magnetic Flux Density of Permanent Magnet

Fig.7.9 shows the size of the special type magnet and the analysis process of the magnetic flux density of the magnet. The diameter of this special magnet is 30 mm, which is same with the size of the original round magnet.

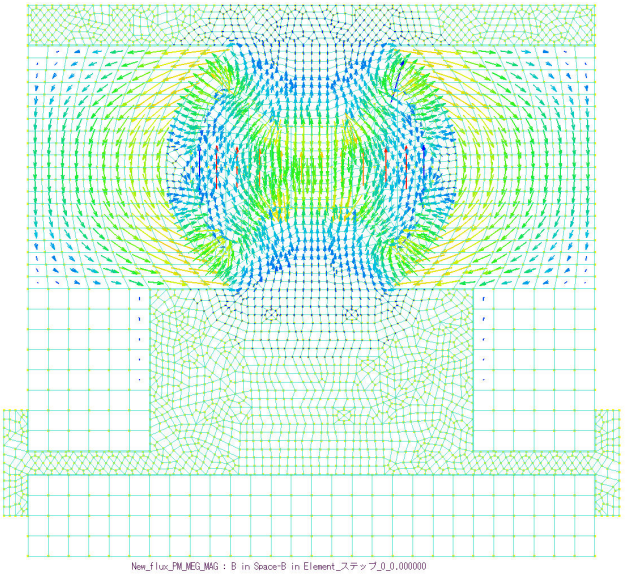

Fig.7.7 Analysis result of magnetic flux field (0 degree)

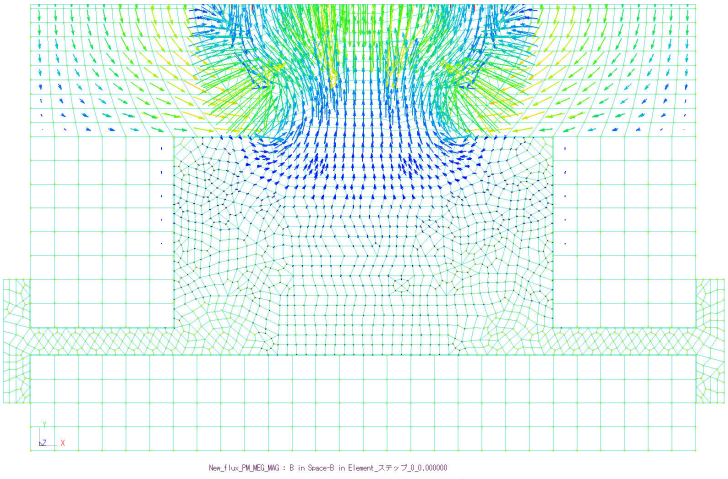

Fig.7.8 Enlarged analysis result with 4 times (0 degree)

Fig.7.10 shows the analysis results of magnetic flux field of the special type magnet. The results show that the magnetic flux density varies as falling off between two pick periods, which is similar to the shape of the saddle. Therefore, when the magnetic poles of this special type magnet stop at the vertical direction, the leakage of the magnetic flux from the magnetic poles will be much less than that in original mechanism using the round magnet. This agrees with the results shown in Fig.7.7 and Fig.7.8.

7.2.2.4 Analysis of Magnetic Flux Density

Fig.7.11 shows the analysis results of the magnetic flux density between the iron cores and the suspended object. The results indicate that the magnetic flux density between the iron cores and the suspended object also resembles to a sine curve, although the magnetic flux

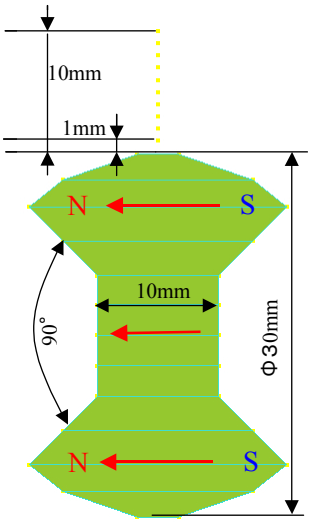

Fig.7.9 Analysis of magnetic flux field of the special type magnet

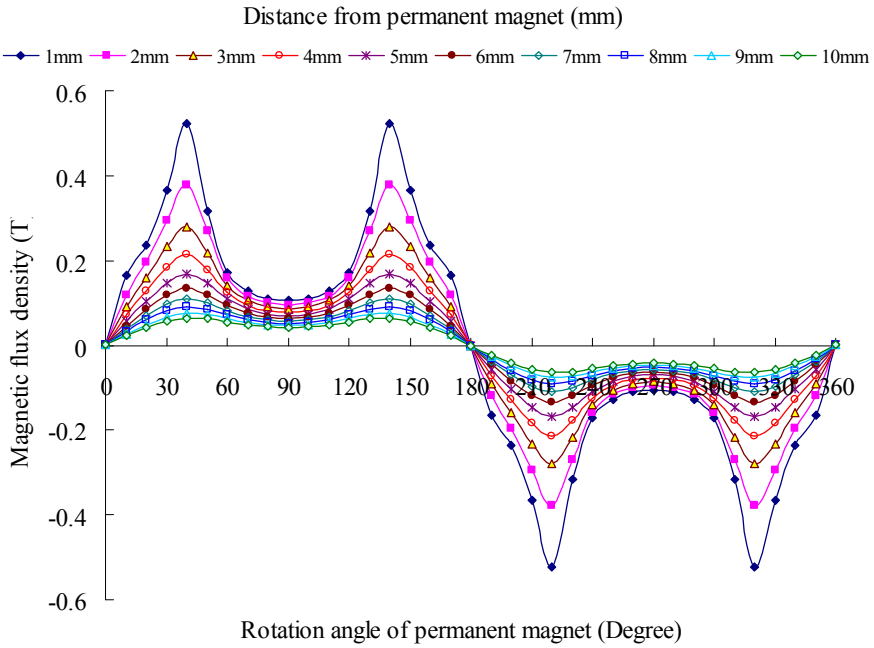

Fig.7.10 Analysis results of magnetic flux field of the special type magnet

density of the special type magnet resembles to the shape of the saddle.

7.2.2.5 Analysis of Attractive Force

Fig.7.12 shows the analysis results of the attractive force between the iron cores and the suspended object. The attractive force from the iron cores also resembles to the results of the original mechanism. The results indicate that the rotation of the angle of the special type magnet can control the suspension force, and the special type magnet does not change the force characteristics of the mechanism.

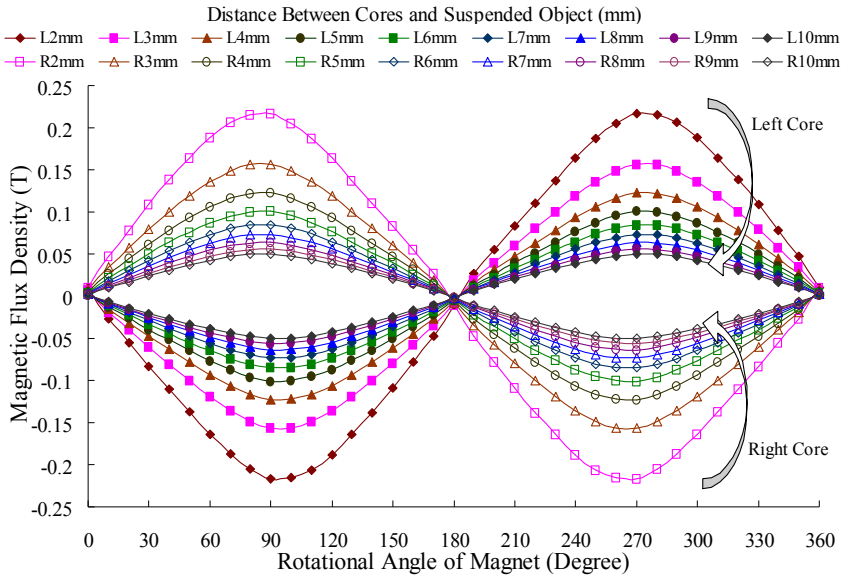

Fig.7.11 Analysis results of magnetic flux density using the special type magnet

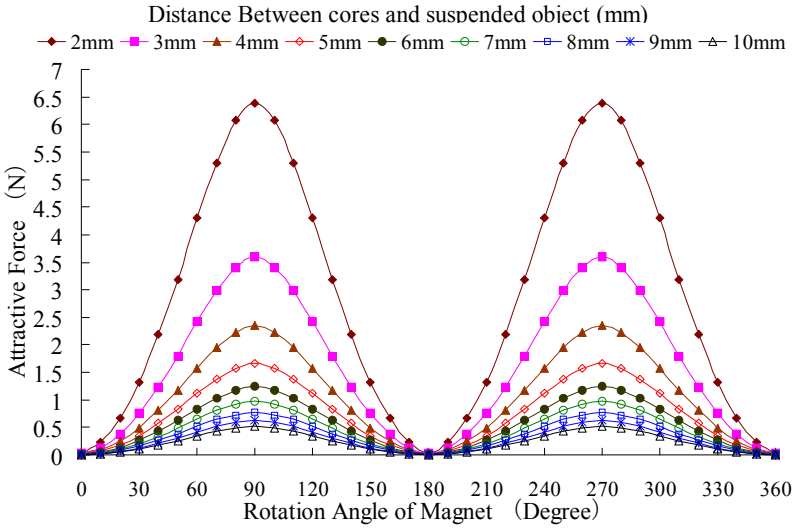

Fig.7.12 Analysis results of attractive force using the special type magnet

7.2.3 IEM Analysis for Extending the Length of Cores Method

7.2.3.1 Analysis Model

Fig.7.13 shows the analysis model using the extended iron cores. The length of the iron cores is 80 mm in this model, which is 30 mm longer than the cores of the original mechanism. This method is going to reach the aim of reducing the leakage of the magnetic flux by extending the distance between the magnet and the suspended object, i.e. enlarging the magnetic reluctance between the magnet and the suspended object.

Moreover, the IEM analysis was also examined using the different length of the iron cores, which was changed from 40 mm to 80 mm, and the increased length of each time was 5 mm.

7.2.3.2 Analysis of Magnetic Flux Field

The analysis of the magnetic flux field of the mechanism was just examined when the length of the iron cores was 80 mm. Fig.7.14 shows the analysis result when the magnet stops at zero degree. Fig.7.15 shows the 4-time enlarged figure of the lower side of Fig.7.14. From these results, we can see that the leakage of magnetic flux around the magnet is same as the original mechanism, however, since the distance is large between the magnet and the suspended object, there is no magnetic flux arrive to the suspended object. There results indicate that the extending the length of the iron cores method can obviously improve the semi-zero suspension force characteristics.

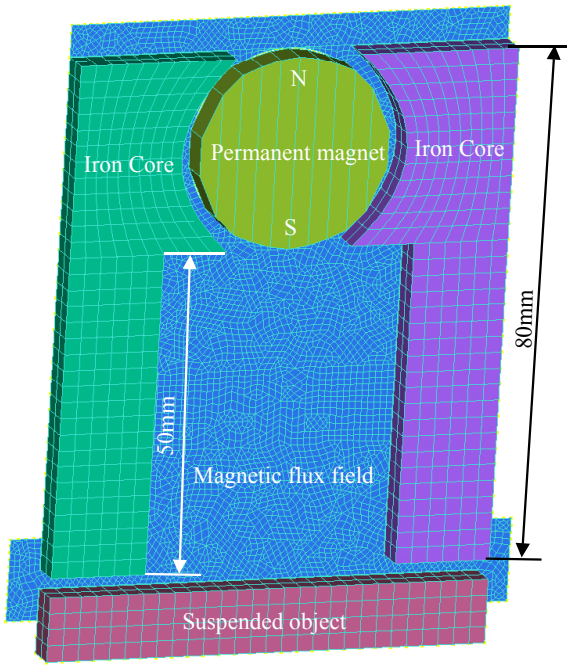

Fig.7.13 IEM analysis model of extending the iron cores

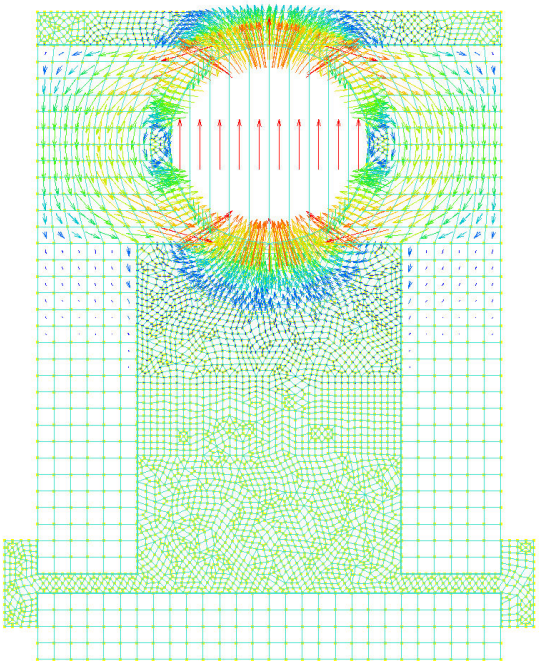

Fig.7.14 Analysis result of magnetic flux field (0 degree)

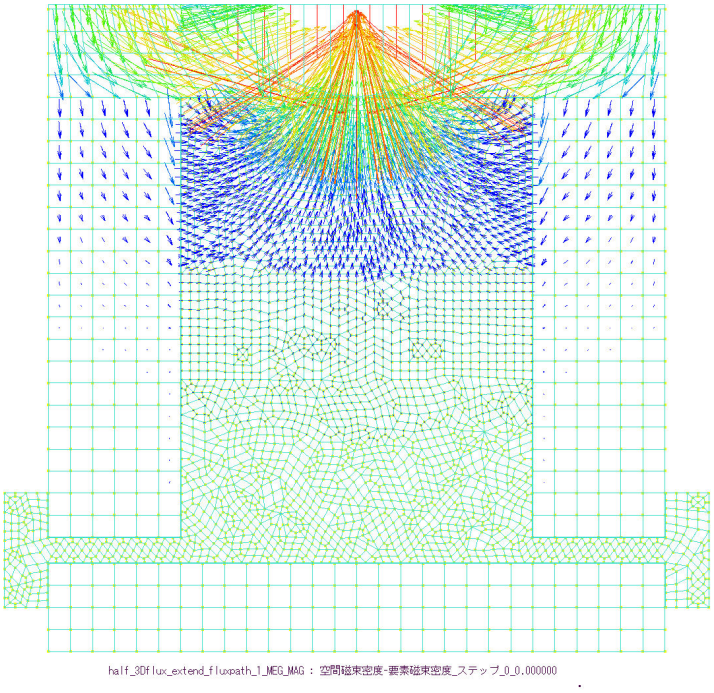

Fig.7.15 Enlarged analysis result with 4 times (0 degree)

7.2.3.3 Analysis of Magnetic Flux Density

Fig.7.16 shows the analysis results of magnetic flux field using the extended iron cores method where the length of cores is 80 mm. These results are a little different from the results of the original mechanism. The intensity of the magnetic flux density is samller than the original mechanism. The weakness of the magentic flux density between the iron cores and

the suspended object is caused by the increasing magnetic reluctance and the leakage of magnetic flux of the long iron cores. This also can be understood from Fig.7.15.

7.2.3.4 Analysis of Attractive Force

Fig.7.17 shows the analysis results of attractive force using the extended iron cores method where the length of cores is 80 mm. The attractive force becomes a little weaker than the original mechanism, however, the attractive forces at 0 degree and 180 degrees are obviously samller than the original mechanism.

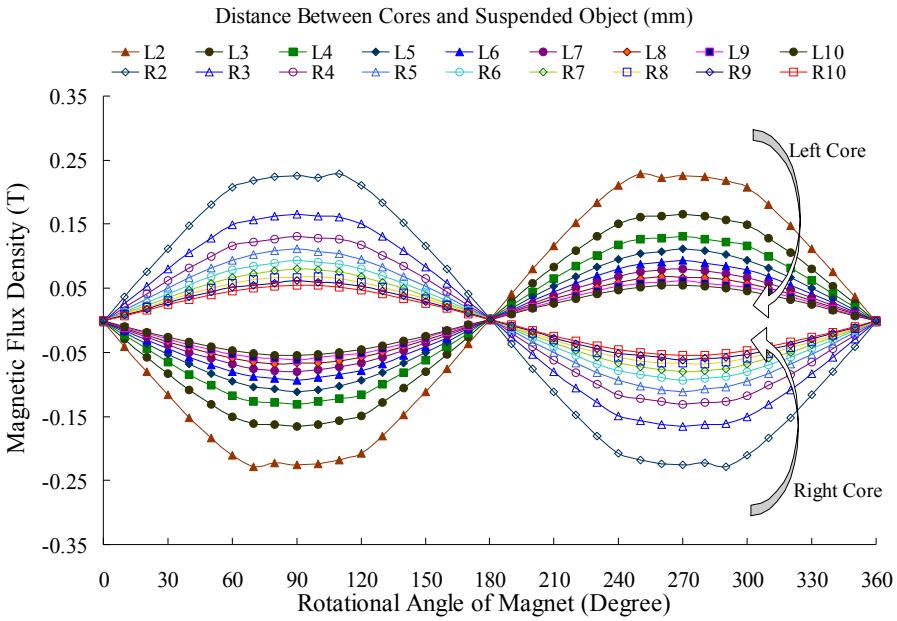

Fig.7.16 Analysis results of magnetic flux density using the extended cores

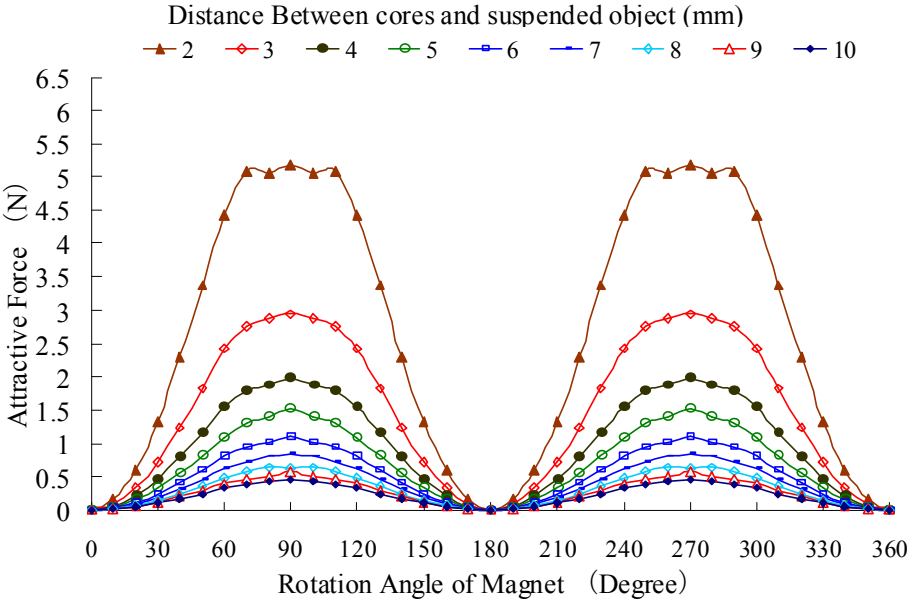

Fig.7.17 Analysis results of attractive force using the extended cores

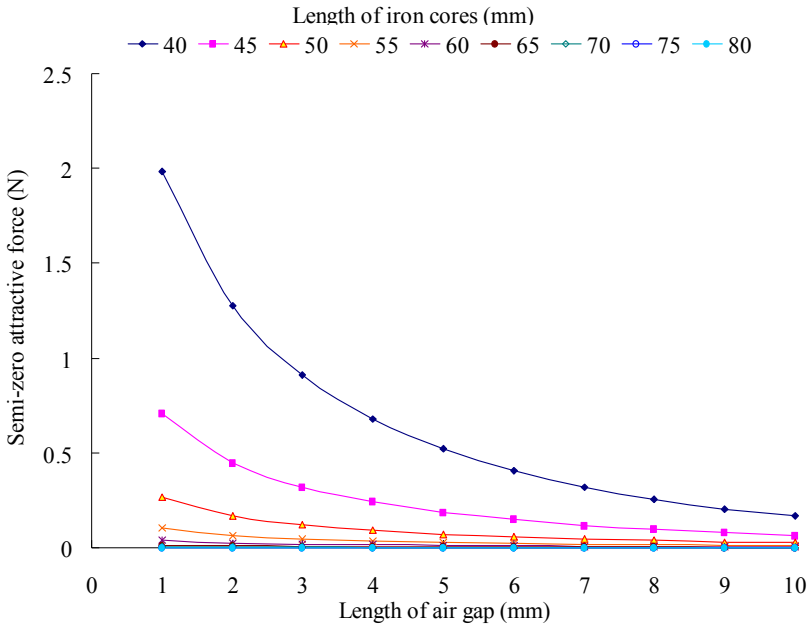

Fig.7.18 Semi-zero suspension force characteristics using different length of iron cores

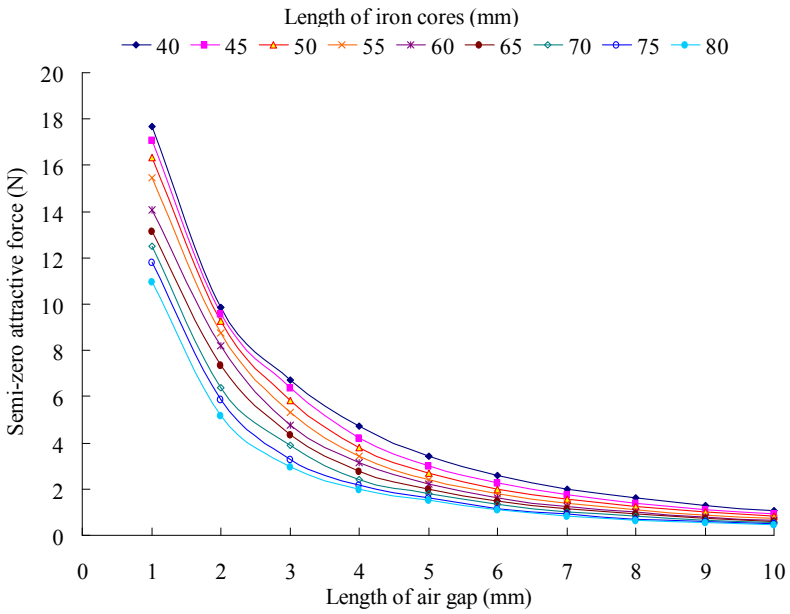

Fig.7.19 Maximum suspension force characteristics using different length of iron cores

Moreover, the semi-zero and the maximum suspension force characteristics were also examined when the length of the iron cores was varied by 5 mm and from 40 mm to 80 mm. Fig.7.18 shows the semi-zero suspension force characteristics using different length of iron cores, and Fig.7.19 shows the maximum suspension force characteristics using different length of iron cores. These results indicate that the longer iron cores can generate the better semi-zero suspension force characteristics, but the maximum attractive force characteristics becomes worse.

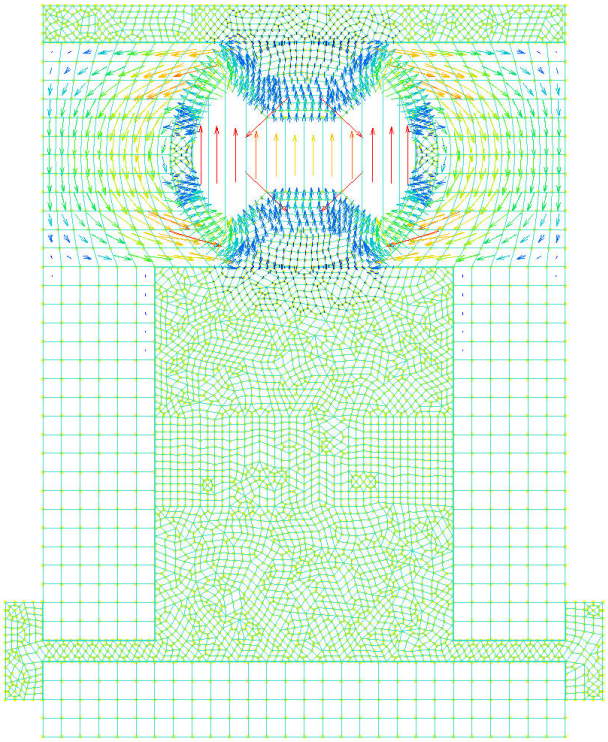

Fig.7.20 Analysis result of magnetic flux field (0 degree)

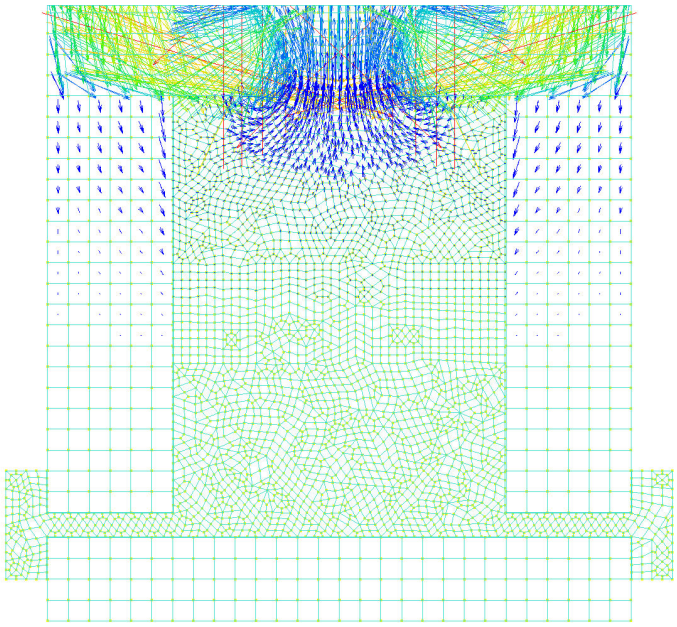

Fig.7.21 Enlarged analysis result with 8 times (0 degree)

7.2.4 IEM Analysis for Combination Method

7.2.4.1 Analysis of Magnetic Flux Field

The improvement method of the combination of the special type magnet and the extended iron cores was also examined by IEM analysis. The used analysis model was just changing the round magnet to the special type magnet in the model shown in Fig.7.13. The

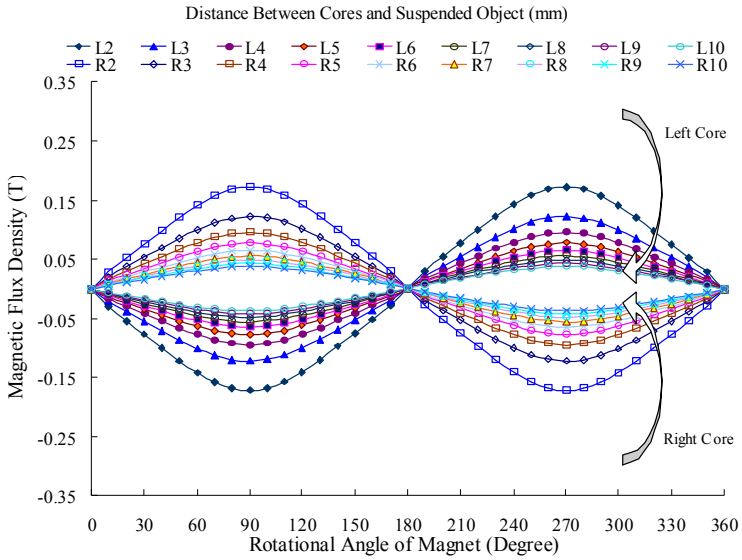

Fig.7.22 Analysis results of magnetic flux density using combination method

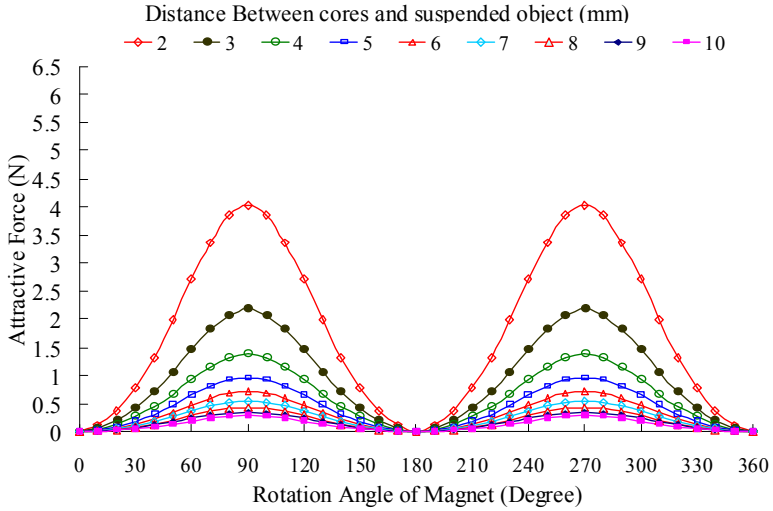

Fig.7.23 Analysis results of attractive force using combination method

result of the magnetic flux field of the mechanism is shown in Fig.7.20 when the magnet stops at zero degree. Fig.7.21 shows the 8-time enlarged figure of the lower side of Fig.7.20. From these results, we can see that even though the arrows are enlarged to 8 times, the arrival magnetic flux to the suspended object cannot be seen in the figure. Therefore, the combination method can obviously improve the semi-zero suspension force of the mechanism, and may induce the semi-zero suspension force almost zero.

7.2.4.2 Analysis of Magnetic Flux Density

Fig.7.22 shows the analysis results of magnetic flux density of the iron cores. From the results, we can see that the maximum magnetic flux density becomes smaller, but the symmetry of two iron cores becomes better than those of the former models.

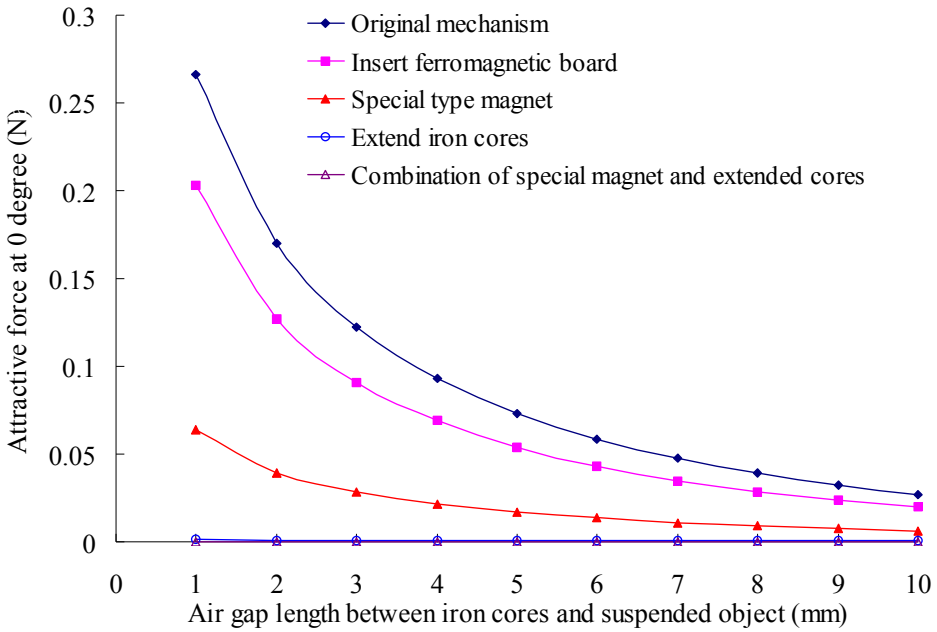

Fig.7.24 Comparing zero attractive force characteristics

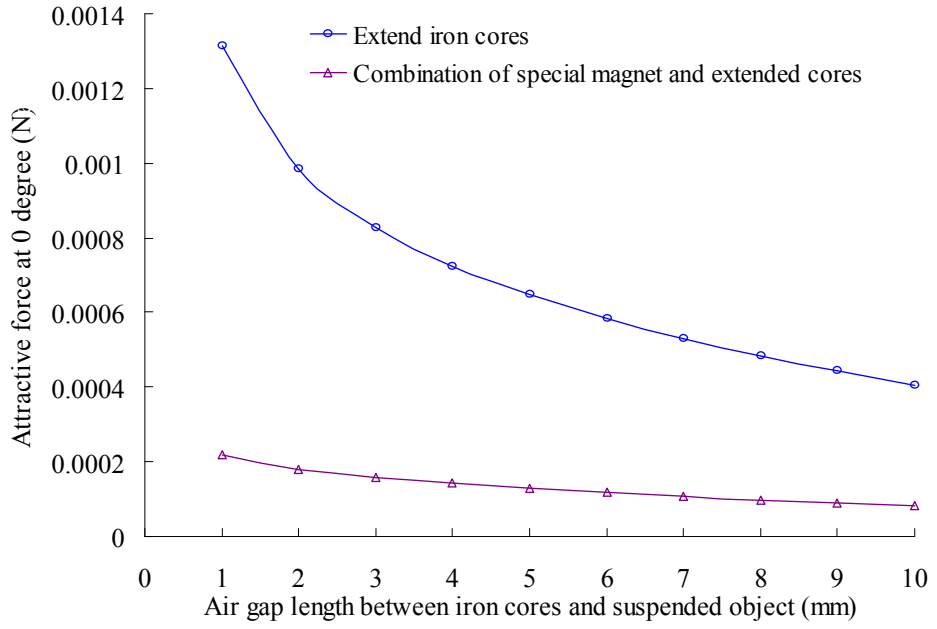

Fig.7.25 Comparing zero attractive force characteristics between extended iron cores method and combination method

7.2.4.3 Analysis of Attractive Force

Fig.7.23 shows the analysis results of attractive force of the iron cores. The results indicate that the maximum force becomes smaller, but the graph shape becomes more regular, and the linearity beomes better than the model only using the extended iron cores.

7.2.5 Comparison of Semi-Zero Attractive Force Performance

In order to evaluate the four improvement methods, the analysis attractive forces are compared with the original mechanism when the magnet stops at 0 degree.

Fig.7.24 shows the comparison results of the semi-zero attractive force between the improvement methods and the original mechanism. The results indicate that all the improvement methods have the effect, but the results of using extended iron cores method and the combination method are best, the attractive forces at zero degree of these two methods are almost zero.

Moreover, in order to compare the effect of using extended iron cores method and the combination method, the comparison results between these two methods are shown in Fig.25. From Fig.25, we can see that the effect of the combination method is much better than the method using the extended iron cores, and the semi-zero attractive force is almost equal to 0.0001 N constantly, and the air gap length between the iron cores and the suspended object is almost no impact to the semi-zero attractive force characteristics.

7.3 Performance Comparison by Experimental Examinations

Moreover, in the light of the four improvement methods, the magnetic flux density and the attractive force of the experimental prototype were also carried out by experimental examinations. According to the results of IEM analysis, the method of inserting a ferromagnetic board has an inconspicuous improvement. Therefore, only the attractive forces in 0 degree and 180 degrees were measured, and compared with other methods.

7.3.1 Experimental Examinations for Special Type Magnet Method

7.3.1.1 Measurement of Magnetic Flux Density of Magnet

Fig.7.26 shows the measument results of the magnetic flux density of the special type magnet. The results are similar to the IEM analysis results, and indicate that when the magnetic poles stop in the vertical direction in the mechanism, the leakage of the magnetic flux will be a little. Using this magnet, the measurement of the magnetic flux density and the attractive force of the iron cores were also carried out.

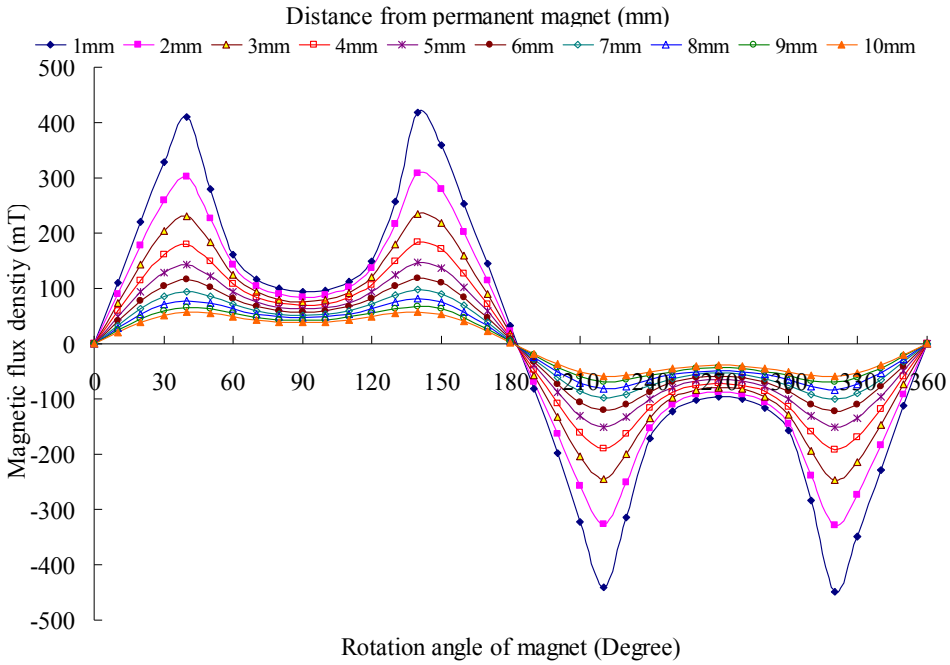

Fig.7.26 Measurement result of magnetic flux density of the special type magnet

7.3.1.2 Measurement of Magnetic Flux Density

Fig.7.27 shows the measurement results of the magnetic flux density of the iron cores. Although the graph shape of the magnetic flux density of the magnet is like a saddle, the magnetic flux density is also similar to a sine curve according to the rotational angle of the magnet. These results indicate that the special type of the magnet only changes the magnetic flux density of the magnet, but not influences the magnetic flux density of the iron cores.

7.3.1.3 Measurement of Attractive Force

Fig.7.28 shows the measurement results of the attractive force of the iron cores. These results are similar to the results of the original mechanism, but the graph shape becomes thin, and the linearity of the attravtive force becomes good towards to the rotational angle of the magnet. Moreover, it can be seen that the attractive forces at 0 degree and 180 degrees are smaller than the result of the original mechanism.

7.3.2 Experimental Examinations for Extending the Length of Cores Method

7.3.2.1 Measurement of Magnetic Flux Density

Fig.7.29 shows the measurement results of the magnetic flux density of the extended iron cores. The results are similar with the IEM analysis results. The long iron cores make the graph shape of the flux density even around 90 degrees. The flux leakage of the long iron cores cause some flux cannot arrive the air gap between the iron cores and the suspended

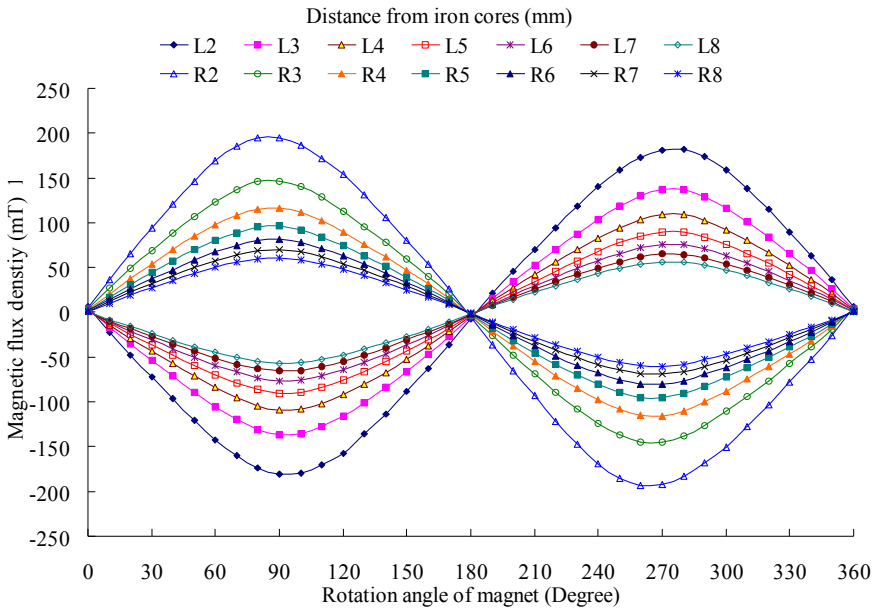

Fig.7.27 Measurement result of magnetic flux density of the iron cores

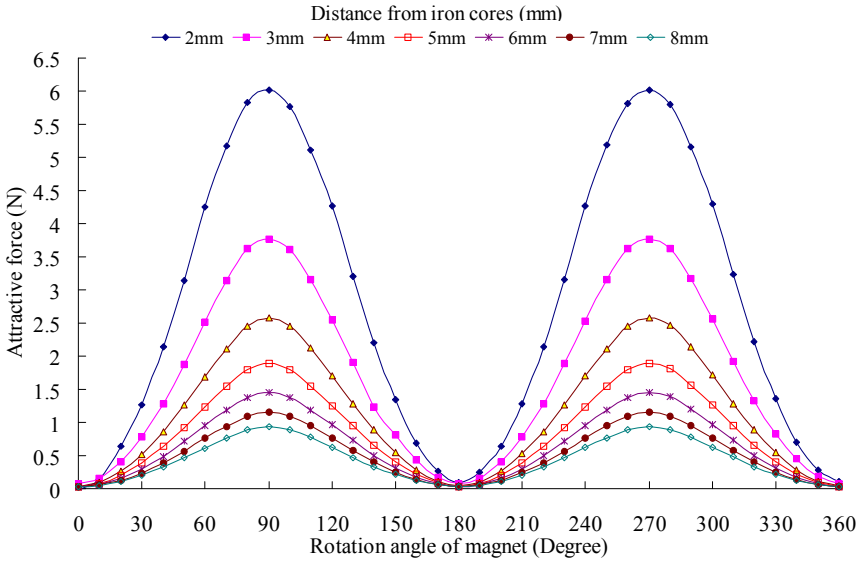

Fig.7.28 Measurement result of attractive force of the iron cores

object.

7.3.2.2 Measurement of Attractive Force

Fig.7.30 shows the measurement results of the attractive force using the extended iron cores. From the results, we can see that, the maximum force becomes small, and the force variations become unconspocuous from 60 to 120 degrees and from 240 to 300 degrees. And the weak variation of force cause the system uncontrol in those areas. However, the semi-zero attractive force at 0 and 180 degrees becomes almost zero.

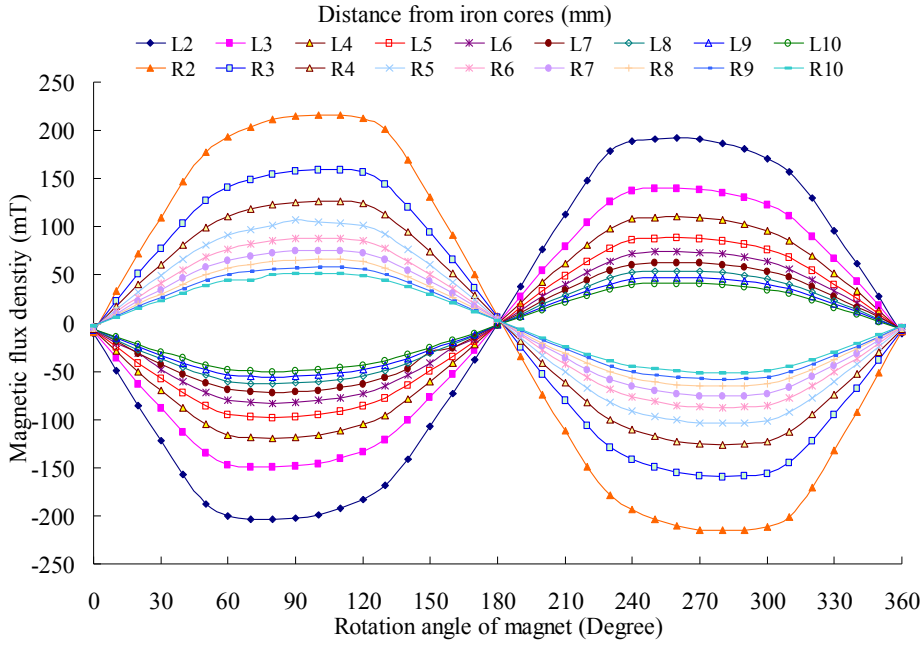

Fig.7.29 Measurement result of magnetic flux density of the iron cores

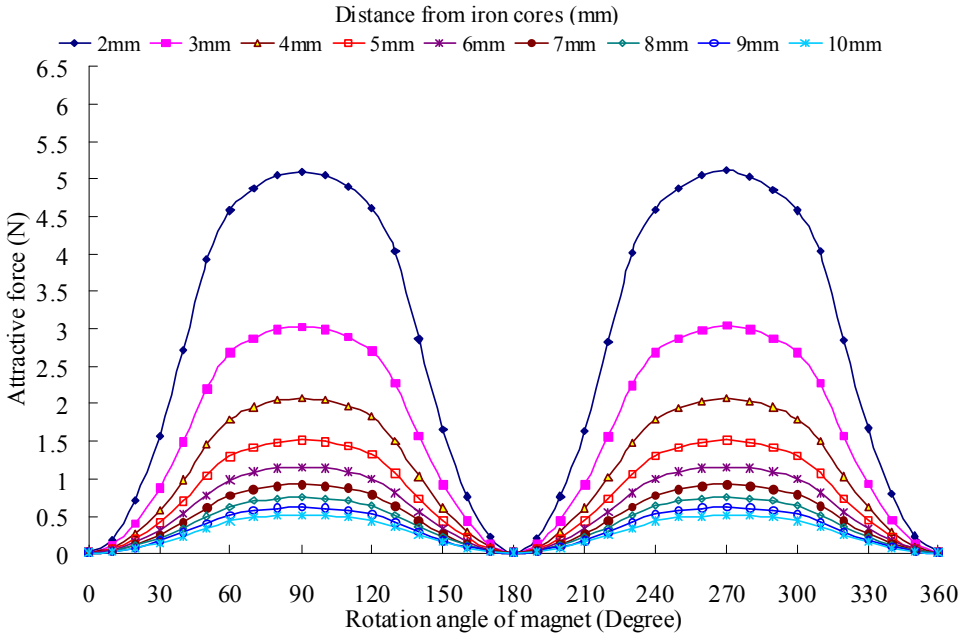

Fig.7.30 Measurement result of attractive force of the iron cores

7.3.3 Experimental Examinations for Combination Method

7.3.3.1 Measurement of Magnetic Flux Density

Fig.7.31 shows the measurement results of magnetic flux density using the combination method with the extended iron cores and the special type permanent magnet. In this figure,

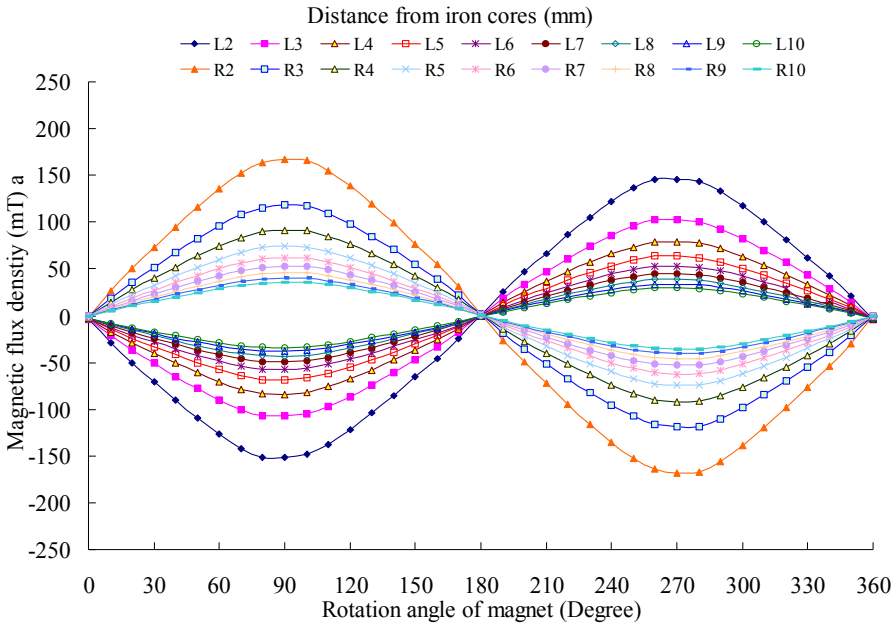

Fig.7.31 Measurement result of magnetic flux density of the iron cores

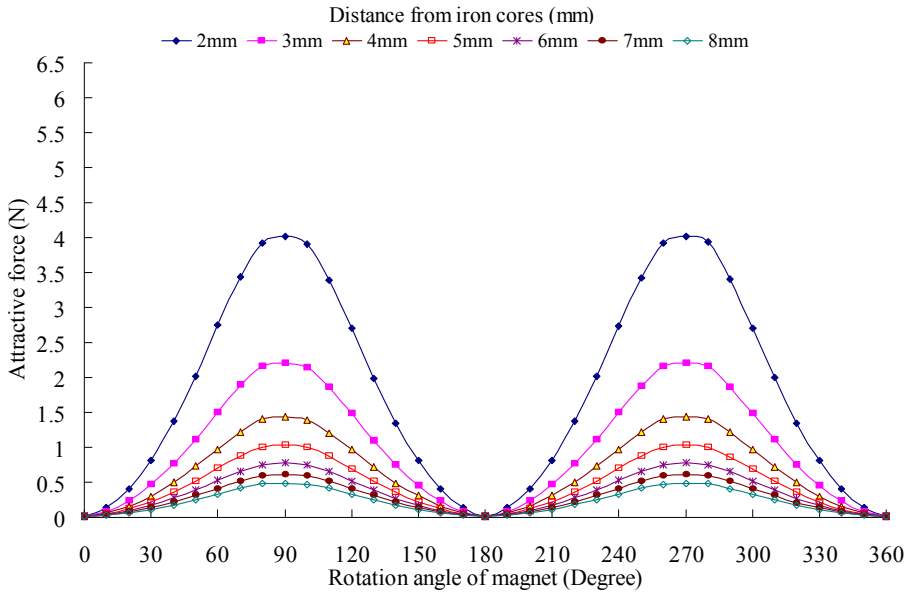

Fig.7.32 Measurement result of attractive force of the iron cores

the magnetic flux density is also weaker than the results with the shot iron cores and the special magnet. But the graph shape is better than the results with the long iron cores and the round magnet.

7.3.3.2 Measurement of Attractive Force

Fig.7.32 shows the measurement results of the attractive force using the combination

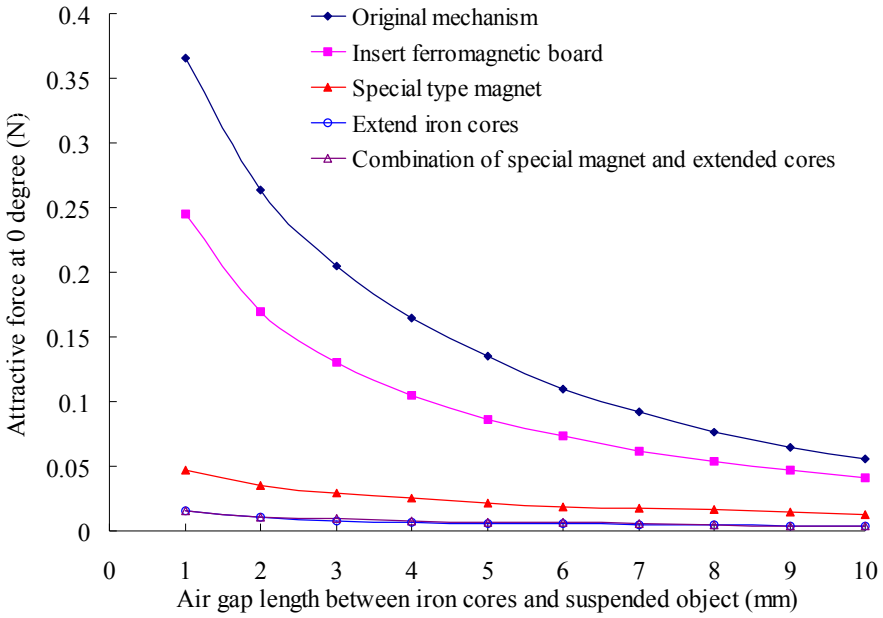

Fig.7.33 Comparison of zero attractive force characteristics

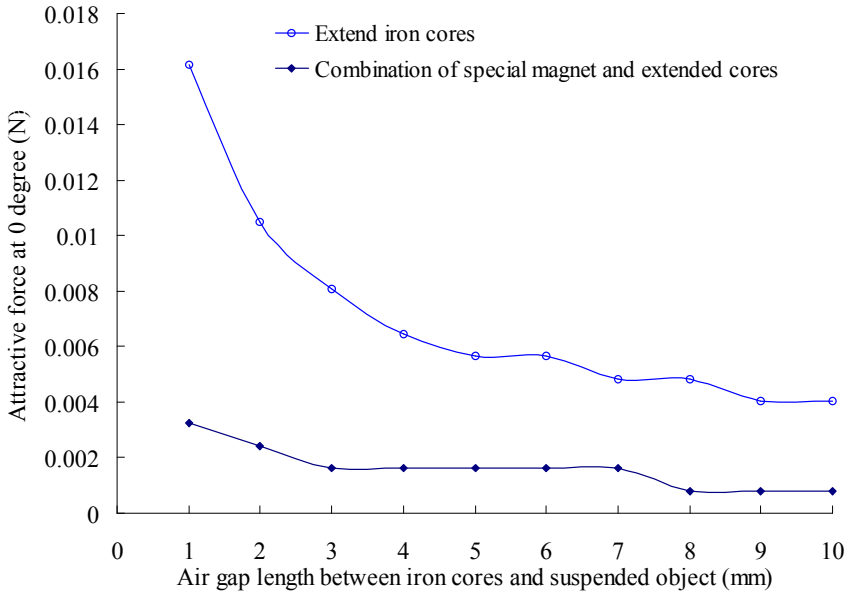

Fig.7.34 Comparing zero attractive force characteristics between extended iron cores method and combination method

method with the extended iron cores and the special type permanent magnet. The results shows that, the attractive force becomes weaker than the results with the shot iron cores and the special magnet, the controllable range of the attractive force, however, becomes wider than the results with the long iron cores and the round magnet. Moreover, the semi-zero

attractive force is also almost zero like Fig.7.30, and the comparison results will be shown in next session.

7.3.4 Comparison of Semi-Zero Attractive Force Performance

In order to evaluate the four improvement methods, the measurement attractive forces are compared with the original mechanism when the magnet stops at 0 degree. The comparison results are shown in Fig.7.33. From the results, we can see that, the semi-zero attractive forces of the improvement methods are smaller than the results of original mechanism. Therefore, all the improvement methods are available. The improvement effect using the special type permanent magnet is conspicuous, and is better than the inserting ferromagnetic board method. However, the improvement effect of using extended iron cores and the combination method is best, and the graphs of these two methods are almost overlapping.

In order to compare the improvement effect between the extended iron cores method and the combination method, the results of these two methods are shown in Fig.7.34. The results indicate that, the improvement effect of the combination method is much better than the method only using the extended iron cores.

7.4 Suspension Examination Using the Special Type Permanent Magnet Method

In order to examine the suspension performance of the improved mechanism, the suspension examination was carried out using the special type permanent magnet method.

7.4.1 Numerical Simulation of Suspension

Using the same mathematical model shown in last chapter and the different parameters, the

Table.7.1 Parameters using in numerical simulation

Parameter	Value	Parameter	Value
m (kg)	0.232	c_1 (N/(m/s))	0.1
d_0 (mm)	1.8	c_2 (N/(m/s))	85
Δd_f (mm)	1.8	J (kgm^2)	6.37×10^{-4}
Δd_τ (mm)	0	k_t (Nm/A)	0.69
θ_0 (degree)	35.4	k_m (Nm^2)	8.69×10^{-5}
g (m/s^2)	9.8	k_τ (Nm^2)	0

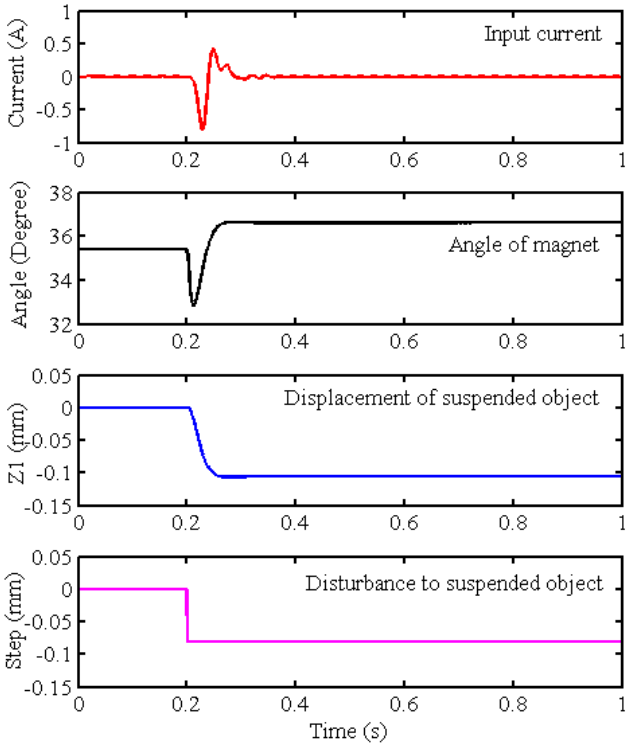

Fig.7.35 Simulation results with a suspended object of 0.232 kg

numerical simulation was carried out. The parameters show in Table.7.1, which are measured from the experimental prototype and the measurement experiment. We chose the state weighting matrix Q and input weighting matrix R as following:

$$Q = \begin{bmatrix} 10000000000 & 0 & 0 & 0 \\ 0 & 1000000 & 0 & 0 \\ 0 & 0 & 1 & 0 \\ 0 & 0 & 0 & 1 \end{bmatrix} \tag{7.1}$$

$$R = 1 \tag{7.2}$$

Using MATLAB software, the feedback gain K is calculated as following:

$$K = \begin{bmatrix} 177250 & 2208 & 391.23 & 1.31 \end{bmatrix} \tag{7.3}$$

In the simulation, the nonlinear attractive force and the nonlinear rotational torque are used directly, and the mass of suspended object is 0.232 kg. An input disturbance of a step of -0.08 mm was applied to the displacement of the suspended object, and the response was recorded until 1 second. And the simulation results are shown in Fig.7.35. The figures show the input current of motor, the angle of magnet, the displacement of suspended object, and the

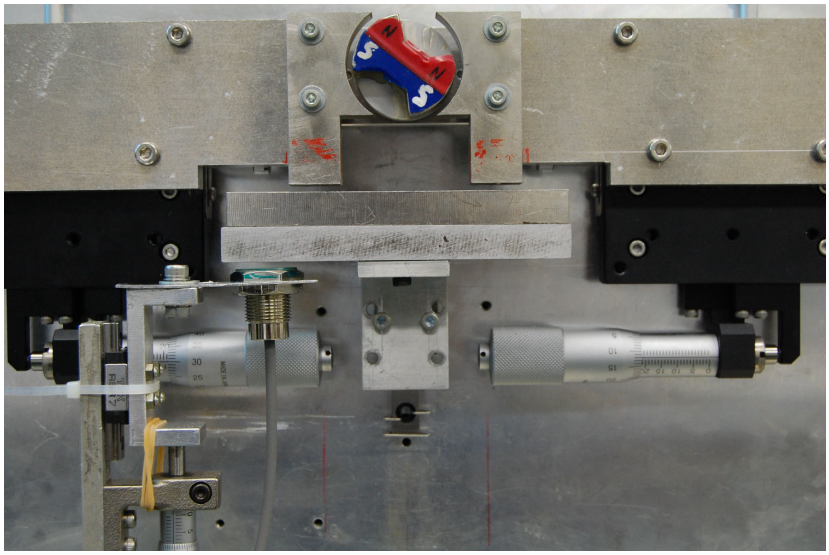

Fig.7.36 Suspending photograph with the special type magnet

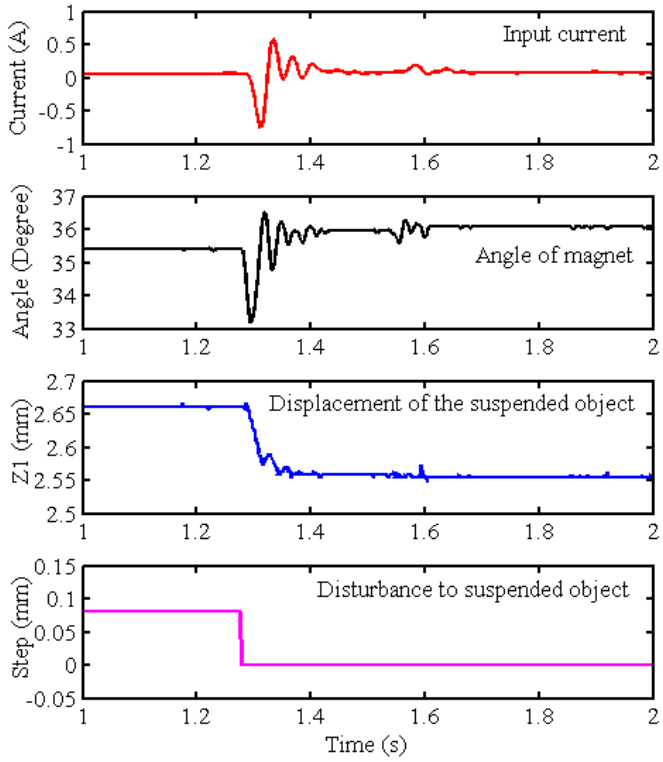

Fig.7.37 Experimental results with a suspended object of 0.232 kg

input disturbance from up to down. The results indicate that the system using the special type magnet also can realize the stable suspension.

7.4.2 Experimental Suspension

Using the experimental prototype shown in last chapter, where the used magnet was changed to the special type permanent magnet, the experimental suspension was succeeded. The suspension photograph using the special permanent magnet is shown in Fig.7.36.

Fig.7.27 shows the step response results when the mass of suspended object is 0.232 kg, and the step input is –0.08 mm. In the figures, the input current, the rotational angle of magnet, and the displacement of suspended object are recorded from 1 second to 2 seconds. The results indicate that the suspended object can be suspended stably and the input current is almost zero at the stable state. This is same with the results in last chapter.

The results indicate that the magnetic suspension system using a special type magnet not only can improve the semi-zero attractive force performance, but also can realize the stable suspension as the original mechanism have realized.

7.5 Conclusions

This chapter focused on the improvement of the semi-zero suspension force of the proposed magnetic suspension mechanism, and proposed four improvement methods, which are inserting the ferromagnetic board, using a special type magnet, extending the iron cores, and combination of the special type magnet and the extended cores. The performance of the mechanism using each improvement method was examined by IEM analysis and measurement experiment. All the results indicated that, every method could improve the semi-zero suspension force characteristics. However, using the method of the special type magnet or the extended iron cores could obtain the obvious improvement, and using the combination method could obtain an almost zero suspension force characteristics. Moreover, only using the extended iron cores, the semi-zero force characteristics were inproved, but the controllable range of the attractive force becomes narrow. Using the combination of the special permanent magnet and the extended iron cores, the semi-zero attractive force characteristics were improved, basing on no reduction of the controllable range of the attractive force.

In addition, the suspension examinations were also carried out with the improved mechanism using the special type permanent magnet in numerical simulation and the experiment. The results indicated that the improved mechamsim also could suspend the suspended object stable.

Chapter 8 Simultaneous Suspension of Two Iron Balls

8.1 Introduction

Magnetic suspension is technology for supporting or manipulating objects without contact by means of magnetic forces. Magnetic suspension system has many advantages, which are no contact, no friction, no dirt and lubrication free. Using these advantages, many magnetic suspension mechanisms have been proposed [9]. Moreover, these mechanisms have been developed and used in noncontact conveyance vehicles, high-speed transportations and motors, dirt-free factories and outer space. These magnetic levitation systems use various methods to control the suspension force. Two types of systems are electromagnetic suspension systems, which control the coil current so as to change the magnetic force in order to levitate an object stably; and mechanical magnetic suspension systems, which use permanent magnets to control the magnetic reluctance so as to vary the suspension force in order to achieve stable suspension. Moreover, there are two methods for controlling magnetic reluctance in mechanical magnetic suspension systems [24], i.e. changing the air gap between magnets and ferromagnetic objects by moving the permanent magnet [38], and varying the flux by changing the flux path of the magnetic circuit. Many researchers have proposed magnetic suspension systems using flux path control method. Mizuno et al. have proposed a magnetic suspension system with a permanent magnet and three flux-path control modules consisting of a ferromagnetic plate, a voice coil motor (VCM), and a displacement sensor [31]. This system controls the attractive force of the magnet by changing the flux path with the flux-path control modules. Ueno and Higuchi presented a magnetic levitation technique using flux path control method with a composite of magnetostrictive and piezoelectric materials [33].

Moreover, some multiple magnetic suspension systems have been proposed. Yamamoto et al. have discussed a series magnetic suspension system with an electromagnet, a permanent magnets and a magnetic target [71]. Yamamoto's suspension system realized an indirect suspension of a magnetic target through an actively controlled permanent magnet, whose position is controlled by the electromagnet. Sakurada et al. have proposed a parallel magnetic suspension of two-floater using one signal amplifier [72]. Moreover, Sakurada has confirmed that there were minus feedback gains in the current control of the parallel two-fold magnetic suspension.

This chapter proposes a noncontact magnetic suspension system for levitating two different weight iron balls simultaneously using flux path control method [35]. In this system, the magnetic flux is generated from a disk-type permanent magnet, and passes through two iron cores to arrive two iron balls. Therefore, the suspension force of two cores can be changed simultaneously at same variation rate by varying the angle of the permanent magnet that is driven by a rotary actuator. This proposed suspension system of two-ball is similar to the parallel-type double inverted pendulum system, which consists of two different length pendulums and a cart or a linear motor [73]. In the double inverted pendulum system, two pendulums can be maintained the balance at the up-right position through the motion control of the cart in one degree.

In this chapter, first, the suspension principle of two iron balls is explained, and a prototype is introduced. Second, the characteristics of this system are examined by IEM analysis and some basic experiments. Third, a model is created, and the controllability is proved, theoretically. Finally, the simulation and experimental results of suspension are shown and discussed.

8.2 Suspension Principle

The suspension principle of this magnetic suspension system can be understood from Fig.8.1, a schematic diagram showing a disk permanent magnet, two iron cores and two iron balls. The permanent magnet is in the center of diagram, and has an N pole of 90 degrees and an S pole of opposite side 90 degrees in radial direction. Two iron cores, resembling a pair of opposite letters of “F”, and are installed beside the permanent magnet. Two iron balls have different size, and are located under the two cores, respectively.

First, the followings will be assumed:

(1) The distance between two iron balls is far enough, and comparing with the attractive force from the iron cores, the attractive force between two balls can be neglected.

(2) The rotation angle of permanent magnet is 0 degree at the situation shown in Fig.8.1 (a).

Fig.8.1 (a) shows that the magnetic poles of the permanent magnet are aligned in the vertical direction, and the N pole is at the upper side and the S pole is in the lower side. In this case, the facing angle of the N pole and S pole to each core are same, so all magnetic flux comes from the N pole and is absorbed into the S pole through the upper part of each core, respectively. There is no magnetic flux arrive at two iron balls, so zero attractive force generates between the cores and the levitated iron balls. However, Fig.8.1 (b) shows the permanent magnet rotated 20 degree, the facing angle of the N pole becomes bigger than the S pole in the right core, and that is reverse in the left core. Since that, some flux coming from N pole passes the right core, and arrives at the right ball; and some flux passes through the left

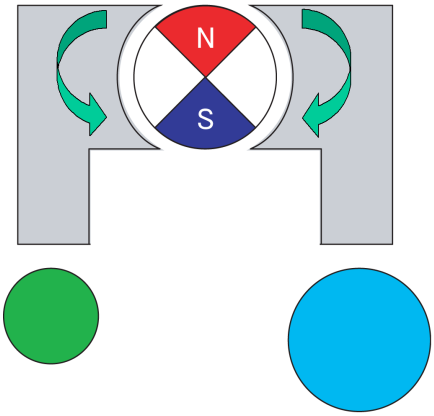

(a) Rotation angle of magnet is 0 degree.

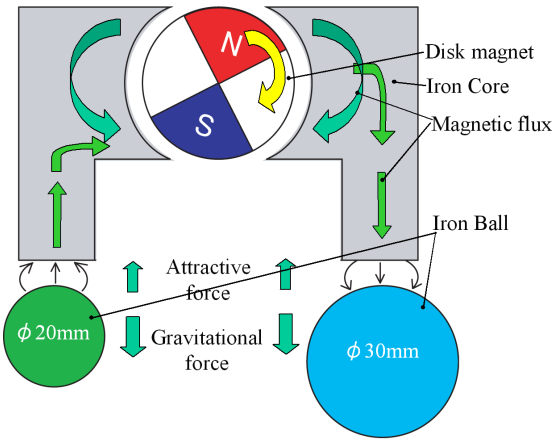

(b) Rotation angle of magnet is 20 degree.

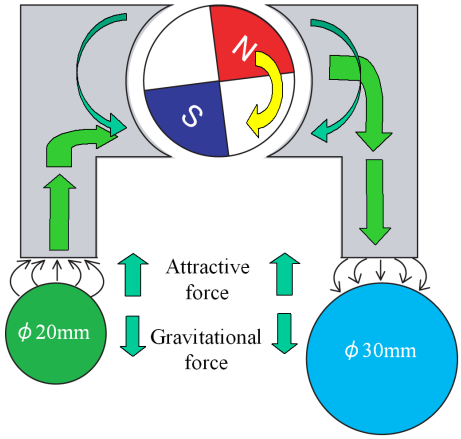

(c) Rotation angle of magnet is 20 degree.

Fig.8.1 Principle of flux path control magnetic suspension

iron ball and left core, and returns to the S pole. Consequently, the attractive force is generated between cores and iron balls. Moreover, Fig.8.1 (c) shows the permanent magnet rotated 40 degree. The flux flowing through two iron balls becomes more as the rotation angle of magnet becomes larger. As a result, the attractive force between two cores and two iron balls can be changed by means of varying the rotation angle of permanent magnet simultaneously.

In addition, since the natural frequency of an iron ball depends on its weight, and the small ball has a higher natural frequency. Since the rotation of the magnet affects the two iron balls directly, if the magnet rotates same angle, the small ball tends to respond intensively and moves a large distance.

Consequently, simultaneous suspension of two iron balls can be realized using the proposed flux path control method, theoretically.

8.3 Experimental Prototype

8.3.1 Experimental Prototype

Fig.8.2 shows the schematic of the proposed magnetic suspension mechanism. And an experimental prototype of the proposed magnetic suspension system was constructed, and the

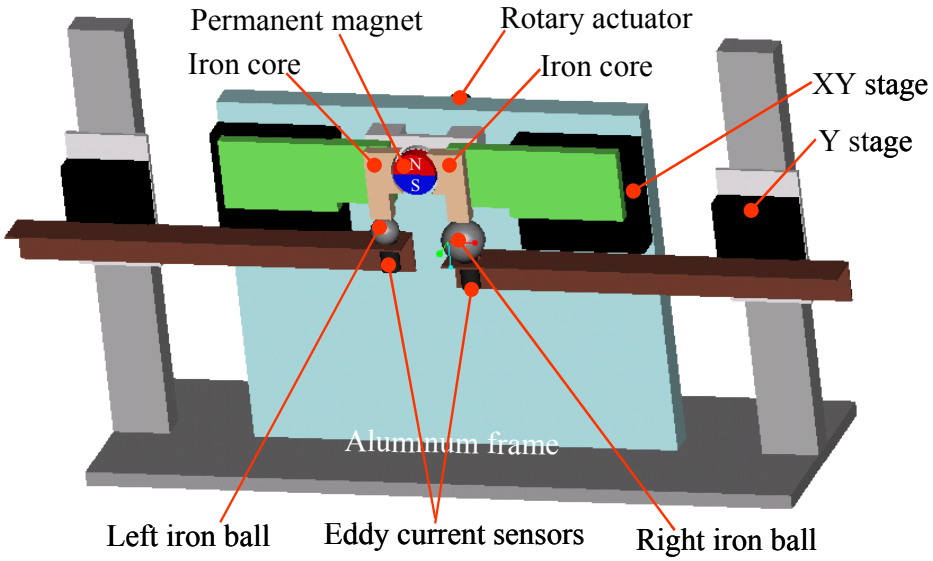

Fig.8.2 The schematic of the magnetic suspension mechanism

photograph of the prototype is shown in Fig.8.3. This prototype consists mainly of a disk permanent magnet, a rotary actuator containing a gear reducer and an encoder, a pair of opposite F-type permalloy cores, two different size iron balls and two eddy current sensors. The disk permanent magnet, which is in the center of the opposite F-type cores, is a neodymium magnet and magnetized in the radial direction. The diameter of the magnet is 30 mm and the thickness is 10 mm. The magnet is installed on the shaft of a rotary actuator. The rotary motor is at behind of the magnet, cannot be seen in Fig.8.3. The encoder of the actuator measures the rotation angle of the magnet. The thickness of the two permalloy cores is 10 mm that is same as the magnet. The diameter of iron ball under the left core is 20 mm, and the weight is 35.8 g. The diameter of iron ball under the right core is 30 mm, and the weight is 109.9 g. The position of the two levitated balls is measured by two eddy current sensors, of which the measurement range is 3.5 mm and the measurement error is less than 0.7 μm.

8.3.2 Control System

The configuration of the system is shown in Fig.8.4. The position of two balls and the angle of magnet are measured, and returned to a DSP controller. Then the DSP controller calculates the current to control the rotary actuator. The actuator drives the magnet rotate to an

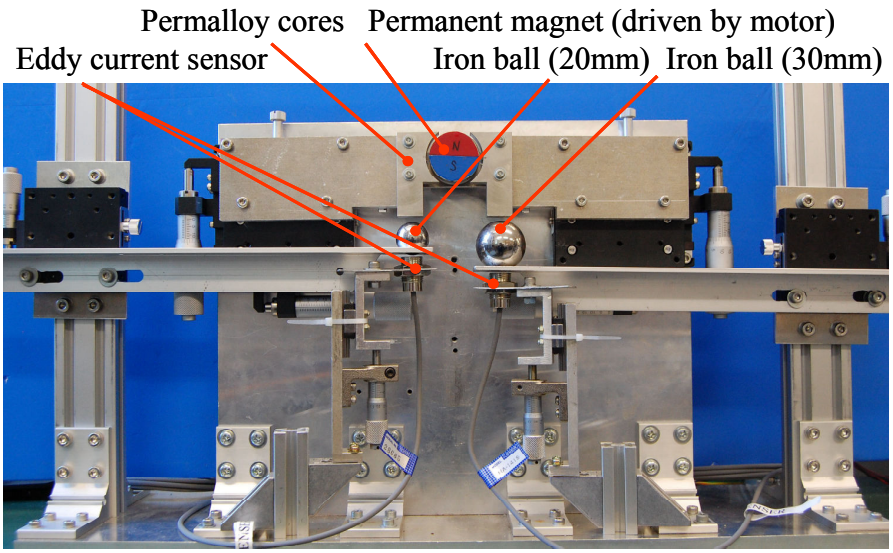

Fig.8.3 Photograph of experimental prototype

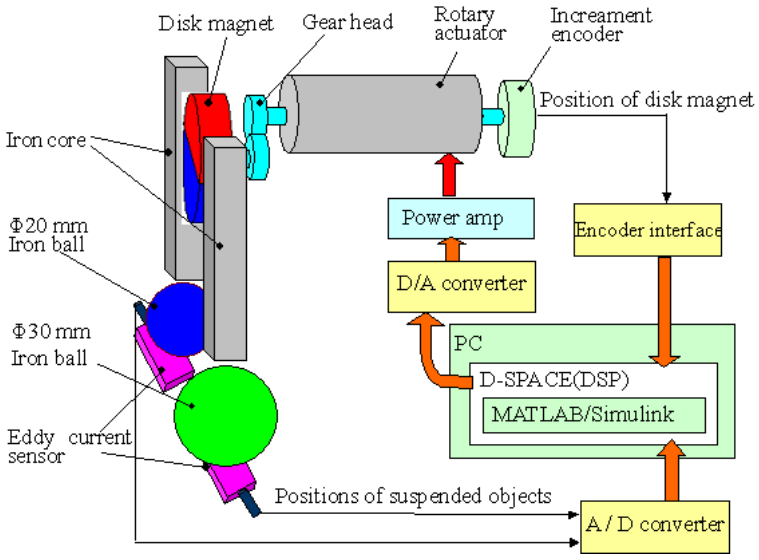

Fig.8.4 Configuration of the magnetic suspension system

appropriate angle. As a result, two iron balls will be suspended without contact.

The control system of the suspension system is shown in Fig.8.5. According to feedback of the positions of two iron balls and the rotation angle of magnet, this control system uses three PD controllers to calculate the current of the rotary motor.

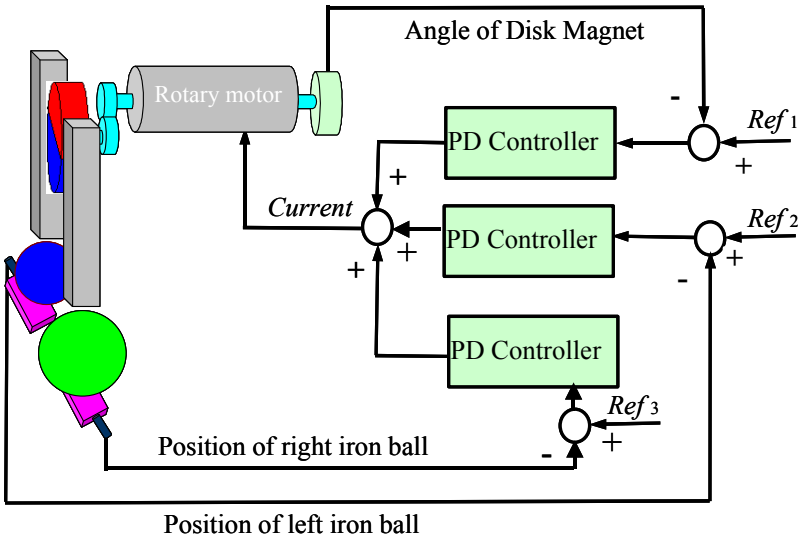

Fig.8.5 Block diagram of control system

8.4 Basic Characteristics Examination by IEM Analysis

8.4.1 Analysis of Magnetic Flux Path

In ELF/Magic software, a 3-D analysis model was created in the same dimension with the experimental prototype, and shown in Fig.8.6. In the model, in order to get a short calculation time, a half of model of the mechanism was created since the mechanism has a symmetry construction in the thickness direction (z direction in the model). And the magnetic flux field in air space is expressed as the blue field in 2-D, and in the middle position of the thickness direction of the mechanism. The magnet is the roundness in the center of the cores, and when the N pole and S pole are arranged as shown in Fig.8.6, the rotational angle of the magnet is assumed as 0 degree. The diameter of left iron ball is 20mm, and that of right iron ball is 30 mm. The air gap between the magnet and the iron cores is 2mm. The length of air gap between the left iron core and the left iron ball is 1.97mm, and the length of air gap between the right iron core and the right iron ball is 1.25 mm, which are the measured equilibrium air gaps of two iron balls, when the magnet stopped at 40 degrees.

Using the analysis model shown in Fig.8.6, the magnetic flux field was analyzed. The analysis results are shown in Fig.8.7 to Fig.8.11. In the figures, the direction of arrows express the direction of the magnetic flux, and the size and color of the arrows express the intensity of the magnetic flux density.

Fig.8.7 shows the analysis result when the magnet stops at 0 degree. There is almost no magnetic flux arrived to the two iron balls, so there are no attractive force between iron cores and the iron balls.

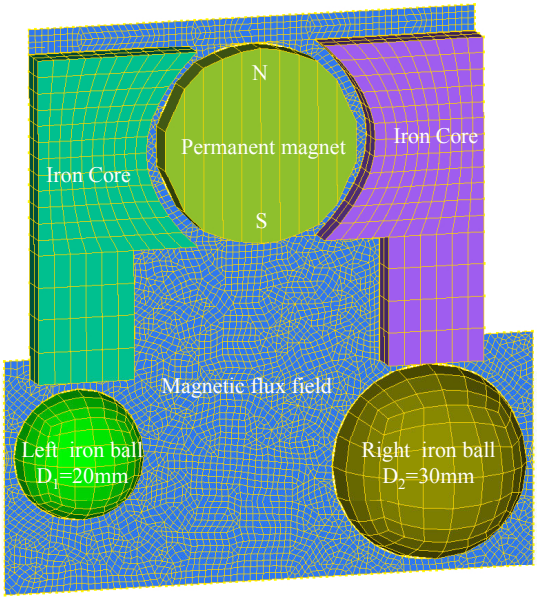

Fig.8.6 3-D model for IEM analysis

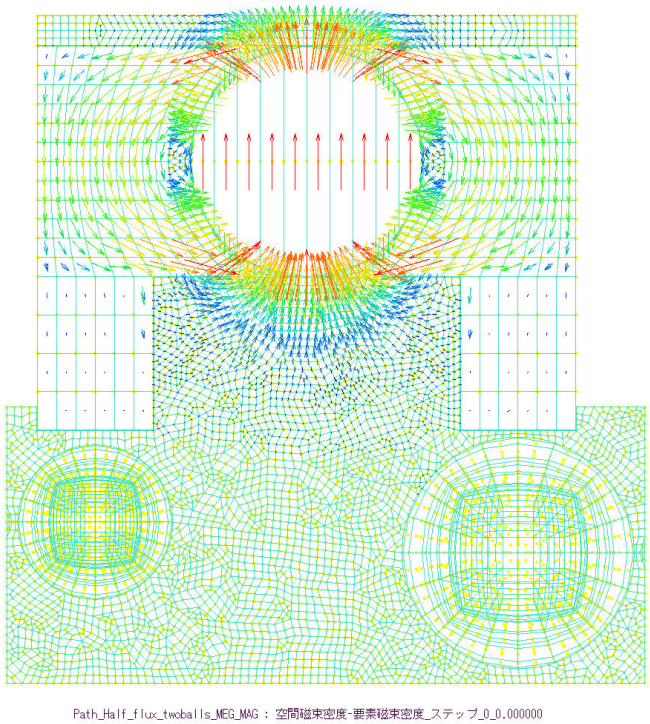

Fig.8.7 Analysis result of magnetic flux field (0 degree)

Fig.8.8 shows the analysis result when the magnet stops at 40 degree. From this result, we can see that there is some magnetic flux arrived to the two iron balls, so the attractive force are generated to support the gravitational force of the balls.

Fig.8.9 shows the 5-time enlarged arrow size of Fig.8.8. The figure indicate that since there is some magnetic flux leakage in the mechanism, some magnetic flux returns to the magnet

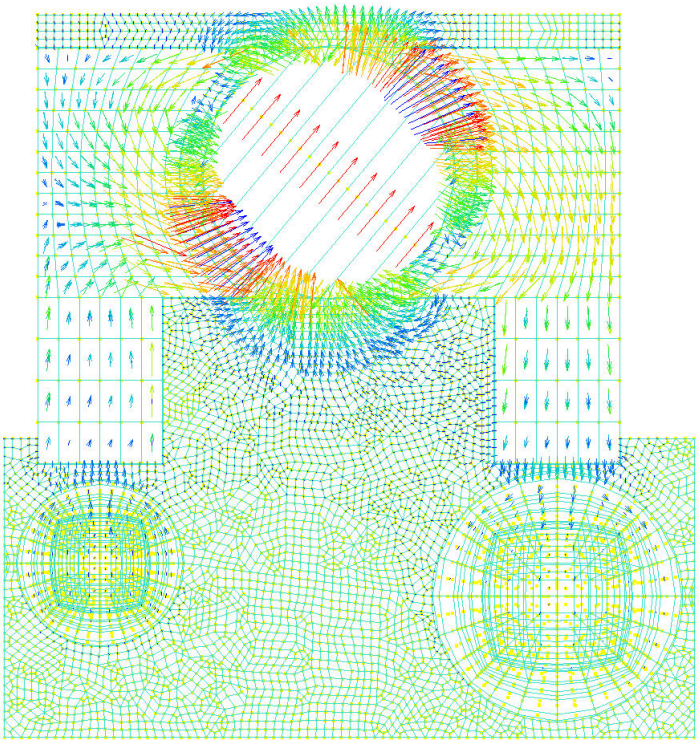

Fig.8.8 Analysis result of magnetic flux field (40 degree)

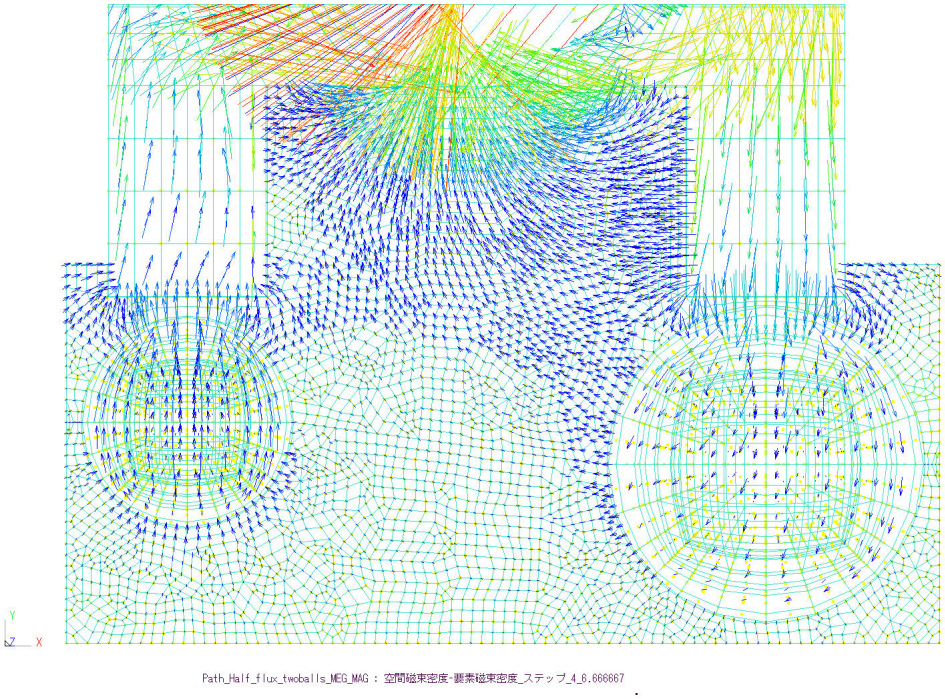

Fig.8.9 Enlarged analysis result with 5 times (40 degree)

directly through the air space, especially in the right iron ball side. That may cause some force in the horizontal direction of the iron ball when the iron balls are suspended.

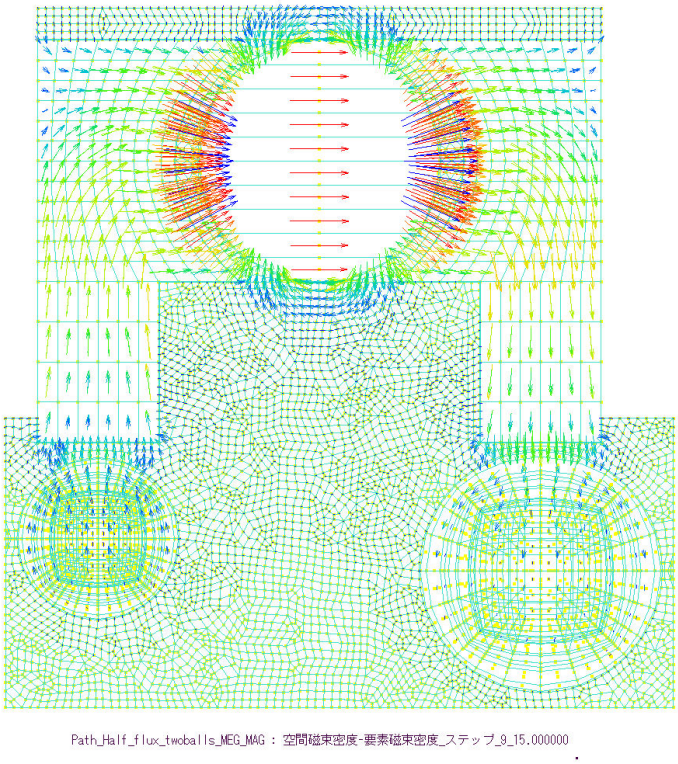

Fig.8.10 Analysis result of magnetic flux field (90 degree)

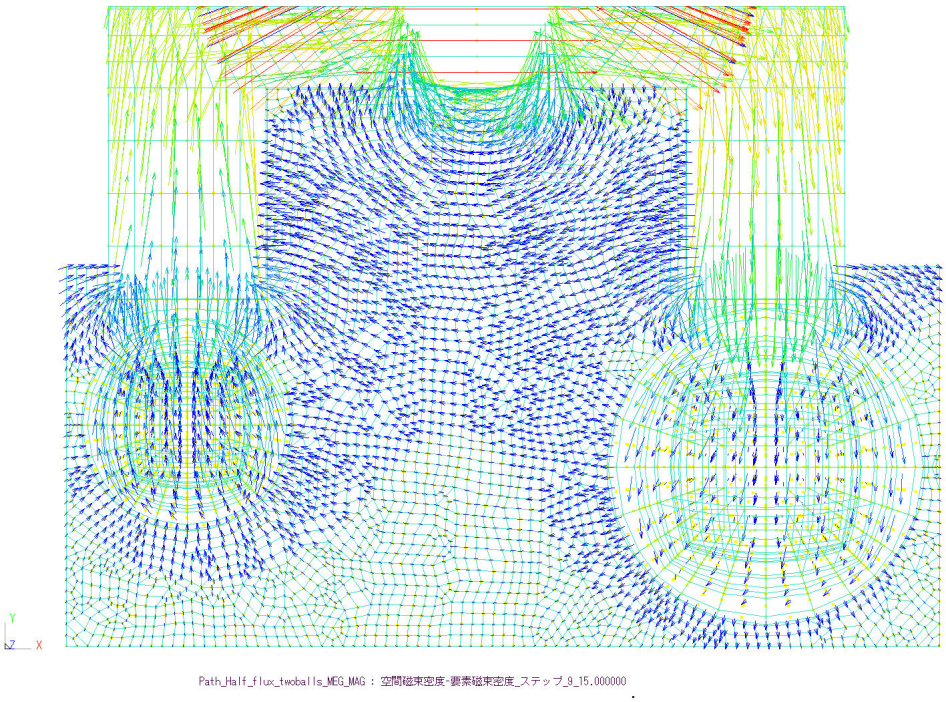

Fig.8.11 Enlarged analysis result with 5 times (90 degree)

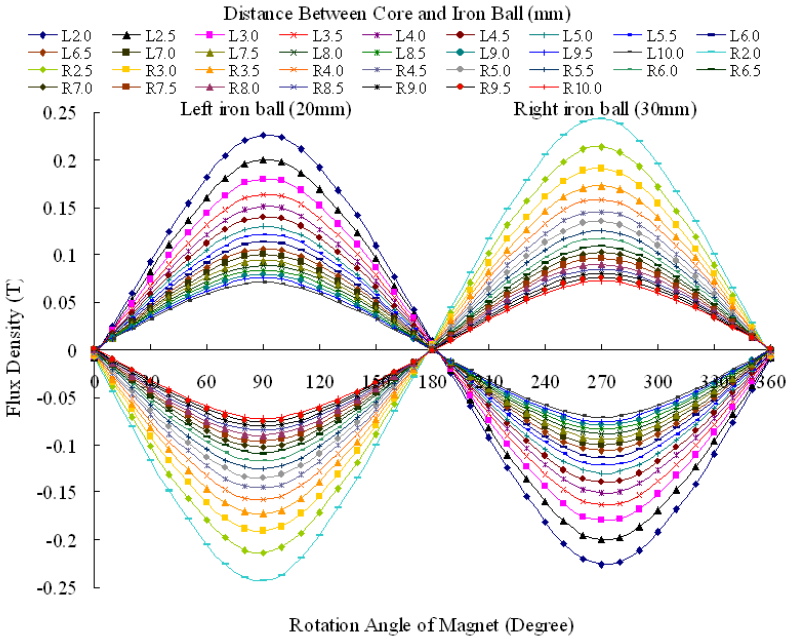

Fig.8.12 Magnetic flux density between cores and two iron balls in IEM

Fig.8.10 shows the analysis result when the magnet stops at 90 degree. This result shows that the arrival magnetic flux to the iron balls is much more than that in Fig.8.8. Fig.8.11 shows the 5-time enlarged arrow size of Fig.8.10. From this figure, we can understand that the right iron ball absorbs the magnetic flux from the right iron core, and the attractive force generates. And then, the magnetic flux is released to the air space from the right iron ball. The left iron ball absorbs the magnetic flux from the air space, and mainly releases the flux to the left iron core, finally the magnetic flux returns to the S pole of the magnet through the left core. Moreover, we can see that the left iron ball absorbs some magnetic flux released by the right iron ball in the air space between two iron balls. That will cause the attractive force between two iron balls. As a result, when the two iron balls are suspended, the equilibrium point in the horizontal direction will no be at the just below position of the iron cores, and will be at some position closing with each other.

8.4.2 Analysis of Magnetic Flux Density

The magnetic flux densities and attractive forces from the cores were analyzed, when the permanent magnet was rotated at 10 degrees as one step in one revolution. The air gap length between the left core and the left ball was changed from 2 mm to 10 mm, and increased at 0.5 mm as a step, when the right ball was fixed at the air gap length of 2 mm, For the right iron ball, the left iron ball was fixed at the air gap length of 2 mm.

Fig.8.12 shows the analysis results of magnetic flux density. In the figure, the horizontal axis expresses the rotation angle of permanent magnet, the vertical axis expresses the magnetic flux density on the surface of iron ball, and the parameters on the top of figures

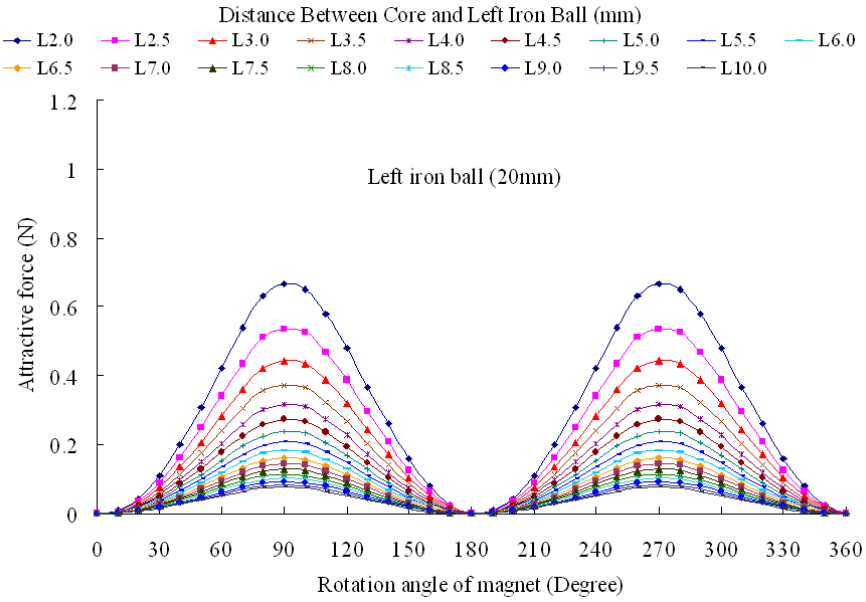

Fig.8.13 Attractive force between left core and left iron ball in IEM

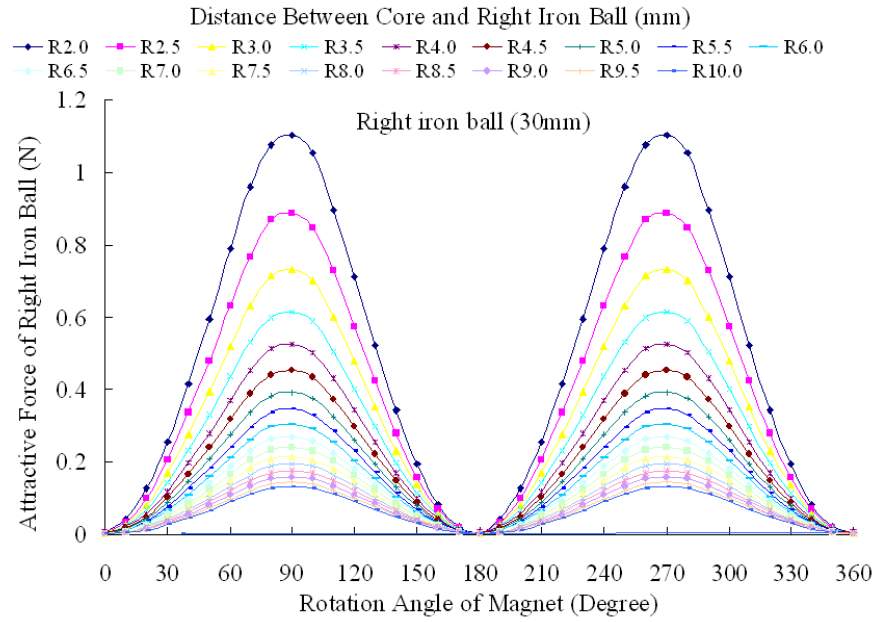

Fig.8.14 Attractive force between right core and right iron ball in IEM

express the distance between the core and iron ball. The graph of magnetic flux density resembles sine curve according to the magnet's angles at all distance, and smaller distance yielded greater flux density. The flux density on the surface of big iron ball is always large. Moreover, the direction of the flux is changing at about 180 degrees. The magnetic flux density of the big right iron ball is larger than the small left iron ball at the same air gap length.

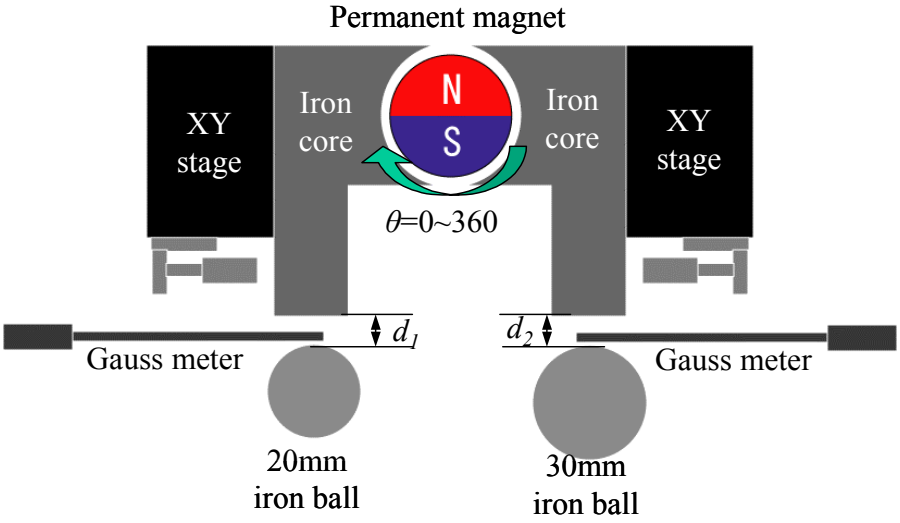

Fig.8.15 Schematic of the measurement experiment for magnetic flux density

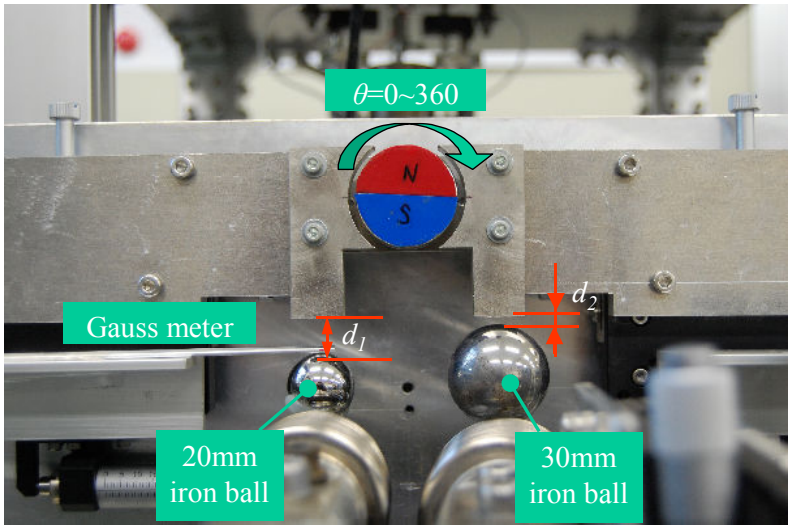

Fig.8.16 Photograph when measuring the magnetic flux density of left ball

8.4.3 Analysis of Attractive Force

Fig.8.13 shows the results of the attractive force between the left iron core and the left iron ball. Fig.8.14 shows the results of the attractive force between the right iron core and the right iron ball. As shown in the figures, the force curve in each position varies according to the rotated angle of the magnet, and has 2 maximum points at about 90 degrees and 270 degrees and has 2 approximately zero points at about 0 degree and 180 degrees. The forces become smaller when the gap becomes larger, and the attractive force of big ball is large.

8.5 Basic Characteristics Examination by Measurement Experiment

Moreover, in order to know the basic characteristics of the proposed prototype, the measurement experiments were also carried out using the manufactured mechanism.

8.5.1 Magnetic Flux Density

Fig.8.15 shows the schematic of the measurement experiment for magnetic flux density near the surface of the two iron balls using gauss meters. Fig.8.16 shows the photograph when measuring the magnetic flux density of left iron ball. In the measurement experiment, when the rotational angle θ of the permanent magnet was rotated at 10 degrees as one step in one revolution, and the air gap length d2 was fixed at 2 mm, the flux density was measured with the changing range of the air gap length d1 from 2 mm to 10 mm, and the changing step was 1 mm. Moreover, the similar experiment was implemented for the right iron ball. The measurement results of the magnetic flux density are shown in Fig.8.17 and Fig.8.18. Fig.8.17 shows the relationship between the magnetic flux density and the rotational angle of the permanent magnet. The results show the relationship between the magnetic flux density and the rotational angle as a sine curve, which are similar to the IEM analysis results. Fig.8.18

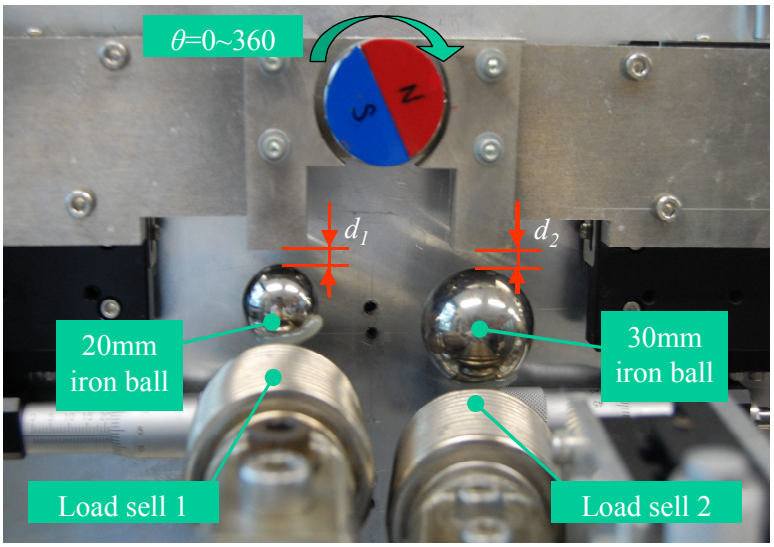

Fig.8.19 Photograph of measurement experiment for attractive force

shows the relationship between the magnetic flux density and the distance between the core and the iron ball. The results indicate that the magnetic flux density is inverse proportion to the distance between the core and the iron ball.

8.5.2 Attractive force

The attractive force between the iron cores and the iron balls were measured using two load

cells. Fig.8.19 shows the photograph of the measurement experiment. The same processes of the experiments for the attractive force were carried out with the experiments for the magnetic flux density.

The measurement results of the attractive force of the left iron ball are shown in Fig.8.20 and Fig.8.21. Fig.8.20 shows the relationship between the attractive force and the rotational angle of the magnet. Fig.8.20 indicates that the attractive force is similar to the square the sine relationship to the rotational angle of the magnet. There are two almost zero points appearing at 0 degree and 180 degrees, and two peak forces appearing at 90 degrees and 270 degrees. Therefore, the attractive force can be controlled through changing the angle of the magnet. Fig.8.21 shows the relationship between the attractive force and the distance between the iron

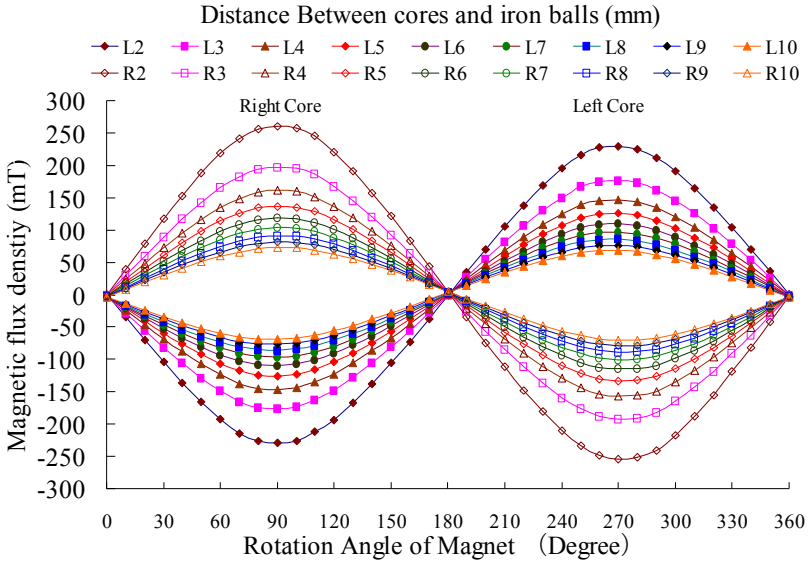

Fig.8.17 Relationship between flux density and rotational angle

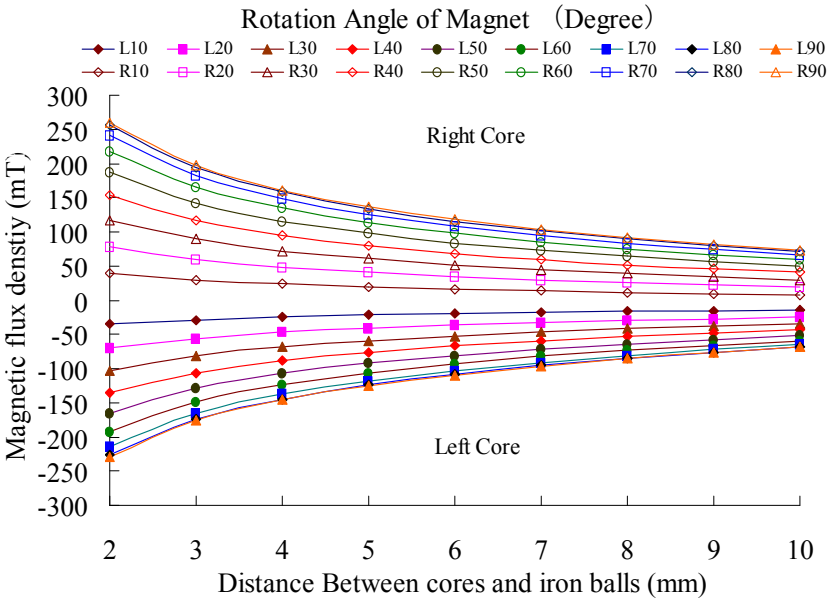

Fig.8.18 Relationship between flux density and air gap

core and the iron ball. The results indicate that the attractive force is almost square of the inverse proportion to the distance.

The measurement results of the attractive force of the right iron ball are shown in Fig.8.22 and Fig.8.23. Fig.8.22 shows the relationship between the attractive force and the rotational angle of the magnet. Fig.8.23 shows the relationship between the attractive force and the distance between the iron core and the iron ball. The results of the right iron ball is similar to the results of the left iron ball, the attractive force of the right ball, however, is larger than the left ball' at all same points.

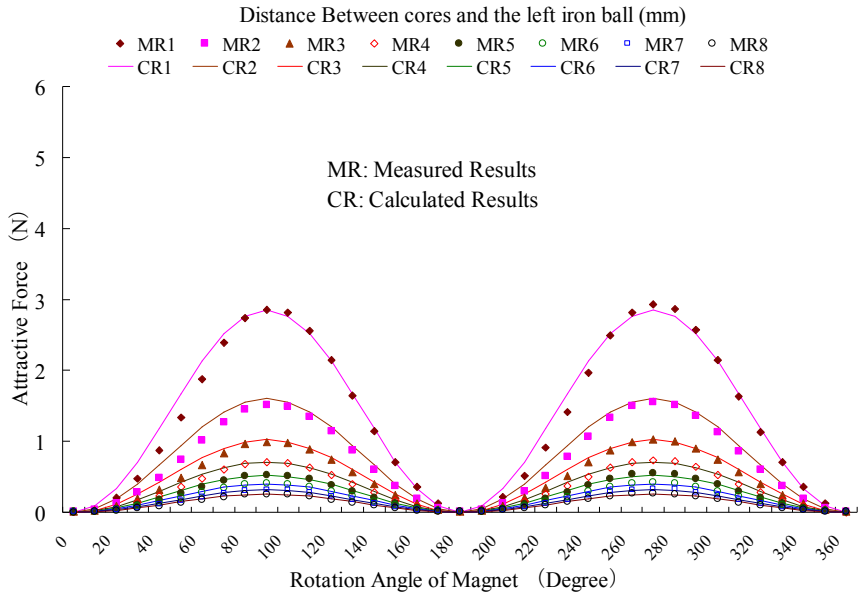

Fig.8.20 Relationship between force and rotational angle of left ball

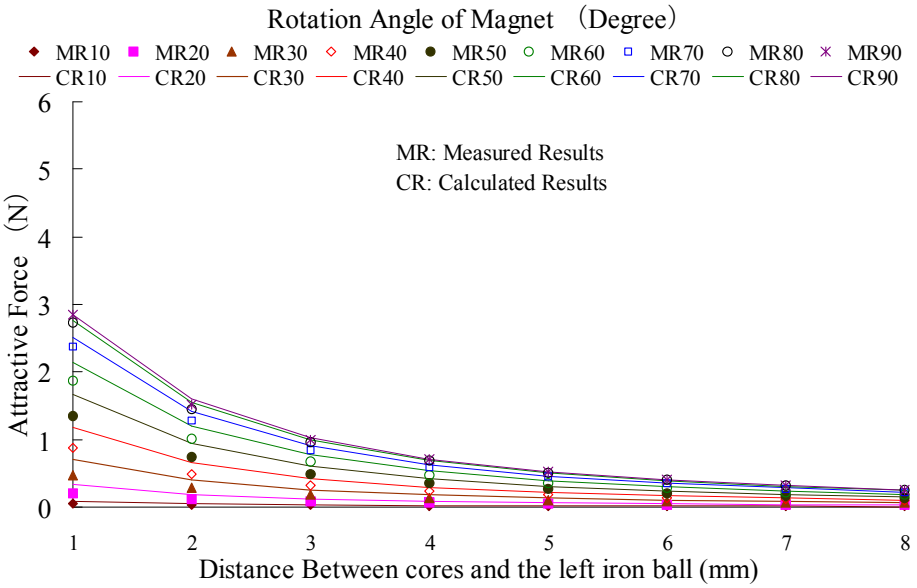

Fig.8.21 Relationship between force and air gap of left ball

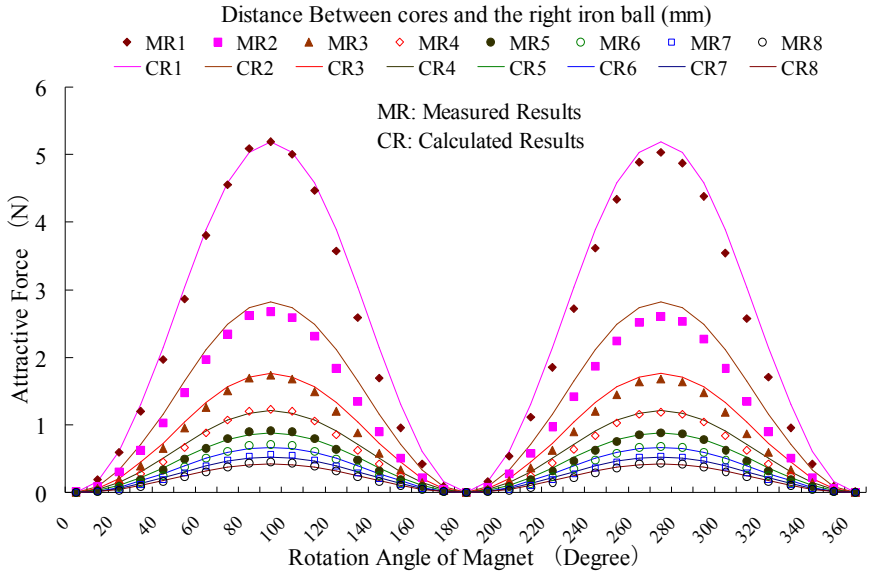

Fig.8.22 Relationship between force and rotational angle of right ball

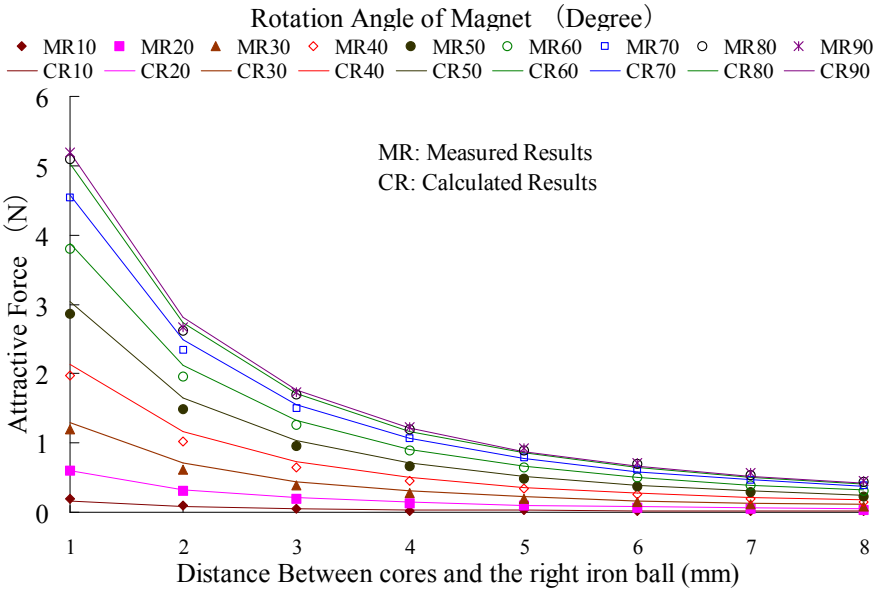

Fig.8.23 Relationship between force and air gap of right ball

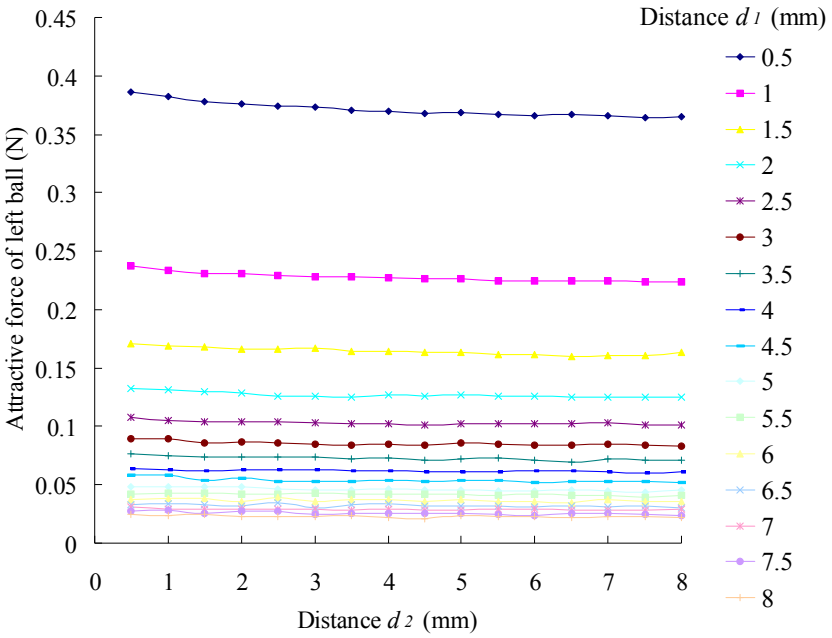

Fig.8.24 Interaction examination results of left iron ball

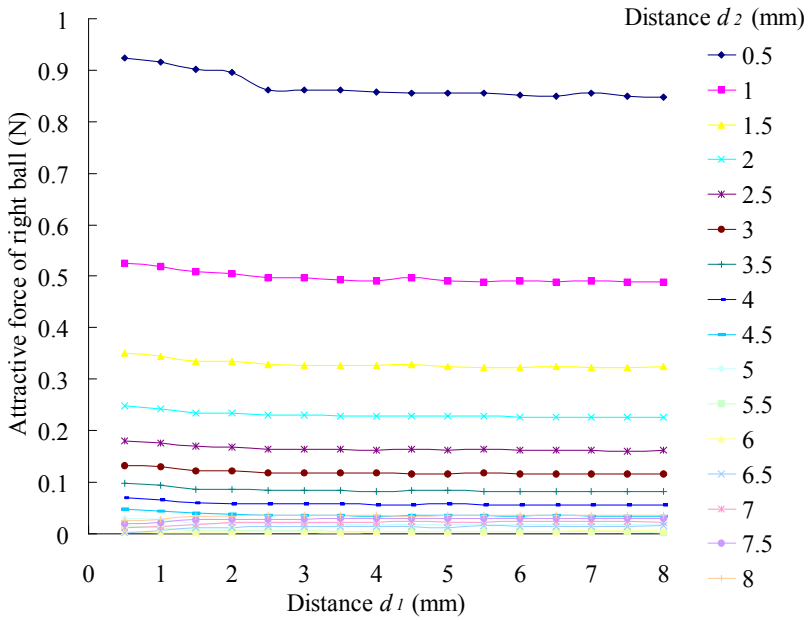

Fig.8.25 Interaction examination results of right iron ball

8.5.3 Examination of Interaction between Two Iron Balls

In order to examine the interaction between two iron balls in the suspension direction, the examination experiments were carried out. The interaction between two iron balls in the suspension direction means that, when the rotational angle of the magnet is fixed, e.g. the angle is fixed at 30 degrees, whether the movement of one side iron ball influences the suspension force of the other side iron ball or not. The experimental device and the parameters are same with the measurement device shown in Fig.8.19. The examination

experiment of left iron ball was carried out as following:

(1) Fix the rotational angle θ of magnet to 30 degrees.

(2) Fix d_1 to 0.5 mm.

(3) Measure the attractive force of the left iron ball when changing d_2 from 0.5 mm to 8 mm at a step of 0.5 mm.

(4) Increase d_1 at the step of 0.5 mm, and repeat (3).

(5) Repeat (3) and (4), until d_1 reach 8 mm.

Moreover, the examination experiment of the right iron ball was carried out in the same process with the left ball'.

Fig.8.24 shows the interaction examination results of the left iron ball. Fig.8.25 shows the interaction examination results of the right iron ball. The results indicate that there is almost no interaction between two iron balls. Although, a little influence occurs when the right iron ball is at 0.5 mm, but that displacement range will not be used in the suspension experiments. As a result, it is feasible to suspend two iron balls simultaneously.

8.6 Theoretical Feasibility Analysis

In order to investigate the feasibility of the proposed magnetic suspension system, a model is setup, and the controllability of the experimental system are checked for simultaneous suspension of two balls.

8.6.1 Suspension Force Modeling

For setting up the model, first, the following is assumed:

One half of the permanent magnet is N pole and the other half part is S pole.

The flux coming out from the magnet and absorbed to the magnet is in proportion to the area facing to the iron core.

The magneto-resistance of the iron cores is small enough and all magnetic flux passes through the two iron cores.

Second, according to the result in Fig.8.17 and Fig.8.18, the relationship of the flux flowing through iron ball, the rotation angle of permanent magnet and the distance between core and iron ball can be considered as:

$$Q = k_Q \frac{\sin\theta}{d} \tag{8.1}$$

where,

Q : the magnetic flux flowing through the levitated object

k_Q : the constant of magnetic flux

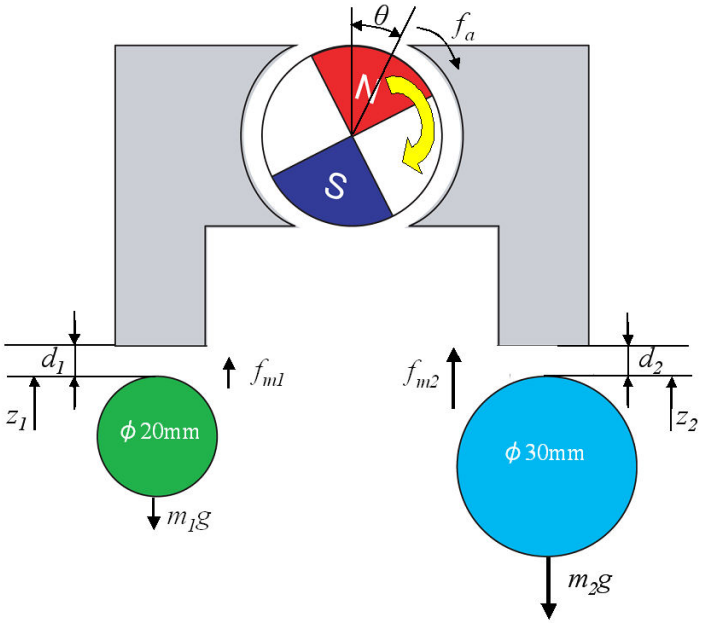

Fig.8.24 Model of suspension system

θ : the rotated angle of the magnet (positive is the clockwise direction)

d : the distance between core and iron ball

Moreover, according to the results from Fig.8.20 to Fig.8.23, we can consider that the attractive force is in proportion to the square of the flux. Then the attractive force f_{mi} (i=1, 2) between core and iron ball can be expressed as,

$$f_{mi} = k_{mi} \frac{\sin^2 \theta}{\left(d_i + \Delta d_{mi}\right)^2} \tag{8.2}$$

Where k_{mi} is a proportionality coefficient of attractive force and Δd_{mi} is a compensation coefficient of air gap. Comparing the attractive force calculated by Equation (8.2) with the measurement results, the coefficients k_{m1} and k_{m2} can be decided as 2.56×10^{-5} (Nm^2) and 4.06×10^{-5} (Nm^2). And the coefficients Δd_{m1} and Δd_{m2} can be decided as 2 mm and 1.8 mm. The comparison results shown in Fig.8.20 to Fig.8.23, where the solid line expresses the calculation force and the point mark expresses the measurement force. The comparison indicates that Equation (8.2) expresses the measurement results of the attractive force very well, and the validity of attractive force model is proved.

8.6.2 Motion Equations of Motor and Two Suspended Iron Balls

A model of this simultaneous suspension system is created and shown in Fig.8.24. According to the model and the assumptions, the motion equations of the magnet and two

iron balls are, respectively,

$$J\ddot{\theta} = c\dot{\theta} + k_{\tau}\sin 2\theta + k_t i \tag{8.3}$$

$$m_1\ddot{z}_1 = k_{m1}\frac{\sin^2\theta}{\left(d_1 + \Delta d_{m1} - z_1\right)^2} - m_1 g \tag{8.4}$$

$$m_2\ddot{z}_2 = k_{m2}\frac{\sin^2\theta}{\left(d_2 + \Delta d_{m2} - z_2\right)^2} - m_2 g \tag{8.5}$$

where,

m_1 : the mass of left iron ball

m_2 : the mass of right iron ball

z_1 : the displacement of left iron ball

z_2 : the displacement of right iron ball

f_{m1}: the attractive force between the left core and iron ball

f_{m2}: the attractive force between the right core and iron ball

k_{m1}: the constant of the attractive force between the left core and iron ball

k_{m2}: the constant of the attractive force between the right core and iron ball

d_1: the distance between the left core and iron ball

d_2: the distance between the right core and iron ball

J: the moment of inertia of motor and magnet

c: the damping constant of motor and reducer.

f_a: the driving force of motor

k_t: the torque constant of motor

k_{τ}: the torque constant of magnet

i: the input current of motor

8.6.3 Analysis of Controllability

In the motion equations of this system, the attractive force f_m is represented as a nonlinear function of the rotation angle of permanent magnet and the distance between core and iron ball. Moreover, the attractive force becomes larger as the rotation angle increases and becomes smaller as the distance decreases. Through linearization of the attractive force around the equilibrium position, the linear relationship of attractive force, rotation angle and the distance can be obtained.

$$\tau = \frac{2k_\tau(1-2(\sin\theta_0)^2)}{J}\Delta\theta \tag{8.6}$$

$$\Delta f_{mi} = \frac{2k_{mi}(\sin\theta_0)^2}{\left(d_{i0}+\Delta d_{mi}\right)^3}\Delta z_i + \frac{k_{mi}\sin 2\theta_0}{\left(d_{i0}+\Delta d_{mi}\right)^2}\Delta\theta \tag{8.7}$$

where,

$i = 1,2$

Δf_{jm}, Δz_i, $\Delta\theta$: the small value around the equilibrium position

θ_0, d_{i0} : the value at the equilibrium position

Moreover, assuming that:

$$d_{mi} = d_{i0} + \Delta d_{mi} \tag{8.8}$$

According to the equations from Equation (8.2) to Equation (8.8), the state space equation and the output equation are represented as:

$$\begin{aligned} \dot{x} &= Ax + Bu \\ y &= Cx \end{aligned} \tag{8.9}$$

where

$$x = \begin{pmatrix} z_1 & \dot{z}_1 & z_2 & \dot{z}_2 & \theta & \dot{\theta} \end{pmatrix}'$$

$$A = \begin{bmatrix} 0 & 1 & 0 & 0 & 0 & 0 \\ \frac{2k_{m1}(\sin\theta_0)^2}{m_1 d_{m1}^3} & 0 & 0 & 0 & \frac{k_{m1}\sin 2\theta_0}{m_1 d_{m1}^2} & 0 \\ 0 & 0 & 0 & 1 & 0 & 0 \\ 0 & 0 & \frac{2k_{m2}(\sin\theta_0)^2}{m_2 d_{m2}^3} & 0 & \frac{k_{m2}\sin 2\theta_0}{m_2 d_{m2}^2} & 0 \\ 0 & 0 & 0 & 0 & 0 & 1 \\ 0 & 0 & 0 & 0 & \frac{2k_\tau(1-2(\sin\theta_0)^2)}{J} & \frac{c}{J} \end{bmatrix}$$

$$B = \begin{pmatrix} 0 & 0 & 0 & 0 & 0 & \frac{k_t}{J} \end{pmatrix}'$$

$$C = \begin{pmatrix} 1 & 0 & 0 & 0 & 0 & 0 \\ 0 & 0 & 1 & 0 & 0 & 0 \\ 0 & 0 & 0 & 0 & 1 & 0 \end{pmatrix}$$

$$u = i$$

The controllability matrix of the system of Equation (8.9) is,

Table.8.1 Parameters using in numerical simulation

Parameter	Value	Parameter	Value
m_1 (kg)	0.06233	c_1 (N/(m/s))	0
m_2 (kg)	0.13479	J (kgm^2)	6.37×10^{-4}
d_{10} (mm)	2.2	k_t (Nm/A)	0.69
d_{20} (mm)	1.8	k_{1m} (Nm^2)	2.56×10^{-5}
Δd_{m1} (mm)	2	k_{2m} (Nm^2)	4.0645×10^{-5}
Δd_{m2} (mm)	1.8	g (m/s^2)	9.8
θ_0 (degree)	40		

$$P_c = \begin{pmatrix} B & AB & A^2B & A^3B & A^4B & A^5B \end{pmatrix} \tag{8.10}$$

Then determinant of the controllability matrix is,

$$\det(P_c) = \frac{-4k_{m1}^{\ 2}k_{m2}^{\ 2}k_t^{\ 6}\sin^4\theta\sin^4 2\theta(d_{m1}^{\ 3}k_{m2}m_1 - d_{m2}^{\ 3}k_{m1}m_2)^2}{d_{m1}^{\ 10}d_{m2}^{\ 10}J^6m_1^{\ 4}m_2^{\ 4}} \tag{8.11}$$

When,

$$d_{m1}^{\ 3}k_{m2}m_1 - d_{m2}^{\ 3}k_{m1}m_2 \neq 0 \tag{8.12}$$

$$Rank(Pc) = 6 \tag{8.13}$$

According to the characteristic of the suspension system, when the mass of two iron balls is different, the determinant of the controllability matrix is nonzero, and the controllability matrix is full rank. Consequently, the proposed magnetic suspension system is controllable, and suspension feasibility is verified, theoretically.

8.7 Numerical Simulation Examination

In this feasibility study, first, the control system is introduced. Second, the feedback gains are calculated using the LQR (linear quadratic regulator) full state feedback control law with the linear mathematical model of Equation (8.9). Finally, the numerical simulation is carried out with a nonlinear attractive force.

8.7.1 Control System

Fig.8.25 shows the structure of the control system. In this control system, three PD controllers are used to realize the suspension of two iron balls stably and simultaneously.

8.7.2 Calculation of Feedback Gains

All the parameters using in the numerical simulation are shown in Table.8.1, which are measured from the experimental prototype. Moreover, the values of k_{m1} and k_{m2} are measured from Fig.8.20 to Fig.8.23.

Many methods can design the controller for a linear system. In terms of linear control theory, due to this proposed system is controllable and observable, the LQR can be used to get the feedback gains.

Based on the characteristics of the system and Equation (8.9), we chose the state weighting matrix Q and input weighting matrix R as following:

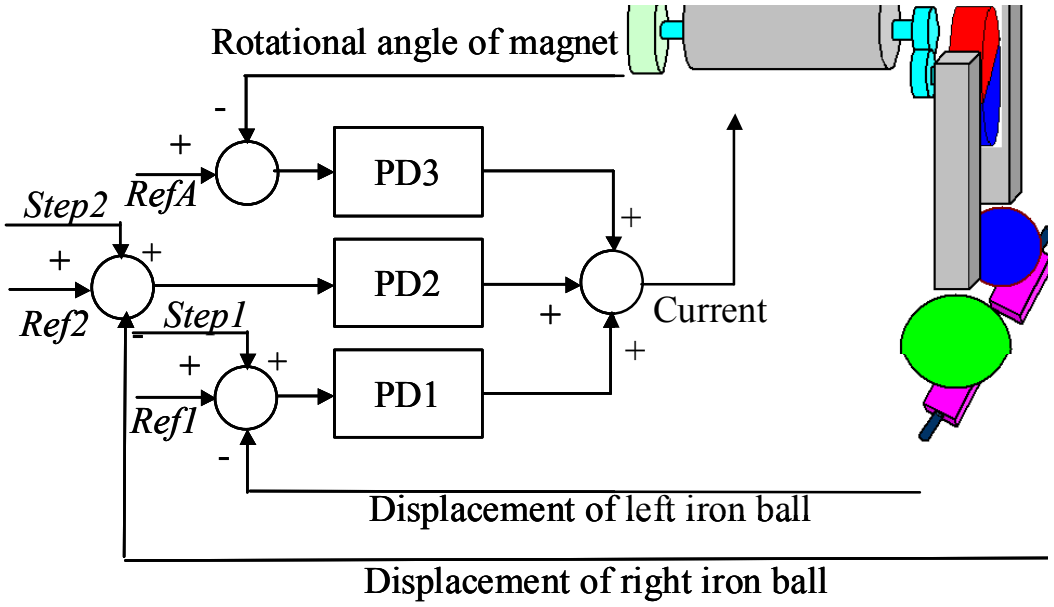

Fig.8.25 Structure of control system

$$Q = \begin{bmatrix} 10000000000 & 0 & 0 & 0 & 0 & 0 \\ 0 & 1000000 & 0 & 0 & 0 & 0 \\ 0 & 0 & 1000000000 & 0 & 0 & 0 \\ 0 & 0 & 0 & 1000000 & 0 & 0 \\ 0 & 0 & 0 & 0 & 1 & 0 \\ 0 & 0 & 0 & 0 & 0 & 0 \end{bmatrix} \tag{8.14}$$

$$R = 1 \tag{8.15}$$

Using MATLAB software, the feedback gain K is calculated as following:

$$K = \begin{bmatrix} -9669000 & -140810 & 10908000 & 147060 & 466.64 & 0.9282 \end{bmatrix} \tag{8.16}$$

8.7.3 Numerical Simulation

Using the nonlinear attractive force model and the calculated feedback gain, the simulation

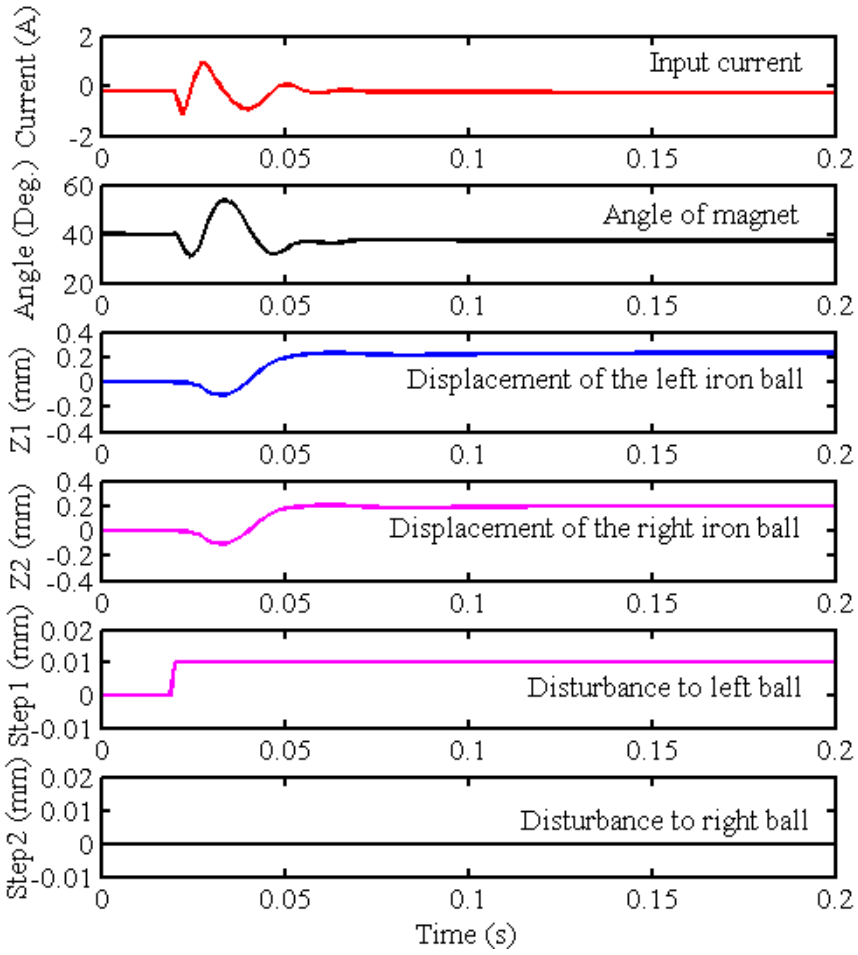

Fig.8.26 Simulation results when a step is applied to left iron ball

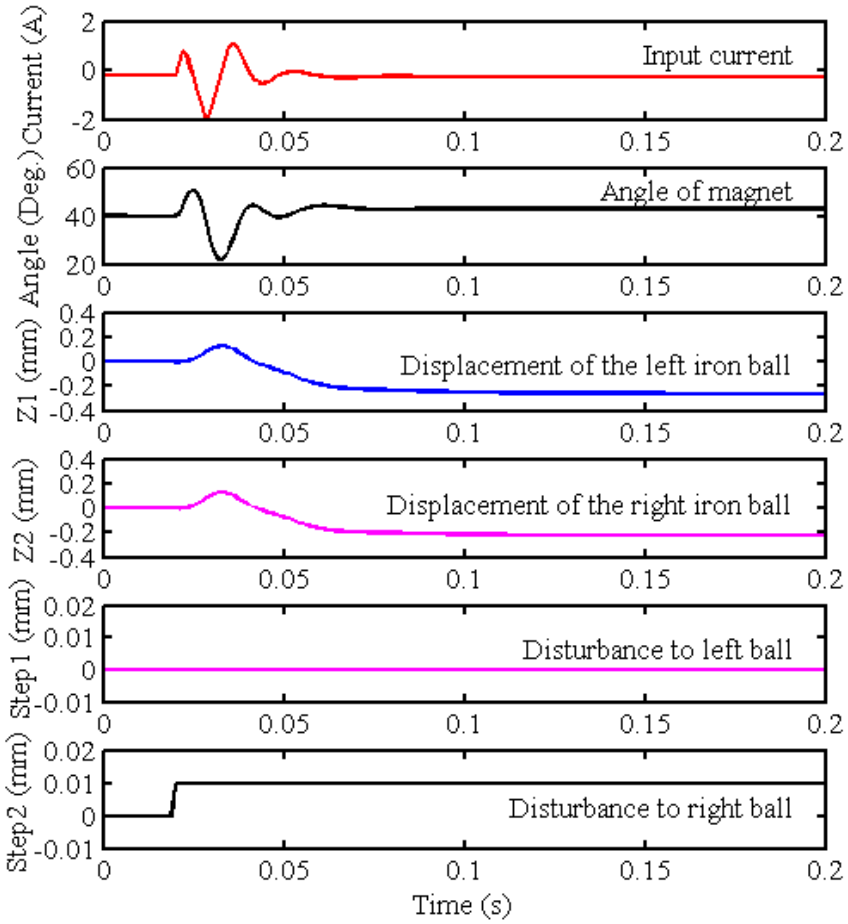

Fig.8.27 Simulation results when a step is applied to right iron ball

was carried out. The simulation results show in Fig.8.26 and Fig.8.27. In the simulation, when the two iron balls were levitated, a 0.01 mm step value was added to the two iron balls as a disturbance, respectively. After the step was added, the input current of motor, the rotational angle of magnet, and two iron balls' displacements were recorded. The step was added at 0.1 second, and the responses were recorded until 0.5 second. The variations of current, angle, displacements, and the disturbances were plotted, with the upward direction as positive.

Fig.8.26 shows the simulation results when the step is applied to the left iron ball. In the figure, after applying the step, the system reinstates the steady suspensions of two iron balls quickly. The step drives the left iron ball move upward, and for maintaining the suspension force equal with gravitational force of the iron ball, the rotational angle of magnet becomes small a little. However, the variation of rotational angle also directly affects the suspension of the right iron ball. In order to also suspend the right iron ball stably, the system moves the right iron ball up a little distance at same time with the left iron ball. Since the gravitational force of iron balls is supported by the two iron cores fixed on the frame, the motor just drives the magnet' rotation, and the input current of motor returns to zero after returning to the equilibrium state.

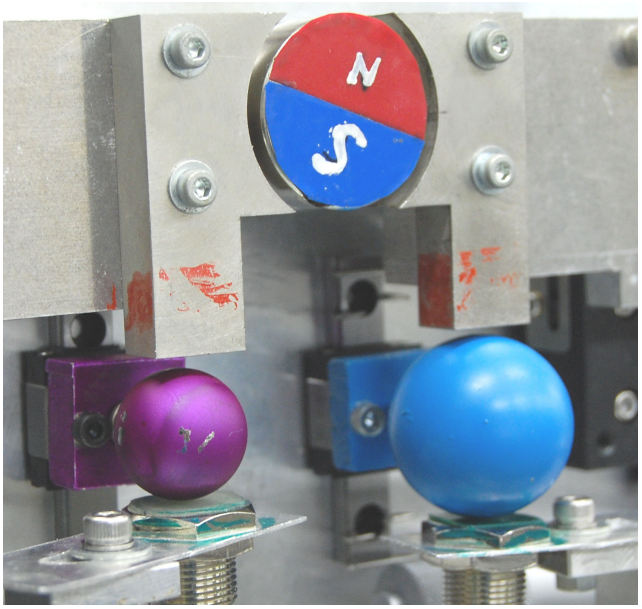

Fig.8.28 Photograph of the suspension device with linear rails

Fig.8.27 shows the simulation results when the step is applied to the right iron ball. The results in Fig.8.26 indicate that, the suspensions of two iron balls can also be realized stably after applying the disturbance to the right iron ball. However, the movements of two iron balls are downward, and the final angle of the magnet increases, which are reverse to the results in Fig.8.26. The different signs of the feedback gains for the two iron balls' suspension cause these differences. The feedback gains for left ball are minus, and the ones for right ball are plus.

Consequently, all the simulation results indicated that this proposed system could simultaneously suspend two iron balls steadily.

8.8 Experimental Suspension

Using the experimental prototype, the suspension was carried out. However, the equilibrium position in the horizontal direction is not just at the lower center of the iron cores. It caused the stable suspension to be realized difficultly. In order to limit the iron balls move in the suspension direction only, the iron balls were installed onto two linear rails and the suspension was succeeded. Fig.8.28 shows the suspension photograph using the mechanism with the linear rails. After using the linear rails, the suspended unit included the iron ball, the block of the linear rail, and the connecting parts. In this situation, the mass of the left suspended unit was 62.33 g, and the mass of the right suspended unit was 134.79 g. In the suspension experiments, the used feedback gains are same with the gains used in simulations.

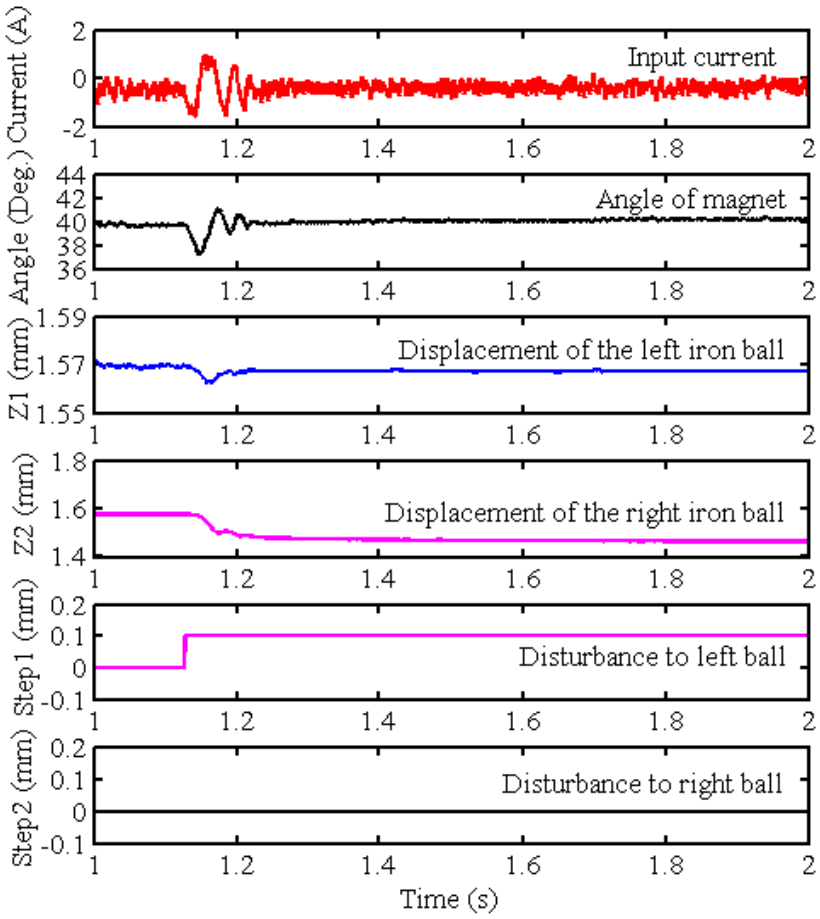

Fig.8.29 Experimental results of step response to the left iron ball

In order to examine the stability of the suspension, a step response experiment was carried out for two iron balls respectively. In the experiments, the step response with 0.1 mm was applied after 1.2 s, and the response results were recorded until 2.2 s. The step response results are shown in Fig.8.29 and Fig.8.30. In the figures, the variations of current, angle, displacements, and the disturbances were plotted, with the upward direction as positive.

Fig.8.29 shows the step response results of the left iron ball. After applying the step disturbance. The system returns to stable state immediately. The upward step of the left iron ball made two iron balls move downward at same time. This movement is reversing to the simulation results. In the simulation, the upward step got an upward response. The difference may be caused by the different feedback gains and the different initial values between the simulation and the experiment. Moreover, we can understand the results as that, in the experiment, the two iron balls reach the stable suspension state without vibrations after applying the disturbance; and in the simulation, the two iron balls reach the stable suspension state after a vibration and reach another stable state. The rotational angle of the magnet decreased firstly, and then increased to maintain the balance state after applying the step disturbance. In the final state, the two iron balls moved down, and the rotational angle of

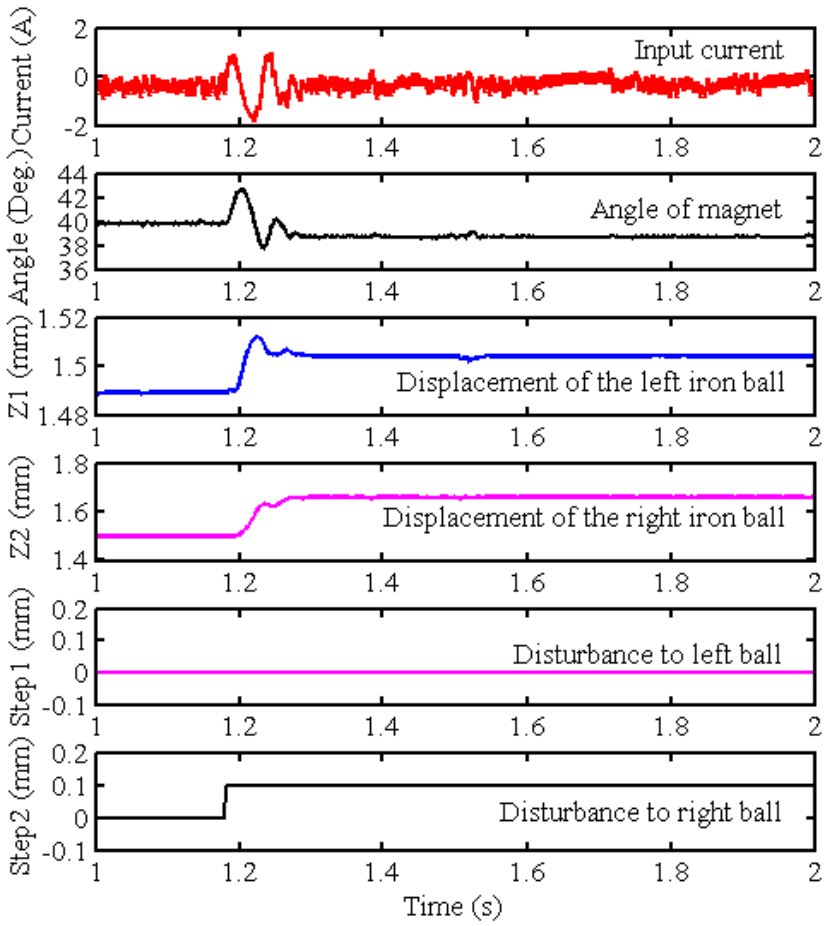

Fig.8.30 Experimental results of step response to the right iron ball

magnet increased.

Moreover, Fig.8.30 shows the step response results of the right iron ball. The system also reaches the second stable suspension state quickly. However, the movement of the two iron balls is reversing to the results in Fig.8.29. This is caused by the inverse sign of the feedback gains, and agrees with the simulation results. The response of this system between simulation and experimental results is consistent with each other.

However, the final value of the stable state is reverse between the simulation results and the experimental results. The upper step that was applied to the left iron ball causes the two iron balls moving upward in simulation, and downward in experiment. And the upper step that was applied to the right iron ball causes the two iron balls moving downward in simulation, and upward in experiment.

8.9 Examination of results' validity

In order to examine the validity of the simulation results and the experimental results, the

initial values and final values of the simulation and experimental results when the upper step was applied to the left iron ball, were concluded and shown in Table.8.2. And all the values were input to the stable state eqations of this system from Equation (8.17) to (8.19), the results of all the equations were 0. This indicates that all the results of simulation and experiment are satisfied with the motion equations, and the validity of the results is proven.

Table.8.2 Results of validity examination

	Simulation		Experiment	
	Initial value	Final value	Initial value	Final value
$Refz_1$ (mm)	0	0	1.5	1.5
$Refz_2$ (mm)	0	0	1.5	1.5
z_1 (mm)	0	0.2399	1.569	1.567
z_2 (mm)	0	0.2075	1.577	1.47
θ (deg.)	40	37.68	39.74	40.12
i (A)	-0.26	-0.255	-0.26	-0.262
Eq.1	0	0	0	0
Eq.2	0	0	0	0
Eq.3	0	0	0	0

$$Eq.1 = k_\tau \sin 2\theta + k_t i \tag{8.17}$$

$$Eq.2 = k_{m1} \frac{\sin^2 \theta}{\left(d_1 + \Delta d_{m1} - z_1\right)^2} - m_1 g \tag{8.18}$$

$$Eq.3 = k_{m2} \frac{\sin^2 \theta}{\left(d_2 + \Delta d_{m2} - z_2\right)^2} - m_2 g \tag{8. 19}$$

8.10 Conclusions

In this chapter, a simultaneous suspension system of two iron balls was proposed using a disk type permanent magnet and a rotary motor. This system controlled the suspension force by varying the flux path. An experimental prototype was manufactured. The magnetic flux field, the magnetic flux density and the attractive force of the system were analyzed by IEM analysis. Some basic measurement experiments were carried out using the experimental prototype. According to the results of the basic experiments, a mathematical model was created, and the feasibility of the proposed system was verified by the theoretical examinations. A numerical simulation was completed, and the experimental suspension was succeeded with the linear rails. All the results indicate the following conclusions:

The simultaneous suspension of two iron balls could be realized using the proposed magnetic suspension system, which controlled the suspension forces by a variable flux path control mechanism.

The minus feedback gains were affirmed in this simultaneous suspension system.

Since the inverse sign of the feedback gains of two iron balls, the movement of two iron balls is reversing each other.

However, the final states of the simulation and experiment results are a little different, and now we are investigating the reasons.

The characteristics of this system are similar to the parallel-type double inverted pendulum system, so this system can be applied as an examination device of the control system for education.

Chapter 9 General Conclusions

Until now, basing on the advantages of the magnetic suspension systems, many magnetic suspension systems have been developed and applied in many fields. Most existing magnetic suspension systems are using the electromagnetic magnet or including coils. In the light of the drawbacks of the coils, which are the heat generation, the relative large dimensions, and the large energy consumption with a lower efficiency, the magnetic suspension systems using the coils cannot be used in some special places, where needs a miniature dimension and the energy-saving characteristics. Based on the all-around considerations of the above coil's drawbacks and the development of permanent magnets, this thesis was proposed and completed.

This thesis focused on the magnetic suspension systems and the control systems using permanent magnets. First, an overview of the research background was introduced in a classification way, and the structure of this thesis was shown in chapter 1. Second, the research contents about the magnetic suspension systems using permanent magnets were exposited in three parts.

Part I proposed a zero power control method using a spring and an integral feedback loop, and examined the zero power control method on two kinds of magnetic suspension systems with permanent magnets and linear actuators.

Chapter 2 examined the zero power control method on a hanging type magnetic suspension system that could be applied as a noncontact conveyance vehicle. In chapter 2, the hanging type suspension principle was explained, and an experimental prototype was set up. A mathematical model was created. The suspension feasibility of the system was examined theoretically. The realization of zero power control was analyzed in device, mathematical model, and control system. The numerical simulations and experiments were carried out in five cases. All the simulation and experimental results indicated that this hanging type magnetic suspension system could be suspended stably. Moreover, comparing the results in the five cases, the validity of the zero power control was examined.

Chapter 3 discussed the zero power control method in a magnetic suspension system of an iron ball that could be applied as a noncontact manipulation mechanism. All the examination results in theoretical and experimental indicated that the iron ball could be suspended stably using the experimental prototype, and the zero power suspension could be realized using the proposed zero power control method.

This chapter proposed a hanging type magnetic suspension system using a permanent magnet and the VCM. In order to reduce the power consumption of the system in the stable

suspension state, a kind of zero power control method was proposed for this hanging type magnetic suspension system using a spring and an integral feedback loop of current.

Therefore, using this two proposed magnetic suspension systems, the miniature transmission device and the noncontact manipulation mechanism can be developed; and combining the proposed zero power control method, the zero power noncontact supporting also can be realized. The developed systems can be applied in some special places, e.g. the constant temperature plant.

Moreover, many control methods can realize the zero power control, but this thesis just discussed the method using the current integral feedback loop. The load observer control method may be regarded as the next step of the research. For the hanging type magnetic suspension system, this thesis just investigated the stable suspension in one dimension, and the controllable movement of the device has not been touched. The controllable movement of the hanging type magnetic suspension device in the horizontal plane may be the next step of this research.

Part II proposed a novel noncontact spinning mechanism using disk-type permanent magnets and rotary actuators, and analyzed the rotational characteristics of the mechanism by IEM analysis and the experimental measurement.

Chapter 4 proposed a novel noncontact spinning mechanism using disk-type permanent magnets and rotary actuators. In chapter 4, the noncontact spinning principle was exposited, and the experimental prototype was set up to investigate the proposed method. The mathematical model was created, and the simulation of spinning was carried out. And the noncontact spinning experiments were also carried out using one driving magnet, two driving magnets, and four driving magnets. The results indicated that a levitated iron ball could be spun using the remanent magnetizations and the rotational disk magnets. The iron ball could be spun regardless of the number of driving magnets used, however, as more magnets were used, the iron ball was spun more smoothly, but the velocity limit decreased.

In order to clarify the rotational characteristics of the noncontact spinning mechanism, chapter 5 analyzed the magnetic flux field variation and the rotational torque characteristics of the mechanism by IEM analysis and the experimental measurement. The results indicated that since the magnetic flux filed around the iron ball varied smoothly and the rotational torque was almost constant in every rotational angle of the magnets, the rotational state was stable and responded quickly when four magnets were used as the driving magnets. However, the attractive force in the horizontal direction was also large when using four magnets, and the horizontal force influence the stability of the suspension, as a result, the limit of the spinning velocity of the iron ball decreased.

However, in this thesis, the spin of the iron ball was not feedback to the control system and only the velocity of the iron ball was examined. Therefore, it may be the next step of this research that using the feedback signal controls the spin angle of the iron ball.

Part III proposed a mechanical magnetic suspension system using the variable flux path control method. This system could generate a semi-zero suspension force, the variable magnetic poles, and semi-zero power suspension.

Chapter 6 examined a magnetic suspension of a cuboid suspended object using the proposed variable flux path control mechanism. In chapter 6, the principle of the variable flux path control mechanism was exposited, and an experimental prototype was constructed. The magnetic flux variation in the mechanism was examined by IEM analysis, and the basic characteristics were examined by the IEM analysis and the measurement experiments. According to the experimental results, the mathematical model was created, and the suspension feasibility was investigated theoretically. The numerical simulation and the experiment of suspension were succeeded, and the energy-saving characteristics were also examined. All results indicated that this system could suspend the object stably in the suspension direction, and this system generated the variable magnetic poles of the stators, generated the semi-zero suspension force, and realized two kinds of semi-zero power suspension. However, the semi-zero suspension force characteristics were not very good, since the leakage of the magnetic flux between the magnet and the suspended object.

Chapter 7 proposed four methods to improve the semi-zero suspension force characteristics of the variable flux path control mechanism. The four improvement methods were inserting the ferromagnetic board, using a special type magnet, extending the iron cores, and combination of the special type magnet and the extended cores. The performance of the mechanism using each improvement method was examined by IEM analysis and measurement experiment. All the results indicate that, every method can improve the semi-zero suspension force characteristics. However, using the method of the special type magnet or the extended iron cores can obtain the obvious improvement, and using the combination method can obtain an almost zero suspension force characteristics. Moreover, the suspensions of the simulation and experiment were also carried out using the special type permanent magnet, and the results indicated that the improvement just improved the semi-zero suspension force characteristics of the mechanism, but not influenced the suspension characteristics.

Chapter 8 proposed a simultaneous suspension of two iron balls using the variable flux path control mechanism. An experimental prototype was manufactured. The magnetic flux field, the magnetic flux density and the attractive force of the system were analyzed by IEM analysis. Some basic measurement experiments were carried out using the experimental prototype. According to the results of the basic experiments, a mathematical model was created, and the feasibility of the proposed system was verified by the theoretical examinations. A numerical simulation was completed, and the experimental suspension was succeeded with the linear rails.

In addition, the magnetic suspension systems that were introduced in this part III, have

been realized the suspension using the state feedback control method. However, the robustness of the suspensions still should be strengthened, so the robust control method or the adaptive control method may be used to examine the robust suspension in these magnetic suspension systems. Moreover, the simultaneous suspension of two iron balls without the linear rails has not been succeeded since the magnetic flux leakage of the mechanism causes the horizontal attractive force to two iron balls. Finding the stable points of suspension in the horizontal direction and the improvement of the suspension mechanism will be the futural work of this research.

Reference

[1] J. Jin, T. Higuchi, and M. Kanemoto, "Electrostatic Levitator for Hard Disk Media", IEEE Trans. Industrial Electronics, Vol. 42, No. 5, pp. 467-473, 1995

[2] J. U. Jeon and T. Higuchi, "Electrostatic Suspension of Dielectrics", IEEE Trans. Industrial Electronics, Vol. 45, No. 6, pp. 938-946, 1998

[3] T. Kato, S. Tsukada, Y. Ishino, M. Takasaki, and T. Mizuno, "Electrostatic Suspension Using Variable Capacitors", Journal of Dynamics and Design, Vol. 3, No. 4, pp. 617-626, 2009

[4] AIR BEARING TECHNOLOGY, Westwind Air Bearings, a division of GSI Group Ltd. www.westwind-airbearings.com

[5] Teruyoshi HORIUCHI, Kazuyuki AONO, and Hiroaki HIYOSHI, "Development of Aerostatic Bearing Spindle for Precision Machine Tools", NTN TECHNICAL REVIEW, No.74, pp. 34-376, 2006

[6] How Acoustic Levitation Works. http://science.howstuffworks.com/acoustic-levitation2.htm

[7] Takuro NOZOE, and Nobuo TANAKA, "Relationship between Vibration Intensity and Transportation Force in 2-dimention Non-contact Transportation Using Ultrasonic Wave Levitation", Dynamics and Design Conference 2008, CDROM, P.254, Nara, Japan, 2008.

[8] Junpei TANAKA, and Nobuo TANAKA, "Non-contact Transportation Using Ultrasonic Levitation (Position Control Using Low Frequency)", Dynamics and Design Conference 2009, CDROM, P.633, Sapporo, Japan, 2009.

[9] B.V. Jayawant, "Electromagnetic levitation and suspension techniques", Edward Arnold, London, 1981.

[10] G. Schweitzer and E.H. Maslen, "Magnetic Bearings : Theory, Design, and Application to Rotating Machinery", Springer Dordrecht Heidelberg London New York, 2009.

[11] Hannes BLEULER, "A Survey of Magnetic Levitation and Magnetic Bearing Types", JSME International Journal, Series III, Vol.35, No.3, pp.335-342, 1992.

[12] R. Moser, Y. Regamey, J. Sendtner, and H. Bleuler, "Passive Diamagnetic Levitation for Flywheels", The Proceeding of 8th International Symposium on Magnetic Bearings. pp. 599-603, Mito, Japan, 2002.

[13] R. Moser, J. Sendtner, and H. Bleuler, "Diamagnetic Suspension System for Small Rotors ", Journal of Micromechatronics, VSB, Vol.1, No.2, pp. 131-137, 2001.

[14] R.E. Pelrine, “Room Temperature, Open-loop Levitation of Microdevices Using Diamagnetic Materials”, Proceeding of IEEE Micro Electro Mechanical Systems, Napa Valley, Canada, 1990

[15] K. Geim, M. D. Simon, M. I. Boamfa, L. O. Heflinger, “Magnet levitation at your fingertips”, Nature, 400, pp. 323–324, 1999.

[16] S. Komatsu，K. Oka，and H. Taguch, “Masato Sakamoto, Positioning Mechanism for Superconductive Levitation System”, Proceedings of the Asia-Pacific Symposium on Applied Electromagnetics and Mechanics, CDROM, Sydney, Australia, 2006.

[17] J. Wang, S. Wang, Z. Ren, X. Dong, G. Lin, J. Lian, C. Zhang, H. Huang, C. Deng, and D. Zhu, “A Scheme of Maglev Vehicle Using High Tc Bulk Superconductors” Applied Superconductivity, IEEE Transactions on, Vol. 9, Issue 2, Part 1, pp. 904-907, 1999.

[18] M. Ono, S. Koga, H. Ohtsuki, “Japan's Superconducting Maglev Train” Instrumentation & Measurement Magazine, IEEE, Vol. 5, Issue 1, pp. 9-15, 2002.

[19] Y. Tsutsui, and T. Higuchi, “A Suspension of Soft Magnetic Materials Using High Tc Superconductors”, IEEJ Transaction on Industry Application, Vol.115D, No.4, pp. 495-500, 2000.

[20] J.W. Henn, M. Sc, D. Phil, “Linear Perturbation Models for a.c. Magnetic Suspension Systems: Experimental and Theoretical Results”, IEE PROC, Vol. 127, No. 2, pp. 64-74, 1980.

[21] S. Hagihara, M. Eng., “Performance and Stability of a Magnetic Suspension Device Using a Tuned LCR Circuit”, PROCEEDING OF THE INSTITUTION OF ELECTRICAL ENGINEERS CONTROL AND SCIENCE, Vol.125, No.2, pp. 153-156, 1978.

[22] S. Suziki et al., “HSST-03 system”, IEEE Trans. Magn., Vol.20, pp. 1675-1677,1984.

[23] M. Morishita, T. Azukizawa, S. Kanda, N. Tamura, and T. Yokuyama, “A New Maglev System for Magnetically Levitated Carrier System”, IEEE Transactions on Vehicular Technology, Vol.38, No.4, pp. 230-236, 1989.

[24] K. Oka and T. Higuchi, “Magnetic Levitation System by Reluctance Control: Levitation by Motion Control of Permanent Magnet”, International Journal of Applied Electromagnetics in Materials, Vol. 4, pp.369-375, 1994.

[25] K. Oka, T. Higuchi, and T. Shiraishi, “Hanging Type Mag-lev System with Permanent Magnet Motion Control”, Electrical Engineering in Japan, Vol. 133, No. 3, pp.63-70, 2000.

[26] K. Oka, “Noncontact Manipulation with Permanent Magnet Motion Control”, Proceeding of the 4th International Symposium on Linear Drivers for Industry

Applications, LDIA2003, pp.259-262, Birmingham, UK, September 8-10, 2003.

[27] T. Cui, Y. Fujiwara, and K. Oka, “2 DOF Maglev System with Permanent Magnet Motion Control”, SICE Annual Conference 2005 in Okayama, Okayama University, Japan, pp.3859-3862, August 8-10, 2005

[28] K. Oka and T. Cui, “2 DOF Suspension Mechanism for Noncontact Manipulation with Permanent Magnet Motion Control”, Proc. of Mechatronics and Robotics 2004, CDROM, pp. 383-387, 2004

[29] K. Oka, Y. Fujiwara, T. Cui and C. Li, “Noncontact Spinning Mechanism Using Linearly Actuated Magnets”, Proc. of the 5th International Symposium on Linear Drivers for Industry Applications, LDIA2005, CDROM, pp.552-555, Awaji Yumabutai, Hyogo, Japan, September 25-28, 2005.

[30] T.S. Cui, K. Oka, and K. Masaki, “Magnetic Levitation System Using Permanent Magnet and Linear Actuator - Study of Push-Pull Levitation Mechanism”, The Japan Society Applied Electomagnetics and Mechanics, Vol. 14, No. 1 pp. 120-125, 2006.

[31] T. Mizuno, Y. Hirai, Y. Ishino, and M. Takasaki, “Flux-Path Control Magnetic Suspension System Using Voice Coil Motors”, Journal of System Design and Dynamics, Vol.1, No.2, pp.147-158, 2007.

[32] M. Furutachi, S. Inaba, Y. Ishino, M. Takasaki, and T. Mizuno, “Three-Dimensional Force Measurement and Control of a Flux-path Control Magnetic Suspension”, Journal of System Design and Dynamics, Vol.2, No.6, pp.1239-1249, 2008.

[33] T. Ueno, and T. Higuchi, “Zero-Power Magnetic Levitation Using Composite of Magnetostrictive/Piezoelectric Material”, IEEE Transactions on Magnetics, Vol.437, No.8, pp.3477-3482, 2007.

[34] T. Ueno, J. Qiu, and J. Tani, “Magneto-Electric Composite Element of Giant Magnetostrictive and Piezoelectric Materials and Its Application of Magnetic Force Control to Magnetic Levitation System”, Transactions of the Japan Society of Mechanical Engineers, Series C, Vol.67, No.658, pp. 1897-1904, 2001.

[35] K. Oka, N. Ninomiya, L. Chen, and Y. Fujiwara, “Magnetic Suspension System with Variable Flux Path Mechanism Using Rotary Actuator”, The 10th International Symposium on Magnetic Bearings, CDROM, p.86, 2006.

[36] D.M. Rote, Y. Cai, “Review of dynamic stability of repulsive-force maglev suspension systems”, Magnetics, IEEE Transactions on, Vol.38, No.2, pp. 1383-1390, 2002

[37] S.C. Mukhopadhyay, J. Donaldson, G. Sengupta, S. Yamada, C. Chakraborty, D. Kacprzak, “Fabrication of a repulsive-type magnetic bearing using a novel arrangement of permanent magnets for vertical-rotor suspension”, Magnetics, IEEE Transactions on, Vol.39, No.5, pp. 3220-3222, 2003

[38] T. Mizuno, H. Sekiguchi and K. Araki, “Repulsive Magnetic Bearing Using Motion Control of Permanent Magnets (Stabilization in the Axial Direction) ”, Transactions of the Japan Society of Mechanical Engineers, Series C, Vol. 64, No.628, pp. 187-192, 1998.

[39] Lee O. Heflinger, Torrance CA, S. L. Ridgway, and Santa Monica CA, “Spin stabilized magnetic levitation”, American Journal of Physics, Vol.65, No.4, pp. 286-292, 1997.

[40] J. Meins, L. Miller, “THE HIGH SPEED MAGLEV TRANSPORTATION SYSTEM TRANSRAPID”, IEEE Transactions on Magnetics, Vol.24, No.2, pp 808-811, 1988

[41] H. Uwe, H. Reinhard, and H. Josef, “Advanced static power converter and control components for TRANSRAPID maglev system”, Proceedings of Power Conversion Conference 2002, Vol.3, pp. 1045-1049, Osaka, Japan, 2002.

[42] K. Nagata, M. Takahashi, I. Miyashita, “Linear Motor Drive System for the Normal Conductivity Maglev Vehicle HSST-05”, IEEJ Transactions on Industry Applications, Vol.110-D, No.1, pp. 23-31, 1990.

[43] M. Brune and I. Detomb, “APPLICATION OF ACTIVE MAGNETIC BEARINGS IN TURBOCOMPRESSORS AND TURBOEXPANDERS OF THE GAS INDUSTRY”, Chemical and Petroleum Engineering, Vol. 38, No. 7-8, pp.459-463, 2002.

[44] T. Mizuno, K. Araki, and H. Bleuler, “Stability Analysis of Self-sensing Magnetic Bearing Controllers”, IEEE Transactions on Control Systems Technology, Vol.4, No.5, pp.572-579, 1996.

[45] G. -M. Punier, A. Gelen and D. Bolusse, “Centrifugal compressors fitted with active magnetic bearings”, Chemical and Petroleum Engineering, Vol. 35, No. 5, pp. 254-259, 1999.

[46] X. Song, A.L. Throckmorton, A. Untaroiu, S.M. Patel, P.E. Allaire, H.G. Wood, and D.B. Olsen. “Axial Flow Blood Pumps”, ASAIO Journal 2003, Vol.49, pp. 355-364, 2003.

[47] Steven W. Day, James C. McDaniel, Houston G. Wood, Paul E. Allaire, Xinwei Song, Phillip P. Lemire, and Scott D. Miles, “A Prototype HeartQuest Ventricular Assist Device for Particle Image Velocimetry Measurements”, Artificial Organs, Vol. 26, No. 11, pp. 1002-1005, 2002.

[48] X.W. Song, A. Untaroiu, H. G. Wood, P. E. Allaire, A. L. Throckmorton, S. W. Day, and D. B. Olsen, “Design and Transient Computational Fluid Dynamics Study of a Continuous Axial Flow Ventricular Assist Device”, ASAIO Journal 2004, Vol.50, pp. 215-224, 2004.

[49] K. Sekine, M. Asakawa, Y. Mitamura, “Development of an axial flow blood pump:

characteristics of a magnetic fluid seal", The Japanese Society for Artificial Organs 2001, Vol.4, pp. 245-251, 2001.

[50] M. Morishita et al., "A new Maglev system for magnetically levitated carrier system", IEEE Trans. Vehicular Tech, Vol. 38, No. 4, pp. 230-236, 1989.

[51] Y. Suda, T. Wada, Y. Michitsuji and T. Iwasa, "Control of MAGLEV System with Tilting Control by Rotor", Proceeding of Dynamics and Design Conference 2002, CD-ROM, p.446, Kanazawa, Japan, 2002.

[52] J.H. Park and Y.S. Baek, "Design and Analysis of a Maglev Planar Transportation Vehicle", IEEE Trans. Magnetics, Vol. 44, No. 7, pp. 1830-1836, 2008.

[53] M. Morishita and T. Azukizawa, "Zero Power Control Method for Electromagnetic Levitation System", Trans. IEE of Japan, Vol.108-D, No.45, pp.447-454, 1988.

[54] M. Morishita, and H. Iton, "The Self-gap-detecting Zero Power Controlled Electromagnetic Suspension System", Trans. IEE of Japan, Vol.126-D, No.12, pp.1667-1677, 2006.

[55] M.E. Hoque, M. Takasaki, Y. Ishino, H. Suzuki and T. Mizuno, "An Active Micro Vibration Isolator with Zero-Power Controlled Magnetic Suspension Technology", JSME International Journal, Series C, Vol. 49, No. 3, pp. 719-726, 2006.

[56] M.D. Noh, J.F. Antaki, M. Ricci, G. Jeff, D. Paden, "Magnetic Design for the PediaFlow Ventricular Assist Device", Artificial Organs, Vol.32, No.2, pp. 127-135, 2007.

[57] T. Misuno, Y. Hirai, Y. Ishino, and T. Misuno, "Flux-Path Control Magnetic Suspension System Using Voice Coil Motors", Journal of System Design and Dynamics, Vol.1, No.2 (2007), pp.147-158, 2007.

[58] Y. Fujiwara, T.S. Cui, and K. Oka, "Magnetic Levitation System with Permanent Magnet Motion Control (Study of Spinning Mechanism)" (in Japanese), Dynamics and Design Conference 2008, No.04-5, p.517, 2004.

[59] K. Oka and T.S. Cui, "Zero Power Control for Magnetic Suspension System with Permanent Magnet Motion Control", International Conference on Electrical Machines and Systems, CD-ROM, 2004.

[60] E. Shameli, M.B. Khamesee and J.P. Huissoon, "Nonlinear Controller Design for a Magnetic Levitation Device", Microsyst Techno, Vol.13, pp. 831-83, 2007.

[61] T. Mizuno, and Y. Takemori, "A Transfer-Function Approach to the Analysis and Design of Zero Power Controllers for Magnetic Suspension System", The Transactions of The Institute of Electrical Engineers of Japan, Vol. 121, No. 9, pp. 933-940, 2001.

[62] T. Misuno, and R. Yoshitomi, "Vibration Isolation System Using Zero-Power Magnetic Suspension (1st Report, Principle and Basic Experiments)" (in Japanese), Transactions of the Japan Society of Mechanical Engineers, Series C, Vol.68,

No.673, pp. 2599-2604, 2002.

[63] T. Misuno, D. Kishita, M. Takasaki, and Y. Ishino, “Vibration Isolation System Using Zero-Power Magnetic Suspension (2st Report, Introduction of Weight Support Mechanism)” (in Japanese), Transactions of the Japan Society of Mechanical Engineers, Series C, Vol.72, No.715, pp. 714-722, 2006.

[64] Y. Ishino, T. Misuno, M. and Takasaki, “In Creasing the Load Capacity of Magnetic Suspension by a Stiffness Switching Control” (in Japanese), Dynamics and Design Conference 2008, No.08-14, p.658, 2008.

[65] Kim, Y.H., Kim, K.M. and Lee, J., Zero Power Control with Load Observer in Controlled-PM Levitation, IEEE Transactions on Magnetics, Vol.37, No.4, pp.2851-2854, 2001.

[66] Non, M.D., Antaki, J, F., Ricci, M., Gardiner, J., Paden, D., Wu, J.C., Prem, E., Borovetz, H. and Paden, B.E., Magnetic Design for the PediaFlow Ventricular Assist Device, Artificial Organs, Vol.32, No.2, pp.127-135, 2007.

[67] T. Nakamura and M.B. Khamesee, “A Prototype Mechanism fro Three-Dimensional Levitated Movement of a Small Magnet”, IEEE/ASME Transactions on Mechatronics, Vol. 2, No. 1 pp. 41-50, 1997.

[68] S. Verma, H. Shakir and W.J. Kim, “Novel Electromagnetic Actuation Scheme for Multiaxis Nanopositioning”, IEEE Transactions on Magnetics, Vol. 42, No. 8 pp. 2052-2062, 2006.

[69] K. Ikuta, S. Makita and S. Arimoto, “Non-Contact Magnetic Gear for Micro Transmission Mechanism”, Proceedings of the 1991 IEEE Micro Electro Mechanical System, pp.125-130, Nara, 1991.

[70] Manual of ELF/Magic, ELF Company.

[71] Yamamoto, M. Kimura, and T. Hikihara, “A Study on Indirect Suspension of Magnetic Target by Actively Controlled Permanent Magnet”, 11th International Symposium on Magnetic Bearings, pp.182-188, Nara, Japan, 2008.

[72] T. Sakurada, Y. Maruyama, Y. Ishino, M. Takasaki, and T. Mizuno, “Multiple Magnetic Suspension Systems 4th report: Realization of Parallel Magnetic Suspension of two floator”, The 52th Automatic Control Union Lecture, G5-2, CD-ROM, Osaka, Japan, 2009.

[73] C.N. Lu, C.C. Tsai, M.C. Tsai, K.V. Ling, and W.S. Yao, “Application of Model Predictive Control to Parallel-Type Double Inverted Pendulum Driven by a Linear Motor”, The 33th Annual Conference of the IEEE Industrial Electronics Society, Nov.5-8, pp.2904-2909, Taipei, Taiwan, 2007.

Relevant papers of this research

✧ Publication for Journal

[1] Feng SUN and Koichi OKA, Zero power control for hanging type maglev sytem with permanent magnet and VCM, Trans. of JSME Series C, Vol. 75, No.753, (2009-5), pp.1383-1388

[2] Feng SUN and Koichi OKA, Zero Power Non-Contact Suspension System with Permanent Magnet Motion Feedback, Trans. of JSME, Journal of System Design and Dynamics, Vol.3, No.4 (2009), pp.627-638

[3] Feng SUN and Koichi OKA, Noncontact Spinning Mechanism Using Rotary Permanent Magnets, IEEJ Transactions on Industry Applications, Vol.130, No.7, (2010-7), pp.913-919

[4] Feng SUN, Koich OKA and Yuuta SAIBARA, Magnetic Suspension System by Flux Path Control Using Rotary Actuator, the International Journal of Applied Electromagnetic and Mechanics (Received, will be published)

[5] Feng SUN and Koich OKA, Development of Noncontact Suspension Mechanism Using Flux Path Control Disk Magnet Rotation, Trans. of JSME Series C (Received, will be published)

✧ Publication for International Conference

[1] Feng SUN and Koichi OKA: Zero Power Control for Permanent Magnetic Suspension System, Proceeding of The 11th International Symposium on Magnetic Bearings, No.631, pp. 489-495, Nara, Japan (2008-8)

[2] Feng SUN and Koichi OKA, Noncontact Rotation Control for Suspension Iron Ball Using Disk Magnet, Proceeding of The First Japan-Korea International Joint Symposium on Dynamics and Control, August 4-6, 2009, Sapporo, Japan. No.09-208, pp.155-156

[3] Sun, F., Oka, K. and Saibara, Y., Magnetic Suspension System by Flux Path Control Using Rotary Actuator, Proceedings of 14th International Symposium on Applied Electromagnetics and Mechanics, pp.289-290, Xi'an, China, 2009.

[4] Koichi OKA and Feng SUN, Noncontact Spinning Mechanism Using Rotary Permanent Magnets, Proceeding of the 7th International Symposium on Linear Drivers for Industry Applications 2009, No.PS2.1, pp. 125-128, Incheon, Korea, (2009-9)

[5] Koichi OKA and Feng SUN, Zero Power Control for Mechanical Magnetic Suspension System Using Spring Force, Proceeding of 6th Japanese-Mediterranean Workshop on Applied Electromagnetic Engineering for Magnetic, Superconducting and Nano Materials, pp. 251-252, Bucharest, Romania, (2009-7)

[6] Feng SUN, Koichi OKA and Toru TAKECHI, Simultaneous Noncontact Suspension of Two Iron Balls Using Flux Path Control Mechanism, Proceeding of The 10th International Conference on Motion and Vibration Control, No.10-203, 2A14, Tokyo, Japan, (2010-8).

[7] Feng SUN, Akira TSURUMI and Koichi OKA, Torque Analysis of a Noncontact Spinning System Using Linearly Actuated magnets, Proceeding of Asia-Pacific Symposium on Applied Electromagnetics and Mechanics 2010, pp.108-109, Kuala Lumpur, Malaysia, (2010-7).

[8] Feng SUN and Koichi OKA, Characteristics Analysis of Magnetic Suspension Mechanism with Variable Flux Path Control, Proceeding of The 12th International Symposium on Magnetic Bearings, No.11, pp. 154-160, Wuhan, China, (2010-8).

✧ Publication for Domestic Conference

[1] 孫鳳，岡宏一：永久磁石の吸引力を利用した懸垂型磁気浮上機構における零パワ制御，Dynamic and Design Conference 2008，No.660， pp. 373，横浜，日本 (2008-9)

[2] 孫鳳，岡宏一：アクチュエータ駆動による非接触回転駆動機構（円板磁石の回転による駆動），第 21 回「電磁力関連のダイナミクス」シンポジウム，No.20B4-1, pp207-212，長野，日本（2009-5）

[3] 孫 鳳, 岡 宏一, 西原 雄太: 回転モータを利用した浮上システムの開発 , Dynamic and Design Conference 2009，No.436， pp. 231，札幌，日本 (2009-8)

[4] 孫 鳳, 岡 宏一, 運動制御による鉄球の回転機構のトルク特性, 電気学会 リニアドライブ研究会, LD-09-051 p.23, 産業技術総合研究所秋葉原事業所大会議室 2 (千代田区,東京) 日本（2009-10）

[5] 孫 鳳，岡 宏一，円板磁石の回転による非接触回転駆動機構，SICE Annual Conference 2009, CD-ROM of SICE 2009, 高知工科大学(香美市, 高知県), 日本（2009-11）

[6] 孫 鳳, 岡 宏一, 運動制御に基づく磁気浮上機構の零パワー制御, 第 52 回自動制御連合講演会，CD-ROM, 大阪大学基盤工学研究科 (豊中市,大阪府), 日本（2009-11）

[7] 武智 徹，孫 鳳，岡 宏一, 円板磁石の回転を用いた磁路制御形非接触浮上機構, SICE Annual Conference 2009, CD-ROM of SICE 2009, 高知工科大学(香美市, 高知県), 日本（2009-11）

[8] 西原 雄太，孫 鳳，岡 宏一：永久磁石を用いたロータリー式磁気浮上機構，日本機械学会中四国学生会 第 39 回学生員卒業研究発表講演会，No.1205，pp.239，山口大学(宇部市，山口県)，日本（2009-3）

[9] 岡 宏一，孫 鳳，永久磁石とリニアアクチュエータを利用した非接触浮上機構の零パワー制御，第 11 回「運動と振動の制御」シンポジウム，No.B22，pp. 291-294，アクロス福岡 (福岡市，福岡県)，日本（2009-9）

[10] 岡 宏一，孫 鳳，永久磁石と回転形モータを磁路制御型磁気浮上機構，第 11 回「運動と振動の制御」シンポジウム，No.B27，pp. 452-455，アクロス福岡 (福岡市，福岡県)，日本（2009-9）

[11] 岡宏一，孫鳳，永久磁石の回転による磁路制御形磁気浮上機構の浮上性能の評価，電気学会 半導体電力変換/リニアドライブ合同研究会，SPC-09-186/ LD-09-76，pp. 115-120，浜名湖かんざんじ荘(浜松市，静岡県)，日本（2009-12）

[12] 武智徹，孫鳳，岡宏一，楠川量啓，永久磁石を用いた磁路制御形非接触浮上機構開発，日本設計工学会四国支部平成 21 年度研究発表講演会論文集，pp.11-14，香川大学（高松，香川），日本（2010-3）

[13] 鶴身輝，孫鳳，岡宏一，楠川量啓，永久磁石を用いた非接触浮上・回転機構の開発，日本設計工学会四国支部平成 21 年度研究発表講演会論文集，pp.15-18，香川大学（高松，香川），日本（2010-3）

[14] 孫鳳，鶴身輝，岡宏一，円盤磁石の回転駆動による非接触回転装置のトルク特性分析，第 22 回「電磁力関連のダイナミクス」シンポジウム，20B2-2，pp.346-349，九州，日本（2010-5)

[15] 孫鳳，鶴身輝，岡宏一，永久磁石を用いた非接触回転駆動機構のトルク特性，Dynamic and Design Conference 2010，京都，日本 (2010-9) (発表予定)

[16] 孫鳳，岡宏一，武智徹，円板磁石を用いた可変磁路制御機構による２つの鉄球浮上，Dynamic and Design Conference 2010，京都，日本 (2010-9) (発表予定)

[17] 孫鳳，鶴身輝，岡宏一，永久磁石の運動制御を用いた非接触回転機構-回転トルク特性の考察，第 53 回自動制御連合講演会，高知城ホール (高知市,高知県)，日本（2010-11）(発表予定)

ACKNOWLEDGEMENTS

My deepest gratitude goes first and foremost to my supervisor Prof. Koichi Oka, who led me into the world of magnetic suspension, for his constant encouragement and guidance in my pursuing the Ph.D. degree. He gave me the chance to continue doctoral course and guided me all the 3 years. Without his consistent assistance and instruction, I cannot receive the fruit of research, and also this thesis could not have reached its present form. His ethos of dedication and perfectionism to work will have a far-reaching impact on my life. I am also greatly indebted to his kind family. Mrs. Oka helped me a lot on my Japanese. Her serious and earnest attitude makes me moved deeply.

Next, I am also very grateful to Prof. Yoshio Inoue, Prof. Shuoyu Wang, Prof. Fumiaki Takeda, and Prof. Kyoko Shibata for their insightful comments on my thesis. Many valuable advices were gotten from them, so this thesis can be improved.

As a SSP student, I would like to appreciate Kochi University of Technology for supporting me to study here. I would also like to express my thanks to Shenyang University of Technology who recommended me to study at Kochi University of Technology.

As a foreign student, I really appreciate Prof. Mikiko Ban and all the staff in IRC. They make me live happily and comfortably in Japan.

Much-appreciated co-operations and helps come from the lab-mates, especially from Mr. Saibara, Mr. Tsurumi, Mr. Takechi, Mr. Tachibana, thank them for their friendship and contributions to my work. Without the nice staff of Oka lab, the research could never have been fulfilled.

Last, but not least, I would like to appreciate my parents, particularly my wife for their generous love and support to my life all along. I also owe my sincere gratitude to my friends who gave me their help and time in listening to me and helping me work out my problems during the difficult course of the thesis.